LATE QUATERNARY GEOMORPHOLOGY OF ARROYOS IN THE MIXTECA ALTA, OAXACA, MEXICO

by

Genevieve A. Holdridge

(Under the Direction of David S. Leigh)

ABSTRACT

Land degradation in drylands is one of the most critical, ongoing global environmental issues, and gullying and arroyos constitute some of the more serious elements of desertification. The overarching goal was to examine how late Quaternary climate, land use, and environmental change influenced the dryland stream dynamics of the Río Culebra watershed, located in the semi-arid Mixteca Alta in southwestern Mexico. This goal was examined through three separate, but interrelated studies. The first study (Chapter 2) examined the sediment yield and land use of the dryland fluvial system of the Río Culebra watershed. Conservative bedload yield estimates on two tributary arroyos demonstrated that despite headwater conservation, the yield is still relatively high, and suggest the need for larger scale conservation efforts. Present channel bed stratigraphy containing predominantly massive, coarser deposits contrasts the prevalence of finer bedded sediments in the Quaternary stratigraphy, which indicate a different flood regime in the past. The second study (Chapter 3) concerned the uncertainty of the relative contributions of anthropogenic versus climatic drivers on land degradation. The alluvium-paleosol chronology was examined against regional climatic conditions and indicated that greater incision occurred

during wetter periods, while alluvial deposition and paleosol formation occurred during transitional wet and dry periods, supporting the "wet-dry-wet" model of arroyo cycles. Comparing the paleoclimatic-paleohydrological relationship of terminal Pleistocene and early Holocene strata versus the late Holocene strata indicated that widepsread agricultural activities greatly impacted sediment rates and influenced the timing and nature of landscape response to climate change. The third study (Chapter 4) addressed the need for better understanding the local paleoenvironment. The local paleoenvironment, as reflected in soil organic matter $\delta^{13}C$ values and paleosol data is comparable to the paleoclimatic and paleoenvironmental reconstruction from central and southwestern Mexico. The paleoenvironment of Culebra watershed was impacted by lama-bordo (i.e., check dam) and agricultural terrace constructions and the increased importance of maize cultivation and succulent plant managment during the late Holocene. The results of these studies illustrate the need to understand long-term climatic, hydrologic and land use variability in order to find solutions to dryland desertification in the present.

INDEX WORDS: Quaternary stratigraphy, Arroyo cycles, Sediment yield, Erosion, Land use, Paleohydrology, Incision, Agradation, Semi-arid, Dryland streams, Stable carbon isotopes, Check dams, Mixteca Alta, Mexico

LATE QUATERNARY GEOMORPHOLOGY OF ARROYOS IN THE MIXTECA ALTA, OAXACA, MEXICO

by

GENEVIEVE A. HOLDRIDGE

BA, University at Albany-SUNY, 2001

MS, Bilkent University, Turkey, 2004

MPhil, University of Cambridge, United Kingdom, 2006

A Dissertation Submitted to the Graduate Faculty of The University of Georgia in Partial Fulfillment of the Requirements for the Degree

DOCTOR OF PHILOSOPHY

ATHENS, GEORGIA

2016

LATE QUATERNARY GEOMORPHOLOGY OF ARROYOS IN THE MIXTECA ALTA, OAXACA, MEXICO

by

GENEVIEVE A. HOLDRIDGE

Major Professor:	David S. Leigh
Committee:	George A. Brook
	L. Bruce Railsback
	David F. Porinchu

Electronic Version Approved:

Suzanne Barbour
Dean of the Graduate School
The University of Georgia
August 2016

"Nothing is softer or more flexible than water,
yet nothing can resist it."
-Lao Tzu

ACKNOWLEDGEMENTS

Thanks to various sources of funding, I was able to complete my dissertation including the following: the Fulbright Garcia-Robles (2012-2013); the Geologic Society of America Grant (2013); the USAID Small Projects Grant (2014); and the Summer Dissertation Write-up Grant UGA (2016). Also thanks to my opportunity as a Peace Corps Response Volunteer, I was able to work on part of my project for an extra year as well as work with many local communities in the Mixteca Alta.

There are many people to thank as I could not have achieved this PhD without their help, support, insight and experience. Firstly, I would like to thank the administraters of many municipalities in the Coixtlahuaca District for giving me permission and support to conduct my work. In particular, I would like to thank the municipalities of San Juan Bautista Coixtlahuaca and Santa Maria Nativitas and the administrators therein. I would like to thank colleagues at the Biosphere Reserve for their enormous support with logistics in the field and their interest in my project that resulted in my position as a Peace Corps Response Volunteer. Thanks to Rafael Arzarte Aguirre, Roberto Navarro, Socorro Garcia, and Fernando Reyes, I learned so much about the region, and was able to co-organize two foros in the Coixtlahuaca district. I am grateful to the employees - my friends- at the Peace Corps including Heather Zissler, Beatriz Charles and especially Angel Pineda, who was my director and helped me coordinate my new position and logistics.

I would also like to thank the geoarchaeological team with whom I started my research in Coixtlahuaca, in particular Gabby Garcia Ayala and Stefan Brannan. I am so greatful to the

project´s co-director, Steve Kowalewski, who like another committee member, offered tons of support and shared his expertise on the archaeology and anthropology of the region; this project would never have been completed without his support.

Professors from other insitutions also offered their support such as lecturer Gerardo Roman Gonzalez Rojas at the Institute of Tehuacan, who helped organize water quality analyses from Coixtlahuaca, and Lorenzo Selem for insightful discussions (Geographer at the National Autonomous University of Mexico (UNAM) in Mexico City. Also David Gale, (astrophysicist, University of the Americas, Puebla) who was such a good friend – thanks for showing me the Azteca! In particular, I would like to thank JP Bernal at UNAM (Geochemist, Queretaro campus), also like another committee member, took me in as one of his students and included me on his caving projects and stalagmite research. He offered much support despite my unsuccessful attempt to incorporate stalagmite work into my dissertation (but not unsuccessful for long….!). Thanks to him for all the insightful discussions about geochemistry, geomorphology and archaeology, etc., - but most especially his friendship. Thanks to Julie Hemple for letting me stay at her house in Queretaro and for teaching me about Mexican literature, and thanks to the other students at UNAM (Queretaro campus) and my friends in the group: los Musicos Queretaros!

I lived in Coixtlahauca for three years and have met so many wonderful people, including Chavela Garcia Juarez and her family, thanks to them for the mezcals, dinners, and teaching me so much about the local Oaxacan culture. I am grateful for the dinners with Regina and her family, and Florinda and her family. Lucia, thank you for the interesting talks! Most especially I would like to thank mi tía, Altagracia Garcia Lara, who is my adopted aunt, with whom I lived with for almost 2 years, and with whom I have shared many meals and heartfelt talks. Her

children and grandchildren, the rest of the Garcia Lara family, have shown so much support while I lived in the village. In particular, I would like to recognize Blademir Victor Garcia Lara who is very insightful, an engineer in his own right, and who has succeeded in conserving much of his land in the headwaters of Sandage. He serves as a model for all of us. Thanks to Fidelia Garcia Juarez (Victor´s wife) for her insight and support and their son Richy who has helped me so much in the field. Finally, many other field and lab workers were employed by me, but Juan Carlos Juerez Jimenez, Karen Betanzos and Berenice Lara were exceptional employees and I could not have done this without them.

My lab work involved isotopes and I appreciate the support of Julia Cox in the Geology Isotope Lab, and the scientists at the Center for Applied Isotopes: especially Doug Dvorocek and Alex Cherkinsky. Much of my writing and map-making took place in the Center for Geospatial Research, and I thank the the lab for its support (and safetly) in particular, Tommy Jordan, Magarite Madden, Sergio Bernardes, David Cotten, Roberta Samli, and Brandon Adams. To my fellow physical geographers, thanks for all the good discussions and the impetus to finish! In particular Jake McDonald, Pete Akers and Lixin Wang. To other friends who have enriched my life and opend my mind, especially Brooke Tave, Guy Savir, Mike and Alicia Coughlan, Tiffany Videl, Shadrock Roberts, Megan Westbrook, Peter Baas, Megan MacMuller, Isaac Lungu and Mohammed Yaffa.

Thanks to my committee, firstly David Porinchu for his critical and insightful comments. I am so grateful to Bruce Railsback, who taught me so much and helped me achieve something with my undateable stalagmites. Thanks to George Brook (best soccer player), as I have learned so much from him and who has given much support over the years. I would have never made it without his help, and dare I say friendship! Finally, to my advisor David Leigh, thanks for

believing in me. It has been tough as I have been in the field so much. Thanks to David for all of his insight, knowledge, guidance and support. I have learned so much from him - from field methods to better writing. I am so happy we worked together. *Salud!*

To Stuart and Laina Swiny, thanks for all the support over the years. They are like family to me and my life would have not been the same if I had not attended that excavation on Cyprus with them all those years ago (2001)! To all my family, thank you so much for being there for me! In particular, I would like to thank my Aunt and Uncle, Ruth Harman and Jack Holdridge, who live in Athens. We have become so close, and thanks to them for sticking with me through the ups and downs. I will never forget it and will always be there for them. Thanks to my parents, Louise and Jim Holdridge, who have been behind me, pushed me, and who have never given up on me. Also, I am grateful to my father, an excellent writer and editor, who did last minute edits on my dissertation writing. I love you all!

TABLE OF CONTENTS

Page

LIST OF TABLES

Page

LIST OF FIGURES

Page

CHAPTER 1

INTRODUCTION

1.1 Overview and Objectives

Land degradation in drylands is identified as one of the most critical, ongoing global environmental issues by the United Nations (UN Report, 2011). Drylands are defined as regions that have an aridity index of between 0.03-0.75 (Table 1.1) (UN Report, 2011). Drylands cover approximately 40% of the Earth's land surface, and contain around 30% of the world's population (UN Report, 2011). Land degradation is defined as the damage to land productivity in drylands that results from unsustainable land use practices and recent climate change (Annan, 2006; UN Report, 2011). Drylands, especially semi-arid and arid environments, are characterized by rainfall variability and unstable hydrological regimes, leaving them particularly vulnerable to land degradation (Sivakumar, 2007). Gullying and arroyo formation are types of soil erosion that constitute one of the more serious elements of desertification, causing severe damage to terrestrial and aquatic ecosystems (Dregne, 2002).

Notwithstanding the importance of other external factors (i.e., tectonics and base level), the degree to which humans versus climate influence gullying and arroyo formation has been one of the most prominent debates in geomorphology since the early 20th century. A study by Waters and Haynes (2001) demonstrated that climate change alone generates arroyos, while land use effects (e.g., cultivation, deforestation) on soil erosion and gullying have also been confirmed as drivers by a number of studies (Walling, 1999; Knox, 2001; Poesen et al., 2003; Gellis et al.,

2004; Walling and Collins, 2008; Svoray and Markovitch, 2009). Geoarchaeological and geomorphological research also supports that prehistoric land use practices, such as agriculture and deforestation as well as population pressures and land abandonment, resulted in land degradation during the late Holocene (Butzer, 1992; Denevan, 1992; O'Hara et al., 1993; Waters and Ravesloot, 2000; McAuliffe et al., 2001; Fisher et al., 2003; Wilkinson, 2005a; Butzer et al., 2008).

Although the overarching link between climate change, human activities, and desertification is well documented for the last century (Karl and Trenberth, 2003; Giurma et al., 2008), the relative contributions of anthropogenic versus climatic factors are unclear. This uncertainty calls for more studies on the long-term climatic variability, land use change, and related hydrologic responses in drylands (Poesen et al., 2003; Benito et al, 2010).

Research Objectives: This research focuses on late Quaternary arroyo processes, forms, and functions in the semi-arid environment of the Río Culebra Valley, located in the Mixteca Alta of southwestern Mexico. The overarching goal is to examine past and present dryland stream dynamics in relation to climatic, land use, and environmental change. Although drylands cover hyper-arid to sub-humid climates, in this research the term drylands in relation to the Mixteca Alta will refer to a semi-arid environment, and the term 'all drylands' will denote the entire ensemble of dryland environments. Three research objectives will be addressed in three separate, but interrelated chapters, as follows:

Research Objective 1 (RO1): to study the channel bed morphology, bedload and flow characteristics of the present ephemeral stream system in order to better understand erosion in the region, as well as offer insight on interpreting the alluvial stratigraphy; Chapter 2 provides data and interpretations related to this objective;

Research Objective 2 (RO2): to determine the relationship between paleoclimatic fluctuations and arroyo formation prior to widespread agriculture in the region, and compare the results from the pre-agricultural stratigraphy to the late prehistoric and modern agricultural time periods in order to better discern the influences of climate versus anthropogenic drivers; Chapter 3 provides data and interpretations related to this objective;

Research Objective 3 (RO3): to examine paleoenvironmental change represented by stable carbon isotopes in soil organic matter, and along with the paleoclimate information provided by paleosols, to establish how the site specific record of paleoenvironmental change corresponds with regional paleoenvironmental and paleoclimatic fluctuations; Chapter 4 provides data and interpretations related to this objective.

1.2 Rationale

According to Graf (1979) the term 'arroyo' was first used in the southwestern United States by Dodge (1902), who defined them as: 'steep-walled, flat-floored trenches excavated in valley floors". In some literature gullies denote smaller incised channels and are located in the headwaters, while arroyos represent larger incised channels and are situated in valley bottoms, but in other studies they are synonymous (as they will be used here) (Goudie, 2013). The terms gullies and arroyos are also referred to as ephemeral streams, dryland rivers (Bull and Kirkby, 2002), and barrancas (local name in Oaxaca, Mexico), but the latter three terms typically refer to continuous channels, whereas gullies and arroyos can be continuous or discontinuous (Bull, 1997). Flow in arroyos is usually ephemeral, but occasionally they contain perennial (i.e., when

supplied by a spring) or intermittent groundwater inflow (Bull, 1997; Goudie, 2013). Additionally, in some regions arroyos undergo cycles of incision and aggradation, though it is uncertain why they form and how they operate. The dryland streams in the study area are continuous arroyos, having mainly ephemeral flow, but some streams are spring-fed perennial streams and all demonstrate cycles of erosion and incision. To clarify, in this research 'dryland streams' in the context of the Mixteca Alta will represent semi-arid dryland streams, but when referring to all dryland streams the term 'all dryland streams' will be used.

Present arroyo formation has been linked to various combinations of climate-independent (i.e., drainage area and morphometry, geology, slope, surficial crusts), climate-dependent (i.e., rainfall and temperature, flood frequency and magnitude, vegetation type and amount), and anthropogenic causes (i.e., grazing, overpopulation, agriculture) (Jansson, 1988; Bull, 1991; Bull, 1997; McFadden and McAuliffe, 1997; Hereford, 2002; Poesen et al., 2003; Avni, 2005; Valentin et al., 2005; Jones et al., 2010). The combination of factors varies at times and for different locations making it difficult to understand and predict arroyo formation. Internal factors are important, as sensitive lithologies will produce higher amounts of sediment yield in comparison to basins with more resistant lithologies with the same climate and land use (McFadden and McAuliffe, 1997).

The overarching climatic and anthropogenic drivers and their relative contributions toward arroyo formation are still uncertain (e.g., Boardman et al., 2010; Goudie, 2013). While the connection between gully formation and climate, without human intervention, has been substantiated (Waters and Haynes, 2001), contradictory hypotheses concerning arroyo formation still endure (e.g., Borejsza et al., 2008; Solleiro-Rebolledo et al., 2011). Some studies maintain that incision occurs during wet periods and alluviation in dry periods (Waters and Haynes, 2001;

Hereford, 2002), while others support base level control (i.e., dry periods cause base level to fall and vice versa) (e.g., Haynes, 1968). In other cases, it has been argued that changes in intensity, magnitude and frequency of precipitation regimes can affect arroyo cycles instead of adhering to more general 'wet' and 'dry' terms (Leopold, 1976; Butzer et al., 2008; Huckleberry et al., 2013). Arroyo cycles have been associated with climatic fluctuations on various time scales, such as increasing ENSO intensity during the late Holocene (Waters and Haynes, 2001) and millennial scale fluctuations associated with the strength of the North American Monsoon on a '1,500-year cycle' (Mann and Meltzer, 2007). However, neither study indicates the precise nature of how these large-scale climatic fluctuations would affect flood and sediment characteristics. Rainfall associated with arroyo activity is characterized by high intensity and low duration storms, when much sediment is eroded and transported from the catchment (Poesen et al., 2003; Valentin et al., 2005); however, the present link between climatic drivers, such as ENSO and rain intensity have not been clearly established.

Even though research has shown that gullying is a major contributor to erosion and desertification in drylands, there are still many uncertainties concerning the effects that future land use modifications will have on hydrologic responses for dryland streams (Poesen et al, 2003; Valentin et al., 2005; Sinha et al., 2012). Although the effects of various land use activities on increased soil erosion and sedimentation have been well documented (e.g., Walling, 1999; Wilkinson, 2005b; Walling and Collins, 2008), in many cases the severity and complexity of local erosion are not well understood (Fox et al., 2016). Equally important is the need for more understanding on how prehistoric land use and the accrual of land use over millennia influences gullying. For example, some studies suggest that unsustainable agricultural practices during the prehistoric periods in conjunction with a high population produced high rates of erosion (e.g.,

Melville, 1990; Butzer, 1992, O'Hara et al., 1993). Conversely, other studies have shown that increased erosion was associated with land abandonment following a period of intensively well-managed landscapes sustained by higher populations (e.g., Fisher et al., 2003; Redman, 2005). Some studies on recently abandoned, terraced landscapes support the latter (Lesschen et al., 2009), though conservation efforts have only recently been assessed (Polyavok et al., 2014).

Despite a limited understanding of the effects that climate change has on gullying without human intervention, it has been argued that human activities have more severe impacts on arroyo formation than climate change alone (e.g., Garcia-Ruiz, 2010). Teasing out human intervention and/or climatic processes is very difficult in both the past and the present and confounded by the fact that various climatic drivers can be reflected in similar fluvial responses, or equifinality (Knox, 1993). Attaining a baseline of 'natural' responses of a basin to climatic events is essential before attempting to assess how population fluctuations and land use activities affect landscape response. Furthermore, the majority of research concerning the relationship between land degradation and climate fluctuations concentrates on the last 200 years, neglecting to place this within the context of both long-term climate variability and land use change (Mayewski et al., 2004; Quigley et al., 2011). Deciphering the relationship between climate and arroyo cycles may only be achieved by understanding both long- and short-term climatic fluctuations and landscape response.

Research concerning the connection between human activities, climate change and arroyos falls in line with studies of sediment erosion during the latter part of the 19th century into the early part of the 20th century, many of which were made in the southwestern U.S. (Bryan, 1925; Bull, 1997). For instance, the Langbein-Schumm curve (Langbien and Schumm, 1958) implies that semi-arid environments promote very high sediment yield, due to sufficient rain to

produce runoff, but insufficient rain to promote much vegetation growth (Figure 1.1). Although it is clear that vegetation type and amount interacts with atmospheric and climatic conditions, land use, and local factors to affect erosion (e.g., Abrahams et al., 1994), the relative contribution of vegetation change as compared to extreme events in causing incision and aggradation has been debated in recent studies (e.g., Antinao and McDonald, 2013; Pelletier, 2014). Vegetation change both reflects overarching drivers and interacts with them to influence landscape response. Therefore, incorporating several local and regional paleoclimatic and paleoenvironmental proxies helps avoid equifinality while providing a more complete understanding of land use and climate change.

Studies of process and form in relation to dryland streams have offered insight to aspects of fluvial geomorphology such as hydrology, hydraulics, and channel sediments (Tooth, 2000). Notions of thresholds and equilibrium have been exemplified through research on arroyo incision and aggradation (Schumm and Hadley, 1957; Graf, 1979; Schumm, 1979). Studies on ephemeral streams have shown that they contain a much higher amount of sediment load than perennial counterparts (e.g., Laronne and Reid, 1993; Renard et al., 2008). It has been recognized that much insight on Quaternary stratigraphy may be gained from examining present flood and channel bed deposits to better understand stream behavior (Reid and Frostick, 1987; Reid, 2002; Benvenuti et al., 2005; Billi, 2008). Despite some increased interdisciplinary discussion on applying knowledge of obtained from short-term, process and form relationships in all present dryland stream systems to better understand older sediments (Tooth, 2009), the application toward better understanding the long-term hydrological conditions of the Quaternary still requires attention. Investigations of semi-arid dryland alluvial flood deposits emphasize the more erosive incision phase, while ignoring the aggradation phase (Benvenuti et al., 2005; Jones

et al 2010). This is partially due to the difficulty in contriving generalizations concerning the alluvial sequences, which constitute a number of undated, discrete events (Harvey and Pederson, 2011). More reliance on present process-form relationships between sediment and flow may alleviate these challenges by providing potential interpretations for sedimentary successions.

Conversely, in other areas like Mexico, the emphasis has been on paleosols with less regard for the alluvium (Sedov et al., 2009; Solliero-Rebolledo et al., 2011). Paleosols indicate either local or widespread landscape stability (Benvenuti et al., 2005; Solliero-Rebolledo et al., 2011), but the intricacies of alluvial paleosol formation are often overlooked. Examining the timing and characteristics of alluvial paleosols has the potential to offer valuable information about the paleohydrology and alluvial stratigraphy of dryland stream systems (Aslan and Autin, 1998).

Additionally, examining the effects of climate change on near-surface processes will provide a better understanding of the paleoclimatic fluctuations that affected similar stratigraphy and features in the past (Kochel and Miller, 1997). Reid (2002) suggests that only large changes will modify channel form and behavior in dryland streams, which may apply to some present, dryland streams. Small changes in climate, however, can result in relatively large changes in flood magnitude and frequency (Knox, 1993). Changes in internal dynamics and land use, especially if widespread, may also produce threshold-crossing changes in dryland stream behavior in conjunction with climate change.

1.3 Summary

Contradictory hypotheses concerning arroyo formation still endure because more studies on paleosol-alluvium sequences are needed to connect paleoclimate drivers and paleohydrologic

responses before evaluating widespread land use change. In addition, more fluvial geomorphological studies need to evaluate paleoenvironmental and paleoclimatic data against paleosol-alluvial sequences. Our incomplete understanding of the natural variability of flood characteristics and sediment yield in drylands is both due to the inadequate application of present climate-hydrologic relationships to interpreting past alluvium as well as the lack of a long-term perspective needed to more fully understand present systems. Finally, more research is needed to understand the relationship between climate fluctuations, land use change and hydrologic responses over the *longue durée* in order to untangle the interaction between desertification, climate, and land use change in prehistoric to recent times. This dissertation seeks to contribute to a better understanding of these complex issues.

1.4 References

Abrahams, A.D., Parsons, A.J., Wainwright, J., 1994. Resistance to Overland-Flow on Semiarid Grassland and Shrubland Hillslopes, Walnut Gulch, Southern Arizona. Journal of Hydrology 156, 431-446.

Annan, K., 2006. Protecting Drylands, Preventing Poverty, Deserts and Desertification: Don't Desert Drylands! Message of United Nations Secretary General, United Nations Environment Programme Report, World Environment Day, http://www.unep.org/ - wed/2006/downloads.PDF/WED2006Booklet_en.pdf. Last accessed January, 2015.

Antinao, J.L., McDonald, E., 2013. A reduced relevance of vegetation change for alluvial aggradation in arid zones. Geology 41, 11-14.

Aslan, A., Autin, W.J., 1998. Holocene flood-plain soil formation in the southern lower Mississippi Valley: Implications for interpreting alluvial paleosols. Geological Society of America Bulletin 110, 433-449.

Avni, Y., 2005. Gully incision as a key factor in desertification in an and environment, the Negev highlands, Israel. Catena 63, 185-220.

Benito, G., M. Rico, Y. Sanchez-Moya, A. Sopena, V. R. Thorndycraft, Barriendos, M., 2010.

The impact of late Holocene climatic variability and land use change on the flood hydrology of the Guadalentin River, southeast Spain. Global and Planetary Change, 70, 53-63.

Billi, P., 2008. Bedforms and sediment transport processes in the ephemeral streams of Kobo basin, Northern Ethiopia. Catena 75, 5-17.

Boardman, J., Foster, I., Rowntree, K., Mighall, T., Gates, J., 2010. Environmental Stress and Landscape Recovery in a Semi-Arid Area, The Karoo, South Africa. Scottish Geographical Journal 126, 64-75.

Borejsza, A., I. R. Lopez, C. D. Frederick, Bateman, M. D., 2008. Agricultural slope management and soil erosion at La Laguna, Tlaxcala, Mexico. Journal of Archaeological Science, 35, 1854-1866.

Bryan, K., 1925. Date of Channel Trenching (Arroyo Cutting) in the Arid Southwest. Science (New York, N.Y.) 62, 338-344.

Bull, W.B., 1991. Geomorphic Responses to Climate Change. Oxford University Press, Oxford.

Bull, W.B., 1997. Discontinuous ephemeral streams. Geomorphology 19, 227-276.

Bull, L.J., Kirkby, M.J., 2002. Dryland River Characteristics and Concepts, in: Bull, L., J., Kirkby, M. J. (Ed.), Dryland Rivers: Hydrology and Geomorphology of Semi-Arid Channels. John Wiley & Sons Ltd., West Sussex.

Butzer, K.W., 1992. The America Before and After 1492 – An Introduction to Current Geographical Research. Annals of the Association of American Geographers 82, 345-368.

Butzer, K.W., Abbott, J.T., Frederick, C.D., Lehman, P.H., Cordova, C.E., Oswald, J.F., 2008. Soil-geomorphology and "wet" cycles in the Holocene record of North-Central Mexico. Geomorphology 101, 237-277.

Denevan, W.M., 1992. The pristine myth: the landscape of the Americas in 1492. Annals of the Association of American Geographers 82, 369-385.

Dregne, H. E., 2002. Land degradation in the drylands. Arid Land Research and Management, 16, 99-132.

Fisher, C. T., H. P. Pollard, I. Israde-Alcantara, V. H. Garduno-Monroy, Banerjee, S. K., 2003. A reexamination of human-induced environmental change within the Lake Patzcuaro Basin, Michoacan, Mexico. Proceedings of the National Academy of Sciences of the United States of America, 100, 4957-4962.

Fox, G.A., Sheshukov, A., Cruse, R., Kolar, R.L., Guertault, L., Gesch, K.R., Dutnell, R.C.,

2016. Reservoir Sedimentation and Upstream Sediment Sources: Perspectives and Future Research Needs on Streambank and Gully Erosion. Environmental Management 57, 945-955.

García-Ruiz, J. M., 2010. The effects of land uses on soil erosion in Spain: A review. Catena, 81, 1-11.

Gellis, A.C., Pavich, M.J., Bierman, P.R., Clapp, E.M., Ellevein, A., Aby, S., 2004. Modern sediment yield compared to geologic rates of sediment production in a semi-arid basin, New Mexico: Assessing the human impact. Earth Surface Processes and Landforms 29, 1359-1372.

Graf, W., 1979. The Development of Montane Arroyos and Gullies. Earth Surface Processes and Landforms 4, 1-14.

Giurma, I., C. R. Giurma-Handley, I. Craciun, Antohi, C. M., 2008. Global Dimming- An Environmental Hypothesis on Climate Change. Environmental Engineering and Management Journal, 7, 417-421.

Goudie, A. S., 2013. Arid and Semi-Arid Geomorphology. Cambridge: University of Cambridge Press.

Harvey, J.E., Pederson, J.L., 2011. Reconciling arroyo cycle and paleoflood approaches to late Holocene alluvial records in dryland streams. Quaternary Science Reviews 30, 855-866.

Haynes, C.V., Jr., 1968. Geochronology of late-Quaternary alluvium, in R.B. Morrison & H.E. Wright, Jr. (Eds.), Means of correlation of Quaternary successions, 591–631, Salt Lake City: University of Utah Press.

Hereford, R., 2002. Valley-fill alluviation during the Little Ice Age (ca. AD 1400-1880), Paria River basin and southern Colorado Plateau, United States. Geological Society of America Bulletin 114, 1550-1563.

Huckleberry, G., Duff, A.I., 2008. Alluvial cycles, climate, and puebloan settlement shifts near Zuni Salt Lake, New Mexico, USA. Geoarchaeology-an International Journal 23, 107-130.

Huckleberry, G., J. Onken, W. M. Graves, Wegener, R., 2013. Climatic, geomorphic, and archaeological implications of a late Quaternary alluvial chronology for the lower Salt River, Arizona, USA. Geomorphology, 185, 39-53.

Jansson, M.B., 1988. A Global Survey of Sediment Yield. Geografiska Annaler Series a-Physical Geography 70, 81-98.

Jones, L. S., M. Rosenburg, M. D. Figueroa, K. McKee, B. Haravitch, Hunter, J., 2010.

Holocene valley-floor deposition and incision in a small drainage basin in western Colorado, USA. Quaternary Research, 74, 199-206.

Karl, T. R., Trenberth, K. E., 2003. Modern global climate change. Science, 302, 1719-1723.

Knox, J.C., 1993. Large Increases in Flood Magnitude in Response to Modest Changes in Climate. Nature 361, 430-432.

Knox, J. C., 2001. Agricultural influence on landscape sensitivity in the Upper Mississippi River Valley. Catena, 42, 193-224.

Kochel, R. C., Miller, J. R., 1997. Geomorphic responses to short-term climatic change: An introduction. Geomorphology, 19, 171-173.

Langbein, W.B., Schumm, S.A., 1958. Yield of sediment in relation to mean annual precipitation. Trans Amer Geophys Union 39, 1076-1084.

Laronne, J.B., Reid, I., 1993. Very High-Rates of Bedload Sediment Transport by Ephemeral Desert Rivers. Nature 366, 148-150.

Lesschen, J. P., J. M. Schoorl, Cammeraat, L. H., 2009. Modelling runoff and erosion for a semi-arid catchment using a multi-scale approach based on hydrological connectivity. Geomorphology, 109, 174-183.

Leopold, L. B., 1976. Reversal of Erosion Cycle and Climatic Change. Quaternary Research, 6, 557-562.

Mann, D.H., Meltzer, D.J., 2007. Millennial-scale dynamics of valley fills over the past 12,000 C-14 yr in northeastern New Mexico, USA. Geological Society of America Bulletin 119, 1433-1448.

Mayewski P.A., E.E. Rohling, J.C. Stager, K. Wibjörn, K. A. Maasch, L. D. Meeker, E. A. Meyerson, F. Gasse, S. van Kreveld, K. Holmgren, J. Lee-Thorp, G. Rosqvist, F. Rack, M. Staubwasser, R. R. Schneider, Steig, E. J., 2004. Holocene climate variability. Quaternary Research, 62, 243-255.

McAuliffe, J.R., Sundt, P.C., Valiente-Banuet, A., Casas, A., Viveros, J.L., 2001. Pre-columbian soil erosion, persistent ecological changes, and collapse of a subsistence agricultural economy in the semi-arid Tehuacan Valley, Mexico's 'Cradle of Maize'. Journal of Arid Environments 47, 47-75.

McFadden, L.D., McAuliffe, J.R., 1997. Lithologically influenced geomorphic responses to Holocene climatic changes in the Southern Colorado Plateau, Arizona: A soil-geomorphic and ecologic perspective. Geomorphology 19, 303-332.

Melville, E. G. K., 1990. Environmental and Social-Change in the Valle-del-Mezquital, Mexico,

1521-1600. Comparative Studies in Society and History, 32, 24-53.

O'Hara, S.L., Street-Perrott, F.A., Burt, T.P., 1993. Accelerated soil erosion around a Mexican highland lake caused by prehispanic agriculture. Nature 362, 48-51.

Pelletier, J.D., 2014. The linkages among hillslope-vegetation changes, elevation, and the timing of late-Quaternary fluvial-system aggradation in the Mojave Desert revisited. Earth Surface Dynamics 2, 455-468.

Poesen, J., Nachtergaele, J., Verstraeten, G., Valentin, C., 2003. Gully erosion and environmental change: importance and research needs. Catena 50, 91-133.

Polyakov, V.O., Nichols, M.H., McClaran, M.P., Nearing, M.A., 2014. Effect of check dams on runoff, sediment yield, and retention on small semiarid watersheds. Journal of Soil and Water Conservation 69, 414-421.

Quigley, M. C., T. Horton, J. C. Hellstrom, M. L. Cupper, Sandiford, M. 2010. Holocene climate change in arid Australia from speleothem and alluvial records. Holocene, 20, 1093-1104.

Redman, C. L., 2005. Resilience theory in archaeology. American Anthropologist, 107, 70-77.

Reid, I., 2002. Sediment Dynamics of Ephemeral Channels, in: Bull, L.J., Kirkby, M.J. (Eds.), Dryland Rivers: Hydrology and Geomorphology of Semi-Arid Channels. John Wiley & Sons Ltd., Wests Sussex.

Reid, I., Frostick, L.E., 1987. Flow Dynamics and Suspended Sediment Properties in Arid Zone Flash Dynamics and Suspended Sediment Properties in Arid Zone Flash Floods. Hydrological Processes 1, 239-253.

Renard, K.G., Nichols, M.H., Woolhiser, D.A., Osborn, H.B., 2008. A brief background on the U.S. Department of Agriculture - Agricultural Research Service Walnut Gulch Experimental Watershed. Water Resources Research 44.

Schumm, S.A., Hadley, R.F., 1957. Arroyos and the Semiarid Cycle of Erosion. American Journal of Science 255, 161-174.

Schumm, S. A. (1979) Geomorphic Thresholds - Concept and Its Applications. Transactions of the Institute of British Geographers, 4, 485-515.

Sedov, S., Solleiro-Rebolledo, E., Terhorst, B., Sole, J., Flores-Delgadillo, M.D., Werner, G., Poetsch, T., 2009. The Tlaxcala basin paleosol sequence: a multiscale proxy of middle to late Quaternary environmental change in central Mexico. Revista Mexicana De Ciencias Geologicas 26, 448-465.

Sinha, R., Latrubesse, E.M., Nanson, G.C., 2012. Quaternary fluvial systems of tropics: Major

issues and status of research. Palaeogeography Palaeoclimatology Palaeoecology 356,1-15.

Sivakumar, M. V. K., 2007. Interactions between climate and desertification. Agricultural and Forest Meteorology, 142, 143-155.

Solleiro-Rebolledo, E., Sycheva, S., Sedov, S., McClung de Tapia, E., Rivera-Uria, Y., Salcido-Berkovich, C., Kuznetsova, A., 2011. Fluvial processes and paleopedogenesis in the Teotihuacan Valley, Mexico: Responses to late Quaternary environmental changes. Quaternary International 233, 40-52.

Svoray, T., Markovitch, H., 2009. Catchment scale analysis of the effect of topography, tillage direction and unpaved roads on ephemeral gully incision. Earth Surface Processes and Landforms 34, 1970-1984.

Tooth, S., 2000. Process, form and change in dryland rivers: a review of recent research. Earth-Science Reviews 51, 67-107.

UN, 2011. Global Drylands: A UN system-wide response. United Nations Environmental Management Group.

Valentin, C., Poesen, J., Li, Y., 2005. Gully erosion: Impacts, factors and control. Catena 63, 132-153.

Walling, D.E., 1999. Linking land use, erosion and sediment yields in river basins. Hydrobiologia 410, 223-240.

Walling, D.E., Collins, A.L., 2008. The catchment sediment budget as a management tool. Environmental Science & Policy 11, 136-143.

Waters, M.R., Haynes, C.V., 2001. Late Quaternary arroyo formation and climate change in the American Southwest. Geology 29, 399-402.

Waters, M.R., Ravesloot, J.C., 2001. Landscape change and the cultural evolution of the Hohokam along the middle Gila River and other river valleys in south-central Arizona. American Antiquity 66, 285-299.

Wilkinson, T.J., 2005a. Soil erosion and valley fills in the Yemen highlands and southern Turkey: Integrating settlement, geoarchaeology, and climate change. Geoarchaeology- an International Journal 20, 169-192.

Wilkinson, B.H., 2005b. Humans as geologic agents: A deep-time perspective. Geology 33, 161-164.

Table 1.1. Characteristics of Drylands. Drylands are subdivided into various environments based on their aridity index. The aridity inex is the ratio between average annual precipitation and annual potential evapotranspiration (AAP/APE – Aridity Index) (information from UN Report, 2011; Goudie, 2013).

Environment	Aridity Index	Typical Average Annual Precipitation Range	Examples of Associated Biome(s)
Hyper-arid	<0.05	<150 mm	Desert
Arid	0.05-0.2	150 – 300 mm	Desert-like steppe
Semi-arid	0.2-0.5	300 – 600 mm	Grassland, Savannah, Steppe
Dry sub-humid	0.5-0.65	600 - 800 mm	Dry Forest

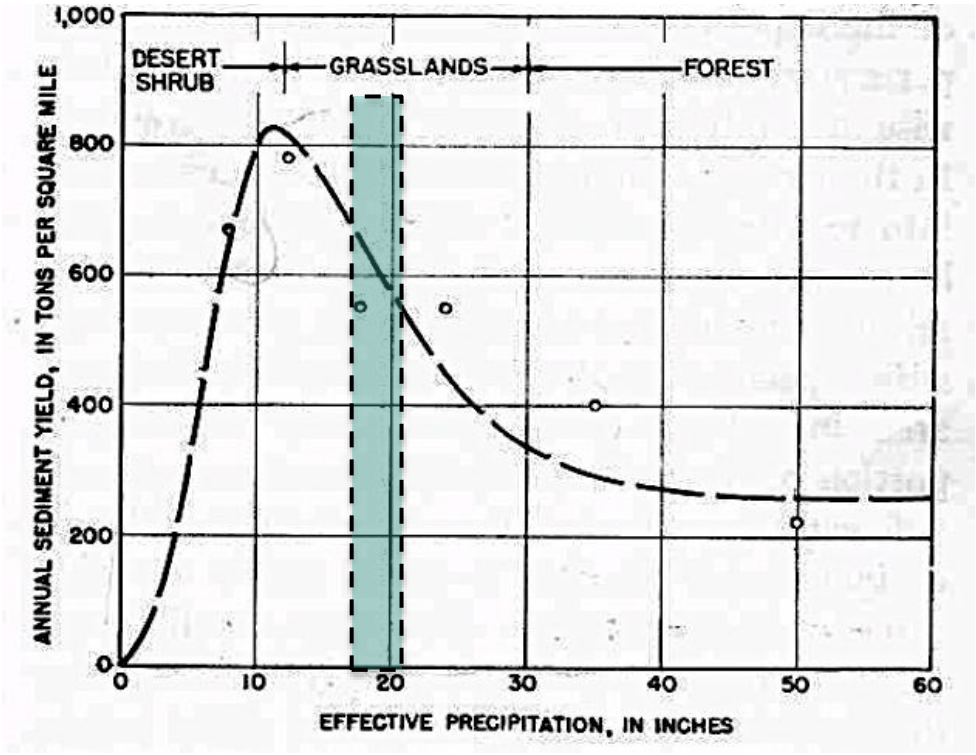

Figure 1.1. The Langbein-Schumm curve. The highlighted area represents the approximate range of effective precipitation in which the Mixteca Alta lies (modified from Langbein and Schumm, 1958).

CHAPTER 2

GEOMORPHIC CHARACTERISTICS AND BEDLOAD YIELD ESTIMATES OF A DRYLAND EPHEMERAL STREAM IN SOUTHWESTERN MEXICO[1]

[1] Holdridge, G. A. and Leigh, D. S. To be submitted to the *International Journal of Sediment Research*.

Abstract

Semi-arid dryland streams are known for their very high sediment loads, in particular high bedload yields, resulting from widespread sediment availability and efficient transport. Intense and sporadic rainfall, sparse vegetation cover, erodible geology, and land use change contribute to land degradation. Semi-arid environments are especially vulnerable to widespread erosion. Local communities and governmental agencies attempt to control gullying and arroyo formation by applying various conservation strategies, including check dams. The effectiveness of check dams on downstream sediment yield and geomorphology is still relatively unclear. The dryland fluvial system of the Río Culebra watershed, located in the semi-arid region of the Mixteca Alta, southwestern Mexico, was examined to better understand the present-day sediment yield and check dam effectiveness, and to provide context for past sediment yield. It also offered information concerning prehistoric agricultural landscape management.

A general survey of the watershed was undertaken to evaluate the processes and morphology characterizing the present dryland stream system. A more in-depth study was made on two tributary arroyos to the Culebra to estimate bedload yield and to gain a better understanding of erosion in the region, as well as community efforts to reduce soil erosion. One of the tributary arroyos, Barranca Sandage, contains soil conservation structures in the headwaters that included modern construction of several sediment check dams. The other arroyo, Barranca Sauce, is poorly managed and contains a high proportion of bare ground land cover.

The geomorphic survey suggests that the entire watershed is undergoing internal adjustments or complex response from legacy and recent land use impacts. Conservative bedload yield estimates suggest that even with headwater conservation, the yield is still relatively

high, even during low flow conditions. Continued high bedload yield points to the need for larger scale conservation efforts. The arroyo with more bare ground indicates that transmission loss is also important and influences the bedload yield. Based on conservative estimates of modern daily bedload yield of 17 tonnes in Barranca Sandage and 45 tonnes in Barranca Sauce, the time it would take to fill ancient and modern check dams was calculated to be 23 and 249 years, respectively. The modern bedload sediment yield is at least 4.6 times greater than the prehistoric sediment yield during the late Holocene, based on modeled sedimentation rates associated with the ancient lama-bordos. The examination of present-day processes and forms also offered insight to understanding and interpreting the alluvium-paleosol stratigraphy. Present channel bed stratigraphy associated with scour-and-fill consists of poorly sorted, massive, sandy gravel deposits. Finer bedded sediments are observed in the present patchy floodplain deposits, but are susceptible to erosion. In contrast, the Quaternary stratigraphy is dominated by extensive fine sediment deposits, having bedding and laminations, while coarser, massive strata are observed, but to a lesser extent. The less prevalent coarser strata are analogous to present-day flash floods deposits, whereas the prevalent finer sediments indicates a different flood regime that allowed for the deposition of finer sediments and construction of a more expansive floodplain.

2.1 Introduction and Objectives

Drylands encompass about 40% of global land cover, including hyperarid to sub-humid climate systems. The United Nations (UN) defines drylands as regions that have an aridity index of <0.65 (UN Report, 2011), though the focus here will be on warm, semi-arid drylands (as in Tooth, 2000), in particular the fluvial and dryland geomorphology of the semi-arid environment of the Mixteca Alta, Oaxaca, Mexico. Dryland rivers or streams range from perennial, such as exotic or spring-fed rivers, to ephemeral streams that only flood when it rains. Gullies and arroyos are incised channels, and characterized as either discontinuous (e.g., Bull, 1997) or continuous (e.g., Billi and Dramis, 2003).

Dryland streams, especially in semi-arid environments are known for their high sediment yield (Alexandrov et al., 2009; Langbein and Schumm, 1948), and in particular for their high bedload yield (Laronne and Reid, 1993). Although base level and tectonics are important for driving changes in fluvial systems, human impacts and climate change are considered the primary causes of the high sediment yield and erosion associated with gullying (Byran, 1925; Leopold et al., 1966; Tooth, 2000; Waters and Haynes, 2001; Bull and Kirkby, 2002). Human activities and climate change can result in land degradation, which has already occurred in 10% of all drylands worldwide. Degradation involves soil erosion, water scarcity, reduction of biological activity, all of which negatively impact dryland ecosystems and human populations (UN Report, 2011). Consequently, local communities and governmental agencies have implemented land management techniques to reduce sediment yield and to improve water retention, including the construction of check dams. However, the effectiveness of these check dams depend on how they are constructed and how they relate to the overarching conservation

strategy. Their efficiency has only recently been assessed (Castillo et al., 2014; Polyakov et al., 2014; Zema et al., 2014).

Objectives: This research concerns incised dryland streams in the Río Culebra watershed, situated in the semi-arid environment of the Mixteca Alta, Oaxaca, Mexico (Figure 2.1). The main objective is to examine how the use of check dams in the headwaters of a small watershed impacts the bedload yield and geomorphology downstream. Two related aims will also be examined, listed as follows: 1) to explore the processes and features of the present fluvial system; 2) to use the characterstics of the present system to better understand the sedimentology and paleohydrology of arroyo systems throughout the Holocene (related to subsequent chapters in this dissertation). To begin, a brief overview will be presented concerning dryland streams, including arroyos, as well as conservation measures to preserve sediment and water by using check dams.

2.1.1 Background

Terminology in relation to dryland streams varies considerably, which is partially due to the variations in similar landforms in different drylands (Tooth, 2000). Here the term dryland stream will refer to any channel resulting from water flow that exists in a semi-arid dryland, except when stated otherwise (e.g., all dryland streams denotes the full range of hyperarid to subhumid dryland streams). This includes: arroyos, gullies; perennial (e.g., exotic and spring-fed), intermittent, ephemeral, continuous, discontinuous, incised, and aggrading channels. Studies distinguish discontinuous ephemeral streams (Bull, 1997), also referred to as arroyos, gullies, ephemeral gullies, and slope gullies on hillslopes from continuous ephemeral streams, also designated as stream gullies, which are essentially an established river system (Leopold et al., 1964; Billi and Dramis, 2003; Wakelin-King and Webb, 2007). The term arroyo has been

used to refer to discontinuous or continuous incised channels, which have a cyclical nature of incision and aggradation (Hereford, 1987; Bull, 1997). Arroyo has also been used interchangeably with gully (e.g., DeLong et al., 2014). However, the term gully has been used to describe headwater or smaller discontinuous incised channels (Poesen et al., 2003). Distinguishing gullies, arroyos and ephemeral streams is very unclear in the literature, but it appears to follow a continuum (Poesen et al., 2003). Most studies of dryland streams have been made on small, steep ephemeral channels in the southwestern U.S. and the Mediterranean, which do not completely reflect the wide range of forms that all dryland streams exhibit (Nanson et al., 2002). The dryland streams in southwestern Mexico are incised, continuous, and have channels with both ephemeral and perennial flow. In this paper, arroyos and gullies are terms that will be used interchangeably to denote an incised, continuous channel.

2.1.1.1 Sediment Yield

The Langbein-Schumm curve (Langbein and Schumm, 1958) demonstrates the relationship between high sediment yield and semi-arid landscapes. Low, but sufficient precipitation results in both reduced vegetation cover and increased erosion and transportation of sediment and soil. Although the Langbien-Schumm curve has been criticized for oversimplifying the complexities of global erosion (Walling and Kleo, 1979; Jansson, 1988), there is still a large amount of suspended and bedload sediment mobilized in dryland streams (Nanson et al., 2002). Recent studies have corroborated the high sediment yields in semi-arid ephemeral streams, which involve bedload sediment transport of up to 400 times more than perennial stream *equivalents* (Laronne and Reid, 1993, Reid and Laronne, 1995), and suspended sediment concentrations that are orders of magnitude higher than perennial counterparts in humid and temperate environments (Alexandrov et al., 2009). In particular, it is the high bedload

transport efficiency under moderate boundary shear stress that makes dryland streams so remarkable (Laronne and Reid, 1993; Reid et al., 1998; Cohen et al., 2010). Gullies are extremely efficient at transporting runoff and sediment from hillslopes to more permanent channels, resulting in the removal of sediments and soils and contributing to high sediment yields, especially in drier environments (Poesen et al., 2003; de Vente et al., 2005).

Although dryland streams fall into the continuum of the general fluvial system, they appear to have some defining traits making it useful to examine them as a subset to better understand them (Bull and Kirkby, 2002, Nanson et al., 2002). One of the main differences between perennial and ephemeral bedload transport rates is the lack of an armour layer in the latter (Schick et al., 1987; Laronne et al., 1994). The absence of an armour layer is due to the abundant sediment supply in drylands, whereas armouring occurs when sediment supply is reduced (see Dietrich et al., 1989; Reid, 2002). Perennial flow may also winnow away fine material resulting in armouring of the bed (Reid and Frostick, 1987). Transmission losses are another major difference between perennial streams and ephemeral channels, whereby water infiltrates the dry, permeable channel bed and banks resulting in reduction of streamflow and sediment downstream (Bull, 1991; Shannon et al., 2002). Recharge through dry channel alluvium can contribute to basin-wide/groundwater recharge in wet years, as much of the water infiltrated into hillslopes is lost via evapotranspiration (Renard et al., 2008).

Other traits considered distinctive of drylands and their streams include rainfall variability, vegetation cover (type and amount), flow and flood type, all of which help explain the high sediment yield observed (Bull and Kirkby, 2002). For example, high rainfall intensity and variability characterize many drylands, including the Mixteca Alta, and result in high run-off and erosion, especially with regard to gully formation (Leopold et al., 1964; Graf, 2002; Gellis et

al., 2004). Osborn et al., (1979) showed that rain variability varies rapidly in a short distance (starting at approximately 1-2 km) for convective storms, as they cover small areas. A study in Israel (Alexandrov et al., 2007) concluded that convective storms typically had high intensity rainfall shown to produce high-suspended sediment concentrations in relatively low water discharge. In contrast, frontal storms had lower intensity and longer duration precipitation, resulting in lower suspended sediment concentrations in relatively higher water discharge. Vegetation and climate are intimately linked and various studies show that a low amount of vegetation cover leaves soil vulnerable to raindrop impact (Abrahams et al., 1994; Parsons et al., 1996).

Dryland systems are sensitive and vulnerable to climatic change and human perturbations (Reid, 2002). Research on sediment load, especially bedload, has been hindered due to the intermittent nature of floods and the enormous resources needed to study ephemeral channels. For example, a number of long-term studies on sediment load and flow in perennial streams have continued for more than a century. A few long-term studies exist for ephemeral dryland streams, including the Walnut Gulch in the southwestern U.S., examined since 1953 (Renard et al., 2008), but it does not include bedload. The longest continuous studies of dryland streams that include bedload span 15 (Alexandrov et al., 2009) and 10 years (Cohen et al., 2010), both located in Israel. Bedload transport studies include several semi-automatic monitoring (e.g. Laronne et al., 1992) and fully automatic systems (e.g. Reid et al., 1980).

Check dams are built in ephemeral channels to control water flow, conserve soil, and reduce land degradation by increasing sediment deposition, reducing bed gradient and flow velocity, and are deemed more beneficial when employed over a large area (Romero Diaz et al., 2007; Castillo et al., 2014). Though, it is unclear how effective they are in promoting long-term

landscape stability (Polyakov et al., 2014; Zema et al., 2014) and they have proved both detrimental (Marden et al., 2005) and valuable (Huang et al., 2003; Molina et al., 2008) at a basin-wide scale. Even well designed check dam implementations require long-term management that is costly and laborious to achieve (Boix-Fayos et al., 2008; Grimaldi et al., 2015). Ineffectiveness can result from filling rapidly, piping, and bypassing around the dams causing failures (Nyssen et al., 2004; Polyakov et al., 2014). Scouring downstream can also be a problem (Conesa-Garcia et al., 2007; Romero-Diaz et al., 2012; Castillo et al., 2014).

Few studies (e.g., Polyakov et al., 2014) have examined the downstream sediment yield of check dam constructions in dryland regions. Instead, much research has focused on the effects of bigger dams in perennial streams. More studies are needed on check dams in ephemeral streams (Conesa-Garcia et al., 2007; Zema et al., 2014).

2.2 Study Area

Investigations were conducted in the semi-arid dryland stream system of the Río Culebra watershed located in the municipalities of San Jan Bautista Coixtlahuaca and Santa María Nativitas (17° 43'N, 97° 19'W and 17° 39'N, 97° 20'W, respectively) (Figure 2.1). The Culebra watershed is located in the Mixteca Alta, Oaxaca, Mexico, which is situated about 2300 m amsl (above mean sea level). The Mixteca Alta is a physio-cultural name corresponding to the Mixtec culture and the high altitude ("Alta") (Balkansky et al., 2000) of the Sierra Mixteca. The Sierra Mixteca forms part of the Sierra Madre del Sur mountain range. The region is characterized as a semi-arid climatic regime (BSh Köppen classification), averaging around 528 mm of rain per year. The average annual temperature ranges between 13.2-18.6 ºC (Servicio Meteorologico

Nacional, 2010). The warmest time of the year overlaps with the rainy season, which spans May through October, with peaks in June and September.

The geology of the watershed primarily consists of lower to middle Tertiary siltstones and claystones (shales) referred to as the Yanhuitlan Formation, which were once lakebeds (Santamaria-Diaz et al., 2008). Overlying these beds in places are middle Tertiary volcaniclastics (Teotongo Volcaniclastics) and andesites (Cañada Maria Andesite and Yucudaac Andesite) (Santamaria-Diaz et al., 2008). Gypsum has precipitated in the jointed and fractured Yanhuitlan beds in places, most likely in association with the volcanic activity in the area, and was subsequently affected by groundwater fluctuations. Quaternary alluvium fills most of the valleys, while many hillslopes contain exposed calcrete surfaces (locally referred to as "endeque") and Yanhuitlan beds (Kirkby 1972, Rincon 1999, Leigh et al., 2013). Buried calcrete horizons were observed underlying alluvial fills in some valleys, indicating great antiquity to these pedogenic horizons.

The Río Culebra watershed (~84 km^2) is an incised spring-fed stream flowing from two sources located along the hillslope of the nearby extinct volcano, Monte Verde, Nativitas. The Río Culebra and its ephemeral, incised tributaries form a continuous dryland stream system. This watershed falls within the Biosphere Reserve of Tehuacán-Cuicatlán, one of the most biodiverse places in the world (UNESCO, 2016). It also has a rich cultural history of agriculture and land management (Kowalewsky et al., 2009; Leigh et al., 2013). However, this watershed is highly degraded, such that the National Park Service of Mexico (Comisión Nacional de Áreas Naturales Protegidas, CONANP) and local communities have implemented conservation measures for soil, vegetation, and water resources. However, conservation efforts can be

expensive and time consuming to apply, given that they need to be maintained and require much local labor and time.

The bedload yield of two small tributary watersheds (~4 km^2) to the Culebra, Barrancas Sandage and Sauce was examined between 2013-2014 (Figures 2.1 and 2.2). Barranca Sandage is located in Coixtlahuaca, while Barranca Sauce is situated in the town of Nativitas. The headwaters of Barranca Sandage have been conserved using various techniques including ridge-and-channel terracing, retention ponds, reforestation, and check dams. The check dams, locally known as lama-bordos, include ancient and modern structures in the headwaters of Sandage. The modern structures were built by Bladimir Victor Garcia Lara and his employees, and involved filling the arroyo with old tires and covering them with sediment (these are denoted from hereon as Victor's lama-bordos or VLB for short) (Figure 2.3). The ancient lama-bordos that are intact in the headwaters retain earth behind them and continue as terraces (Figure 2.4), an observation made by Mr. Garcia Lara (Garcia Lara, Pers. Com) and confirmed in a field survey. The conservation efforts in Sandage comprise ~57% of the total watershed area. Barranca Sauce is not managed and ~45% of the total area is bare ground, calcrete and gullied (Table 2.1). Since Barranca Sauce is analogous to Sandage in geology, drainage area, and slope, but differs in land cover, it serves as a good baseline for erosion studies in the Culebra watershed.

2.3 Methods

2.3.1 Geomorphological Survey

The geomorphology of the Río Culebra watershed was explored via an extensive walking survey. Important features such as knickpoints, faulting, and evidence of mass wasting were described and recorded, including GPS waypoints and pictures. Geology and its relation to the

different features were also noted. In addition, other channel bed characteristics were examined for indication of flow conditions and channel form including bed topography, particle size, and material types.

2.3.2 Land Cover

The percentages of land cover (Table 2.1) in Sandage and Sauce were calculated from a land cover map generated in ArcGIS (Esri Software). Land cover classification was made on RGB composites 321 and 432 for Landsat 7 (LE70250482003146EDC00) (USGS, 2011) using a combination of supervised and unsupervised classification techniques. The survey also involved confirming or determining the "ground truth" of different land covers points, with high success, though the resolution of the imagery was fairly low (30 m side on square pixels).

2.3.3 Basin Outlet Measuring Stations

To obtain an estimate of the bedload yield of Barrancas Sandage and Sauce, a monitoring station was set up at the outlet of each watershed (Figures 2.5 and 2.6). Each station consisted of one meander bend leading into an elongated straightaway, at the end of which was placed the measuring station. The stations contained the following: two peak stage recorders, two to four scouring chains, two to five pit traps, electronic stage recorder (stream gauge), one metal staff gauge, and a reference cable. A total of 14 floods were examined in Sandage, while 13 were examined in Sauce.

2.3.3.1 Stream Gauges

Odyssey Capacitance Water Level Probes, electronic stage recorders that are one meter in length, were used to log variations in water levels. They were encased in a PVC tube with a cap, and linked to a metal tube where the water enters during floods (see Figure 2.5). A fine mesh screen was placed in the channel end of the metal tube to block sand-sized and larger particles

from entering, though mud was always trapped within the tube after each flood, which required cleaning after each storm. Due to sedimentation, the Odyssey stage recorders were fairly unreliable, and much of the detailed information on water level was not possible to record.

A metal stake near the stream gauge served as a staff gauge and was marked every 10 cm (white paint) and 25 cm (black electrical tape). It was used to directly estimate depth during floods. A leveled string was attached to a small metal stake as a reference to make standardized cross-section measurements after each flood. A line level was used when stretching the string across the stream to ensure it was level.

2.3.3.2 Peak Stage Recorders and Scouring Chains

The peak stage recorders (PSRs) consist of a metal stake, hammered about one meter into the ground, and a PVC tube attached to the downstream side of the stake with plastic ties. Tiny slits were cut into the bottom five centimeters of the PVC to allow water to enter. Coffee grains were poured into the top of the PVC in between each flood and then the PVC was covered with a fitted cap. The PSRs offered a backup and in most cases the only reliable information concerning the peak flood depth. The PSRs were placed at 3.50 m and 30 m upstream from the monitoring station in Barranca Sandage, and 4.70 m and 47 m upstream from the station in Barranca Sauce.

Scouring chains measuring 50 cm long were vertically buried into the arroyo beds of each watershed, with the tip of each chain flush with the arroyo bed surface. In Sandage, the chains were interred 9 and 18 m upstream from the monitoring station, while in Sauce the chains were buried at 16, 28, and 36 m from the monitoring station. A small metal stake was placed 1 m high on the channel bank with a string attached, which measured the distance to the buried chain in

order to relocate them. Another chain was added in each barranca in 2014: one at 27 m in Sandage, and one at 9 m in Sauce.

2.3.3.3 Pit traps

Two pit traps were placed in Sandage and five pit traps were placed in Sauce in 2013. In 2014 another trap was added in Sandage, while five more traps were added in Sauce (See Figures 2.5 and 2.6). They are a modified version of the *Birkbeck* samplers (Reid et al., 1980, Reid et al., 1995), which are pit traps with covers and slots, set side-by-side in the stream bed at a designated cross-section of the monitoring station. Beneath the original *Birkbeck* pit traps were pressure pillows, which were connected to pressure transducers that offer the submerged weight of the accumulated sediment for each pit trap (Reid et al., 1980; Reid et al., 1995), but our pit traps lack pressure transducers.

In 2013, the pit traps were all the same size, 0.24 m^3 (0.80 m long, 0.50 m wide, and 0.60 m deep), while in 2014, larger pit traps were added 0.48 m^3 (0.80 m long, 0.80 m wide and 0.75 m deep). The pit traps were spaced at about 70 cm apart in Sandage, and 1.50 m apart in Sauce in 2013, while spacing was reduced to 20 cm in between pit traps in 2014. Each pit trap had a cover with a slot that could be opened up to 50 cm wide. The cover and slot allows one to better assess the passage of bedload over the duration of the flow, as it is deposited into the traps in succession instead of in masses (Reid et al., 1980; Reid et al., 1995). Since these were not automatic samplers, there was a finite amount of sediment flux data that was measured. The length of the slot of the samplers in Sandage and Sauce are 0.50 m, an approximation of 66 times the D_{50} and 200 times the D_{16} immediately upstream from the samplers (as recommended in Reid et al., 1995).

The sediments were removed from the pit traps by shoveling them out in layers, placing them into a 20 L bucket, and weighing them on a scale until each pit trap was empty. The sediments were sub-sampled from the traps before removal, and during extraction of successive layers. The procedure for subsampling the contents of each trap during the flood season of 2013 involved taking three 1- 2 kg samples at 15 cm depth intervals, in the upstream, middle and downstream part of the traps, which resulted in about 15- 20 kg sampled from each trap. In 2014, a <1 kg sample was obtained every seven to ten centimeters in the upstream, middle and downstream part of each trap, resulting in 21-30 kg from each. All of the sub-sampled sediments were dried and sieved for particle size characterization of sand and smaller particles, gravel, and boulders, based on U.S. sieve size series ranging from <2 mm to 64 mm at whole phi intervals (2, 4, 8, 16, 32, 64 mm). The weight of particles was recorded according to sieve size and then converted to percent based on the total weight (Appendix I).

2.3.4 Channel Bed Particle Size Analysis

Channel bed particle sizes in Barrancas Sandage and Sauce were determined by pebble counts that followed a combination of methods derived from several studies (i.e., Bunte and Abt 2001; Kondolf et al., 2002a; Gordon et al., 2004; Bunte et al., 2009). The sampled reach was a pre-defined length measuring 20 times the channel width, which measures 90 m in Sandage and 154 m in Sauce. The sampling scheme was integrated over the reach in cross-channel transects located about one cross-section width apart. To sample particles, a tape measure was placed across the channel width and a particle selected with the aid of a sharpened pencil at a pre-determined interval. After a brief mapping survey of each channel bed, it was determined that the spacing between particle selection was to be 35 cm in Sauce and 20 cm in Sandage. The surveys produced over 400 particles sampled, 400 being the minimum number of particles

defined as representative of the channel bed (Gordan et al., 2004). The particle size was measured using a template on graph paper with model sieve sizes in millimeters (recommended in Kondolf et al., 2002a, pg. 358 to reduce observer bias). Size, shape, and material type were recorded for each particle. The smallest particle size recorded was 2 mm, and anything smaller was labeled as <2 mm. If a particle was partially buried it was labeled with an "E" or mostly buried as "B". Determination of the roundness and material of the 2-4 mm sized particles was aided by a 10x handheld magnifying lens.

2.4 Results and Discussion

2.4.1 Geomorphic survey

The Río Culebra is incised in various areas along its entire length, but its deepest section was 37 m deep along its middle section. Further downstream, just before it joins with the Río Grande, it is much less incised. All tributary arroyos are incised ephemeral streams that feed into the perennial stream of the Río Culebra. The tributary arroyos are incised between 5 to 25 m deep.

Knickpoints were examined along the Río Culebra and many of its tributaries (Figure 2.1). Some of the knickpoints were artificial, clearly created by concrete-surfaced fords and bridge structures causing the channel to steepen and erode. Ford and bridge structures were built across Culebra and its tributaries including Sandage. The incision rate immediately downstream of the bridge at the outlet of Sandage was 22 cm per year between 2011 and 2013, as determined by measuring and comparing the depths of the incision in 2011 and 2013 (Figure 2.7). An overflow dam along Culebra's middle section also serves as an artificial knickpoint. Knickpoints are observed in the more resistant andesite flows located in the upstream section of

the Culebra (Figure 2.8a). Other knickpoints occur along igneous dikes and in more resistant layers of the Yanhuitlan beds (Figure 2.8b). Victor's lama-bordo (i.e., check-dam) constructions in Sandage may partially explain the large number of knickpoints in this arroyo, but the bridge downstream is also affecting its channel form.

Earthquakes do occur in the Coixtlahuaca District, but no recent major earthquakes or active faults have been documented (Servicio Sismologico Naciónal, 2014). No faults were observed in the Quaternary strata within the survey area based on an extensive pedestrian survey of more than 100 km^2. Since the Tertiary shales are jointed and easily erodible and no recent faults have been observed, it was concluded that the deep incision that characterizes this valley is directly related to past (and present) climate fluctuations and human activities, rather than tectonic activity or base level change.

Clearly, all of the channels are internally adjusting to recent human impact, but they may also be undergoing long-term intrinsic adjustment due to the basin-wide incision that occurred approximately 350 years ago in relation to the Spanish conquest (Leigh et al., 2013). The former land use in the Natividad phase and Colonial period may have influenced the timing of incision and contributed legacy sediments to the entire watershed, but especially along Sandage. The internal channel bed adjustments represented by the knickpoints on Río Culebra are probably due to a combination of factors, including: short-term adjustments to the overflow dam, construction of bridges, and pumping further downstream to water crops; and long-term adjustments to past human activities and climatic fluctuations. Knickpoints observed on other barrancas are also affected by the internal adjustments of the mainstem, the Río Culebra. Depositional fan-like features were observed at some tributary junctions with the Río Culebra, while other tributary junctures were erosional and incising.

Mass wasting and side-wall gullying (Bull, 1991) have been observed in several areas along the entire system. Collapse of channel bank alluvium and mass wasting of the Yanhuitlan beds were noticed in various parts of the Culebra watershed (Figure 2.9). Undercut arroyo banks result in collapse of overhanging alluvium. Root action and the differential weathering between layers of single grained sediments versus cohesive paleosols causes weaknesses in the steep banks, resulting in side-wall collapse, especially when it rains. Mass wasting is an erosive process that contributes sediment to the system (Malmon et al., 2004; DeLong et al., 2014). Downstream channel erosion and widening via mass wasting and incision have been associated with channel degradation upstream (Bridge, 2003: 340).

Ephemeral streams apparently are unstable because they alternate between the two states of aggradation and incision. It is unclear by these observations if the system as a whole is incising or aggrading. It is also uncertain whether the system is adjusting inherently/internally or by external forcing mechanisms (climate and/or land-use change). Both incision and aggradation are observed in different areas in the watershed, which suggests that it is in a transitional phase of adjustment to some new conditions. In summary, the entire basin appears to be undergoing "complex response" to various factors and at different timescales (Schumm and Hadley, 1957; Schumm, 2005).

2.4.2 Channel characteristics

All observed and recorded floods (except one in Sauce), including 12 floods in Sauce and 14 in Sandage, covered the entire channel, even when the flow was only five cm deep. During the falling stage of major floods, flow in both barrancas typically occupied one channel measuring between 50 cm to 1 m in width, and 1 to 3 cm deep. However, more than one channel has been observed flowing during the falling stage in Sauce. Since all but the smallest of flows

typically occupy the entire cross-section (as in Bridge, 2003), referred to henceforth as the main channel, the arroyos are characterized as single threaded ephemeral streams having some braiding, especially in Sauce. After most floods, the resulting bed topography had clear, but subtle bedforms and channels, whereas after other floods, bed topography such as bars and channels were harder to discern. The present arroyo channel bed is comprised of a moderately heterogenous mix of sand and fine gravel, with some larger gravel, pebbles, cobbles, silt, clay and boulders (see section 4.3.1).

A study on a sand and gravel-bed ephemeral channel in Spain indicated that it also alternates between more complex and less complex macroform topography with the overall tendency towards the latter of "not creating long-term complex topography" (Singer and Michaelides, 2014). Failure of ephemeral channels to maintain complex topography has been linked to spatial variability in streamflow, transmission losses, and geomorphic thresholds of particle entrainment (Singer and Michealides, 2014). The lack of bedforms and frequent horizontal bedding in some sand-dominated ephemeral streams that have sporadic boulder sized particles, has been connected to the flashy nature of the floods (Billi, 2007).

Bars in Barrancas Sandage and Sauce are characterized as alternate or unit bars, and they generally have an elongated shape, are very flat, and measure only a few centimeters thick (Figure 2.10) (similar to description in Billi, 2008). They contain a large array of particle sizes, ranging from silt to boulders, and the larger particles tend to occur in clusters. The bars appear to be produced by low sediment transport and flow conditions during receding floods (Reid and Frostick, 1997; Billi, 2016). Sufficient energy in receding floods results in movement of smaller particles, streamline bars and cause braiding in channels (Billi, 2016). The bars have proportionately more gravel, pebbles and cobbles than the channels, which are mainly comprised

of sand and fine gravel (similar to Laronne and Schlomi, 2007). Flow is confined in minor channels within the main channel during the end of receding floods, which explains the relative abundance of sand observed within these minor channels. However, stringers or lenses of fine to medium gravel also exist within the minor channels. Walking surveys and observations in conjunction with the scouring chains suggest the bars move in pulsations during certain flows.

In some gravel dominated ephemeral streams, the channel bed contained bars and flats (Powell et al., 2012; Billi, 2016). However, the elongated bars and sheets in Sandage and Sauce resembled other streams with more sandy particles (Hassan et al., 2003; Hassan et al., 2009). During some falling stage flows silt and sand settled out over the surface of the channel bed, which potentially limited channel infiltration in subsequent floods. In a few cases channel bed structures were not observable due to trampling by goat herds (Bull and Kirkby, 2002).

2.4.2.1 Particle size

The particle size data for each arroyo during the flood seasons of 2013 to 2014 is summarized in Figure 2.11. Since fines were not examined in detail in the field, particle size data were always skewed in favor of larger particle sizes (Kondolf et al., 2002b). The <2 mm fraction was labeled as 1 mm to facilitate graphing. In Sandage, D_{50} measured 2 mm, while in Sauce D_{50} was 3 mm. D_{85} measured 8 mm in Sandage whereas D_{85} in Sauce was 10 mm. The <2mm fraction was not examined in detail for shape and material, but it was noted that the Yanhuitlan material was very common.

Most of the studied particles in both barrancas consisted of Yanhuitlan material, though it comprised slightly more of the channel bed in Sauce (Figure 2.12, a and b). The second most common material in Sandage is calcrete, while in Sauce it is gypsum. Other materials include volcanic rocks, chalcedony, mud aggregates eroded from buried A horizons, and a few seeds.

The slightly higher amount of Yanhuitlan materials in Sauce reflects the higher amount of exposed Yanhuitlan beds throughout the watershed, whereas the slightly higher amount of calcrete in Sandage accounts for the higher percentage of intact calcrete covering the land surface (Table 2.1). Chalcedony and the occasional obsidian flake represent anthropogenic contributions to the sediment load. Obsidian was observed in the channel bed, but not during the particle size analysis.

In both barrancas, the dominant shape of the particles comprising the channel bed is sub-angular, followed by sub-round and then angular shape (Figures 2.12, c and d). The majority of the Yanhuitlan particles have a sub-angular and angular shape, probably reflecting the fresh material supplied from the hillslope and channel banks and short transport distances. The Yanhuitlan also breaks easily, and its concoidal fracture results in angular edges, therefore some of the angular shape may be explained by the continued breaking of particles into smaller pieces during successive flows. Gypsum particles also had mainly sub-angular and angular shapes. A large number of Yanhuitlan particles have sub-round and round shapes, which have been rounded due to transport and may suggest they were eroded and recycled from channel bank alluvium in addition to rounding simply by continuous downstream transportation.

2.4.3 Scouring

Scour and fill amounts varied at different points of the reach and during different floods (Table 2.2). The maximum scour and fill in Sandage was 24 cm and 23 cm, respectively, and occurred during a high discharge event (flood 6). During another high flow event, almost the same amount of scour and fill was observed for chain 2, but none was observed for chain 1 (flood 5). Further, similar scour and fill were also observed for floods that were less than bankfull (e.g., flood 4). The minimum amount of scour for chain 1 during many floods,

especially in 2013, was probably due to its location in an alternate bar with larger particles. In Sauce, the maximum scour and fill was 23 cm and 30 cm, respectively, which occurred during flood 8. This flood was the largest flow recorded in the two-year study, and scour and fill was high for all chains. Similar to Sandage, chains 2 and 3, located in alternate bars did not demonstrate much scour and fill for floods 1- 4, after which the bar seemed to have migrated or to have been completely reworked. Scour and fill in ephemeral streams occur locally and sporadically, and are connected to bed form migration and bed reworking (Foley, 1978; Hassan, 1990). Vertical exchange of buried particles with scoured and transported particles is important to consider as particles can be exhumed and reburied in successive floods (Schick et al., 1987; Hassan, 1990).

In the Río Culebra, the stratigraphy related to the scouring chains was examined and described as follows (Figure 2.13). The most common stratigraphy involved poorly sorted, massive, matrix-supported sand and gravel deposits. The matrix typically consisted of medium to coarse sand and fine gravel supporting sporadic clasts of medium gravel and sometimes larger particles. Similar matrix-supported sand and gravel deposits were also commonly observed in ephemeral streams in Israel (Hassan et al., 2009). The matrix is unusual in that it is comprised of relatively coarse particles versus silt and clay, which is analogous to similar deposits in ephemeral streams studied by Laronne and Schlomi (2007). These types of deposits resemble hyper-concentrated or debris flows in perennial streams, but they differ in matrix composition (Hassan et al., 2009). The relatively coarse matrix deposits have been attributed to the sporadic, flashy nature of floods along with high sediment supply and transport, which result in poor vertical sorting and simultaneous deposition (Laronne and Schlomi, 2007; Hassan et al., 2009). Others have found evidence for hyperconcentrated flows in high gradient sandy channel beds,

which are represented by undisturbed boulders transported near the surface, vertical sorting of several distinct layers, and the lack of longitudinal sorting (Billi, 2008).

A few fining- and coarsening-upward sequences were also observed, having silt and clay deposited over (or found below) more sandy and gravelly layers. Fining-upward sequences occurred more frequently than coarsening upwards. All sequences consisted of moderately sorted beds of gravel and/or sand or laminations of fine sand to silt and clay.

2.4.4 Insights relating to Quaternary alluvium and stratigraphy

The present deeply incised dryland system has eroded into and exposed alluvium-paleosol sequences that were deposited since at least 30,000 years ago. The emphasis of this section will be on the non-pedogenic alluvial stratigraphy recorded in studied profiles (Chapter 3) spanning the terminal Pleistocene-early Holocene transition (record starts ~15,500 cal BP) to the latest Holocene. Similar to the modern bedload, the Quaternary alluvium primarily contains abraded particles of Yanhuitlan sediments, while calcrete, volcaniclastics and andesites, and gypsum constitute a smaller proportion. Since the present channel is transporting eroded alluvium that contains volcanic particles, it implies that strata containing rounded volcanic particles are most likely derived from eroded alluvium versus fresh hillslope material. Rounded particles found in alluvium, especially of more resistant materials like volcanic materials, have been rounded during transport in prior incision and aggradation episodes. Conversely, if a stratum contains *only* Yanhuitlan and calcrete, it hints that the source is from freshly eroded hillslopes. Particle size analyses made on studied profiles indicate that most layers contain a majority of <2 mm sized particles (see Chapter 3), and thus are generally finer textured than bed load observed from modern floods.

Stratigraphy recorded from the studied profiles (summarized in Chapter 3), as well as descriptions made on alluvium in various parts of the watershed, indicated that lithofacies and bedding properties varied from clear bedded and laminated to massive and single grain deposits (Figure 2.14). In general, laminations and beds were well sorted, while single grain deposits were moderately to poorly sorted and massive deposits poorly sorted. Normal graded and a few reverse graded sequences involved particle sizes ranging from medium and coarse gravel to silt and clay, and some of these sequences were clearly bedded or laminated, while in others the bedding was less apparent. Silt and clay laminations and sandy beds were much more common than gravel bedding. Some trough cross-beds were observed in some sandy and fine gravel deposits, indicating bedload deposits. Poorly sorted, massive sandy-gravel deposits were also common. Coarse sediments over undisturbed laminae observed in the profiles may result from *en masse* bed transport making the larger fraction buoyant and less likely to incise (as in Billi, 2008).

In sum, the stratigraphy contained both massive and coarser as well as finer and bedded deposits, though the latter was more prevalent. Although thin laminae (less than 0.50 cm) of fine sediments are sometimes deposited on the surface of the present channel bed during receding flood flows, they were usually eroded in the subsequent flood. Fining-upward sequences and silt and clay are common in stream systems where bedload ultimately gets overlain by suspended sediments such as on stable bars and floodplains. Deposition of fine sediments, especially laminated fine sediments, is observed along some areas of present patchy floodplain construction in Sandage and Sauce. However, in deeper floods these floodplain strata were vulnerable to erosion. A study on flash flood sediments in the southwestern U.S. suggests that the bedload fraction is transport-limited, whereas the fine sediment is supply-limited (Malmon et al., 2004).

However, the high suspended sediment load of Sandage and Sauce suggests that there is a substantial supply of fine sediments. Instead, the flashy nature of the present floods results in transport of fine sediments, whereas the extensive fine sediment deposits observed in the stratigraphy indicate a different flood regime that allowed for the deposition of finer sediments and construction of a more expansive floodplain and possibly stable bars. The distinct flood regime reflected in the Quaternary alluvium (as summarized in Chapter 3) is suggestive of diverse paleoclimatic conditions. Conversely, the less prevalent coarser strata, such as the poorly sorted, massive, sandy gravel deposits and the normally and reverse graded sequences of sandy and gravelly texture are analogous to the present-day flash floods deposits.

2.4.5 Bedload transport

During the 2012-2013 rainy seasons a total of 14 and 13 floods were recorded in Sandage and Sauce, respectively. However, several floods in each barranca overfilled the pit traps. This was due to an underestimation of bedload transport as well as financial limitations. Thus, the results offer minimum estimates of bedload transport by each barranca.

2.4.5.1 Discharge and Suspended Sediment Grab Samples

The sporadic, flashy, and hazardous nature of ephemeral floods meant that it was very difficult to be present during a flash flood, especially at the remote monitoring station of Sauce. Therefore, velocity was measured directly with a FloMeter 2000 for only four floods in Sandage and two in Sauce during the end of the flood season in 2012 and beginning of 2013. In Sandage, velocity measurements were obtained at five points across the entire cross-section for the duration of the flood. In the case of Sauce, flow was visibly faster, and wading was not possible, therefore representative measurements of velocity were obtained from the bank. Due to the unreliability of the Odyssey stage recorders (e.g., sedimentation, destruction and vandalism), the

information from the peak stage recorders was used as the primary depth estimate. Velocity for subsequent floods was calculated using the Manning equation. The Manning n value used in the equation was 0.02, which was within the range of back calculations done from the range of velocity measurements obtained during some of the flash floods.

Suspended sediment grab samples were also obtained along with velocity measurements from two flash floods in each barranca during the end of the flood season in 2012. Suspended sediment grab samples were analyzed to estimate specific density of the highly concentrated fluid (Tables 2.3 and 2.4).

By chance, two flood bores were directly observed in Barranca Sauce. Flood bores in ephemeral streams are defined as the front end of the surge of water that advances downstream over the dry channel during a flood. One was a high velocity, turbulent flow, similar to the bores described by Hassan (1990), while the other was extremely low velocity (slower than a walking pace), and possibly 1-2 cm deep. The latter mainly transported silt, clay and fine sand (as observed in the traps afterwards). The non-flashy nature of this flood reflected transmission loss as it descended downstream. Both flows had foam at the bore (also observed by Hassan, 1990), though the low velocity flow had more foam.

2.4.5.2 Pit Trap Observations

The size of the opening on the metal cover was determined by studying the distribution of the particle size of the streambed. The size of the opening ideally optimizes a balance between duration of flow that one would like to sample and the maximum particle size sampled. Therefore, the drawback with the metal covers is that very large particle size sediments will not be collected (Bergman et al., 2006). For the majority of floods, slots were opened to 12 cm in Sauce and 9 cm in Sandage, which is equivalent to D_{90} in both barrancas. The openings are

equivalent to 5% of the channel width in Sandage and 5.5% of the width in Sauce. Bergman et al. (2006) report that 9.2% of the channel width was covered in their study. During a few floods the slot openings varied between 2.5 to 11 cm in Sandage and 2.5 and 13.2 cm in Sauce (see Appendix I). The maximum value of 50 cm as an opening in Sauce is due to the tops of three of the pit traps being torn off during a large flood in September of 2013, which were not replaced until mid-flood season of 2014.

The downstream end of the trap contained larger particles than in the upstream area, which suggests that particles were deposited at the downstream end first and then progressively towards the upstream end. In Sandage, it was also noticed that the south trap filled more during floods than the north trap, which is due to the helical flow of the slightly meandering main channel (see Figure 2.2). For example, the north trap was not as full as the south trap (and middle trap in 2014) during the following floods: 1, 2, 3, 8, and 10. The faster flow strikes the cut bank, which is adjacent to the south trap, causing it to fill more than the north trap in almost every flood. The difference between trap sedimentation was less pronounced in Sauce, possibly because this channel segment is overall straighter. Nonetheless, traps 1 and 2 in Sauce seemed to fill up less.

The combined range of particle sizes from all traps for each flood in Sandage during the 2013-2014 rainy seasons is presented in Figure 2.15. The difference between the D_{50} and D_{85} particle size indicates that there is some fluctuation in particle size. For example D_{50} ranges from 1.5 to 3.2 mm, while D_{85} ranges from 3.8 to 23 mm. However, the average particle size distribution for flood season 2013 does not differ greatly from that in 2014. As expected the range in particle sizes in the pit traps corresponds to that along the channel bed, excluding cobbles and boulders.

2.4.5.3 Bedload Yield

The bedload yield (Q_b) for Sauce and Sandage in metric tons per year is presented in Tables 2.3 and 2.4; however, the values are considered minimum estimates for floods that filled the traps. The bedload flux was calculated by dividing the total sediment in kilograms measured for each flood by product of the area and the average time for the main portion of each flood to pass. Bedload discharge was estimated based on a 45-minute flood. The time for the main portion of the flood to pass, based on direct observations of various flash floods was between 35 to 75 minutes. Falling stage typically lasted longer, but consisted of a channel less than 50 cm in width and 1-2 cm in depth. Note that the Q_b estimates with missing data start to become evident at around 1 $kg^{-1}m^{-2}$ s^{-1} in both Sandage and Sauce as they do not go any higher (Figure 2.16). The rates that are associated with floods that did not fill up the traps were considered the most accurate. Plotting the estimated bedload discharge values against other streams indicates that Sauce and Sandage fall within the range of other ephemeral streams (Figure 2.17), but the Sauce and Sandage estimations are semi-quantitative.

Reid et al. (1995, 1998) illustrate a strong relationship between bedload flux and channel average boundary shear stress in ephemeral streams in Israel, which was confirmed after 10 years of data collection (Cohen et al., 2010). Due to the pit traps filling during some floods limited discerning the relationship between shear stress and stream power in Sandage and Sauce. The bedload-shear-stress relationship in the ephemeral streams in Israel was best approximated by the Meyer-Peter and Muller (1948) capacity transport equation (Reid and Laronne, 1995; Reid and Laronne, 1996). In sandy streams, the Meyer-Peter and Muller equation overestimated the bedload transport (e.g., Billi, 2011), which appears to be the case in Sandage and Sauce. The results using the equation by Martin (2003), which is for sandy-gravel streams, seemed to

overlap better with the bedload flux data from smaller floods (i.e., stages less than 15 centimeters) (see Figures 2.16a and b). Despite the low number of small floods, there seems to be a perceptible association between Q and Q_b as demonstrated in Figures 2.16c and d. Comparing the data with bedload transport equations supports the idea that bedload transport was underestimated when the traps were full and data were missed, but the Martin (2003) equation appears to offer a good approximation of Q_b for the larger floods.

The average estimated bedload yield per day is 17 tonnes in Sandage and 45 tonnes in Sauce, which is roughly 4.5 t/km^2/day and 11 .8 t/km^2/day in Sandage and Sauce, respectively. An estimate of sediment removed from Sandage per year is 117 tonnes, while that in Sauce is 191 tonnes, all of which is removed during 2% of time during the year. It was found that both Sandage and Sauce overlap considerably, but Sandage appears to have slightly lower bedload yield. In comparison to the bedload yield of streams in different environments (Figure 2.18) gathered by information from Preciso et al. (2012) the values for Sandage and Sauce fall between those of another documented semi-arid stream, Nahal Yatir (Reid et al., 1995), and a flashy Mediterranean perennial stream, the Arbucies River (Batalla, 1997).

2.4.6 Check-dam Evaluation

Despite the existence of Victor's modern lama-bordos and conservation efforts in the headwaters of Sandage, a remarkable amount of sediment still leaves this watershed. Even at its lowest estimate, the yield in tonnes per day is comparable to other semi-arid ephemeral streams. The bedload yield for Sauce was slightly higher on comparable smaller flows, but not as high as expected, which may be explained by transmission losses. Lower yields in Sandage versus Sauce may be partially due to the check dams and other conservation efforts in Sandage, but the reduction in yield is estimated to not be more than 37%.

A study on two small ephemeral watersheds before and after check dam construction in the southwestern U.S. showed that a change in runoff and sediment yield was undetectable for large storms, but it indicated that the number of runoff events from smaller storms decreased by 60% (Polyakev et al., 2014). Sediment supply downstream was also reduced in other dammed arroyos with varying outcomes on channel geomorphology (Boix-Fayos et al., 2007). The results from these studies confirm that the impact of check dam implementation on sediment yield is variable and complex.

Scouring is difficult to avoid downstream from a check dam, and the spatial extent, spacing between dams, and type of constructions will determine their effectiveness in storing and scouring sediments (Conesa-Garcia and Garcia-Lorenzo, 2010). It is unclear how much scouring occurs just downstream from the final check dam in Sandage, and if it has caused some of the incision and knickpoints downstream. Much scouring occurs downstream from the bridge near the basin outlet (see Figure 2.7), which may also have caused the outlet area to become narrower. Incision along tributary arroyos is also affected by the downcutting of the Río Culebra in relation to human activities along the midstream and downstream areas.

A survey of the headwaters to Sandage found that vegetation cover is widespread in areas, and includes undergrowth. Standing water was observed in retention ponds and in some parts of the contour terraces during the rainy season. Finally, Victor's lama-bordos have collected sediments that erode from adjacent hillslopes during floods. Although not quantified by hillslope erosion plots, the apparent amelioration of bare and exposed slopes in the headwaters based on land cover classification and field reconnaissance resulted from conservation strategies, including check dams, which was also found in another study by Boix-Fayos et al. (2007). Further downstream, no conservation has been applied to the hillslopes,

there are no check dams, and land use on the abandoned terrace adjacent to Sandage includes easily erodible agricultural land.

As observed in other regions, part of the problem of soil erosion concerns managing the sources of sediment that come from the upstream areas such as hillslopes, but it is also necessary to mitigate erosion from the channel, its banks, and agricultural gullies and rills along the middle and downstream areas. It is also important to understand how managing one part of the stream affects the rest of the watershed (Fox et al., 2016). The relatively high sedimentation rates observed in the basin outlet in Sandage are related to several factors: 1) lack of basin-wide conservation efforts; and 2) the internal adjustments to both (a) Victor's lama-bordo installments upstream; and (b) the behavior of the Río Culebra downstream. Thus, it appears that in such an erodible basin, management strategies have to be basin-wide (not just in the headwaters) to be completely successful. In sum, the check dams and conservation efforts have had beneficial impacts on the landscape, but these are spatially limited. Similar limitations were also observed by Kondolf et al. (2002b), who assert that conservation should be implemented on longer-term and basin-wide scales (i.e., geomorphic scales), instead of applying spatially limited techniques and short-term solutions.

2.4.6.1 Estimations of Check Dam Filling

Based on a number of factors, including geology, check dam type, number and spacing, climate and vegetation, check dams will fill at various rates (Bussi et al., 2013; Polyakev et al., 2014). In some cases filling of deep arroyos, such as those in Culebra, is needed, whereas in others filling is highly undesireable, but hard to avoid. If designed properly, when a check dam becomes filled, it further serves to reduce slope and erosive capacity of flow (Conesa-Garcia and Garcia-Lorenzo, 2010).

The average estimate of bedload yield from smaller floods in Sandage was 117 t yr^{-1}. The average dry weight of the sediments of a filled trap with a volume of 0.24 m^3 is 323 kg, resulting in an approximated bulk density of 1,347 kg m^{-3} for the sediment. Converting kg yr^{-1} to m^3 yr^{-1} results in: 117,000 kg yr^{-1}/1,347 kg m^3 = 87 m^3 yr^{-1}. The average distance between two of Victor's lama-bordos is 175 m and using 10 m for the average width and 15 m for average depth, the total volume was estimated as 21, 619 m^3 (Figure 2.19). Thus, it is estimated that it would take 249 years to fill up, given conservative estimates of present sediment yield.

The prehistoric farmers in the area used basin wide strategies of landscape mitigation including check dams and terracing from 3,500 cal BP to 500 cal BP (Kowalewski et al., 2009; Leigh et al., 2013). Modelled sedimentation rates behind one of the studied ancient lama-bordos (Chapter 3) using the package for 'classical' age-modelling (CLAM) of radiocarbon sequences (Blaauw, 2010; version 2.2) in R (R Core Team, 2013; version 0.98.1103) indicated that it filled in about 105 years at a rate of 4.55 cm yr^{-1}. The maximum space between four ancient lama-bordos along Sandage, two of which have been dated to the Cruz phase, is 60 m. Using 60 m as the length between the ancient lama-bordos, a width of 10 m, and a depth of 5 m, the estimated volume is 1990 m^3 (Figure 2.19). It is estimated that it would take only about 23 years to completely fill when using the modern sediment yield of 87 m^3 yr^{-1}.

Although the bedload yield in Sandage serves as a minimum estimate, the time to fill the dam based on modern rates contrasts the modelled rate behind the ancient lama-bordo, which was about 105 years to fill. The available data indicate that modern bedload sediment yield is at least 4.6 times faster than the prehistoric sediment yield during the late Holocene. Two reasons, which are not mutually exclusive, can account for this observation: 1) the sediment trapped behind the check dams further upstream meant that downstream check dams would fill slower;

and 2) climate and hydrologic regime were different in the past. The geomorphological survey indicated that the present system is not in an aggrading phase, whereas at approximately 3,700 cal BP, the arroyos were starting to aggrade (Leigh et al., 2013). Furthermore, the stratigraphy of the arroyo side-walls is finer and has more bedding than in the present channel bed deposits. The coarser and massive deposits more typical of the present day ephemeral stream deposits reflect the present climate regime, whereas finer deposits and aggradation must reflect diverse paleoclimatic conditions.

2.5 Conclusion

A geomorphic survey in the Río Culebra watershed offered insight on the state of the present dryland stream system. In general, both incision and aggradation was observed throughout the watershed in association with natural features and artificial constructions. These observations in conjunction with historic land use changes and paleoclimatic fluctuations suggest that the system is undergoing complex response to intrinsic and extrinsic factors at various scales. A more in-depth, semi-quantitative study on the channel morphology, bedload and flow characteristics of two tributary arroyos, Barrancas Sandage and Sauce presented information on several form related processes. For instance, channel bed morphology is relatively subtle and channel and bars appear to form during receding flows, similar to other sand-gravel dominated ephemeral streams. Scour-and-fill occurs sporadically and variably across the channel and between floods, and supports high bedload flux and equal mobility as determined for other ephemeral streams. Channel bed morphology and stratigraphy offers invaluable insight on channel bank alluvial stratigraphy. For example, massive, coarse sandy to fine gravel matrix-supported deposits in some alluvial strata resemble the deposits of present flash floods. Overall

finer deposits, with clear laminations and beds are observed in present patchy floodplain deposits, contrasting the prevalence of these finer deposits in the alluvial stratigraphy. The overall finer deposits support more expansive floodplain construction during previous aggradation episodes.

Bedload yield and flow characteristics for the more conserved watershed, Sandage, and the poorly managed watershed, Sauce, produced some unexpected results. Bedload yield from comparable small floods indicated that Sandage had higher sediment yields than expected, while Sauce had lower yields than expected. Although the bedload yield in Sauce was overall higher than in Sandage, the relatively lower yields in the former are linked to transmission losses in the bare ground of the headwaters, and in the channel bed. The relatively high sediment yields in Sandage are attributed to the focus of conservation efforts in the headwaters while no management is effected on vulnerable downstream areas. The stability of vegetation, and the retention of soil and water in the headwaters are noteworthy, but the effect on downstream morphology and flow are also important to consider. In summary, it seems that a basin-wide conservation strategy is needed, especially on vulnerable land use in the downstream area of Sandage, and possibly in other areas along the Culebra. Noteably in the past, basin-wide conservation was employed in Barranca Sandage in the Cruz phase, and in the Culebra watershed in the Natividad phase. Finally, the modest estimations of bedload yield suggest that Victor's lama-bordos are filling at least at a moderate rate and will ultimately require maintenance. This highlights the need to consider temporal scale if long-term watershed management is the aim. The geoarchaeological data suggests that lama-bordos were managed over many generations, especially along Sandage. In conclusion, these observations emphasize the need to consider conservation at various temporal and spatial scales.

2.6 References

Abrahams, A.D., Parsons, A.J., Wainwright, J., 1994. Resistance to Overland-Flow on Semi-Arid Grassland and Shrublands Hillslopes, Walnut Gulch, Southern Arizona. Journal of Hydrology 156, 431-446.

Alexandrov, Y., Cohen, H., Laronne, J.B., Reid, I., 2009. Suspended sediment load, bed load, and dissolved load yields from a semiarid drainage basin: A 15-year study. Water Resources Research 45.

Alexandrov, Y., Laronne, J.B., Reid, I., 2007. Intra-event and inter-seasonal behaviour of suspended sediment in flash floods of the semi-arid northern Negev, Israel. Geomorphology 85, 85-97.

Balkansky, A.K., Kowalewski, S.A., Perez Rodriguez, V., Pluckhahn, T.J., Smith, C.A., Stiver, L.R., Beliaev, D., Chamblee, J.F., Heredia Espinoza, V.Y., Santos Perez, R., 2000. Archaeological survey in the Mixteca Alta of Oaxaca, Mexico. Journal of Field Archaeology 27, 365-389.

Batalla, R.J., 1997. Evaluating bed-material transport equations using field measurements in a sandy gravel-bed stream, Arbucies River, NE Spain. Earth Surface Processes and Landforms, 22(2): 121-130.

Bergman, N., Laronne, J.B. and Reid, I., 2007. Benefits of design modifications to the Birkbeck bedload sampler illustrated by flash-floods in an ephemeral gravel-bed channel. Earth Surface Processes and Landforms, 32(2): 317-328.

Billi, P., 2007. Morphology and sediment dynamics of ephemeral stream terminal distributary systems in the Kobo basin (northern Welo, Ethiopia). Geomorphology 85, 98-113.

Billi, P., 2008. Bedforms and sediment transport processes in the ephemeral streams of Kobo basin, Northern Ethiopia. Catena 75, 5-17.

Billi, P., 2011. Flash flood sediment transport in a steep sand-bed ephemeral stream. International Journal of Sediment Research 26, 193-209.

Billi, P., 2016. Channel processes and sedimentology of a boulder-bed ephemeral stream in the western Afar margin. Zeitschrift Fur Geomorphologie, 60(1): 35-52.

Billi, P., Dramis, F., 2003. Geomorphological investigation on gully erosion in the Rift Valley and the northern highlands of Ethiopia. Catena 50, 353-368.

Blaauw, M. (2010) Methods and code for 'classical' age-modeling of radiocarbon sequences. Quaternary Geochronology 5(5): 512-518.

Boix-Fayos, C., de Vente, J., Martinez-Mena, M., Barbera, G.G., Castillo, V., 2008. The impact

of land use change and check-dams on catchment sediment yield. Hydrological Processes 22, 4922-4935.

Bridge, J.S., 2003. Rivers and Floodplains: Forms, Processes, and Sedimentary Record. Blackwell Science Ltd, Oxford.

Bryan, K., 1925. Date of Channel of Channel Trenching (Arroyo Cutting) in the Arid Southwest. Science (New York, N.Y.) 62, 338-344.

Bull, L.J., Kirkby, M.J., 2002. Dryland Rivver Characteristics and Concepts, in: Bull, L., J., Kirkby, M. J. (Ed.), Dryland Rivers: Hydrology and Geomorphology of Semi-Arid Channels. John Wiley & Sons Ltd., West Sussex.

Bull, W.B., 1991. Geomorphic Responses to Climate Change. Oxford University Press, Oxford.

Bull, W.B., 1997. Discontinuous ephemeral streams. Geomorphology 19, 227-276.

Bunte, K., Abt, S.R., 2001. Sampling frame for improving pebble count accuracy in coarse gravel-bed streams. Journal of the American Water Resources Association 37, 1001-1014.

Bunte, K., Abt, S.R., Potyondy, J.P., Swingle, K.W., 2009. Comparison of Three Pebble Count Protocols (EMAP, PIBO, and SFT) in Two Mountain Gravel-Bed Streams1. Journal of the American Water Resources Association 45, 1209-1227.

Bussi, G., Rodriguez-Lloveras, X., Frances, F., Benito, G., Sanchez-Moya, Y., Sopena, A., 2013. Sediment yield model implementation based on check dam infill stratigraphy in a semiarid Mediterranean catchment. Hydrology and Earth System Sciences 17, 3339-3354.

Castillo, C., Perez, R., Gomez, J.A., 2014. A conceptual model of check dam hydraulics for gully control: efficiency, optimal spacing and relation with step-pools. Hydrology and Earth System Sciences 18, 1705-1721.

Cohen, H., Laronne, J.B., Reid, I., 2010. Simplicity and complexity of bed load response during flash floods in a gravel bed ephemeral river: A 10 year field study. Water Resources Research 46.

Conesa-Garcia, C., Garcia-Lorenzo, R., 2010. Bed Scouring-Sedimentation Balance Induced by Check Dams in Semi-arid Catchments with Different Lithology, in: Garcia, C.C., Lenzi, M.A. (Eds.), Check Dams, Morphological Adjustments and Erosion Control in Torrential Streams, pp. 283-306.

Conesa-Garcia, C., Lopez-Bermudez, F., Garcia-Lorenzo, R., 2007. Bed stability variations after check dam construction in torrential channels (South-East Spain). Earth Surface Processes and Landforms 32, 2165-2184.

DeLong, S.B., Johnson, J.P.L., Whipple, K.X., 2014. Arroyo channel head evolution in a flash-flood-dominated discontinuous ephemeral stream system. Geological Society of America Bulletin 126, 1683-1701.

de Vente, J., Poesen, J. and Verstraeten, G., 2005. The application of semi-quantitative methods and reservoir sedimentation rates for the prediction of basin sediment yield in Spain. Journal of Hydrology, 305(1-4): 63-86.

Dietrich, W.E., Kirchner, J.W., Ikeda, H., Iseya, F., 1989. Sediment Supply and the Development of the Coarse Surface-Layer in Gravel-Bedded Rivers. Nature 340, 215-217.

Foley, M.G., 1978. Scour and Fill in Steep, sand-bed ephemeral streams. Geological Society of America Bulletin 89, 559-570.

Fox, G.A., Sheshukov, A., Cruse, R., Kolar, R.L., Guertault, L., Gesch, K.R., Dutnell, R.C., 2016. Reservoir Sedimentation and Upstream Sediment Sources: Perspectives and Future Research Needs on Streambank and Gully Erosion. Environmental Management 57, 945-955.

Garcia Lara, B. V. 2012. Community member of San Juan Bautista Coixtlahuaca, personal communication.

Gellis, A.C., Pavich, M.J., Bierman, P.R., Clapp, E.M., Ellevein, A., Aby, S., 2004. Modern sediment yield compared to geologic rates of sediment production in a semi-arid basin, New Mexico: Assessing the human impact. Earth Surface Processes and Landforms 29, 1359-1372.

Gordan, N.D., McMahon, T.A., Finlayson, B.L., Gippel, C.J., Nathan, R.J., 2004. Stream Hydrology: An Introduction for Ecologists. John WIley & Sons Ltd., West Sussex.

Graf, W.L., 2002. Fluvial Processes in Dryland Rivers. The Blackburn Press, Caldwell.

Griffith, J., G., P., E., P., Eagleton, D. 2013. Method to Estimate Sediment Storage Volume for Rock Filter Dams and Stone Check Dams. Office of Design Policy and Support, Georgia Department of Transportation.

Grimaldi, S., Angeluccetti, I., Coviello, V., Vezza, P., 2015. Cost-Effectiveness of Soil and Water Conservation Measures on the Catchment Sediment Budget-The Laaba Watershed Case Study, Burkina Faso. Land Degradation & Development 26, 737-747.

Hassan, M.A., 1990. Scour, Fill, and Burial Depth of Coarse Material in Gravel Bed Streams. Earth Surface Processes and Landforms 15, 341-356.

Hassan MA, Ergenzinger P. 2003. Tracers in fluvial geomorphology. In Tools in Fluvial Geomorphology, Kondolf GM, Piegay H (eds). John Wiley & Sons: Chichester; 397–423.

Hassan, M.A., Marren, P.M., Schwartz, U., 2009. Bar structure in an arid ephemeral stream. Sedimentary Geology 221, 57-70.

Hereford, R., 1987. Sediment-Yield History of a Small Basin in Southern Utah, 1937-1976-Implications for Land Management and Geomorphology. Geology 15, 954-957.

Huang, M.B., Gallichand, J., Zhang, P.C., 2003. Runoff and sediment responses to conservation practices: Loess plateau of china. Journal of the American Water Resources Association 39, 1197-1207.

Jansson, M.B., 1988. A Global Survey of Sediment Yield. Geografiska Annaler Series a-Physical Geography 70, 81-98.

Kirkby, M., 1972. The Physical Environment of the Nochixtlan Valley, Oaxaca. Vanderbilt University, Nashville.

Kondolf, G., M., Lisle, T.E., Wolman, G.M., 2002a. Bed Sediment Measurement, in: Kondolf, G.M., Piegay, H. (Eds.), Tools in Fluvial Geomorphology. John Wiley & Sons Ltd., West Sussex.

Kondolf, G.M., Piegay, H., Landon, N., 2002b. Channel response to increased and decreased bedload supply from land use change: contrasts between two catchments. Geomorphology 45, 35-51.

Kowalewski, S.A., Balkansky, A. K., Walsh, L. R. S., Pluckhahn, T. J., Chamblee, J. F., Rodriguez, V. P., Espinosa, V. Y. H., Smith, C. A., 2009. Origins of the Nuu: Archaeology in the Mixteca Alta, Mexico. University Press Colorado, Boulder.

Langbein, W.B., Schumm, S.A., 1958. Yield of sediment in relation to mean annual precipitation. Trans Amer Geophys Union 39, 1076-1084.

Laronne, J.B., Reid, I., 1993. Very high-rates of bedload transport by ephemeral desert rivers. Nature 366, 148-150.

Laronne, J.B., Reid, I., Yitshak, Y. and Frostick, L.E., 1992. Recording Bedload Discharge in a Semiarid Channel, Nahal Yatir, Israel. Erosion and Sediment Transport Monitoring Programmes in River Basins, 210, 79-86 pp.

Laronne, J.B., Reid, I., Yitshak, Y., Frostick, L.E., 1994. The non-layering of gravel streambeds under ephemeral flood regimes. Journal of Hydrology 159, 353-363.

Laronne, J.B., Shlomi, Y., 2007. Depositional character and preservation potential of coarse-grained sediments deposited by flood events in hyper-arid braided channels in the Rift Valley, Arava, Israel. Sedimentary Geology 195, 21-37.

Leigh, D.S., Kowalewski, S.A., Holdridge, G., 2013. 3400 years of agricultural engineering in Mesoamerica: lama-bordos of the Mixteca Alta, Oaxaca, Mexico. Journal of Archaeological Science 40, 4107-4111.

Leopold, L.B., Wolman, G.M., Miller, J.P., 1964. Fluvial Processes in Geomorphology. Dover Publications, Inc., New York.

Malmon, D.V., Reneau, S.L., Dunne, T., 2004. Sediment sorting and transport by flash floods. Journal of Geophysical Research-Earth Surface 109.

Marden, M., Arnold, G., Gomez, B., Rowan, D., 2005. Pre- and post-reforestation gully development in Mangatu Forest, east coast, North Island, New Zealand. River Research and Applications 21, 757-771.

Martin, Y., 2003. Evaluation of bed load transport formulae using field evidence from the Vedder River, British Columbia. Geomorphology 53, 75-95.

Meyer-Peter, E., and MUller, R. (1948). "Formulas for bedload transport." Proc. Int. Assoc. of Hydr. Struct. Res., 39-64.

Molina, A., Govers, G., Poesen, J., Van Hemelryck, H., De Bievre, B., Vanacker, V., 2008. Environmental factors controlling spatial variation in sediment yield in a central Andean mountain area. Geomorphology 98, 176-186.

Nacional, S.M., 2010. Normales Climatologicas 1971-2000, Estacion 0020019: S. J. Bautista Coixtlahuaca. Comision Nacional del Agua (CONAGUA), Mexico.

Nanson, G.C., Tooth, S., Knighton, A.D., 2002. A Global Perspective on Dryland Rivers: Perceptions, Misconceptions and Distinctions, in: Bull, L.J., Kirkby, M.J. (Eds.), Dryland Rivers: Hydrology and Geomorphology of Semi-Arid Channels. John Wiley & Sons Ltd., West Sussex.

Nyssen, J., Veyret-Picot, M., Poesen, J., Moeyersons, J., Haile, M., Deckers, J., Govers, G., 2004. The effectiveness of loose rock check dams for gully control in Tigray, northern Ethiopia. Soil Use and Management 20, 55-64.

Osborn, H.B., Renard, K.G., Simanton, J.R., 1979. Dense Networks to Measure Convection Rainfall in the Southwestern United-States. Water Resources Research 15, 1701-1711.

Parsons, A.J., Abrahams, A.D., Wainwright, J., 1996. Responses of interrill runoff and erosion rates to vegetation change in southern Arizona. Geomorphology 14, 311-317.

Poesen, J., Nachtergaele, J., Verstraeten, G., Valentin, C., 2003. Gully erosion and environmental change: importance and research needs. Catena 50, 91-133.

Polyakov, V.O., Nichols, M.H., McClaran, M.P., Nearing, M.A., 2014. Effect of check dams on runoff, sediment yield, and retention on small semiarid watersheds. Journal of Soil and Water Conservation 69, 414-421.

Powell, D.M., Laronne, J.B., Reid, I. and Barzilai, R., 2012. The bed morphology of upland single-thread channels in semi-arid environments: evidence of repeating bedforms and their wider implications for gravel-bed rivers. Earth Surface Processes and Landforms, 37(7): 741-753.

Preciso, E., Salemi, E., Billi, P., 2012. Land use changes, torrent control works and sediment mining: effects on channel morphology and sediment flux, case study of the Reno River (Northern Italy). Hydrological Processes 26, 1134-1148.

R Core Team, 2013. R: A language and environment for statistical computing. R Foundation for Statistical Computing, Vienna, Austria. URL: http://www.R-project.org.

Reid, I., 2002. Sediment Dynamics of Ephemeral Channels, in: Bull, L.J., Kirkby, M.J. (Eds.), Dryland Rivers: Hydrology and Geomorphology of Semi-Arid Channels. John Wiley & Sons Ltd., Wests Sussex.

Reid, I., Frostick, L.E., 1987. Flow Dynamics and Suspended Sediment Properties in Arid Zone Flash Floods. Hydrological Processes 1, 239-253.

Reid, I., Laronne, J.B., 1995. Bed-load Sediment Transport in an Ephemeral Stream and a Comparison with Seasonal and Perennial Counterparts. Water Resources Research 31, 773-781.

Reid, I., Laronne, J.B., Powell, D.M., 1998. Flash-flood and bedload dynamics of desert gravel-bed streams. Hydrological Processes 12, 543-557.

Reid, I., Layman, J.T., Frostick, L.E., 1980. The Continuous Measurement of Bedload Discharge. Journal of Hydraulic Research 18, 243-249.

Reid, I., Powell, D.M. and Laronne, J.B., 1996. Prediction of bed-load transport by desert flash floods. Journal of Hydraulic Engineering-Asce, 122(3): 170-173.

Renard, K.G., Nichols, M.H., Woolhiser, D.A., Osborn, H.B., 2008. A brief background on the U.S. Department of Agriculture - Agricultural Research Service Walnut Gulch Experimental Watershed. Water Resources Research 44.

Rincon Mautner, C., 1999. Man and the Environment in the Coixtlahuaca Basin of Northwestern Oaxaca, Mexico: Two Thousand Years of Historical Ecology, Anthropology. University of Texas, Ann Arbor.

Romero-Diaz, A., Alonso-Sarria, F., Martinez-Lloris, M., 2007. Erosion rates obtained from check-dam sedimentation (SE Spain). A multi-method comparison. Catena 71, 172-178.

Romero-Diaz, A., Marin-Sanleandro, P., Ortiz-Silla, R., 2012. Loss of soil fertility estimated from sediment trapped in check dams. South-eastern Spain. Catena 99, 42-53.

Santamaria-Diaz, A., Alaniz-Alvarez, S-A., Nieto-Samaniego, A. F., 2008. Deformaciones cenozoicas en la Cobertura de la Falla Caltepec en la Region de Tamazulapam, sur de Mexico. Revista Mexicana De Ciencias Geologicas 25, 494-516.

Schick, A.P., Lekach, J., Hassan, M.A., 1987. Vertical exchange of coarse bedload in desert streams, in: Frostick, L.E., Reid, I. (Eds.), Desert Sediments: Ancient and Modern. Blackwell Scientific Publications, Oxford.

Schumm, S.A., 2005. River Variability and Complexity. Cambridge University Press, Cambridge.

Schumm, S.A., Hadley, R.F., 1957. Arroyos and the Semi-Arid Cycle of Erosion. American Journal of Science 255, 161-174.

Shannon, J., Richardson, R., Thornes, J., 2002. Modelling Event-based Fluxes in Ephemeral Streams, in: Bull, L.J., Kirkby, M.J. (Eds.), Dryland Rivers: Hydrology and Geomorphology of Semi-Arid Channels. John Wiley & Sons Ltd., West Sussex.

Singer, M.B., Michaelides, K., 2014. How is topographic simplicity maintained in ephemeral dryland channels? Geology 42, 1091-1094.

Tooth, S., 2000. Process, form and change in dryland rivers: a review of recent research. Earth-Science Reviews 51, 67-107.

UN Report, 2011. Global Drylands: A UN system-wide response. United Nations Environmental Management Group.

UNESCO, 2016. Tehuacán-Cuicatlán biosphere reserve. Ecological Sciences United Nations Educational, Scientific and Cultural Organization, http://www.unesco.org/new/en/natural-sciences/environment/ecological-sciences/biosphere-reserves/latin-america-and-the-caribbean/mexico/tehuacan-cuicatlan/. Last accessed June, 2016.

USGS, 2011. Global Land Survey , 2000, Landsat ETM+, 30m LE70250482003146EDC00, United States Geological Survey, Sioux Falls, South Dakota.

Wakelin-King, G.A., Webb, J.A., 2007. Threshold-dominated fluvial styles in an arid-zone mud-aggregate river: The uplands of Fowlers Creek, Australia. Geomorphology 85, 114-127.

Walling, D.E., Kleo, A.H.A., 1979. Sediment yield of rivers in areas of low precipitation: A global view. The Hydrology of Mountainous Areas. IAHS Publ. 128, pp. 479-493.

Waters, M.R., Haynes, C.V., 2001. Late Quaternary arroyo formation and climate change in the American Southwest. Geology 29, 399-402.

Zema, D.A., Bombino, G., Boix-Fayos, C., Tamburino, V., Zimbone, S.M., Fortugno, D., 2014. Evaluation and modeling of scouring and sedimentation around check dams in a Mediterranean torrent in Calabria, Italy. Journal of Soil and Water Conservation 69, 316-329.

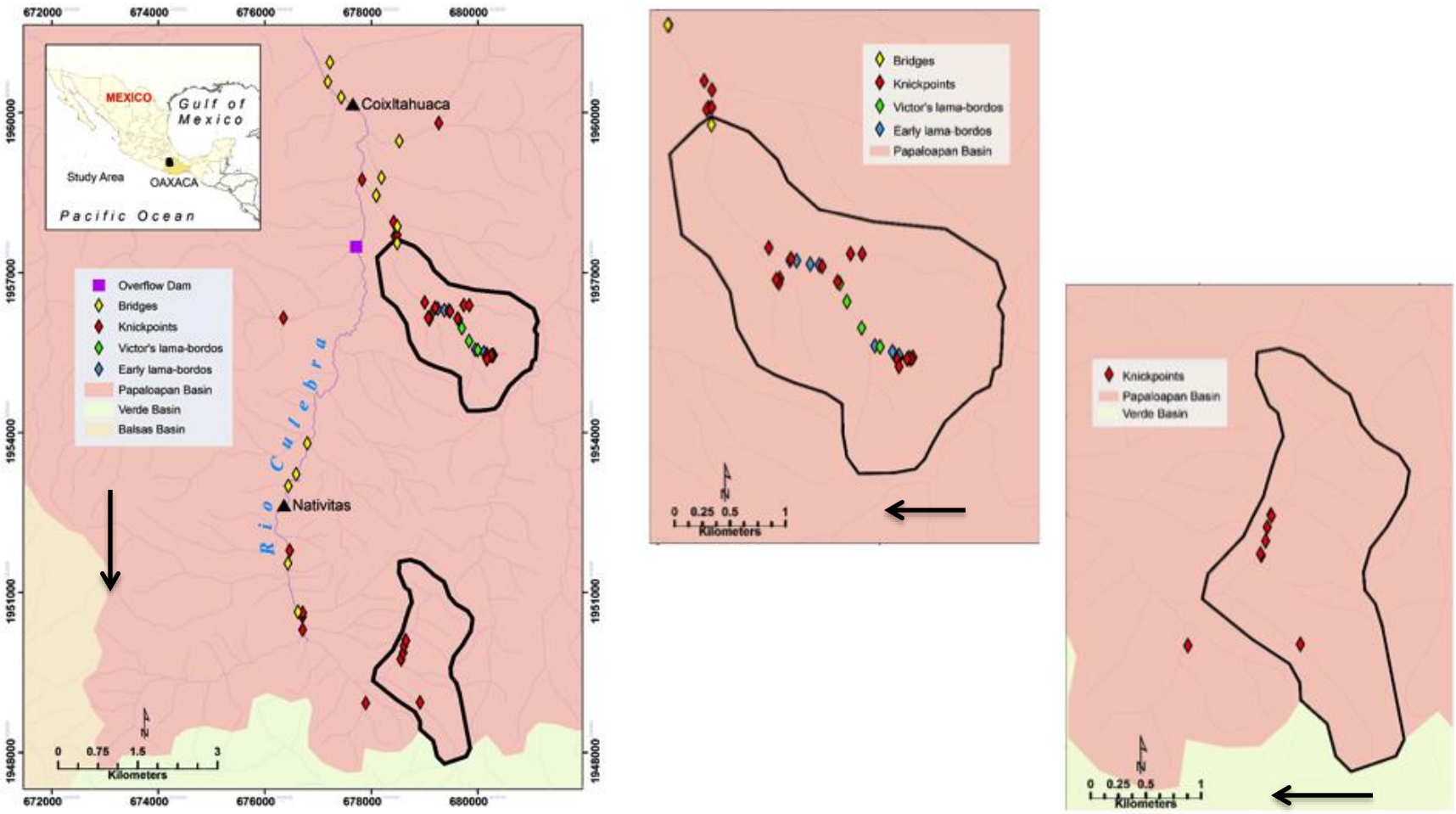

Figure 2.1. Map of the Rio Culebra watershed and its tributaries in Oaxaca, Mexico. Map shows the location of some of the geomorphic attributes in the Culebra watershed and a close-up of Barranca Sauce in Santa Maria Nativitas, and Barranca Sandage in San Juan Bautista Coixtlahuaca. (Black arrows indicate direction of flow).

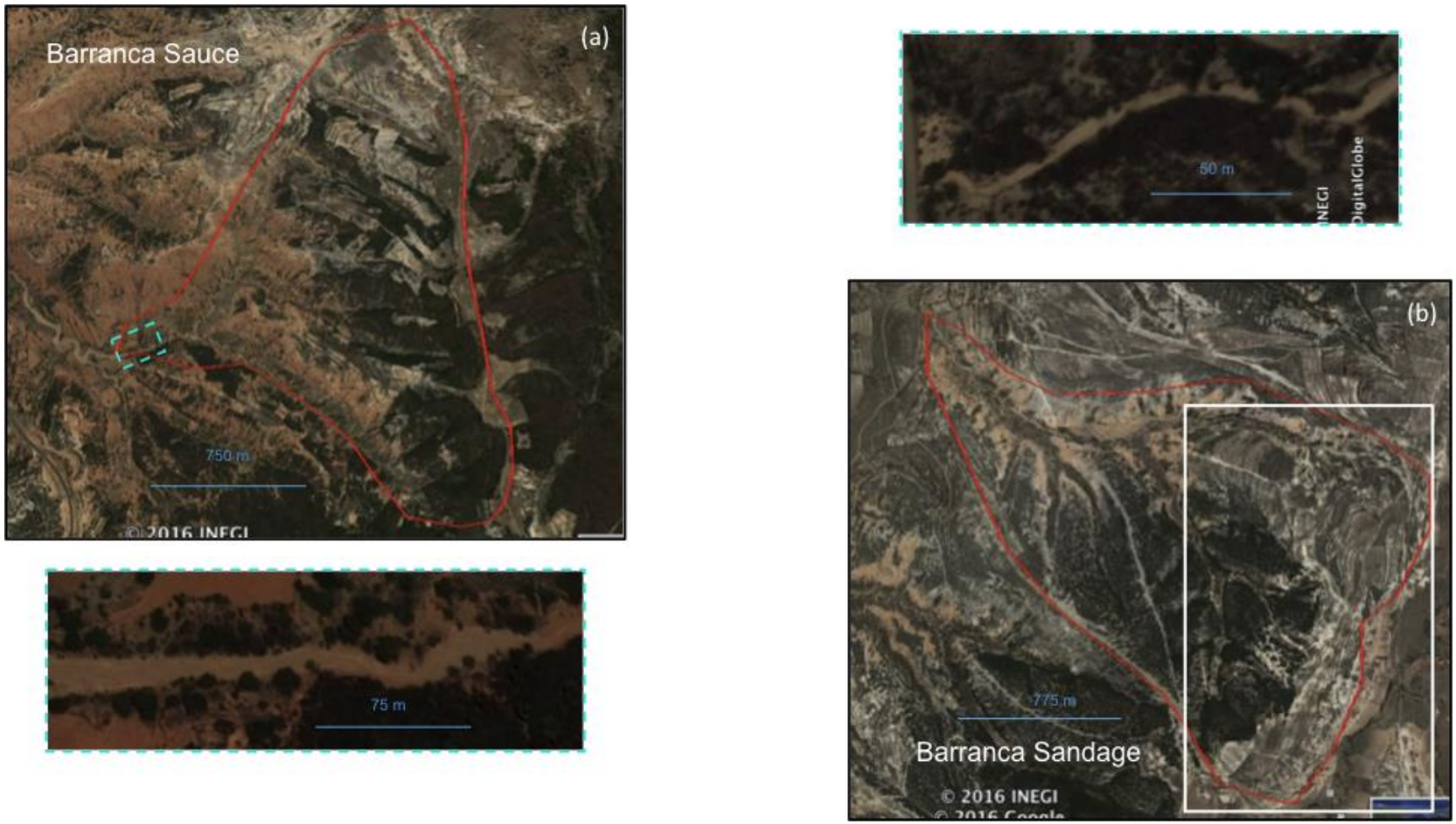

Figure 2.2. Google Earth satellite imagery of (a) Barrancas Sauce and (b) Sandage. A close-up of the study reaches at the basin outlets are shown below each watershed and are outlined by a dashed light blue box in the watershed scale images. Note the bare ground (pinkish orange), endeque/calcrete (white), forest/vegetation cover (dark green), and darker brown and terraced agricultural areas. The area with conservation works is outlined with a solid white box.

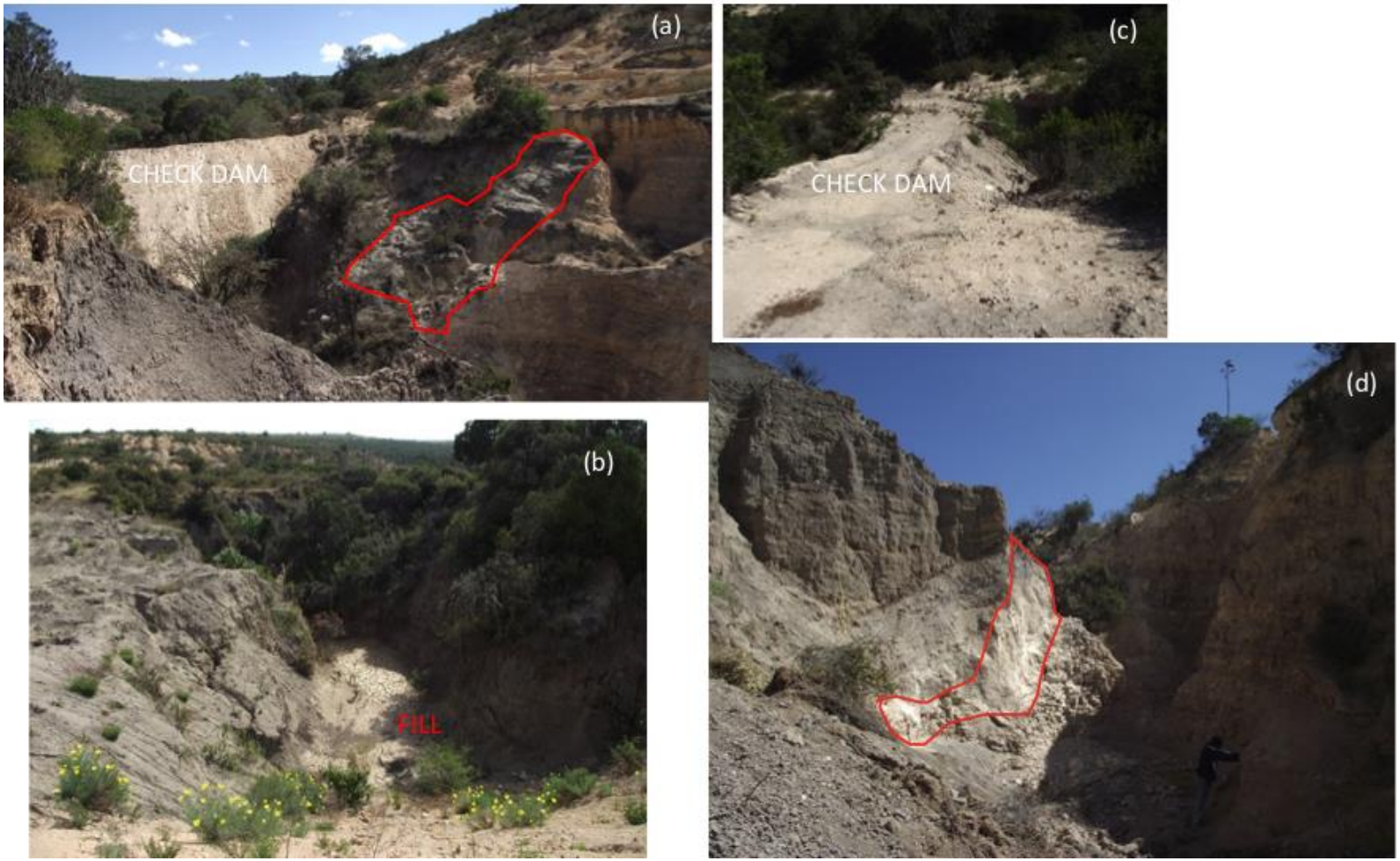

Figure 2.3. Example of a modern check dam (i.e., Victor's lama-bordos). Different views around the check dam include: a view downstream looking upstream (a); a view of fill behind the check dam (b); a view on top of check dam; (c) and a view of the channel bed downstream of check dam (d). Note the endeque/calcrete (outlined in red in Figures 2.3a and d) reached deep into the valley at one point.

Figure 2.4. Intact (a) and blown-out (b) ancient check dam in the headwaters of Barranca Sandage.

Figure 2.5. Monitoring station of Barranca Sandage. The monitoring station includes: three bedload traps (denoted by numbers 1-3), Odyssey stage recorder (4), staff gauge (5) and peak stage recorders in distance (6-7) (one of them has been removed already). The red line indicates the location of bankfull flow.

Figure 2.6. Monitoring station of Barranca Sauce (a). The red line indicates bankfull stage and the white dashed line indicates channel bed width. Note that the basin outlet is much wider than in Sandage (10 m vs. 4m). Figure (b) shows the three of the five pit traps installed in 2013, while figure (c) displays the ten pit traps after five more were added in 2014.

Figure 2.7. Artificial knickpoint created by a bridge on Barranca Sandage. The bridge and associated knickpoint are located immediately downstream from the basin outlet at Sandage. Figure 2.7a shows the incision depth in 2011, while Figure 2.7b demonstrates the amount of incision that occurred between 2011 and 2014.

Figure 2.8. Natural knickpoints in the Río Culebra watershed. Figure 2.8a shows n exposed andesite flow located in the upstream section of the Culebra. Figure2.8b shows a knickpoint in the Yanhuitlan beds located in the downstream section of Barranca Sandage.

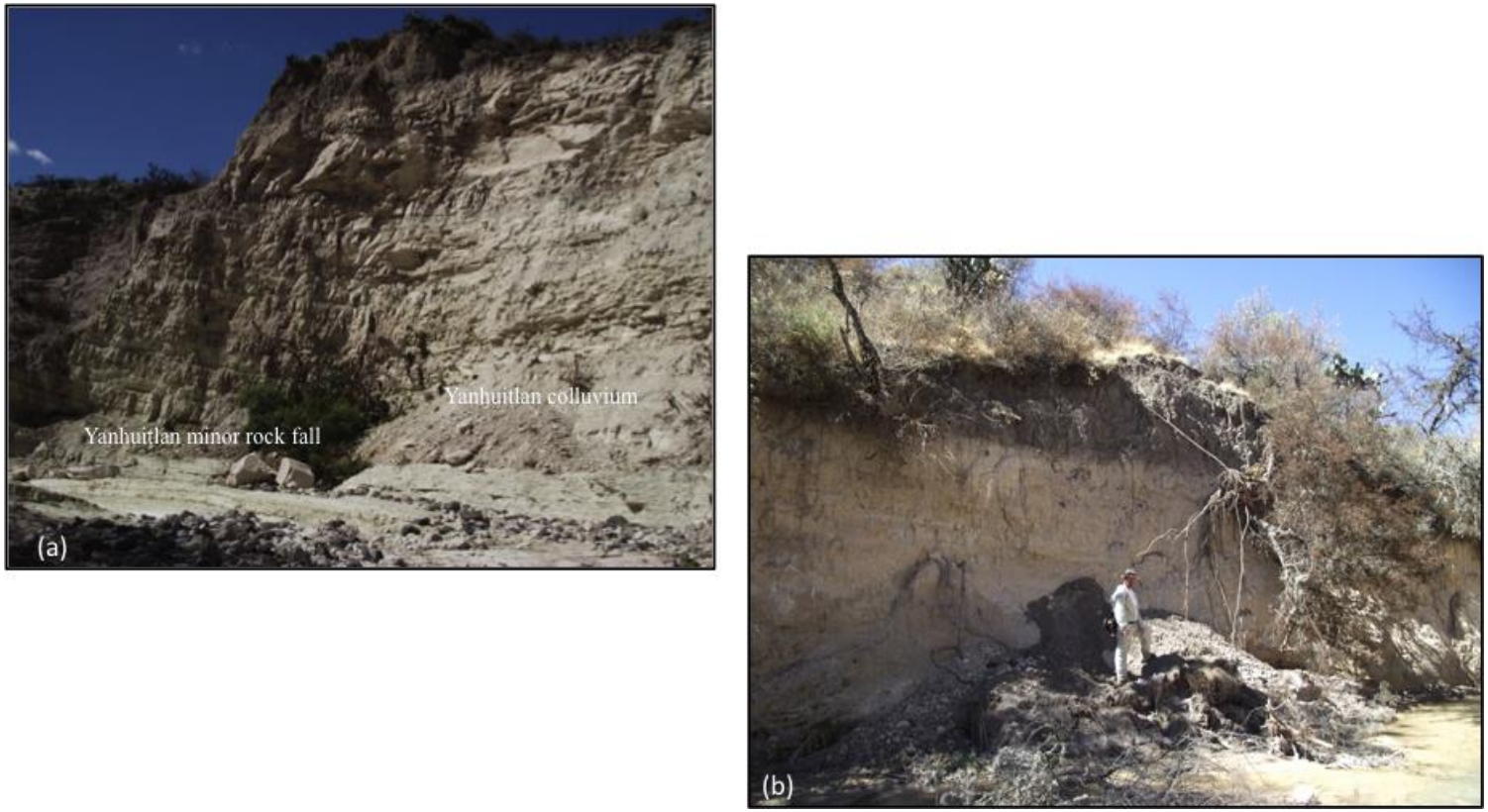

Figure 2.9. Examples of mass wasting in the Yanhuitlan beds (a) and alluvium (b).

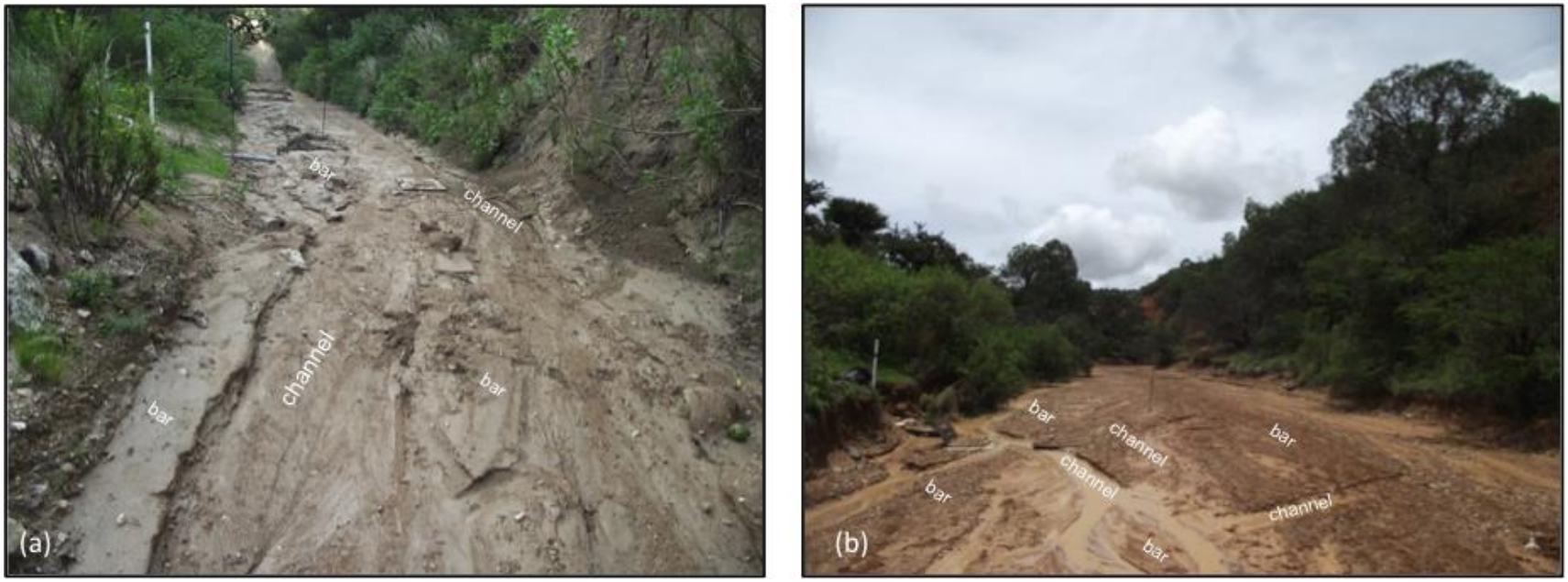

Figure 2.10. Bed topography and morphology in Barrancas Sandage (a) and Sauce (b).

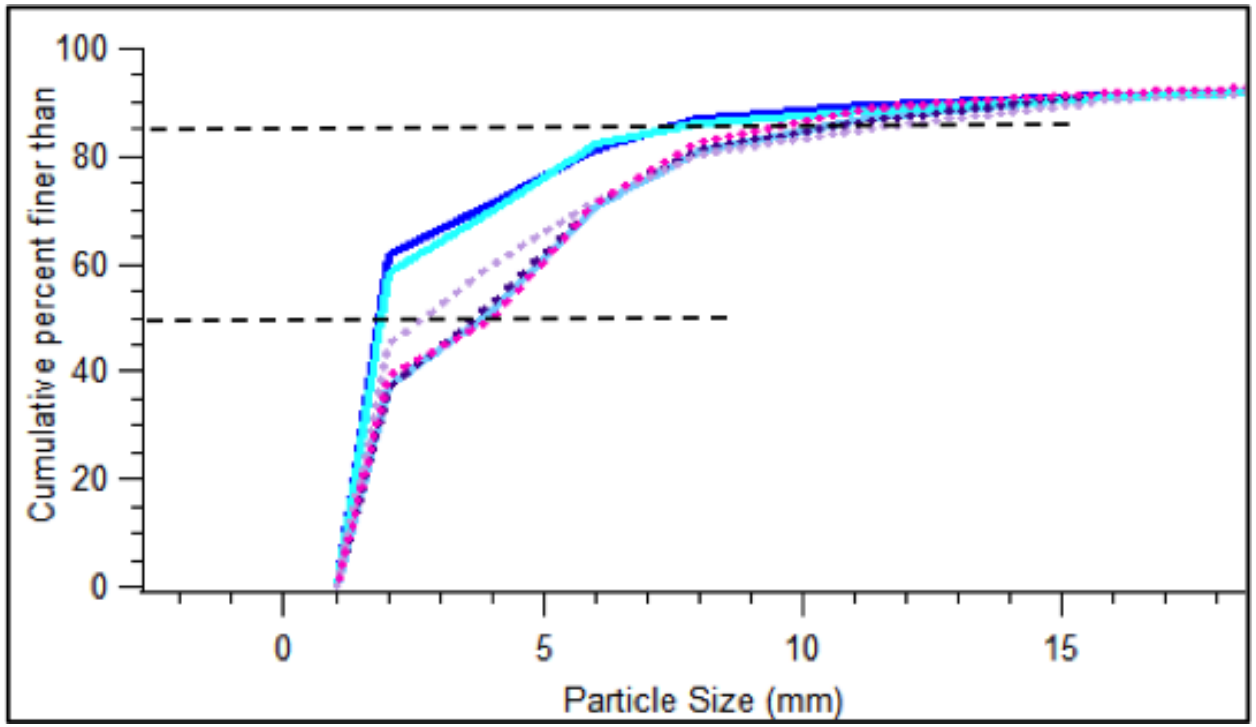

Figure 2.11. Channel bed particle size distribution in Barrancas Sandage and Sauce. The graph shows the cumulative percent finer than a particular particle size of the channel bed in Sandage (shades of blue) and Sauce (pink and purple). The black dashed lines indicate the location of D_{50} and D_{90}.

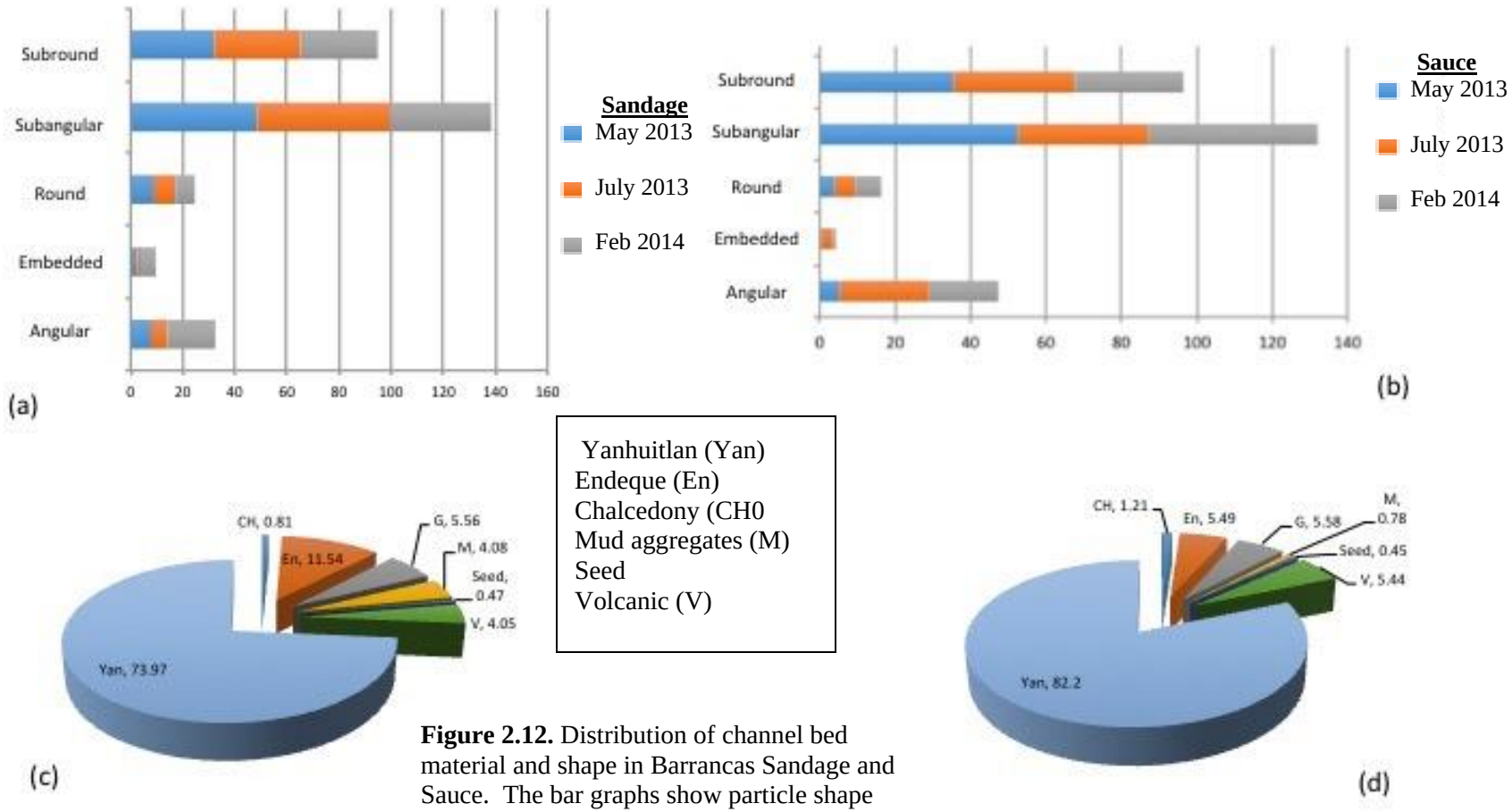

Figure 2.12. Distribution of channel bed material and shape in Barrancas Sandage and Sauce. The bar graphs show particle shape from these separate studies in Sandage (a) and Sauce (b) between 2013-2014. The pie graphs show the distribution of material in Sandage (c) and Sauce (d).

Figure 2.13. Scour-and-fill stratigraphy of the scouring chains in Barrancas Sandage and Sauce. Note the generally massive deposits of poorly sorted sand and fine gravel deposits in both Sandage (a) and Sauce (b). The blue polygons in 2.13a outline a poorly sorted layer of finer sediments. The blue polygon in 2.13b highlights some larger gravel and pebble sized clasts supported in the matrix. The black arrow indicates the downstream direction. Figure 2.13c illustrates how the scouring chains operate (from Gordon et al., 2004).

(a)

(b)

Figure 2.14. Quaternary alluvial stratigraphy in the Culebra watershed. The red and white alternating patterns on the measuring stick are 20 cm each (a), while the small white tip is 5 cm across (b).

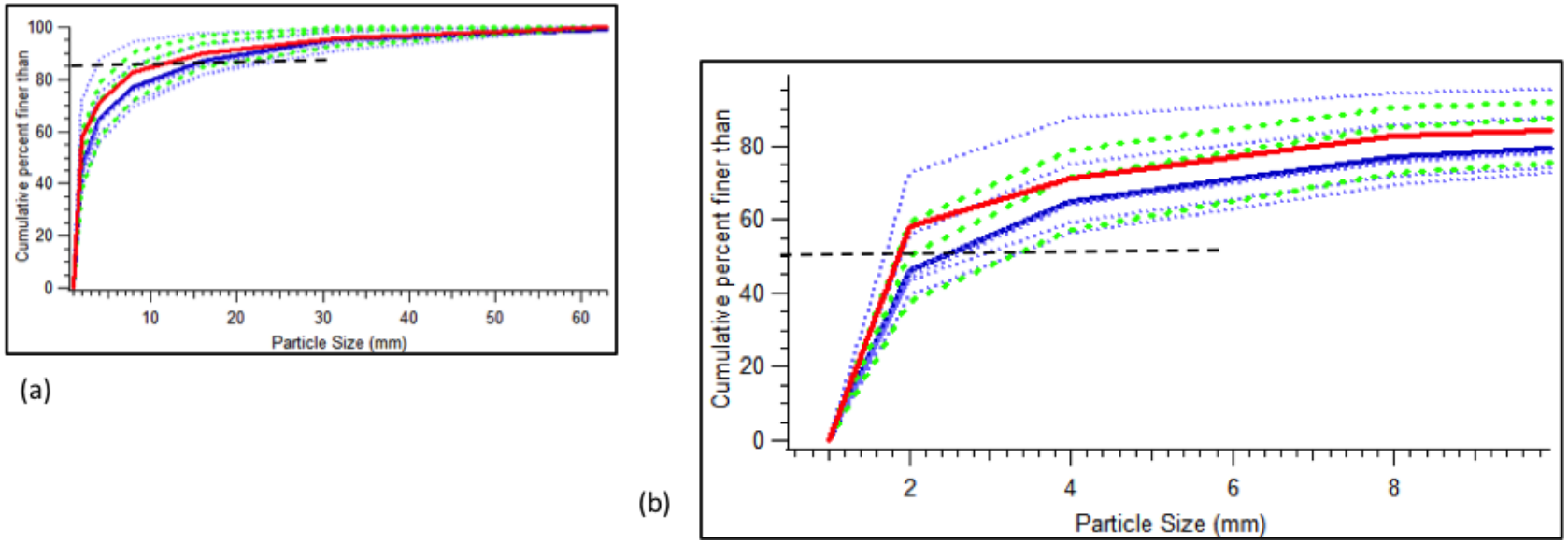

Figure 2.15. Particle size distribution for each floods in Sandage between 2013 (blue and purple) and 2014 (red and green). Figure 2.15b is a focus view of the 0-10 mm particles. The dashed red line marks the D_{50} and D_{85} particle size in Figure 2.15b and a, respectively.

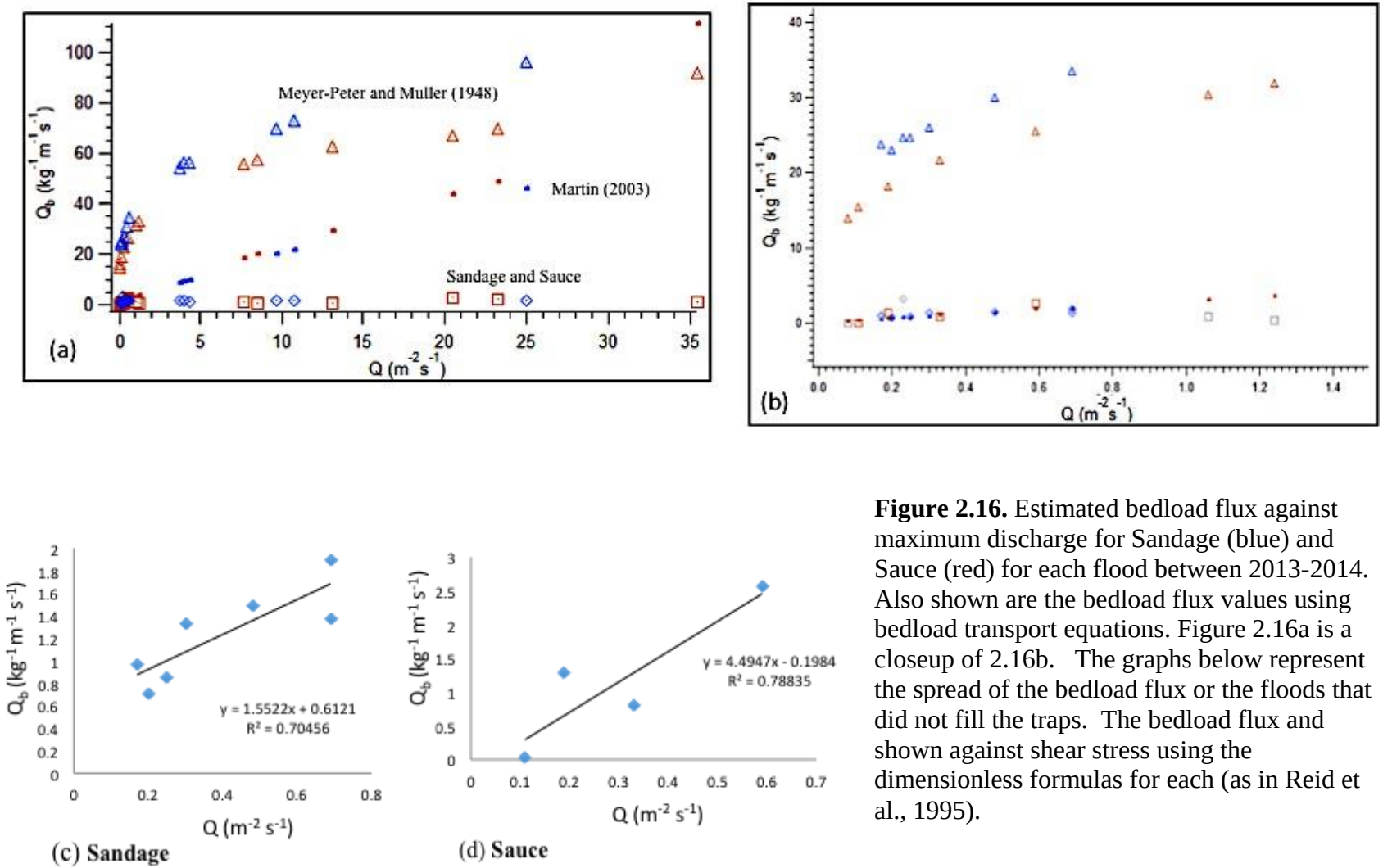

Figure 2.16. Estimated bedload flux against maximum discharge for Sandage (blue) and Sauce (red) for each flood between 2013-2014. Also shown are the bedload flux values using bedload transport equations. Figure 2.16a is a closeup of 2.16b. The graphs below represent the spread of the bedload flux or the floods that did not fill the traps. The bedload flux and shown against shear stress using the dimensionless formulas for each (as in Reid et al., 1995).

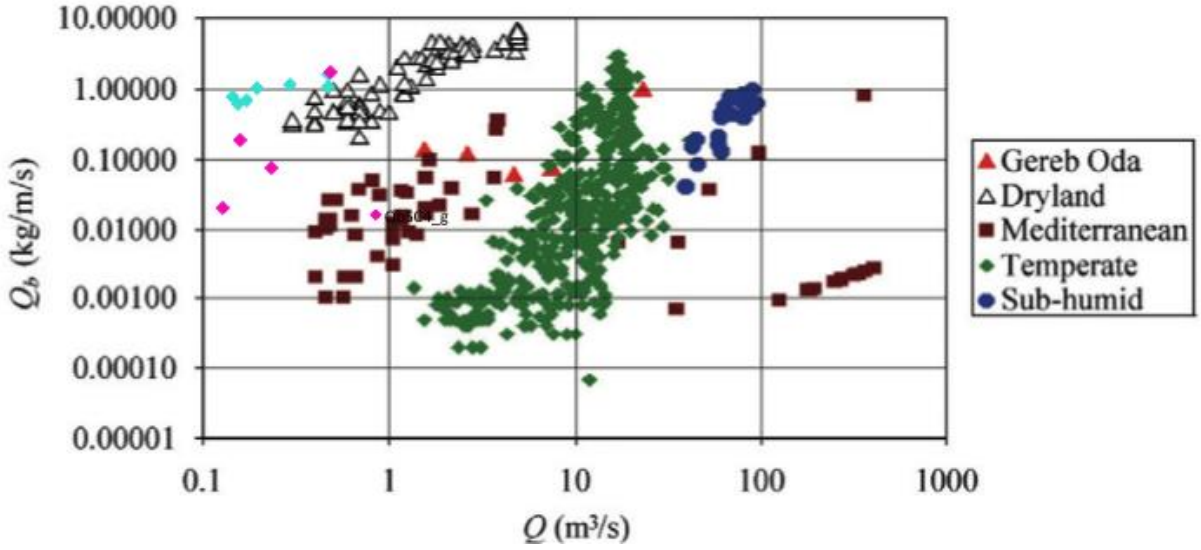

Figure 2.17. Estimated bedload flux values for Sandage (light blue) and Sauce (pink) against streams from other environments (modified from Billi, 2008).

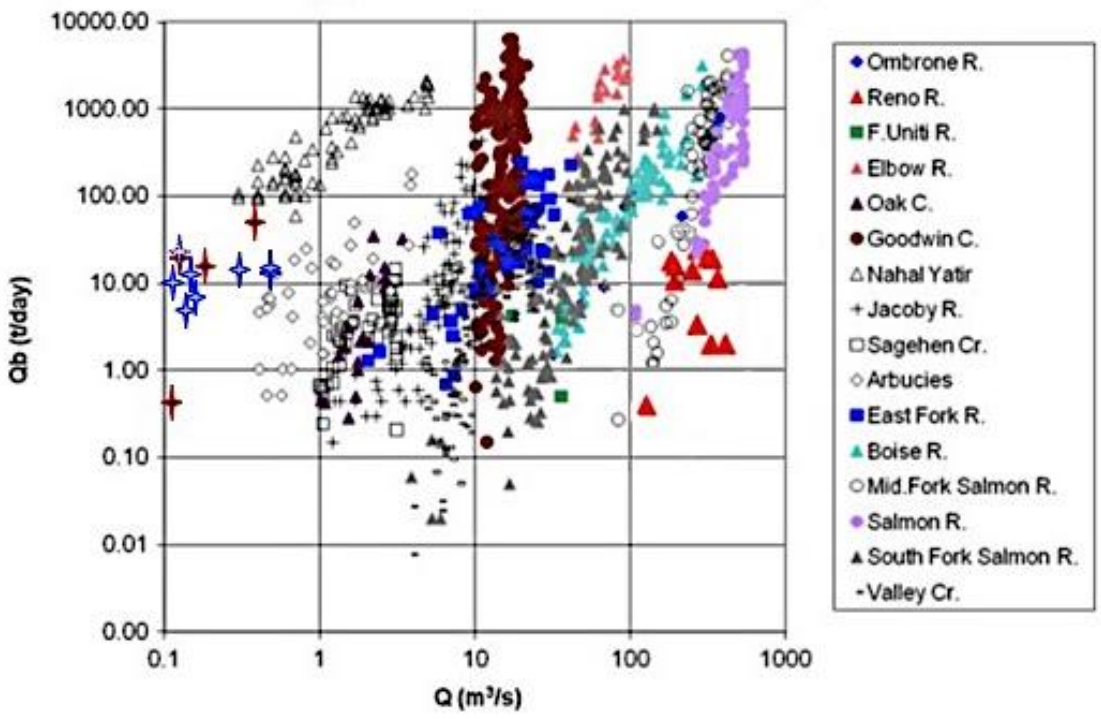

Figure 2.18. Estimated bedload yield in tonnes per day for Sandage (blue crosses) and Sauce (red and black crosses) against streams from other environments (modified from Preciso et al., 2012).

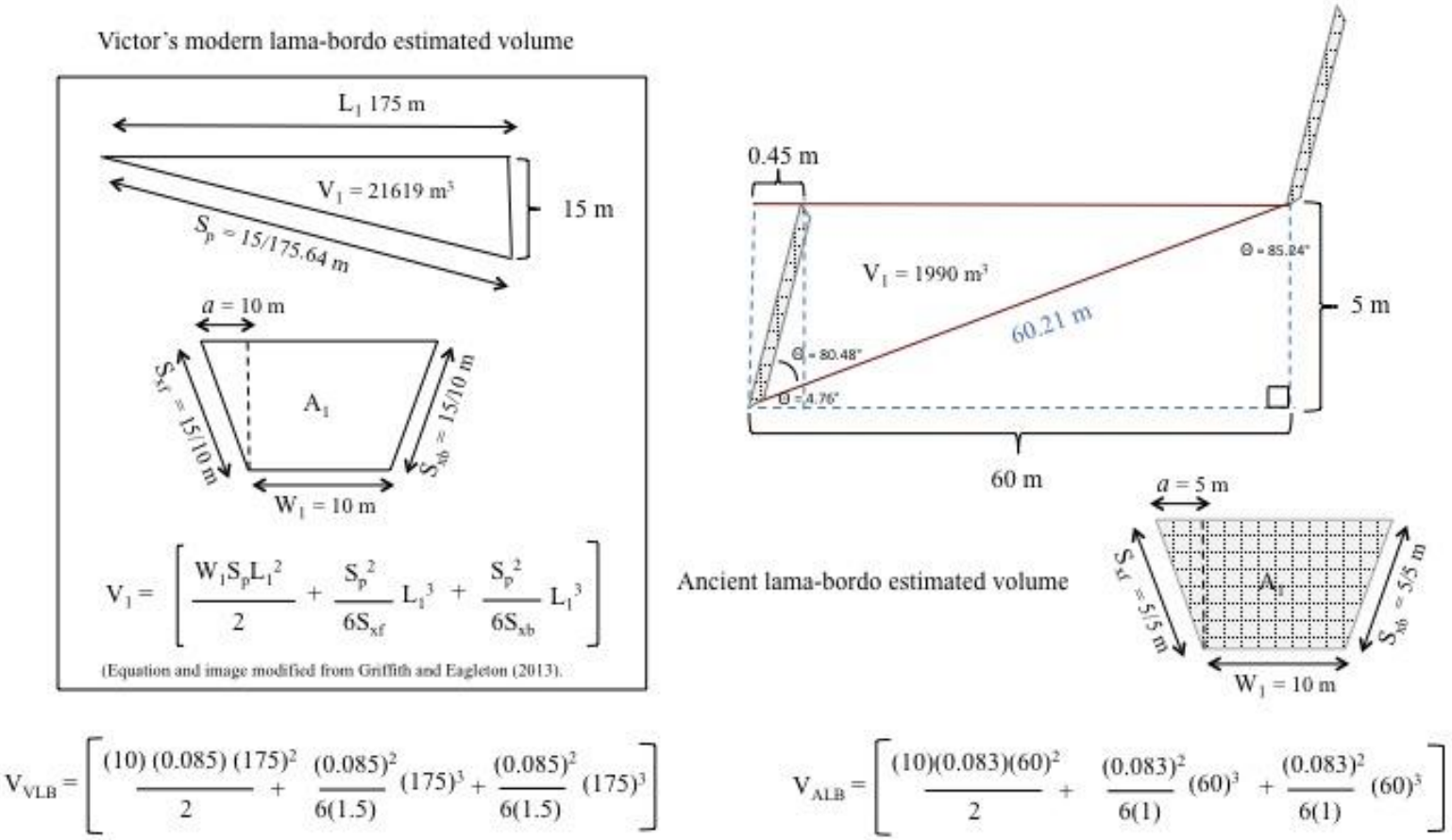

Figure 2.19. Estimations of backfilling behind ancient and modern check dams**.** The figure illustrates the equation and measurements used to estimate the time it would take to fill one of Victor's lama-bordos and one ancient lama-bordo.

Table 2.1. Land cover classification for Barrancas Sandage and Sauce.

Land Cover Class	Sauce %	Sandage %
Forest/vegetation	34	36
Conserved land	0	21
Calcrete	13	18
Bare Rock	28	5
Cropland	21	17
Gullying	4	3

Table 2.2. Scour-and-fill information for Barranca Sandage (a) and Sauce (b) for the flood season of 2013-2014.

(a)

Sandage Flood #	Chain 1 (cm) scour; fill	Chain 2 (cm) scour; fill	Chain 3 (cm) scour; fill
1	2; 1	2; 1	NA
2	0; 0.5	0; 1.5	NA
3	0; 0	7; 7	NA
4	0; 0	20; 15	NA
5	0; 5	18; 22	NA
6	N/A	24; 23	NA
7	N/A	3.5; 3	7; 5
8	1; 1.5	6; 6.5	5; 5
9	2; 0	16; 13	NA
10	4.5; 4	4.5; 0	2; 0
11	0; 3	23; 16	16; 14
12	0; 0.5	0; 0	2; 3
13	21; 21	23.5; 15	5; 3
14	1; 2	5; 5.5	7; 5

(b)

Sauce Flood #	Chain 1 (cm) (scour; fill)	Chain 2 (cm) (scour; fill)	Chain 3 (cm) (scour; fill)
1	14; 17	0; 0	
2	13; 23	0; 0	0; 0
3	4; 0	0; 0.5	0; 0
4	5; 0	6; 0	0; 0
5	15; 21	12; 17	17; 16.5
6	7;7	12;15	NA
7	N/A	N/A	N/A
8	23; 30	22; 19	16; 13
9	2; 2	6; 13	4; 14
10	12; 14	15; 15	0; 5
11	0.5; 0	0; 1	2; 3
12	11; 7.5	13; 5	4; 6
13	13; 8	7; 5	9; 7

Table 2.3. Bedload and flow characteristics for Barranca Sandage during the flood seasons of 2013 and 2014.

Flood	Max Stage (m)	Width (m)	Perimeter (m)	Area (m^2)	Hyd. Radius (m)	Velocity ($m^2\ s^{-1}$)	Q ($m^3\ s^{-1}$)	total sed (kg)	metric t/ day	T (N)	Ω (W/m)	Q_b (kg $m^{-1}\ s^{-1}$)	Reynolds #	Froude #	M-P & M (kg $m^{-1}\ s^{-1}$)	Martin (kg $m^{-1}\ s^{-1}$)
1	0.15	3.8	4.2	0.57	0.14	1.21	0.69	14012.88	14.02	11.48	58.3	1.37	131521.74	0.998	33.26	1.89
2	0.07	3.8	4.2	0.27	0.07	0.73	0.2	7177.8	7.18	5.36	16.42	0.7	37028.99	0.882	22.78	0.61
3	0.08	3.8	4.2	0.31	0.08	0.8	0.25	8657.46	8.66	6.12	20.56	0.85	46376.82	0.904	24.34	0.75
4	0.12	3.8	4.2	0.46	0.11	1.05	0.48	15193.92	15.2	9.18	40.47	1.49	91304.35	0.969	29.77	1.37
5	0.39	4.25	4.45	1.66	0.38	2.42	4.02	19520.98	19.53	31.49	339.03	1.71	683913.05	1.238	55.03	9.02
6	0.65	4.25	4.75	2.77	0.59	3.5	9.67	19097.28	19.1	49.16	817.22	1.67	1648550.73	1.387	68.75	19.74
7	0.08	3.8	4.2	0.31	0.08	0.73	0.23	33616.32	33.62	6.12	18.76	3.28	42318.85	0.825	24.34	0.69
8	0.075	3.8	4.2	0.29	0.07	0.58	0.17	9865.56	9.87	5.74	13.98	0.97	31521.74	0.677	23.57	0.53
9	1.2	4.75	5.1	5.7	1.12	4.39	25.03	20638.56	20.64	94.47	2114.98	1.61	3817391.31	1.281	95.28	46.01
10	0.09	3.8	4.2	0.35	0.09	0.86	0.3	13576.64	13.58	6.89	24.86	1.33	56086.96	0.916	25.8	0.89
11	0.39	4.25	4.45	1.66	0.38	2.6	4.31	14920.32	14.93	31.49	364.25	1.31	734782.61	1.33	55.03	9.62
12	0.36	4.25	4.45	1.53	0.35	2.46	3.77	16440.32	16.45	29.07	318.13	1.44	641739.14	1.31	52.88	8.53
13	0.67	4.5	4.75	3.02	0.64	3.57	10.77	21072.52	21.08	53.65	909.75	1.74	1733260.87	1.394	71.82	21.72
14	0.15	3.8	4.2	0.57	0.14	1.21	0.69	19386.08	19.39	11.48	58.3	1.89	131521.74	0.998	33.26	1.89

Fluid density *pg*	1015 kg m^{-3}
Approx. bulk density	1347 kg m^{-3}
Slope	0.0085
kinematic viscosity	0.00000138 $m^2\ s^{-1}$
D50	2 mm
D85	11 mm

Table 2.3. The table shows the bedload and flow characteristics for Barranca Sandage during the flood seasons of 2013 and 2014.

Table 2.4. Bedload and flow characteristics for Barranca Sauce during the flood seasons of 2013 and 2014.

Flood	Max Stage (m)	Width (m)	Perimeter (m)	Area (m^2)	Hyd. Radius (m)	Velocity ($m^2\ s^{-1}$)	Q ($m^3\ s^{-1}$)	total sed (kg)	metric t/ day	T (N)	Ω (W/m)	Q_b ($kg\ m^{-1}\ s^{-1}$)	Reynolds #	Froude #	M-P & M ($kg\ m^{-1}\ s^{-1}$)	Martin ($kg\ m^{-1}\ s^{-1}$)
1	0.51	10.55	11.54	5.38	0.47	3.8	20.46	84460.32	84.47	45.34	1989	2.97	1405087	1.71	66.03	43.56
2	0.035	10	10.33	0.35	0.04	0.52	0.19	34801.92	34.81	3.3	17.84	1.29	13289.86	0.9	17.93	0.66
3	0.025	10	10.33	0.25	0.03	0.42	0.11	691.22	0.7	2.36	10.09	0.03	7518.12	0.84	15.21	0.4
4	0.02	10	10.33	0.2	0.02	0.36	0.08	143.64	0.15	1.89	6.91	0.01	5144.93	0.81	13.64	0.29
5	0.35	10	10.33	3.5	0.34	2.43	8.5	16665.28	16.67	32.95	825.92	0.62	615543.5	1.32	56.3	19.93
6	0.07	10	10.33	0.7	0.07	0.83	0.59	69153.92	69.16	6.59	56.77	2.57	42304.35	1.01	25.25	1.84
7	0.1	10	10.33	1	0.1	1.05	1.06	23234.72	23.24	9.42	102.49	0.87	76376.82	1.07	30.16	3.12
8	0.9	11.25	11.54	10.13	0.88	3.5	35.44	28226.02	28.23	85.31	5704.91	0.93	3779348	1.96	90.55	111.27
9	0.05	10	10.33	0.5	0.05	0.66	0.33	21532.32	21.54	4.71	32.04	0.8	23876.82	0.95	21.38	1.11
10	0.33	10	10.33	3.3	0.32	2.33	7.7	23122.24	23.13	31.07	748.57	0.86	557891.3	1.3	54.67	18.26
11	0.44	10.55	11.54	4.64	0.41	2.83	13.13	15909.84	15.91	39.12	1275.95	0.56	901362.3	1.37	61.34	29.35
12	0.11	10	10.33	1.1	0.11	1.12	1.24	8033.96	8.04	10.36	119.69	0.3	89195.66	1.08	31.62	3.58
13	0.55	10.55	11.54	5.8	0.51	4	23.2	56720.32	56.73	48.89	2255.58	2	1593406	1.73	68.56	48.72

Fluid density *pg*	1102 kg m^{-3}
Approx. bulk density	1625 kg m^{-3}
Slope	0.009
kinematic viscosity	0.00000138 $m^2\ s^{-1}$
D50	4 mm
D85	11 mm

Table 2.4. The table shows the bedload and flow characteristics for Barranca Sandage during the flood seasons of 2013 and 2014.

CHAPTER 3

LATE PLEISTOCENE AND HOLOCENE ARROYO CYCLES OF THE MIXTECA ALTA, OAXACA, MEXICO[2]

[2] Holdridge, G., Leigh, D. S., Bernal, J.P., and Kowalewski S. To be submitted to *Palaeogeography, Palaeoclimatology, Palaeoecology*.

Abstract

Arroyos are incised, ephemeral dryland streams that aggrade and incise on a cyclical timescale. Arroyo studies are integral to understanding landscape evolution in drylands, but the potential climatic drivers of arroyos are poorly understood. Additionally, human activities in the late Holocene confound climatic influences on arroyo cycles, making it difficult to discern the dominant drivers of erosion and sedimentation in these dryland systems. This paper presents a study on the arroyo cycles in the semi-arid environment of the Mixteca Alta, Oaxaca, Mexico. The characteristics and chronology of the alluvium-paleosol sequences from two watersheds in Coixtlahuaca (this study) and one in Nochixtlan (Mueller et al., 2012) were examined and compared to the regional $\delta^{18}O$ signal from stalagmites from Guererro that date from the terminal Pleistocene to the late Holocene (Bernal et al., 2011; Lachniet et al., 2013). In order to better understand the impact of climate change before widespread agriculture began in the region, the results corresponding to the pre-agricultural era (the terminal Pleistocene through the middle Holocene) were compared to those from the agricultural era in the late Holocene. Overarching regional paleoclimatic conditions partially explained periods of incision, aggradation and paleosol formation, while studies on present-day climate and dryland stream systems offered additional insight on various aspects of arroyo cycles. During the late Holocene, sedimentation rates were estimated to be higher in association with widespread agricultural lama-bordos (i.e., check dams) than in the previous 15,000 years. The lama-bordos were very effective sediment traps, and they supported increasing populations that took advantage of widespread aggradation. In sum, the combination of paleoenvironmental and paleoclimatic information, archaeological material, and modern analogues of arroyos help explain the impact of climate change and human activities on the various geomorphic processes involved in arroyo cycles.

3.1 Introduction

Arroyos are flat-bottomed, incised ephemeral channels with steep walls, typically located in arid to semi-arid environments (Bull, 1997). Studies of recent arroyo formation suggest that a combination of external and internal factors affect cutting and filling, including: precipitation intensity and variability, relief, lithology, soil moisture, vegetation type and cover, drainage basin size and connectivity, duricrusts (e.g., calcrete), and human activities (e.g., deforestation, agriculture, and overgrazing) (e.g., Graf, 2002; Poesen et al., 2003; Schumm, 2005; Valentin, et al 2005). Although, it is recognized that arroyo cycles develop due to a multifarious combination of internal and external factors, in most contexts, human activities and/or climatic fluctuations exert the most influence (Harvey and Pederson, 2011). Arroyo cycles involve incision and aggradation on a cyclical timescale, though it is unclear on what timescale and to which climate phenomena these landforms are responding (Bull, 1991; Mann and Meltzer, 2007). Whether a stream is degrading or aggrading is in part linked to its internal thresholds involving the balance between sediment supply versus water supply (Schumm and Hadley, 1957; Schumm, 2005). However, it is uncertain how external human and/or climatic drivers interact with internal thresholds to produce threshold-crossing adjustments on a regional scale (Prosser et al., 1994; Perroy et al., 2012).

Waters and Haynes' (2001) seminal paper (building on previous research, e.g., Bull, 1997) demonstrated that arroyos can form from climate fluctuations alone. Various climatic factors have been suggested to cause arroyo cycles (as summarized in Hereford, 2002), including the dry-wet-dry fluctuation model, the base level model and variants of the first model, such as wet 'cycles' occurring in an overall dry period (Butzer et al., 2008). Other investigations have invoked more process-based connections, such as the importance of rain intensity (Harvey and

Pederson, 2011), and the relationship between alluvial fills and flood magnitude/frequency (Ely, 1997). Various studies have proposed climatic mechanisms propelling arroyo cycles, such as increased El Niño Southern Oscillation (ENSO) intensity (Waters and Haynes, 2001), and fluctuations in the North American Monsoon strength (Mann and Meltzer, 2007), though these relationships are still unresolved.

Studies of soil erosion during recent (e.g., Walling and Collins, 2008; Svoray and Markovitch, 2009) and prehistoric (e.g., O'Hara et al., 1993; Waters and Ravesloot, 2000; Wilkinson, 2005) times corroborate that human activities, such as agriculture and herding, influence gullying. It is generally agreed that some combination of human and climatic factors have resulted in widespread gully formation and erosion in drylands during the late Holocene period (Bull, 1997; McAuliffe et al., 2001; Avni, 2005; Eriksson, et al., 2006; Borejsza and Frederick, 2010; Constante et al., 2010). However, it is not always easy to identify which anthropogenic factor led to landscape degradation in an area, and it is extremely difficult to determine the degree to which climate versus human activities influence arroyo cycles. Therefore, the history of arroyo cycles and their link to climatic stimuli must be established before attempting to understand the connection between human activities and arroyo cycles (Bull, 1991; Hereford, 2002; Harvey and Pederson, 2011).

Much of the difficulty in deciphering arroyo cycles is due to the relatively poor chronological resolution of alluvial stratigraphy as well as the lack of a locally or even a regionally continuous, high-resolution climatic record, such as one that can be obtained from speleothems. Without external environmental proxies to provide the general climatic trend, it leaves the interpretation of the paleohydrologic record to be derived from alluvium-paleosol sequences that are susceptible to the problem of equifinality (Graf, 1979; Knox 1993; Nordt,

2004). A study by Harden et al. (2010) combined over 700 dates from deposits in the southwestern United States into cumulative probability density function plots and compared them to the $\delta^{18}O$ record from a stalagmite from Pink Panther Cave in Arizona studied by Asmerom et al. (2007). This comparison of dated slackwater and other alluvial arroyo deposits against the stalagmite proxy data has increased our understanding of the relationship between past hydrology and climate. However, despite this and other studies on arroyo cut-and-fill stratigraphy, many questions still remain about the precise nature of overarching climatic phenomena that cause regional scale incision and aggradation, and the relative contributions of anthropogenic and climatic drivers in the late Holocene. Furthermore, there are inconsistencies in the approach to studying arroyos. For example, many studies in the southwestern U.S. emphasize dating arroyo incisions and the sediment fills of the arroyos, while in Mexico many studies focus on paleosols. Finally, there is a need for more rigorous qualitative analyses between climatic fluctuations and alluvial histories.

This paper presents alluvium-paleosol sequences from the Río Culebra in the San Juan Bautista Coixtlahuaca and Santa María Nativitas municipalities, and the Río Inguiro in the Santa Magdalena Jicotlan municipality, both of which are located in the Mixteca Alta, Oaxaca, Mexico. The Mixteca Alta is known for its highly degraded landscape and deep arroyos, locally known as barrancas (Mueller et al., 2012; Leigh et al., 2013). Since the Formative period (local Cruz phase 3,500-2,250 cal BP), prehistoric agriculturalists built check-dams (known as lama-bordos) and terraces to mitigate soil erosion (Kowalewski et al., 2009), and the earliest known lama-bordos were documented in Barranca Sandage in Coixtlahuaca circa 3,500 cal BP (Leigh et al., 2013). Evidence of widespread lama-bordo and terrace constructions is observed by the Post-Classic period (i.e., local Natividad phase, 1,250-430 cal BP) (Kowalewski et al., 2009).

These constructions persist today in various parts of the landscape. The geology, geomorphology and widespread barranca development is similar to the nearby headwaters of the Río Verde watershed in the municipality of Santa María Nochixtlan (Mueller et al., 2012), the results of which are incorporated in the discussion of this paper.

3.1.1 Objectives

The main objectives are twofold: 1) to better understand the relationship between climate and widespread arroyo development during the pre-agricultural era, and 2) to use this climate-arroyo relationship to better discern the impact that humans had during the agricultural era. The results from the Ríos Culebra and Inguiro (this study) were combined with the results from the Río Verde (Mueller et al., 2012) and compared to the stable oxygen isotopic proxy data obtained from stalagmites from various caves in Guerrero (Bernal et al., 2011; Lachniet et al., 2013) to better understand the relationship between the paleoclimate and paleohydrology. For the late Holocene, the grain size data from El Junco Crater Lake (Conroy et al., 2008) was also examined as a proxy for ENSO intensity against the paleosol and alluvium ages. A basin-wide approach, as utilized in this study, can help discern between local developments and intrinsic or complex response and basin-wide response to climatic drivers (e.g., Holliday, 1985).

3.2 Study Area

Stratigraphic investigations were conducted in the arroyos of Coixtlahuaca, Nativitas, and Jicotlan municipalities (Figure 3.1; see Appendix II for coordinates). Profiles in the municipalities of Nativitas and Coixtlahuaca are situated within the Río Culebra watershed (or Culebra watershed), while Jicotlan is located along the Río Inguiro watershed. The profiles in Nochixtlan studied by Mueller et al. (2012) are located in the Río Verde watershed (Figure 3.1).

All of these study sites are located in the Mixteca Alta, Oaxaca, Mexico, which is situated, on average, 2,300 m above mean sea level (amsl). The Mixteca Alta is a part of the Mixteca macroregion, which designates the present area of the Mixtec culture and language groups. The Alta ('high") of Mixteca Alta represents the high altitude, inland semi-arid region, which is distinguished from the Baja ('low") and Costa ("coastal") sub-regions (Balkansky et al., 2000). The Ríos Culebra and Inguiro are situated in the headwaters of the Río Papaloapan, draining the eastern part of the continental divide, created by the Sierra Madre del Sur, towards the Gulf of Mexico. Conversely, the Río Verde watershed drains the western part of this continental divide, towards the Pacific Ocean. Mueller et al., (2012) studied several headwater tributaries to the Río Verde, but their study will be referred to as the Río Verde watershed.

The regional climate is characterized as semi-arid (BSh Köppen classification), with an average temperature of between 13.2-18.6 ºC and receiving an average of approximately 528 mm of rain per year (Servicio Meteorologico Nacional, 2010). The warmest time of the year, May through October, overlaps with the rainy season, which peaks in June and again in September. The high terrain of the Sierra Madre del Sur, in which the Mixteca macroregion is situated, causes a rain shadow in the region, and the North American Monsoon (NAM) is the main source of precipitation. The timing and duration of NAM are predominantly controlled by the movement of the Intertropical Convergence Zone (ITCZ) and the intensity of El Niño Southern Oscillation (ENSO) (Trejo, 2004; Vera et al., 2006). Although no local high-resolution climatic proxies exist for the Mixteca Alta, stalagmite data from Guererro, located 191 kilometers away on a heading of 257° in the Sierra Madre del Sur have been used to estimate high-resolution regional signals of past climate (Bernal et al., 2011; Lachniet et al., 2013). The stalagmite record consists of five different stalagmites from two caves: Juxtlahuaca cave (17°26' N, 99°15' W) and

Cueva del Diablo (18°11' N, 99° 55 W) (Figure 3.1). A strong negative significant correlation (-0.62, with a 5-yr smooth with 0-yr lag) was found between the oxygen isotopes from the Guerreran and rainfall in Oaxaca for the last 128 years (Lachniet and Bernal, accepted in press). These results suggest that the stalagmites from Guerrero can be used as a corollary to the climatic conditions in southwestern Oaxaca from the late Pleistocene to the present (Lachniet and Bernal, accepted in press). The $\delta^{18}O$ isotopic signature from stalagmites is a reflection of the regional climatic processes, which reflects precipitation in the tropics (McDermott, 2004; Fairchild et al., 2006; Lachniet, 2009). Support for regional response to climate also comes from a study on tree growth in Mexico, which indicated that tree growth in southwestern Mexico (as opposed to northwestern and northeastern Mexico) was most sensitive to spring rainfall (April-June), corresponding to the onset of the North American Monsoon (Therrell et al., 2002).

The geology of the study area primarily consists of lower to middle Tertiary siltstones and claystones (shales), referred to as the Yanhuitlan Formation, which is overlain in areas by middle Tertiary volcaniclastics (Teotongo volcaniclastics) and andesites (Cañada Maria andesite and Yucudaac andesite) (Santamaria-Diaz, 2008). Calcrete surfaces (locally referred to as "endeque") are exposed on most hillslopes and barranca development is widespread (Kirkby, 1972; Rincon, 1999; Leigh et al., 2013).

Earthquakes do occur in the Coixtlahuaca District, but no recent major earthquakes or faulting have been documented (Servicio Sismologico Naciónal, 2014). No faults were observed in the Quaternary strata within the survey area based on an extensive pedestrian survey of more than 100 km^2. Since the Tertiary shales are jointed and easily erodible and no recent faults have been observed, it was concluded that the deep incision that characterizes this valley is directly

related to past (and present) climate fluctuations and human activities, rather than tectonic activity or base level change.

The valley fill comprises Quaternary alluvium situated along the mainstem of Río Culebra and its tributaries. The Río Culebra and its tributaries are single-thread dryland streams that have incised from about seven to thirty-seven meters below the ground surface (e.g. the Colonial terrace). The headwaters of the Río Culebra entail an incised spring-fed stream flowing from two sources located along the hillslope of the nearby extinct volcano, Monte Verde, Nativitas.

3.2.1 Archaeology

Archaeological surveys of the Ríos Culebra and Inguiro, and the surrounding areas have shown that the region exhibits a rich material record of cultural changes (Figure 3.2, Table 3.1), especially in the last 3,500 years (Balkansky et al., 2000; Kowalewski et al., 2009). Surveys in 2008 and 2011 indicate that Archaic artifacts exist in the region, but are poorly understood. The Formative period (local Cruz phase) is scattered throughout the Culebra and Inguiro watersheds, but is best preserved along a tributary to the Culebra, Barranca Sandage. The Formative period corresponds to the transition from hunting and gathering to an agricultural way of life (Kowalewski et al., 2009). Since the early Cruz phase, prehistoric agriculturalists built check-dams (locally referred to as lama-bordos) and terraces to mitigate soil erosion (Kowalewski et al., 2009). The earliest known lama-bordos were documented in Barranca Sandage and dated to ~3,500 cal BP (Leigh et al., 2013).

Between 2,250 cal BP to 1,750 cal BP, population remained fairly low during the Ramos phase, but town centers moved to the protected hillslopes. Some agricultural lama-bordos span the entire valley floor. During the early Transición/las Flores phase (1,750-1,250 BP),

population first increased significantly in the Culebra and adjacent watersheds, and then was followed by a sharp population decline and settlement dispersal. Subsequently, during the local Natividad phase (1,250-430 cal BP), population exploded, and one of the major Post-Classic urban centers of the Mixteca emerged in Inguiteria, Coixtlahuaca. Terrace walls are located throughout the valley during this period (Rincon, 1999; Kowalewski et al., 2009).

The Río Verde watershed shares a similar cultural history, including the practice of building lama-bordos and terrace walls that were dated to as early as ~2,990 cal BP (Mueller et al., 2012).

3.3 Methods

After a thorough reconnaissance in the Culebra and Inguiro watersheds, ten profiles were selected for more in-depth descriptions and sampling (Figure 3.3; see Figure 3.1 for location; see APPENDIX II). Arroyo cut-and-fill features and well-represented alluvium-paleosol sequences were selected for examination. The steep, tall, unstable, and erodible nature of arroyo walls made accessing certain strata very dangerous. Thus, most profiles were not recorded in one continuous section. Instead, profiles were described and sampled in several more accessible subsections that combined to represent a continuous section. All of the stratigraphic profiles have been described according to the nomenclature of the USDA Soil Survey (Soil Survey Staff, 1993). For each recorded profile, approximately 50 grams of sediment were obtained by sampling at arbitrary intervals of 30 cm or according to horizon boundaries when they were abrupt. Paleosols were identified and distinguished from unweathered alluvium by a combination of two or more of the following factors: (1) darker color; (2) clear expression of pedogenic structure; (3) evidence for translocation of clay; and (4) evidence for pedogenic

translocation of other minerals (e.g., $CaCO_3$ or Fe_2O_3) (Birkeland, 1984; Schaetzl and Anderson, 2005). It is acknowledged that paleosols form in alluvium and that alluvium serves as the parent material for paleosols. Accordingly, the term "alluvium" will be used to designate the unweathered or apedal sediment that separates paleosols.

3.3.1 Soil Residence Time and Radiocarbon Dates

Multiple samples containing charcoal flecks and organic-rich buried A horizons were taken for ^{14}C dating (Table 3.2). Radiocarbon accelerator mass spectrometry (AMS) analyses were done at the Center for Applied Isotope Studies (CAIS) at the University of Georgia using standard pretreatment techniques. The software program CALIB (Stuiver et al., 2015) was used to calibrate all of the ages based on the INTCAL13 database (Reimer et al., 2013). All ages are presented as the median age in calibrated years before present (cal BP) unless otherwise noted (Table 3.2). All age ranges are equivalent to the two-sigma range calculated by the CALIB software from the original radiocarbon age.

Charcoal samples comprised 23 of 25 alluvium ages and ten of the 22 paleosol ages. The remaining ages came from bulk organic material from buried A horizons and in two instances redeposited organic material was dated to represent alluvium deposits. A total of 31 radiocarbon dates from the Río Verde (Mueller et al., 2012) were incorporated into this study, all of which were from organic-rich buried A horizons.

Problems with both charcoal and bulk organic dates are recognized. For example, both can be eroded and redeposited into much younger alluvium and yield dates much older than the actual time of alluvial deposition. Bulk organic ages can also be affected by soil residence time (SRT) and appear older (Rincon, 1999; Leigh et al., 2013) than the time of burial of the soil surface. Observing the dates against depth for each profile (Figure 3.3), there are a few

instances of inverse stratigraphy illustrating the incorporation of older organic material into younger A horizons, and these inverted ages were not considered further (Figure 3.3, Table 3.2). Age-depth models were constructed with the program R (version 0.98.1103) using the package for 'classical' age-modelling (CLAM) of radiocarbon sequences (Blaauw, 2010; version 2.2), which helped to assess the accuracy of bulk ages versus charcoal ages. It was found that in most cases both were accurate, but the charcoal ages appear more consistent.

In order to consider the SRT for the bulk organic ages, the difference between calibrated charcoal and bulk ages obtained from the organic matter of buried A horizons at five different profiles was examined. The charcoal ages were, on average, 273 years younger than the bulk organic ages with a standard deviation of 22 years. Since there is inherent variability in the calibrated radiocarbon ages, a t-test was conducted to determine if the average variability in the original calibrated date range of the charcoal and organic bulk ages was significantly different from the average difference between the calibrated charcoal and organic bulk ages from the same strata. No significant difference was observed between the 2-sigma error of the original calibrated age range and the average difference between the calibrated charcoal and organic bulk ages from the same strata (see Appendix III). Since only the calibrated age range was incorporated into the qualitative analyses, the 2-sigma error of the original calibrated ages were considered to represent a sufficient amount of variability to compensate for the SRT of an organic age.

3.3.2 Geochemical Analyses, Particle Size Determination and Sedimentation Rates

Geochemical studies involved total elemental analysis on later strata using the four-acid "near-total" procedure (ALS Geochemistry, ME-ICP61). The results of 23 elements were provided in percentages or parts per million. Two of the elements were used to examine

weathering (as described in Buggle et al., 2011). Organic and inorganic content was estimated using the loss-on-ignition procedure applied to subsamples of strata from several profiles. To estimate the percentage of organic carbon, subsamples of each stratum were oven-dried at 105°C, weighed and then heated in a muffle furnace at 550°C for four hours (as recommended in Heiri et al., 2001). After, the samples were cooled, weighed, and then reheated to 950°C for two hours to burn off the inorganic carbon (as in Heiri et al., 2001).

All of the sampled strata were air-dried and sieved for particle size determination using the <2mm U.S. sieve size to seperate <2 mm from >2 mm. The < and >2 mm fraction was weighed and converted to percent based on the total weight. Sedimentation rates were modeled using the CLAM program (Blaauw, 2010) in R software (R software team, 2008). The CLAM program models the sedimentation rate based on the relationship between age and depth of each profile's stratigraphy.

3.3.3 Qualitative Analyses

The calibrated age range of the dated samples from the Ríos Culebra, Inguiro and Verde watersheds were combined to generate summed probability curves. Two different summed probability curves were created using the two-sigma calibrated age range: one for paleosols, and one for alluvium (see APPENDIX III). In order to discern the relationship between past climatic drivers and paleoenvironmental change, the summed probability curves and the $\delta^{18}O$ isotope values from the Guerreran stalagmites were examined qualitatively from the late Pleistocene to the middle Holocene**.**

Difficulties in distinguishing wet versus dry in the $\delta^{18}O$ isotope record during the late Holocene resulted in exploring alternative paleoclimatic proxies for ENSO. Bernal et al. (2011) demonstrated that ENSO was the dominant climatic driver during the late Holocene, following

the shift of the ITCZ towards the south (Haug et al., 2001). The grain size data, in particular the sand percentage data from the El Junco Crater Lake in the Galápagos Islands is a proxy for ENSO frequency and intensity in the eastern tropical Pacific (Conroy et al., 2008). Conroy et al. (2008) found that the amount of sand (%) increased during increased El Niño activity (the negative anomaly of ENSO), which in El Junco corresponds to an increase in the number of intense rainfall events. The sand percentage data were examined against the $\delta^{18}O$ isotope record and the summed probability plots for the late Holocene to discern any relationships between them. The ENSO variability determined from the El Junco record is considered only as an approximation of regional patterns in the eastern Pacific, and it is realized that local conditions in southwestern Mexico may differ to an extent.

3.4 Results

The alluvium-paleosol stratigraphy of ten profiles along the Ríos Culebra and Inguiro were examined in detail (Figure 3.3; see Appendix II for profile descriptions). Two profiles were selected along the middle section of the Río Culebra (profiles C2 and C3), while profile C1 was located in the headwaters of the Río Culebra along the second-order tributary of Barranca Sauce. Four profiles were selected for study along the upper, middle, and lower sections of the tributary Barranca Sandage (profile S4, S5, S6 and S7), and one profile was examined along a first-order tributary to Barranca Sandage (profile S8). Another profile was recorded along the lower section of the tributary Barranca Sandaxne (X9). Finally, one profile was studied along the mid-section of the Inguiro mainstem (I10). The majority of the profiles were studied along Barranca Sandage as it contained the most continuous and well-preserved archaeological evidence. Some of the profiles studied along this barranca were located adjacent to lama-bordos.

3.4.1 Profiles on the Río Culebra

Profiles C1, C2 and C3 reflect much of the long-term depositional and erosional history of this watershed. The headwater location, profile C1, contains well-preserved cut-and-fill stratigraphy, with four clearly recognizable cuts (in addition to the present-day incision) and four fills. Three paleosols bury all of the cut-and-fill stratigraphy, while one early paleosol is situated at the bottom of the profile, into which all of the later arroyos incised.

Profile C2 is located along the midstream of the Río Culebra (Figure 3.4) and contains much information concerning the depositional and landscape history of the basin. Its deposits span the late Holocene to the late Pleistocene (and possibly earlier). Ten paleosols formed in these deposits, providing information about the long-term changes in paleohydrology and stability of the basin. A sequence of tuff deposits overlying a debris flow deposit sets this profile apart from the others, and indicates a time of volcanism and instability in the region sometime during the late Pleistocene.

Profile C3 is located at the confluence of Barranca Sandaxne and Río Culebra. This profile reveals much about the end of the late Holocene with eight meters of fill corresponding to the last 1,200 years. Three weak paleosols with A-C and A-Bw-C sequences formed within these eight meters of late Holocene deposits, alternating with alluvium deposits. Below the eight meters of deposits, about 24 m of stratigraphy was either covered by recent colluvium or was too steep to sample.

3.4.2 Barrancas Sandaxne and Sandage

Two profiles located along the lower sections of Barrancas Sandaxne (X9) and Barranca Sandage (S4) contain evidence for a long alluvial history spanning the late Pleistocene through the late Holocene, though possibly not as continuous as in the Río Culebra. The X9 profile is

located along the downstream part of Barranca Sandaxne after it joins with Barranca Sandage. Profile X9 accounts for approximately 15,000 years of stratigraphy, based on a date from the bottom of this profile, which is around 23 m below the ground surface. Colluvium covered the strata between 9.30 m and 15.50 m below the ground surface, impeding examination. The studied portion of Profile X9 consists of many alluvial deposits interstratified with four major paleosols. The paleosols span the terminal Pleistocene to the middle Holocene, and include two Ab-Bt soil horizon sequences, and two Ab-Bw soil horizon sequences.

S4 is another profile with a long depositional history, which is located on the downstream part of Barranca Sandage, just before it links up with Barranca Sandaxne. The upper seven meters of S4 correspond to the middle and late Holocene, while the bottom six meters span from the early Holocene into the late Pleistocene. This profile contains five paleosols, three of which belong to the terminal Pleistocene-early Holocene transition. The two other paleosols consist of thick cumulic buried A horizons dating to the middle and late Holocene.

The remaining four profiles (S5, S6, S7, and S8) studied along Barranca Sandage contain late Holocene strata, including profiles that are directly associated with lama-bordos. The archaeology associated with the stratigraphy will be addressed in the discussion section (5.1). S5 is in the mid-section of Barranca Sandage and is associated with a well-preserved lama-bordo, behind which 12 m of Holocene alluvium were trapped (Figure 3.5). Profiles S6 and S7 are also located along the mid-section of Barranca Sandage, but closer to the headwaters than S5. S6 is situated about 20 m upstream from a lama-bordo and has five paleosols, three of which are within the upper three meters of strata and belong to the late Holocene. The only profile studied along a first-order tributary was S8, situated along the hillslopes of Barranca Sandage. S8 has

two important paleosols, which entail an Ab-C sequence and an Ab-AB-Bk separated by a thin layer of alluvium.

3.4.3 Río Inguiro

Only one profile, I10, was studied along Río Inguiro in Jicotlan. Profile I10 is located in the upper section of this river, just below the headwaters. The most interesting aspect of this profile, which is set along a meander bend, is the remnants of several lama-bordos. The profile contains five paleosols, with intermittent sediments all dating to the late Holocene. A small stone feature, possibly a wall, is situated above the lowest sediments dating to approximately 4,100 cal BP.

3.4.4 Alluvium-Paleosol Stratigraphy

The profiles present information on the environmental history of the Culebra and Inguiro watersheds since the late Pleistocene to the present. The stratigraphy will be presented according to the following time periods: late Pleistocene (~27,000 to 14,700 cal BP); terminal Pleistocene (14,700 to 11,700 cal BP); early Holocene (11,700 to 8,200 cal BP); middle Holocene (8,200 to 4,300 cal BP); and late Holocene (4,300 cal BP to the present).

3.4.4.1 Late Pleistocene (~27,000-14,700 cal BP)

Only three strata were dated to this period, two of which were paleosols having an age between 30,000 and 27,000 cal BP, while the other stratum comprised a layer of alluvium dating to 15,203 cal BP. Thick (> 2m), dark, cumulic buried A horizons having slickensides were observed in the deepest portions of the stratigraphic profiles at various places in the Culebra and Inguiro watersheds. The upper 5-10 cm of one of these thick buried A horizons was dated along Barranca Sandage, which returned an age of 27,677 cal BP. The other Ab horizon, also located on Barranca Sandage, was dated indirectly by radiocarbon dating of an in-situ horse jaw with

seven teeth (identified by Eduardo Jimenez-Hidalgo), resulting in an age of 29,716 cal BP. No strata have been dated in the Verde watershed corresponding to the late Pleistocene, though early strata are mentioned in the text (Mueller et al. 2012).

A layer of charcoal within a silty matrix, 23 m below ground surface at site X9, had an age of 15,203 cal BP. Part of the cut-and-fill stratigraphy is observed in the lower strata, which contains planar beds at the bottom. Above these beds was a fining upward sequence of large gravel to sand with trough cross-bedding that was covered by a layer with flame structures.

3.4.4.2 Terminal Pleistocene (from 14,700-11,700 cal BP)

Paleosols dating between 13,000 and 12,000 cal BP are situated at the C2 and the X9 profiles. At profile X9, a buried A horizon with abundant charcoal was dated to 12,583 cal BP. This weak paleosol (Ab-Bw-C sequence) was covered by nine meters of alluvium including trough cross-bed stratigraphy, and silty and clay rhythmites. At the top of the thick alluvium was another weak paleosol (Ab-Bw-C sequence), which was capped with by another layer of alluvium with an age of 10,474 cal BP. At profile S4 an alluvial deposit had an age of 11,119 cal BP. At profile C1, an age of 12,520 cal BP corresponded to the middle layers of one of the fills containing charcoal. The bottom of the cut-and-fill at profile C1 was fairly rapid as evidenced by rip-up clasts of this buried A. At profile C2 an Ab horizon (12,717 cal BP) with moderate subangular blocky structure, silty loam texture, and a few calcium carbonate ($CaCO_3$) nodules had formed over silt deposits (A-C sequence). Overlying this Ab, a well-developed paleosol with an A-AB-Btk-Ck sequence developed below alluvium deposited at approximately 9,063 cal BP. This buried A-AB has a cumulic component, and the Btk has $CaCO_3$ nodules, clay films, prismatic structure, and slickensides in its lowermost part.

Some stratigraphy was situated below strata dating to the terminal Pleistocene, making it unclear to which period they belong (e.g., terminal or late Pleistocene). For example, paleosols below strata dating to 12,533, 11,119 and 12,717 cal BP were located at profiles C1, S4, and C2, respectively. Some of these paleosols have a darker color (10YR 4/2) medium to strong prismatic structure, and common, prominent slickensides in the buried A horizon (e.g., indicating polygenesis); whereas other Abs have a browner color (10YR 5/3) and medium to strong subangular blocky structure. Most of the soils have a B horizon, varying between a Bt, Bk, Btk or Bw.

At profile C2, a colluvial layer beneath a terminal Pleistocene paleosol dated at 12,717 cal BP buries a tuff deposit consisting of a massive deposit of medium sand-sized particles. Situated below the tuff is a debris flow with gravel, cobbles, and boulders in a sandy loam matrix. Tuff has been identified in other areas of the Culebra, especially along its mid-section (pers. Obs.; Rincon, 1999) suggesting at one point there must have been an eruption nearby; though at a later date than the andesite flows dating to the middle Tertiary (see Santamaria-Diaz et al., 2008). The paleosol below the debris flow is characterized by an Ab-Bk sequence with manganese nodules, which is about a meter and a half below the bottom of the tuff. Underneath about two meters of unaltered alluvium lies a Bw-BC, the overlying Ab having been eroded. Another paleosol sequence is situated about a meter below the former, having an Ab-Btk with few, distinct clay films, and few, very coarse, irregular-to-spherical $CaCO_3$ nodules between peds.

3.4.4.3 Early Holocene (11,700-8,200 cal BP)

Few strata have been directly dated to the early Holocene, but some strata fall between those dating to the middle Holocene and terminal Pleistocene and are possibly early Holocene

layers. An age of 9,063 cal BP dates a Ck horizon at profile C2, and the overlying solum apparently has been eroded away. Preserved above and below this Ck are about 70 cm of alluvial deposits. At profile X9, a thin Ab paleosol sequence is formed above sediments dating to 10,474 cal BP. A-Bw-BC sequence overlies the former paleosol, and the BC had an age of 9,625 cal BP.

3.4.4.4 Middle Holocene (8,200-4,400 cal BP)

Similar to the early Holocene, few paleosols and alluvium have been dated to the middle Holocene. Above the Ab-Bw-BC sequence (mentioned above) at profile X9 lies an A-Bw-C sequence, which had a cumulic Ab with an age of 6,375 cal BP. Profile S4 contains an A-C paleosol sequence with a prominent cumulic Ab with some evidence for colluvial input. The upper and lower part of the cumulic Ab horizon returned two different ages: 6,282-and 6,620 cal BP, respectively. The only middle Holocene date obtained for alluvium comes from a bulk date on an organic deposit at the bottom of a cut nearby site S5, which cuts into the paleosol dated to the late Pleistocene, approximately 27,677 cal BP. The organic deposit has an age of 6,527 cal BP.

3.4.4.5 Late Holocene (4,300 cal BP to the present)

Many paleosols and alluvium are dated to the late Holocene, due to better preservation of younger sediments, as well as slightly biased sampling to obtain geomorphological data relating to the archaeological findings. At approximately ~4,300 cal BP, paleosols were found in several areas in the Culebra watershed. For example, at profile S4, an age of 4,360 cal BP corresponds to a thin A/C horizon, while at profile S6, a buried A of an A-C sequence returned an age of 4,348 cal BP. At profile S8, a well-developed soil sequence of A-AB-Btk-CK formed along the

hillslope, dating to 4,327 cal BP. The Btk has $CaCO_3$ nodules and clay films. A cumulic paleosol having two dates: 3,511 and 3,547 cal BP is observed at profile S7.

Alluvium was dated between ~4,200-2,700 cal BP at profiles I10, S5, and S4. At profile I10, a massive loamy deposit about a meter below the bottom stones of a lama-bordo dates to 4,183 cal BP. Sediments below a lama-bordo at profile S5 had an age of ~3,500 cal BP (as reported by Leigh et al., 2013). Charcoal recovered from an AB horizon returned an age of 3,834 cal BP at profile S4. A massive silty loam deposit at profile S5 with an age of 2,715 cal BP covered a weak paleosol (A-C sequence) dating to ~2,746 cal BP.

Several strata in the Ríos Culebra and Inguiro watersheds date to approximately 2,000 years ago. At profile S7, for instance, two dates on a cumulic Ab returned ages of 2,143-and 2,329-cal BP, respectively. This buried A was associated with a cluster of rocks that possibly represents a lama-bordo. Underlying this buried A is a Bk with $CaCO_3$ concretions. A buried A at profile C2, belonging to an Ab-Btk-Ck sequence, had an age of 2,028 cal BP. The Ab was clearly cumulic, and it contained some iron oxides on its ped faces, which was also observed on the C horizon above it. Profile C1 contains a small channel with evidence for lateral migration ~2,143 cal BP. The Btk of the same Ab-Btk-Ck sequence had clay films, and both the Btk and Ck had $CaCO_3$ nodules. An age of 1,913 cal BP dates a planar bed of rhythmites of gravelly sand to fine sand at profile I10.

From ~1,500-1,000 cal BP several paleosols and alluvium were observed in the watersheds. At profile C3, thin beds of silt and silt loam had an age of 1,065 and 1,234 cal BP. These strata are located above a thick (~1.50 m) cumulic Ab horizon. A date of 1,626 cal BP at profile S7 corresponds to an alluvial deposit having prismatic structure, which was deposited behind a lama-bordo. Buried A horizons have been dated to 1,291, 1,233, and 1019 cal BP at

sites S6, S7, and I10, respectively. All three sites had an Ab-C sequence, but the buried Abs at profiles S6 and S7 were cumulic with prismatic structure. The paleosol at profile S7 formed just above some fluvial deposits that buried the lama-bordo there.

The uppermost buried As dated to 603, 595, and 447 cal BP at profiles at S4, S8 and C3, respectively, corresponding to the latter part of the Natividad phase. At profile S4, the paleosol is an Ab-Bw-BC-C sequence, with a cumulic Ab. Pottery sherds were found in this buried A at profiles S4 and S7, also belonging to the Natividad phase. This paleosol is evident throughout the Culebra and Inguiro watersheds, and it apparently represents the land surface of the valley floors at the time of Spanish conquest.

3.4.5 Soil and Sediment Characteristics

The results of the loss-on-ignition, particle size, and geochemical analyses are shown for profiles S4 and C2 (Figures 3.6a and b). In general, the organic content tends to be higher for Ab horizons, while inorganic carbon tends to decrease. The $CaCO_3$ content has both detrital and pedogenic origins. Almost all strata contain $CaCO_3$ deposited in root pores and on ped faces, while detrital additions are also widespread but to a lesser extent. A significant increase in $CaCO_3$ in a buried A horizon implies polygenesis. Particle size fluctuates between approximately 75-100% <2 mm, and 0-25% >2 mm, and although sizes of >2 mm mainly correspond to unweathered alluvium, they are also found in some buried A horizons, as the A horizons had alluvium as their parent material.

Weathering indices were calculated from the geochemical analyses made on the upper strata at each profile. A scatterplot of all the elements suggested that Na represents a mobile element, while Ti was immobile, and the weathering index was calculated for Na/Ti (as in Buggle et al., 2011). Examining the Na/Ti ratio with respect to depth and horizon, it is observed

that the ratio tends to decrease for most buried As, while in C horizons the ratio typically increases. This observation supports the interpretation of the former as buried A horizons, which were identified in the field by their darker color (e.g., 10YR 3/1-3/2; 4/1-4/4, 5/2-5/3) and structure. Exceptions to the association between lower Na/Ti ratios and Ab horizons are the higher Na/Ti ratios near the bottom of an Ab at profile S4 and the top of a buried A at profile C2, both around 6 m deep.

Thicknesses of buried A, B, and Ck horizons were plotted against age and it was observed that horizon type and thickness varied across time (Figure 3.6c). The ages of some horizons were modeled using CLAM (Blaauw, 2010) in R (R software team, 2008) in order to obtain a better idea about changes overtime. Before exploring the results it must be emphasized that: 1) some of the thicknesses are only represented by one or two ages; and 2) the late Holocene paleosols seem to fluctuate more than the earlier paleosols, which is probably due, in part, to better preservation of these later paleosols. In general, buried A horizons seem to be thicker starting in the middle Holocene, a trend that continues into the late Holocene. Before ~7,000 cal BP paleosols contain Btk, Ck, and Bw horizons, but around this date two paleosols have a very thick Bt horizon. Throughout the late Holocene the Bw horizon seem to be more widespread as compared to the Bt, Btk, and Ck horizons.

3.4.6 Sedimentation Rates

The average sedimentation rate for the terminal Pleistocene through the middle Holocene was estimated from three profiles (C2, X9, and S4), and was found to be 0.14 cm yr^{-1} (Figure 3.7). During the late Holocene, the average sedimentation rate from strata that was not directly behind a lama-bordo was estimated at 0.21 cm yr^{-1}, while behind the lama-bordos the sedimentation rate was modeled to be around 0.65 cm yr^{-1}. These estimations were derived from

five profiles (S8, S6, C3, and parts of S7 and S5) and two profiles (parts of S7 and S5), respectively. The highest sedimentation rate before the late Holocene occurs in the terminal Pleistocene to early Holocene (between 12,000 and 11,000 cal BP), with a value of 0.035 cm yr^{-1}. Only three sedimentation rate estimates are greater than this, all of which occur in the late Holocene. At approximately 3,500 cal BP, a sedimentation rate of approximately 0.4 cm yr^{-1} is associated with lama-bordos. The highest sedimentation rate of 0.6 cm yr^{-1} occurs ~600 cal BP, and is also associated with lama-bordos, which is almost twice the rate as the fastest rate during the terminal Pleistocene-early Holocene transition. The other value of 0.44 cm yr^{-1} occurs ~800 cal BP, and although this estimate is not directly associated with lama-bordos, this estimate reflects the widespread construction of lama-bordos during the Natividad phase.

Since the ages and resulting sedimentation rate estimations were modeled and then examined collectively, these rates were evaluated against rates estimated on individual profiles based on actual radiocarbon dates (and not a combination of actual and modern ages). Rates were only obtained between actual radiocarbon dates, and did not include strata with major erosional boundaries, well-developed paleosols, but did include cumulic A horizons. The rate behind the lama-bordo at S5 resulted in the highest rate, measuring 4.55 cm yr^{-1}. The sedimentation rates of the terminal Pleistocene to the middle Holocene ranged between 0.06 to 0.55 cm yr^{-1}, while rates in the late Holocene (excluding profile S5) ranged between 0.09 to 0.98 cm yr^{-1} (see Appendix II).

3.4.7 Qualitative Comparison between Alluvium-Paleosol Sequences and Paleoclimate

The $\delta^{18}O$ data from the Guerrero stalagmites were qualitatively compared to the summed probability curves made from the alluvium and paleosol dates from Culebra, Inguiro and Verde

watersheds (Figures 3.8 and 3.9). The $\delta^{18}O$ data are from five different stalagmites from two different caves: Juxtlahuaca and Cueva del Diablo. Although different stalagmites from the same cave and even the same region may have different ranges of $\delta^{18}O$, the overlap in the values between the different Guerreran stalagmites supports that these stalagmites are strong indicators of fluctuations in precipitation amount over time. For example, during the late Holocene, the $\delta^{18}O$ values from the three stalagmites from Juxtlahuaca overlap with the values from the stalagmite from the Cueva del Diablo, strongly supporting the accuracy of the precipitation record (see Lachniet et al., 2013). The range in values is assumed for the terminal Pleistocene, but the values from the latter are from a different stalagmite (JX-10) with no overlapping section with the other stalagmite data. Thus, the very enriched $\delta^{18}O$ values *may* have resulted from to disparities between stalagmites.

In order to compare paleosol formation and alluvial deposition to stable oxygen isotope data from the Guerreran stalagmites, we only included strata that were considered representative of basin-wide scale phenomena. For example, paleosols were considered widespread when they were represented by two or more overlapping dates in either two distinct parts of the same watershed, or two distinct watersheds (e.g., Culebra and Rio Verde). All of the alluvium dates were used, and they correspond to either cut-and-fill stratigraphy, or continuous horizontal deposits. Only ages from the terminal Pleistocene to the late Holocene were examined. No interpolated ages were incorporated into these analyses.

The comparisons suggest that from the terminal Pleistocene through the late Holocene alluvial and paleosol ages overlap and in general, as the relative probability of paleosol ages increases, the relative probability of alluvium ages typically decreases, and vice versa. The

relative probability of both paleosol and alluvium ages is usually low to zero during the wettest periods (Figure 3.9a).

During the terminal Pleistocene to the middle Holocene, the relative probability of alluvium and paleosol ages occurs during relatively drier periods, which consists of transitional climatic regimes (dry to wet and wet to dry, but not the wettest). In cases where the relative probability of ages slightly diverges, the probability of alluvium ages is higher during the wetter end of the transition, while that of paleosols appears to increase during the drier end of the transition.

Since no clear pattern was observed between the $\delta^{18}O$ values and the summed probability curves, the latter was compared with the El Junco sand percentages reflecting ENSO intensity (Conroy et al., 2008) (Figure 3.9b). Paleosol ages appear almost continuous, but seem to slightly favor lower ENSO intensity periods. The probability of alluvium dates slightly favors high ENSO intensity periods and tends to decrease during deep plunges in ENSO intensity. Similar to the terminal Pleistocene to the middle Holocene, the relative probability of alluvium ages overlaps with that of the paleosols ages, but in general as one increases, the other decreases.

3.5 Discussion

In general, paleosols from the Culebra and Inguiro watersheds include Inceptisols (e.g. Ustepts), Mollisols (e.g., Ustolls), Aridisols (e.g., Argids, Calcids, and Cambids) and Vertisols. The dated paleosols of the late Pleistocene resemble Mollisols and Vertisols, while those dated from the terminal Pleistocene to the early Holocene can be classified as Mollisols, Aridisols, Vertisols and Inceptisols. Paleosols corresponding to the middle Holocene can be classified as

Mollisols and Inceptisols. Late Holocene paleosols mainly comprise Inceptisols and Mollisols, but Aridsols exist as well.

The prevailing paleosol characteristics support the idea that since the late Pleistocene, wet and dry fluctuations are an important component of the climate. For example, Stage II secondary $CaCO_3$ accumulation reflects distinctly dry climate conditions (Birkeland 1984), whereas prismatic structure and clay films imply wetter conditions. Slickensides indicate fluctuating wet and dry conditions that lead to swelling and shrinking of the soil (Schaetzl and Anderson, 2005). The prevalence of a dry component to the climate in the area is demonstrated by the widespread Stage I $CaCO_3$ deposited on ped faces and in root pores in most paleosol horizons. The idea that paleosols develop under wet and dry seasonal climatic regimes is supported by polygenetic traits, such as carbonate nodules, slickensides, and prismatic structure in some Ab horizons (Birkeland, 1984). Paleosols with Bt and Btk horizons represent well-developed soils, while those with Bw or Ck are less developed. The nature of paleosol development represented by these sequences appears to alternate over time; however, spatial variation and polygenesis make it difficult to derive a detailed chronology of local paleoenvironmental conditions. In summary, the wet and dry seasonal climatic regime, polygenetic nature of many of the paleosols, and the variations in topographic and hydrologic stability throughout time and space make it challenging to use paleosols to reconstruct the paleoclimate and paleoenvironment.

3.5.1 Links between Paleoclimate and Paleohydrology

The results from the stratigraphic study in the Ríos Culebra and Inguiro watersheds will be discussed along with that of the Verde watershed, and the alluvium-paleosol sequences of all three watersheds will be explored with regard to pre-existing regional paleoclimate data, with

particular reference to the high-resolution $\delta^{18}O$ stalagmite record from Guerrero, in order to better understand the local paleoclimate and paleohydrology.

To facilitate this analysis, the stratigraphy was divided into three groups (I-III, with I being the oldest) based on chronology, which will be summarized below. Mueller et al. (2012) divided their stratigraphy into four groups, but they attributed each group to a fill cycle, which is difficult to confirm. They also did not examine their data with regard to paleoclimate data.

3.5.*1.1 Late Pleistocene, Group I; North Atlantic Sea Surface Temperature Fluctuations*

The stalagmite record starts at approximately 22,000 cal BP, and depleted $\delta^{18}O$ values during the Last Glacial Maximum (LGM) implies a strong North American Monsoon (NAM) and wetter conditions. Two explanations are offered to explain the wetter conditions despite cooler temperatures, high ice volume and lower CO_2 (Lachniet et al., 2013): 1) a relatively high summer insolation that brought about a high ocean-to-land temperature gradient; or 2) a moderately active Atlantic Merdional Overturning Circulation (AMOC) that influenced the strength and the position of the ITCZ, which resulted in a stronger North American Monsoon (NAM). A strong to intermediate (e.g., active) AMOC results in moving warm surface waters northward and maintaining high sea surface temperatures in the North Atlantic, which favors a more northward location for the ITCZ and consequently more precipitation in southwestern Mexico (Lachniet et al., 2013).

The thick horizonation of the Pleistocene soils in the Culebra watershed, having organic-rich Ab horizons, common illuviation and/or vertic features, $CaCO_3$ deposits, and well-developed B horizons all infer that seasonal (dry and wet fluctuations) conditions existed during the early part of Marine Isotope Stage 2. In Central Mexico, the formation of thick paleosols with vertic features (Solleiro-Rebolledo et al., 2011) and the evidence for high lake levels

(Lozano-Garcia and Ortega-Guerrero, 1998) support the notion that the regional climate was wet, with dry fluctuations prior to and ~26,000 cal BP. No late Pleistocene soils were dated in the Verde watershed (Mueller et al., 2012).

Between 27,677 and 15, 203 cal BP, no alluvium or paleosols were dated from any of the watersheds. After 18,000 cal BP, conditions became drier, coinciding with Heinrich Stadial 1 (HS1) (Lachniet et al., 2013). The influx of meltwater into the North Atlantic that occured during Heinrich events led to lower sea surface temperatures, which weakened the AMOC. The outcome of a weakened AMOC is a more southward location for the ITCZ and less precipitation in southwestern Mexico (Lachniet et al., 2013).

The lower strata at the C2 site, including a tuff layer, a thick layer of colluvium, and a debris flow below a date of 12,717 cal BP (e.g., prior to the Younger Dryas), suggest a period of instability possibly associated with volcanic activity. The apparent gap in age in the sediments and soils between 27,677 and 15,203 cal BP may have also been caused by erosion during the climatic fluctuations that occurred during the terminal Pleistocene (e.g., HS1, B/A), or by non-deposition.

3.5.1.2 Terminal Pleistocene - Middle Holocene, Group II, North Atlantic SST

The $\delta^{18}O$ record indicates that in general, high amplitude and relatively low frequency fluctuations characterize the terminal Pleistocene to the early Holocene, which become more moderate towards the middle Holocene (Bernal et al., 2011; Lachniet et al., 2013). Bernal et al. (2011) showed that the North Atlantic SST has a weak-moderate influence on the rainfall in southwestern Mexico via its effect on the position and strength of the ITCZ. Lower North Atlantic SSTs result in a less active or weaker AMOC and consequently a more southward location of the ITCZ (Bernal et al., 2011; Lachniet et al., 2013). These factors bring about less

precipitation in southwestern Mexico.

The summed probability curves suggest that alluvium deposition overlaps with paleosol formation, while typically less paleosol formation and alluviation occur during the wettest periods. Previous studies have suggested that arroyo incision occurs during wetter periods (e.g., Bull, 1991; Waters and Haynes, 2001), which is supported by Harden et al.'s (2010) analysis of over 700 dates in the southwestern U.S.A. Mueller et al (2012) also support the idea of incision during wetter periods, but they do not recognize any incision dates between 14,000 cal BP and 4,000 cal BP.

According to the $\delta^{18}O$ stalagmite record, the wettest periods occur at ~11,500, 10,200, 9,500, 7,000, 6,100, and 4,800 cal BP (Bernal et al., 2011; Lachniet et al., 2013), some of which may correspond to incision periods. For example, fewer alluvium and paleosol dates exist around 11,500, 10,200, 7,000 and 6,100 cal BP, which is consistent with the idea of incision during those times. An organic fill at the bottom of a cut (near profile S5) had an age of 6,527 cal BP, which means the cut would have occurred before, and possibly ~ 7,000 cal BP. A hiatus between 16,125 and 13,544 cal BP in the stalagmite record includes the Bølling-Allerod (B/A) (14,700 to 12,700 cal BP), and may be linked to a wetter climate (e.g., as in Central America, Hodell et al., 2008) though no sub-regional data are available for this timespan. Mueller et al. (2012) also suggest that an incision occurred before 14,000 cal BP, and it is possible that incision occurred during the B/A. Based on interpolated ages, high sedimentation rates are estimated from 15,000 to 13,000 cal BP (~0.17 cm/yr), which spans at least part of the B/A. Since there were several alluvial strata and paleosols dated to ~9,500 cal BP, this time is not indicative of a possible incision date.

The $\delta^{18}O$ stalagmite record indicates that regional conditions become more arid during

the latter part of the B/A, ~13,500 cal BP, and continue to be dry through the Younger Dryas (YD) spanning 12,900 to 11,700 cal BP. However, the sedimentation rates were estimated to be highest between 12,000 and 11,000 cal BP (0.35 cm/yr), spanning from the end of the YD through to the early Holocene. Relatively high sedimentation rates with a mean of 0.21 cm/yr were also estimated between 11,000 and 9,000 cal BP, though according to the $\delta^{18}O$ record, part of this timespan is dry, coinciding with the 10.2 ka event. After 9,000 cal BP, sedimentation rates decrease until the late Holocene.

Similar to HS1, the influx of freshwater into the North Atlantic during theYD weakened the AMOC, which resulted in a southward position for the ITCZ and in turn, a weaker NAM (Lachniet et al., 2013). The influx of freshwater causing the 8.2 ka event explains the drier climate in southwestern Mexico, though it is unclear what caused the weaker monsoon during the early Holocene between 9,000 and 7,500 cal BP, which is indicated by a dry interval in the stalagmite during this timespan (Bernal et al., 2011). Conversely, increased insolation in the northern hemisphere during the transition to the early Holocene, which was associated with the precessional cycle, brought about a more active AMOC and northward position of the ITCZ (Bernal et al., 2011; Lachniet at al., 2013). Maximum insolation occurred approximately 9,500 cal BP (e.g., just before the subsequent cooling event). Warmer temperatures and higher CO_2 also coincided with this more active monsoon (Lachniet et al., 2013).

Paleosol ages in the Verde and Culebra watersheds span the YD, 10.2 and 8.2 ka events Paleosols dating from 14,000- to 10,200 cal BP in the Verde watershed are described as organic-rich, cumulic Abs, having prismatic structure and prominent clay coats. A prominent soil forming between 7,800-8,400 cal BP in the same watershed has no cumulic properties, but is clay-rich with prismatic structure. From 12,717 to 9,063 cal BP in the Culebra watershed no

evidence for cumulic Abs exist, and all Abs examined during that time interval are less than 40 cm thick. According to dated and interpolated ages, Bws alternate with Btk and Ck horizons below buried As between 14,000 and 9,000 cal BP. Some evidence for polygenetic features in both watersheds include $CaCO_3$ deposits and slickensides within buried A horizons.

After 7,000 cal BP, there is evidence for cumulic soils in the Culebra watershed, which have prismatic structure and Bt subsoils. In the Verde watershed, thick (>1.0 m), organic and clay-rich buried A horizons date between 6,000 and 7,000 cal BP. At ~5,000 cal BP, thinner buried A horizons with weaker structure are evident in the Verde watershed.

Although paleosol ages in the Verde and Culebra watersheds span the YD, 10.2 and 8.2 ka events, they do not necessarily represent the direct local response to any of these events. Instead, the paleosol characteristics having ages coinciding with these events are suggestive of the climatic conditions prevalent during these intervals. In addition, the conditions during the YD are evidently much drier than those during the Holocene, but the earliest date on an arroyo cut-and-fill is around 15,000 cal BP, which is during the B/A. Since the earliest date is before the YD, it hints that arroyo cycles occurred through the YD up to the present. Despite the overlap in $\delta^{18}O$ values in stalagmites during the Holocene, the very dry conditions indicated by the stalagmite (JX-10, see Figure 3.8) for the terminal Pleistocene may instead reflect the range in values represented by that one stalagmite and not actually much drier conditions than during the 8.2 ka. If the $\delta^{18}O$ values are correct, the evidence for arroyo cycles in the paleosol-alluvium since the B/A suggests that the range in climatic conditions associated with the position of the ITCZ and variations in AMOC due to the fresh water influx (Lachniet et al., 2013) are conducive to arroyo cycles. Conversely, during the LGM, the active AMOC appears to have been the result of a different set of overarching conditions that, seemingly, were not conducive to arroyo cycles.

The characteristics of the paleosols in the LGM are very different than that from the terminal Pliestocene through the middle Holocene paleosols, which also hints at different local paleoclimatic and paleoenvironemntal conditions.

In summary, the paleosol characteristics and sedimentation rates indicate fluctuating paleohydrologic and local paleoenvironmental conditions during the terminal Pleistocene through the middle Holocene. For example, $CaCO_3$ deposits demonstrate the importance of dry conditions, while prismatic structure and especially slickensides offer evidence for alternating wet and dry conditions, and possibly seasonal fluctuations. Mueller et al., (2012) suggest that cumulic soils indicate a high water table, but according to the $\delta^{18}O$ record their cumulic soils overlapped with drier periods. The local conditions may have differed from the regional $\delta^{18}O$ stalagmite signal; however, the implication that cumulic soils coincide with drier climate is that rain intensity and/or variability may have been low, while alluvial deposition occurring at this time was slow enough to allow for soil formation to occur.

3.5.1.3 Late Holocene and the Human Imprint, Group III, ENSO

Bernal et al., (2011) suggested that ENSO became the dominant driver in the region ~4,300 cal BP, influencing the location of the ITCZ (Magana et al., 2003). The El Niño phase results in less precipitation in southwestern Mexico (Magana et al., 2003; Vera et al., 2006), but apparently increased frequency and intensity of cyclones (Amador et al., 2006). The La Niña phase leads to more summer precipitation (Magana et al., 2003; Vera et al., 2006), and reduced frequency and intensity of cyclones (Amador et al., 2006). An increase in ENSO intensity and frequency has been recognized on millennial timescales, which have been associated with Bond cycles (Moy et al., 2002). A substantial increase in ENSO intensity and frequency is observed for the late Holocene, starting approximately 4,000 cal BP (Conroy et al., 2008).

In general, the frequent fluctuations during the late Holocene make it hard to perceive trends in the $\delta^{18}O$ stalagmite record, especially after 2,000 cal BP. Despite these difficulties, four wetter periods can be discerned in the $\delta^{18}O$ stalagmite record: ~3,700, 1,800, 1,450 and 500 cal BP, which may be possible incision periods. The fill near the bottom stones of two lama-bordos (S5 and another at LB175) and immediately above bedrock was dated to ~ 3,500 cal BP (Leigh, et al. 2013), and offers evidence for an incision event slightly before this time, probably between 3,700 and 4,100 cal BP. Mueller et al., (2012) also suggest an incision event at approximately 4,000 cal BP. From 1,234 to 1,065 cal BP, aggradation was occurring at least at seven meters (or more) below the surface at profile C3, which suggests the basin had undergone incision before this time, even as early as 1,450 cal BP. Mueller et al., (2012) suggested that a basin-wide incision period began ~950 cal BP in the Verde watershed. It is possible that another incision event occurred ~1,800 cal BP, coinciding with a wet period in the $\delta^{18}O$ stalagmite record, but it is unclear. The most recent incision event is proposed to have occurred ~350 years ago (Leigh et al., 2013), which is a short time after the wet period at 500 cal BP is observed in the $\delta^{18}O$ stalagmite record. This incision event coincides with the Colonial period, when population reduction, land abandonment and degradation were widespread (Rincon, 1999; Mueller et al., 2012; Leigh et al., 2013), suggesting that abandonment and lack of maintenance of the lama-bordo and hillslope terrace system may have contributed to arroyo incision.

The sand percentage data from El Junco reflects rainfall variability associated with El Niño events, serving as a proxy for ENSO intensity and frequency. Conroy et al., (2008) emphasized periods of high ENSO intensity and frequency at approximately 4,000 cal BP and in particular, 2,000 cal BP, and indicated a slow increase in ENSO intensity after 3,200 cal BP.

Intense dry periods, indicated by Ck and Bk horizons at ~4,300 and ~2,000 cal BP, correspond to high ENSO intensity periods. The dry period at ~4,300 cal BP occurs about the time of the intense, dry 4.2 ka event (Walker et al., 2012). A paleosol dating to 2,028 cal BP has redox features on its buried A horizon and the sediments above it, but this paleosol also has a well-developed Btk horizon. The redox features suggest a high water table, while the Btk implies dry conditions. The combination of features in this paleosol implies a progressive change of conditions from dry to wet around 2,000 cal BP.

Cumulic Ab and Bw horizons are evident throughout the late Holocene, spanning high and low ENSO intensity periods. All alluvium dates overlapped with higher intensity ENSO periods (e.g., ~4,100, 3,900, 3800, 1,900, 1,600 cal BP), except one dating to 1,100 cal BP. However, the calibrated age range of some of the alluvium dates overlapped with periods of transitional low-high (or vice versa) ENSO intensity, which is similar to the observation for paleosols.

Just before the early Cruz phase is observed in the region, ENSO intensity is relatively high, while the highest ENSO intensity period overlaps with the local Ramos phase spanning 2,250 to 1,600 cal BP. A lower intense ENSO period coincides with the Cruz phase from 3,500 to 2250 cal BP. The Transición/las Flores phase ranging from 1,750 to 1,250 cal BP, and the Natividad phase ranging from 1,250 to 430 cal BP, (Table 3.1) both overlap with high and low intensity ENSO periods. Before inhabitants of the Cruz phase started building lama-bordos, the sedimentation rate was estimated to very high to about 0.34 cm/yr, and comparable to early Holocene rates. During the Cruz phase, populations remained relatively low, though estimated accumulation rates continue to be high, including those directly associated with lama-bordos at 0.42 cm/yr (~3,400 cal BP), and those not directly associated with lama-bordos, with rates of

0.27 cm/yr (~3,200 cal BP). The date of 2,300 cal BP corresponds to the early Ramos phase, when some lama-bordos are evident in the region, though the sedimentation rate is much lower. Since population is lower for both the Cruz and Ramos phases, it is suggested that basin-wide sedimentation rates, in particular rates that were not associated with lama-bordos, fluctuated according to overarching climate change. For instance, during higher ENSO intensity periods, which correspond to a drier climate, rates are lower, for example from 4,300 to 4,000 cal BP and 2,500 to 1,800 cal BP. Higher sedimentation rates are estimated during much of the Cruz phase coinciding with lower ENSO intensity and wetter climate.

Population increased during the subsequent Transición/las Flores phase, peaking ~1,500 cal BP. Two lama-bordos were placed above the paleosol dating to between 2,300 and 2,000 cal BP in the Culebra watershed (Rincon, 1999; this study). Sediments behind this wall were dated to 1,600 cal BP. At approximately ~1,600 cal BP, the estimated accumulation rate increased to 0.22 cm/yr adjacent to lama-bordos, and 0.15 cm/yr not adjacent to lama-bordos. The population declined after 1,500 cal BP.

Starting ~1,100 cal BP, the population increased significantly during the Natividad phase, peaking ~600 cal BP. Lama-bordos and terraces are evident throughout the Culebra watershed, and are associated with the uppermost paleosol that dates from 650-450 cal BP that is preserved in many locations in the watershed. Accumulation rates estimated for the Natividad phase were higher than that estimated for the last 15,000 years. Rates not directly associated with lama-bordos were estimated at 0.43 cm/yr from 1,100 to 600 cal BP), while rates associated with lama-bordos were estimated to be 0.6 cm/yr at approximately 800 cal BP.

According to the archaeological and El Junco data, it appears that population growth was greatest during the transition from a low to high ENSO intensity period between 1,100-700 cal

BP. The high sedimentation rates in the Cruz and the early part of the Natividad phase appears to result from a coupled human-environmental phenomenon, whereby climatic conditions resulted in transportation and deposition of eroded material, and human-constructed sediment traps effectively accelerated the aggradation process. The population rise in the early Transición/las Flores phase corresponds with a slow rise in sedimentation rates, which occurs after ~1,900 cal BP and coincides with an overall high ENSO intensity period. Since sedimentation appears lower, the population growth may be attributed to intense management of the land associated with the lama-bordos and terraces already constructed by many generations of farmers during the Ramos and Cruz phases.

3.5.2 Arroyo Cycles

As mentioned in the introduction, the disruption of the balance between water supply and sediment supply ultimately results in either incision or aggradation in a fluvial environment. However, fluvial environments, and in particular dryland fluvial environments, are complicated, and studies have shown that diverse combinations of factors effect gully erosion (e.g., Dotterweich et al., 2003; Poesen et al., 2003; Capra et al., 2009; Casali et al., 2009; Kertesz and Gergely, 2011; Mousazedeh and Salleh, 2014). In the case of the Culebra, Inguiro, and Verde watersheds, lithology plays a large role as these basins are filled with silty and fine sandy Quaternary alluvium, and their hillslopes consist of weakly consolidated, jointed, and easily erodible siltstones, which is further covered in many places by a caliche horizon that acerbates runoff. Furthermore, this region is characterized by moderate relief terrain. All of these factors make it very susceptible to erosion in certain climatic conditions, and/or under certain land use activities (as discussed in McFadden and McAuliffe, 1997).

Dryland environments are known for their fluctuating and high-intensity rainfall events (Valentin et al., 2005). The Langbein-Schumm (1958) curve demonstrates the relationship between climate and sediment yield, with sediment yield highest in semi-arid environments due to decreased vegetation cover, yet ample rainfall for runoff events. Observations from modern day studies (e.g., Valentin et al., 2005; Lyons et al., 2013) indicate that very high intensity and/or high magnitude rainfall events result in incision. Harden et al.'s (2010) study on radiocarbon dates from alluvial stratigraphy suggested that basin-wide incision occurred during the wettest periods. In light of modern observations and other studies, the distribution of paleosol and alluvium ages with regard to the regional paleoclimate signal supports incision during the wettest conditions. However, as incision does not necessarily occur during every wet period, or concur with the exact dates of all the wettest events, the exact timing and nature of threshold crossing incision events also depends on the internal system dynamics (Schumm and Hadley, 1957; Schumm, 1974). Human-constructed lama-bordos complicate things further, as they artificially encourage aggradation of sediment and discourage incision.

Paleosol formation and alluvial deposition are intricately linked and represent two facets of the hydrological system and paleoenvironment in this fluvially dominated landscape. Examination of the alluvium and paleosol ages with regard to the paleoclimatic record suggests that paleosols and alluvium both form under wet, dry, and transitional conditions (Figure 3.10). In the terminal Pleistocene through the middle Holocene, both tend to develop during transitional and relatively drier periods (compared to incision events) in the Culebra, Inguiro, and Verde watersheds. Conversely, during the late Holocene, they typically occur during the lower intensity ENSO events, and based on the modern relationship between ENSO and southwestern Mexico, these periods are wetter.

Many studies suggest that alluvium aggrades during dry periods (e.g., Mann and Meltzer, 2007), but hydrological studies on dryland ephemeral streams, including arroyos, indicate that they carry high sediment loads during floods and are likely to be transport limited, but not supply limited (Bull and Kirby, 2002). Sediment is readily available in an overall dry climatic regime with intense sporadic rainfall, low vegetation, and soft geology. To aggrade, it would require that the overarching climatic conditions result in net aggradation. Changes in frequency and magnitude of rainfall have been connected to various geomorphic processes (Leopold, 1951), but understanding how wet and dry relates to runoff and flooding in semi-arid environments is not always straightforward even in present-day settings. For example, a study by Turnball et al. (2013) in the southwestern U.S. determined that an increase of rainfall amount actually produced less runoff because less intense rainfall events resulted in less flashy floods. Studies on paleofloods from slackwater deposits in the southwestern US suggest that higher frequency, lower magnitude floods would allow for net aggradation in arroyos (Ely, 1997), and rainfall with lower intensity and variability would favor these types of floods. For paleosols, it seems that a similar precipitation and hydrological regime would favor cumulic soils (e.g., when aggradation slowed enough to allow them to form). Paleosols also form or continue to form on stable areas in the landscape when an arroyo is either incising or aggrading. The varying characteristics and polygenetic nature of the paleosols reflect the fluctuating climatic conditions in which some of them developed.

The entire valley fill contains layers of paleosols interspersed with alluvium. Although soils may form in the arroyo fill during periods of slower aggradation, some studies suggest that arroyos can fill within 300 years (e.g., Huckleberry and Duff, 2008). Observations of cut-and-fill stratigraphy in the Culebra watershed indicate that the bottom of a cut is filled with a couple

of meters of alluvium, whereas paleosols are observed towards the top of the fill and extend beyond the original incision to the surrounding floodplain. In many cases, alluvium covers these paleosols, also extending to the surrounding floodplain. Therefore, it is suggested that when the arroyo is full, channel migration and overbank flooding plays a more important role in the successive aggradation of the entire valley than is typically acknowledged for arroyo systems. For instance, at profile S4 erosional boundaries occur between strata dating to 11,119 cal BP, 6,400 cal BP, and 4,538 cal BP. These deposits occurred chronologically from bottom to top, but not continuously, suggesting that lateral migration or overbank flooding was responsible for their formation, which must have been slow enough at 6,400 cal BP to allow the development of a cumulic Ab. In addition, a few examples of laterally migrating stream channels were observed in the upper strata within the Culebra watershed. A quasi-equilibrium incised state has been proposed to explain an extended period of incision in the southwestern U.S., (Mann and Meltzer, 2007), while more extensive floodplain deposits hint at an extended, quasi-equilibrium 'full state'.

Human activities, such as agriculture, can also influence internal fluvial system dynamics (Patton and Schumm, 1975). Perroy et al. (2012) showed that increased sedimentation from human activities accelerated the date of an incision event, which would have occurred regardless at a later date in relation to climatic fluctuations. The incision estimated at 350 cal BP (Leigh et al., 2013) may have been delayed due to the extensive lama-bordo system that was still intact leading up to that time. The abandonment of the lama-bordo system with its large amount of trapped sediment resulted in a substantial incision event (Mueller et al., 2012; Leigh et al., 2013). The incision event may have occurred regardless, but possibly later than it had if the system had not been dammed. Lama-bordo and terrace construction resulted in very high sedimentation

rates and offers further evidence for human impact on local and basin-wide geomorphic dynamics in relation to arroyo aggradation.

3.6 Conclusion

Examining arroyo stratigraphy in relation to high-resolution, regional paleoclimatic proxies aided in understanding overarching relationships between the paleoclimate and paleohydrology of the Culebra and Inguiro watersheds. Although insightful, even high-resolution proxies, such as stalagmites, cannot provide the detailed insight on the complexities of rainfall intensity and variability that is needed to explain the nuances of dryland systems involving arroyo cycles or to avoid the problem of equifinality. These comparisons offer supporting evidence that wet and dry fluctuations are important to arroyo cycles, but indicate that 'wet' and 'dry' may be too general. Consideration of rainfall intensity and variability must be gained to better understand the processes involved in incision, aggradation, as well as the 'incised' and 'full' phases in arroyo cycles. Studies on present arroyos and other dryland streams offer complementary insight on the connection between overarching climate, geomorphic process and landscape change.

Despite these difficulties, the examination between alluvium-paleosol stratigraphy and chronology, and the regional signal offered by the $\delta^{18}O$ stalagmite record supports the idea that incision occurs during the wettest periods, which has been concluded in other studies, including investigations on present-day arroyos. Polygenesis and varying characteristics in paleosols (e.g., $CaCO_3$ deposits, cumulic properties) allude to the diverse climatic conditions under which they form, and the difficulties in connecting them to particular palaeoenvironmental regimes. Paleosols, formed in alluvium deposits, offered insight on the palaeohydrologic system and past

landscape stability. For example, paleosol formation, in particular cumulic A horizons, indicate that not only is the fill within arroyos important to consider regarding basin-wide aggradation and soil development, but lateral migration and overbank sedimentation are also extremely important.

During the late Holocene, agricultural activities had a direct impact on the entire landscape, especially in terms of sedimentation rates. Low populations suggest that from the Cruz to the Ramos phase the impact of lama-bordos on sedimentation rates was local, the influence of which increased during the early Transición/las Flores phase as population increased. Widespread construction of lama-bordos suggests that the impact on sedimentation rate was basin-wide during the Natividad phase. The high sedimentation rates indicate that the lama-bordos were effective sediment traps. Based on comparisons with overarching climate, sedimentation rates were also linked to climatic fluctuations that favored aggradation, of which inhabitants took advantage by building lama-bordos for agricultural purposes.

3.7 References

Amador, J.A., Alfaro, E.J., Lizano, O.G., Magana, V.O., 2006. Atmospheric forcing of the eastern tropical Pacific: A review. Progress in Oceanography 69, 101-142.

Asmerom, Y., Polyak, V., Rasmussen, J., Burns, S., 2007. Solar Forcings of Holocene Climate: New Insights from a Speleothem Record, southwestern United States. Geological Society of America Bulletin 35, 1-4.

Avni, Y., 2005. Gully incision as a key factor in desertification in an and environment, the Negev highlands, Israel. Catena 63, 185-220.

Balkansky, A.K., Kowalewski, S.A., Perez Rodriguez, V., Pluckhahn, T.J., Smith, C.A., Stiver, L.R., Beliaev, D., Chamblee, J.F., Heredia Espinoza, V.Y., Santos Perez, R., 2000. Archaeological survey in the Mixteca Alta of Oaxaca, Mexico. Journal of Field Archaeology 27, 365-389.

Bernal, J., Lachniet, M., McCulloh, M., Mortimer, G., Morales, P., Cienfuegos, E., 2011. A Speleothem Record of Holocene Climate Variability from Southwestern Mexico. Quaternary Research 75, 104-113.

Birkeland, P.W., 1984. Soils and Geomorphology. Oxford University Press, New York.

Blaauw, M., 2010. Methods and code for 'classical' age-modelling of radiocarbon sequences. Quaternary Geochronology 5.

Borejsza, A., Frederick, C.D., 2010. Fluvial response to Holocene climate change in low-order streams of central Mexico. Journal of Quaternary Science 25, 762-781.

Bouchnak, H., Felfoul, M.S., Boussema, M.R., Snane, M.H., 2009. Slope and rainfall effects on the volume of sediment yield by gully erosion in the Souar lithologic formation (Tunisia). Catena 78, 170-177.

Bull, L., J., Kirkby, M. J., 2002. Dryland River Characteristics and Concepts in Bull, L. J., Kirkby, M. J., eds., Dryland Rivers: Hydrology and Geomorphology of Semi-Arid Channels. West Sussex, John Wiley & Sons Ltd, pp. 3-16.

Bull, W.B., 1991. Geomorphic Responses to Climate Change. Oxford University Press, Oxford.

Bull, W.B., 1997. Discontinuous ephemeral streams. Geomorphology 19, 227-276.

Butzer, K.W., Abbott, J.T., Frederick, C.D., Lehman, P.H., Cordova, C.E., Oswald, J.F., 2008. Soil-geomorphology and "wet" cycles in the Holocene record of North-Central Mexico. Geomorphology 101, 237-277.

Capra, A., Porto, P., Scicolone, B., 2009. Relationships between rainfall characteristics and ephemeral gully erosion in a cultivated catchment in Sicily (Italy). Soil & Tillage Research 105, 77-87.

Casali, J., Gimenez, R., Bennett, S., 2009. Gully erosion processes: monitoring and modelling. Earth Surface Processes and Landforms 34, 1839-1840.

Conroy, J., L. , Overpeck, J., T. , Cole, J., E. , Shanahan, T., M. , Steinitz-Kannan, M., 2008. Holocene changes in eastern tropical Pacific climate inferred from a Galápagos lake sediment record. Quaternary Science Reviews 27, 11661180.

Constante, A., Luis Pena-Monne, J., Munoz, A., 2010. Alluvial Geoarchaeology of an Ephemeral Stream: Implications for Holocene Landscape Change in the Central Part of the Ebro Depression, Northeast Spain. Geoarchaeology-an International Journal 25, 475-496.

Dotterweich, M., 2008. The history of soil erosion and fluvial deposits in small catchments of central Europe: Deciphering the long-term interaction between humans and the environment — A review. Geomorphology 101, 192208.

Ely, L.L., 1997. Response of extreme floods in the southwestern United States to climatic variations in the late Holocene. Geomorphology 19, 175-201.

Eriksson, M.G., Olley, J.M., Kilham, D.R., Pietsch, T., Wasson, R.J., 2006. Aggradation and incision since the very late Pleistocene in the Naas River, south-eastern Australia. Geomorphology 81, 66-88.

Fairchild, I.J., Smith, C.L., Baker, A., Fuller, L., Spotl, C., Mattey, D., McDermott, F., Eimp, 2006. Modification and preservation of environmental signals in speleothems. Earth-Science Reviews 75, 105-153.

Graf, W., 1979. The Development of Montane Arroyos and Gullies. Earth Surface Processes and Landforms 4, 1-14.

Graf, W.L., 2002. Fluvial Processes in Dryland Rivers. The Blackburn Press, Caldwell.

Harden, T., Macklin, M.G., Baker, V.R., 2010. Holocene flood histories in south-western USA. Earth Surface Processes and Landforms 35, 707-716.

Harvey, J.E., Pederson, J.L., 2011. Reconciling arroyo cycle and paleoflood approaches to late Holocene alluvial records in dryland streams. Quaternary Science Reviews 30, 855-866.

Haug, G.H., Hughen, K.A., Sigman, D.M., Peterson, L.C., Rohl, U., 2001. Southward migration of the intertropical convergence zone through the Holocene. Science 293, 1304-1308.

Heiri, O., Lotter, A. F., Lemcke, G., 2001. Loss on ignition as a method for estimating organic and carbonate content in sediments: reproducibility and comparability of results. Journal of Paleolimnology 25: 101-110.

Hereford, R., 2002. Valley-fill alluviation during the Little Ice Age (ca. AD 1400-1880), Paria River basin and southern Colorado Plateau, United States. Geological Society of America Bulletin 114, 1550-1563.

Hodell, D.A., Anselmetti, F.S., Ariztegui, D., Brenner, M., Curtis, J.H., Gilli, A., Grzesik, D.A., Guilderson, T.J., Mueller, A.D., Bush, M.B., Correa-Metrio, A., Escobar, J., Kutterolf, S., 2008. An 85-ka record of climate change in lowland Central America. Quaternary Science Reviews 27, 1152-1165.

Holliday, V.T., 1985. New Data on the Stratigraphy and Pedology of the Clovis and Plainview Sites, Southern High-Plains. Quaternary Research 23, 388-402.

Huckleberry, G., Duff, A.I., 2008. Alluvial cycles, climate, and puebloan settlement shifts near Zuni Salt Lake, New Mexico, USA. Geoarchaeology-an International Journal 23, 107-130.

Kertész, Á., Gergely, J., 2011. Gully erosion in Hungary, review and case study. Procedia - Social and Behavioral Sciences 19.

Kirby, M., 1972. The Physical Environment of the Nochixtlan Valley, Oaxaca, Anthropology. Vanderbilt University, Nashville, TN.

Kowalewski, S.A., Balkansky, A. K., Walsh, L. R. S., Pluckhahn, T. J., Chamblee, J. F., Rodriguez, V. P., Espinosa, V. Y. H., Smith, C. A., 2009. Origins of the Nuu: Archaeology in the Mixteca Alta, Mexico. University Press Colorado, Boulder.

Lachniet, M. Bernal, J.P., accepted in press. Testing a climatic forcing of societal change at Teotihuacán from a 2400 yr Mesoamerican rainfall reconstruction in Weiss, H., ed., Abrupt Climate Change and Societal Collapse.

Lachniet, M., Asmerom, Y., Bernal, J., Polyak, V., Vaquez-Selem, L., 2013. Orbital Pacing and Ocean Circulation-Induced Collapses of the Mesoamerican Monsoon over the past 22,000 yr. Proc Natl. Acad. Sci. U.S.A. 110, 9255-9260.

Lachniet, M.S., 2009. Climatic and environmental controls on speleothem oxygen-isotope values. Quaternary Science Reviews 28, 412-432.

Langbein, W.B., Schumm, S.A., 1958. Yield of sediment in relation to mean annual precipitation. Trans Amer Geophys Union 39, 1076-1084.

Leigh, D.S., Kowalewski, S.A., Holdridge, G., 2013. 3400 years of agricultural engineering in Mesoamerica: lama-bordos of the Mixteca Alta, Oaxaca, Mexico. Journal of Archaeological Science 40, 4107-4111.

Leopold, L.B., 1951. Rainfall frequency: An aspect of climatic variation. Trans Amer Geophys Union 32, 347-357.

Lozano-Garcia, M.D., Ortega-Guerrero, B., 1998. Late Quaternary environmental changes of the central part of the Basin of Mexico; Correlation between Texcoco and Chalco basins. Review of Palaeobotany and Palynology 99, 77-93.

Lyons, R., Tooth, S., Duller, G.A.T., 2013. Chronology and controls of donga (gully) formation in the upper Blood River catchment, KwaZulu-Natal, South Africa: Evidence for a climatic driver of erosion. Holocene 23, 1875-1887.

Magana, V., Vazquez, J.L., Perez, J.L., Perez, J., 2003. Impact of El Nino on precipitation in Mexico. Geofísica internacional 42.

Mann, D.H., Meltzer, D.J., 2007. Millennial-scale dynamics of valley fills over the past 12,000 C-14 yr in northeastern New Mexico, USA. Geological Society of America Bulletin 119, 1433-1448.

McDermott, F., 2004. Palaeo-climate reconstruction from stable isotope variations in speleothems: a review. Quaternary Science Reviews 23, 901-918.

McFadden, L.D., McAuliffe, J.R., 1997. Lithologically influenced geomorphic responses to Holocene climatic changes in the Southern Colorado Plateau, Arizona: A soil-geomorphic and ecologic perspective. Geomorphology 19, 303-332.

Metcalfe, S.E., O'Hara, S.L., Caballero, M., Davies, S.J., 2000. Records of Late Pleistocene-Holocene climatic change in Mexico - a review. Quaternary Science Reviews 19, 699-721.

Mousazadeh, F., Salleh, K.O., 2014. Factors controlling gully erosion development in Toroud basin – Iran. 3rd International Geography Symposium, Geomed2013 120, 506-512.

Moy, C.M., Seltzer, G.O., Rodbell, D.T., Anderson, D.M., 2002. Variability of El Nino/Southern Oscillation activity at millennial timescales during the Holocene epoch. Nature 420, 162-165.

Mueller, R.G., Joyce, A.A., Borejsza, A., 2012. Alluvial archives of the Nochixtlan valley, Oaxaca, Mexico: Age and significance for reconstructions of environmental change. Palaeogeography Palaeoclimatology Palaeoecology 321, 121-136.

Nordt, L., 2004. Late quaternary alluvial stratigraphy of a low-order tributary in central Texas, USA and its response to climate and sediment supply. Quaternary Research 62, 289-300.

O'Hara, S.L., Streetperrott, F.A., Burt, T.P., 1993. Accelerated soil erosion around a Mexican lake caused by prehispanic agriculture. Nature 362, 48-51.

Patton, P.C., Schumm, S.A., 1975. Gully Erosion, Northwestern Colorado- A Threshold Phenomenon. Geology 3, 88-90.

Perroy, R.L., Bookhagen, B., Chadwick, O.A., Howarth, J.T., 2012. Holocene and Anthropocene Landscape Change: Arroyo Formation on Santa Cruz Island, California. Annals of the Association of American Geographers 102, 1229-1250.

Poesen, J., Nachtergaele, J., Verstraeten, G., Valentin, C., 2003. Gully erosion and environmental change: importance and research needs. Catena 50, 91-133.

Prosser, I.P., Chappell, J., Gillespie, R., 1994. Holocene Valley Aggradation and Gully Erosion in Headwater Catchments, Southeastern Highlands of Australia. Earth Surface Processes and Landforms 19, 465-480.

Reimer, P.J., Bard, E., Bayliss, A., Beck, J.W., Blackwell, P.G., Ramsey, C.B., Buck, C.E., Cheng, H., Edwards, R.L., Friedrich, M., Grootes, P.M., Guilderson, T.P., Haflidason, H., Hajdas, I., Hatte, C., Heaton, T.J., Hoffmann, D.L., Hogg, A.G., Hughen, K.A., Kaiser, K.F., Kromer, B., Manning, S.W., Niu, M., Reimer, R.W., Richards, D.A., Scott, E.M., Southon, J.R., Staff, R.A., Turney, C.S.M., van der Plicht, J., 2013. Intcal13 and Marine13 Radiocarbon Age Calibration Curves 0-50,000 years cal BP. Radiocarbon 55, 1869-1887.

Rincon Mautner, C., 1999. Man and the Environment in the Coixtlahuaca Basin of Northwestern Oaxaca, Mexico: Two Thousand Years of Historical Ecology, Anthropology. University of Texas, Ann Arbor.

Santamaria-Diaz, A., Alaniz-Alvarez, S-A., Nieto-Samaniego, A. F.,, 2008. Deformaciones cenozoicas en la Cobertura de la Falla Caltepec en la Region de Tamazulapam, sur de Mexico. Revista Mexicana De Ciencias Geologicas 25, 494-516.

Schaetzl, R., Anderson, S., 2005. Soils: Genesis and Geomorphology. Cambridge University Press, Cambridge.

Schumm, S.A., 1974. Geomorphic thresholds and complex response of drainage systems, in Morisawa, M, ed., Fluvial Geomorphology. State University of New York at Binghamton, Publications in Geomorphology, pp. 299-310.

Schumm, S.A., 2005. River Variability and Complexity. Cambridge University Press, Cambridge.

Schumm, S.A., Hadley, R.F., 1957. Arroyos and the Semiarid Cycle of Erosion. American Journal of Science 255, 161-174.

Servicio Meterologico Nacional, 2010. Normales Climatologicas 1971-2000, Estacion 0020019: S. J. Bautista Coixtlahuaca. Comision Nacional del Agua (CONAGUA), Mexico.

Servicio Sismologico Nacional, 2015. Institute of Geophysics, National University of Mexico. http://www.ssn.unam.mx/. Last accessed February 2016.

Soil Staff Survey, 2003. US Soil Survey. Natural Resources Conservation Service, United States Department of Agriculture, United States.

Solleiro-Rebolledo, E., Sycheva, S., Sedov, S., McClung de Tapia, E., Rivera-Uria, Y., Salcido-

Berkovich, C., Kuznetsova, A., 2011. Fluvial processes and paleopedogenesis in the Teotihuacan Valley, Mexico: Responses to late Quaternary environmental changes. Quaternary International 233, 40-52.

Stuiver, M., Reimer, P. J., and Reimer, R., 2015. CALIB Radiocarbon Calibration, Version 7.1html ed.

Svoray, T., Markovitch, H., 2009. Catchment scale analysis of the effect of topography, tillage direction and unpaved roads on ephemeral gully incision. Earth Surface Processes and Landforms 34, 1970-1984.

Trejo, I., 2004. Clima, in: Garcia-Mendoza, A.J., Ordonez, M., Briones-Salas, M. (Ed.), Biodiversidad de Oaxaca. Universidad Nacional Autonoma de Mexico, Cuidad Universitaria, pp. 67-86.

Turnbull, L., Parsons, A.J., Wainwright, J., Anderson, J.P., 2013. Runoff responses to long-term rainfall variability in a shrub-dominated catchment. Journal of Arid Environments 91, 88-94.

Valentin, C., Poesen, J., Li, Y., 2005. Gully erosion: Impacts, factors and control. Catena 63, 132-153.

Vera, C., Higgins, W., Amador, J., Ambrizzi, T., Garreaud, R., Gochis, D., Gutzler, D., Lettenmaier, D., Marengo, J., Mechoso, C.R., Nogues-Paegle, J., Silva Dias, P.L., Zhang, C., 2006. Toward a unified view of the American Monsoon Systems. Journal of Climate 19, 4977-5000.

Walling, D.E., Collins, A.L., 2008. The catchment sediment budget as a management tool. Environmental Science & Policy 11, 136-143.

Walker, M.J.C., Berkelhammer, M., Bjorck, S., Cwynar, L.C., Fisher, D.A., Long, A.J., Lowe, J.J., Newnham, R.M., Rasmussen, S.O., Weiss, H., 2012. Formal subdivision of the Holocene Series/Epoch: a Discussion Paper by a Working Group of INTIMATE (Integration of ice-core, marine and terrestrial records) and the Subcommission on Quaternary Stratigraphy (International Commission on Stratigraphy). Journal of Quaternary Science 27, 649-659.

Waters, M.R., Haynes, C.V., 2001. Late Quaternary arroyo formation and climate change in the American Southwest. Geology 29, 399-402.

Waters, M.R., Ravesloot, J.C., 2000. Late Quaternary geology of the middle Gila River, Gila River Indian Reservation, Arizona. Quaternary Research 54, 49-57.

Wilkinson, T.J., 2005. Soil erosion and valley fills in the Yemen highlands and southern Turkey:

Integrating settlement, geoarchaeology, and climate change. Geoarchaeology-an International Journal 20, 169-192.

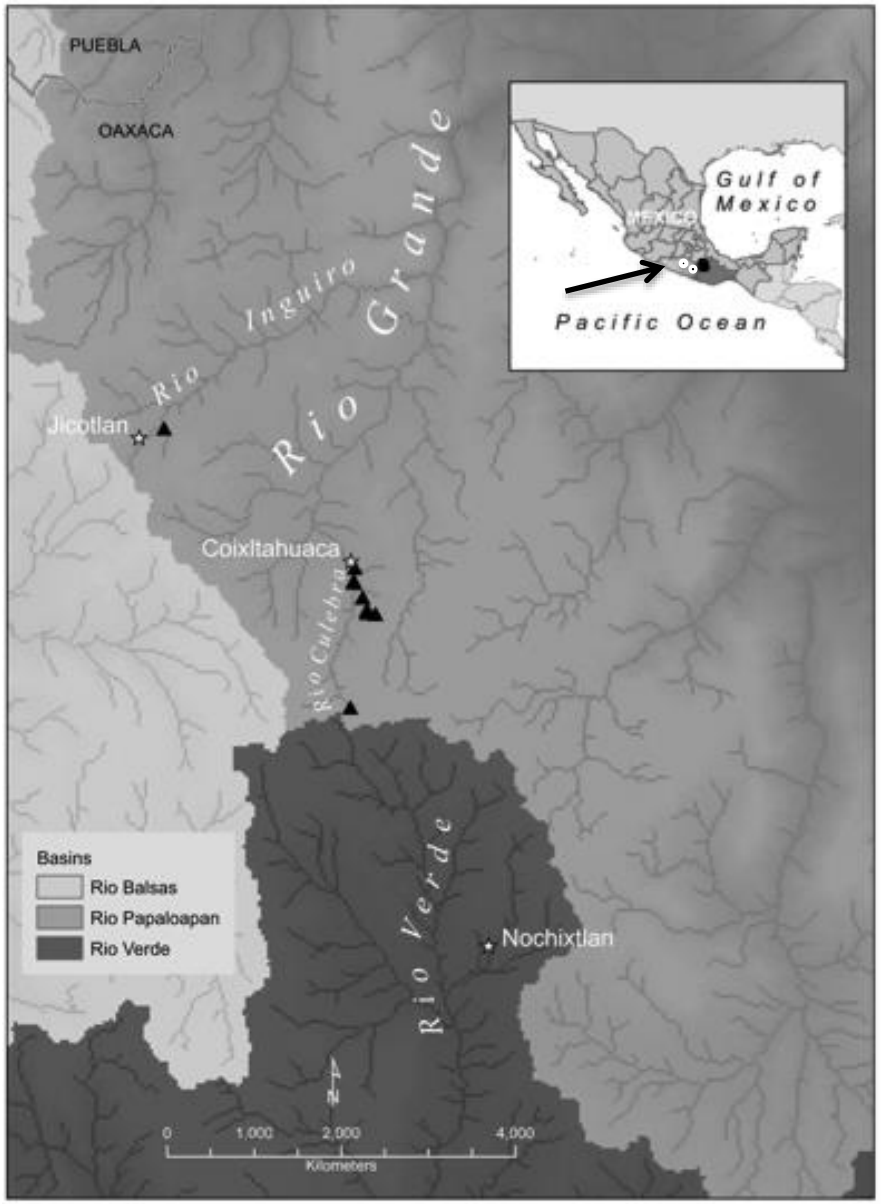

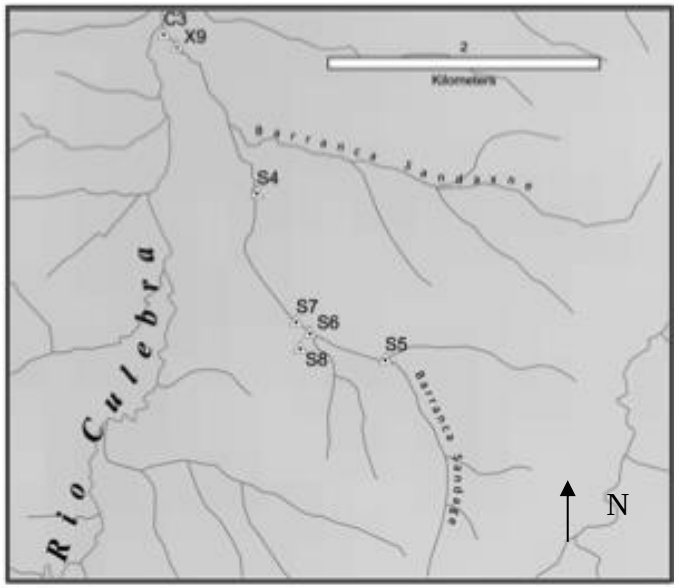

Figure 3.1. Map of study area. The map shows the location of the study area including the Río Culebra, Inguiro and Verde watersheds, along with the municipalities of Coixtlahuaca, Nochixtlan, and Jicotlan (indicated by stars). The main map and detail map show the location of the profiles in the study (black triangles). Each profile is labeled as it is in the text. The general location of the study area (black square) in the state of Oaxaca (very dark gray) is shown in the inset map as well as the location of the stalagmites from the Cueva del Diablo and Juxtlahuaca caves in Guerrero (indicated by the two white circles and an arrow on the inset map) (DEM data from USGS, 2015).

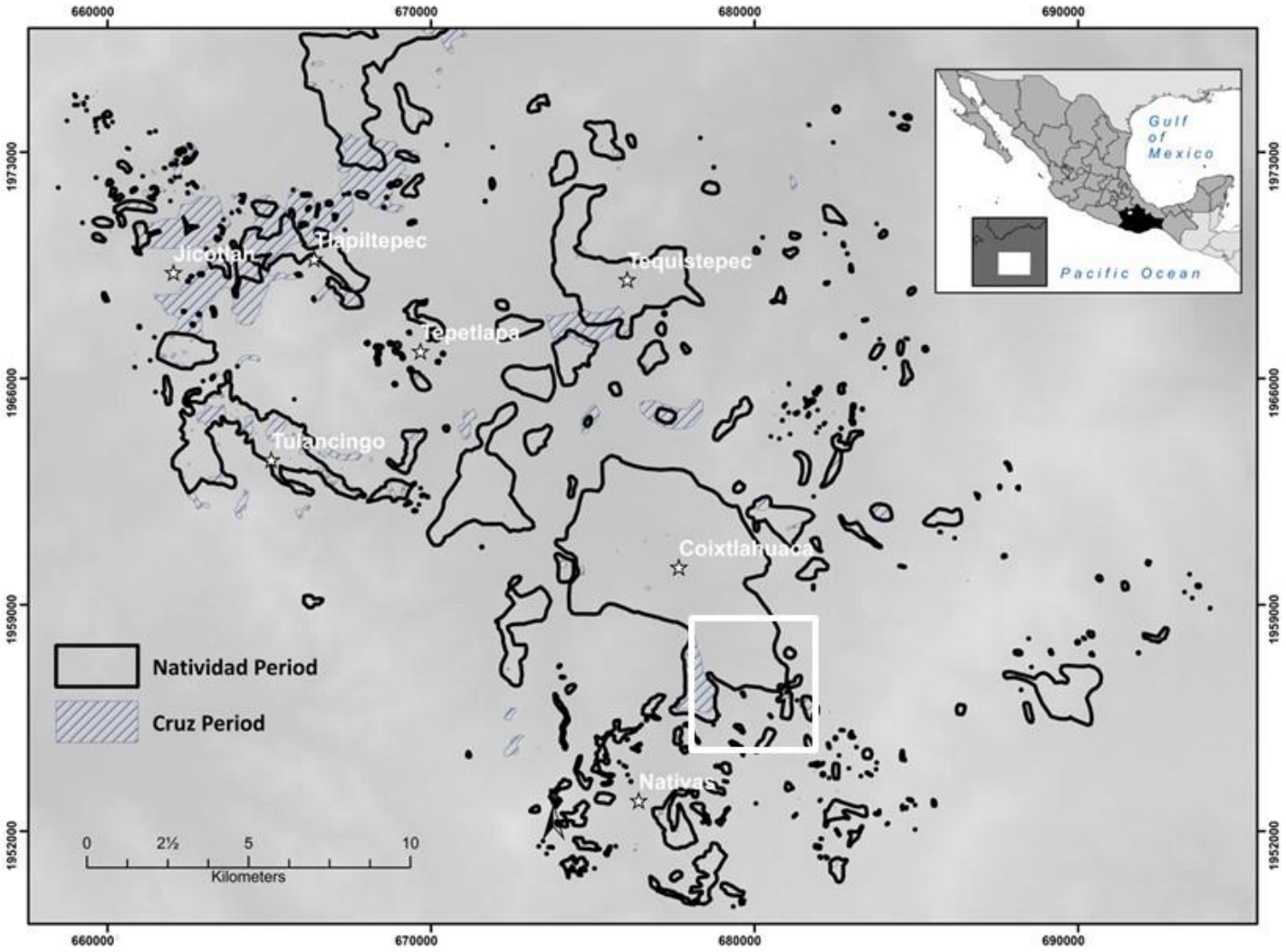

Figure 3.2. Map showing settlement locations in the Río Culebra valley from the Cruz to the Natividad phase. Information is based on an archaeological surveys in 2009 and 2011 (modified from Kowlewski et al., 2009, forthcoming; DEM data from USGS, 2015). White box outlines locations of Barrancas Sandage and Sandaxne.

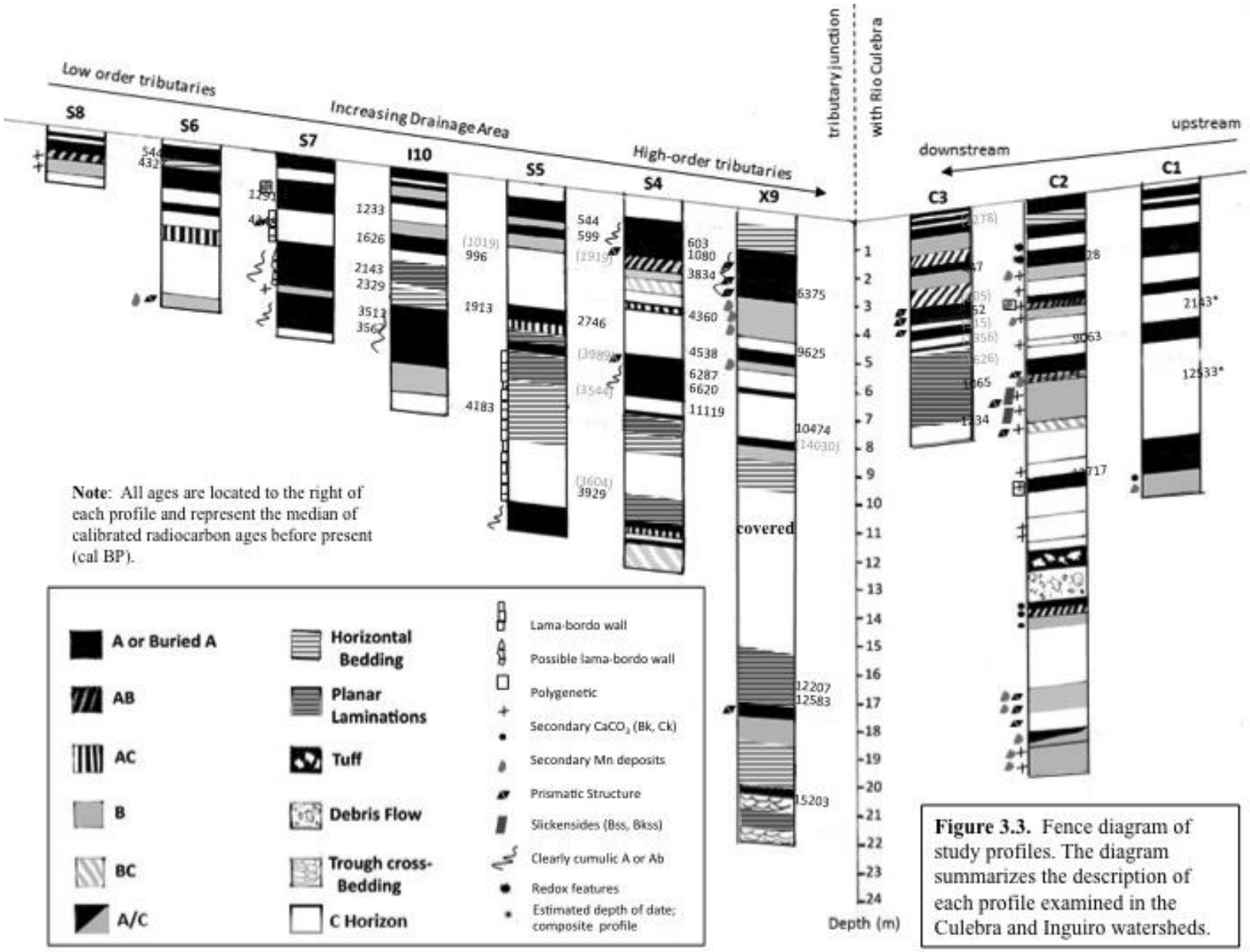

Figure 3.3. Fence diagram of study profiles. The diagram summarizes the description of each profile examined in the Culebra and Inguiro watersheds.

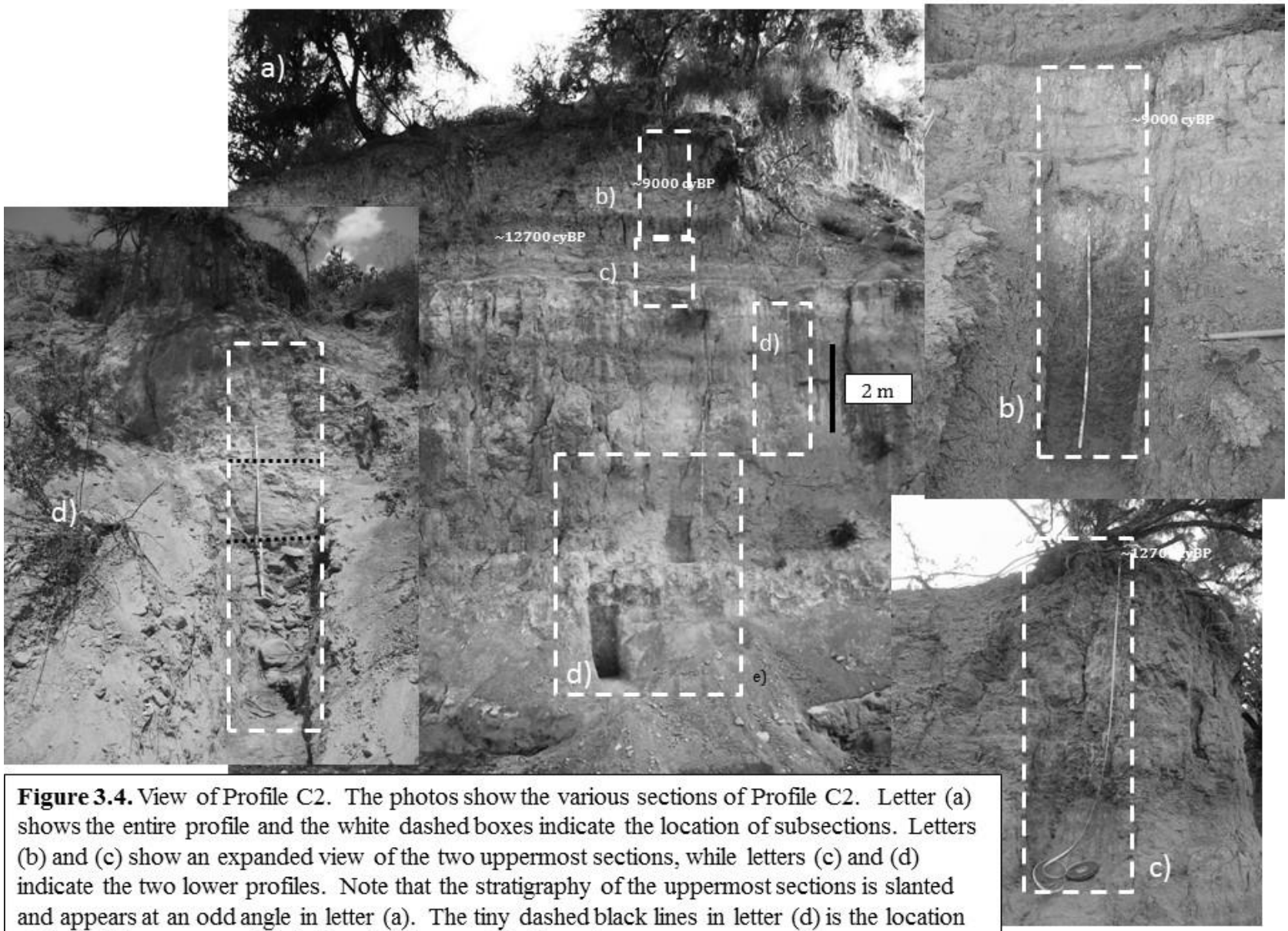

Figure 3.4. View of Profile C2. The photos show the various sections of Profile C2. Letter (a) shows the entire profile and the white dashed boxes indicate the location of subsections. Letters (b) and (c) show an expanded view of the two uppermost sections, while letters (c) and (d) indicate the two lower profiles. Note that the stratigraphy of the uppermost sections is slanted and appears at an odd angle in letter (a). The tiny dashed black lines in letter (d) is the location of the tuff layer over a debris flow (as discussed in the text).

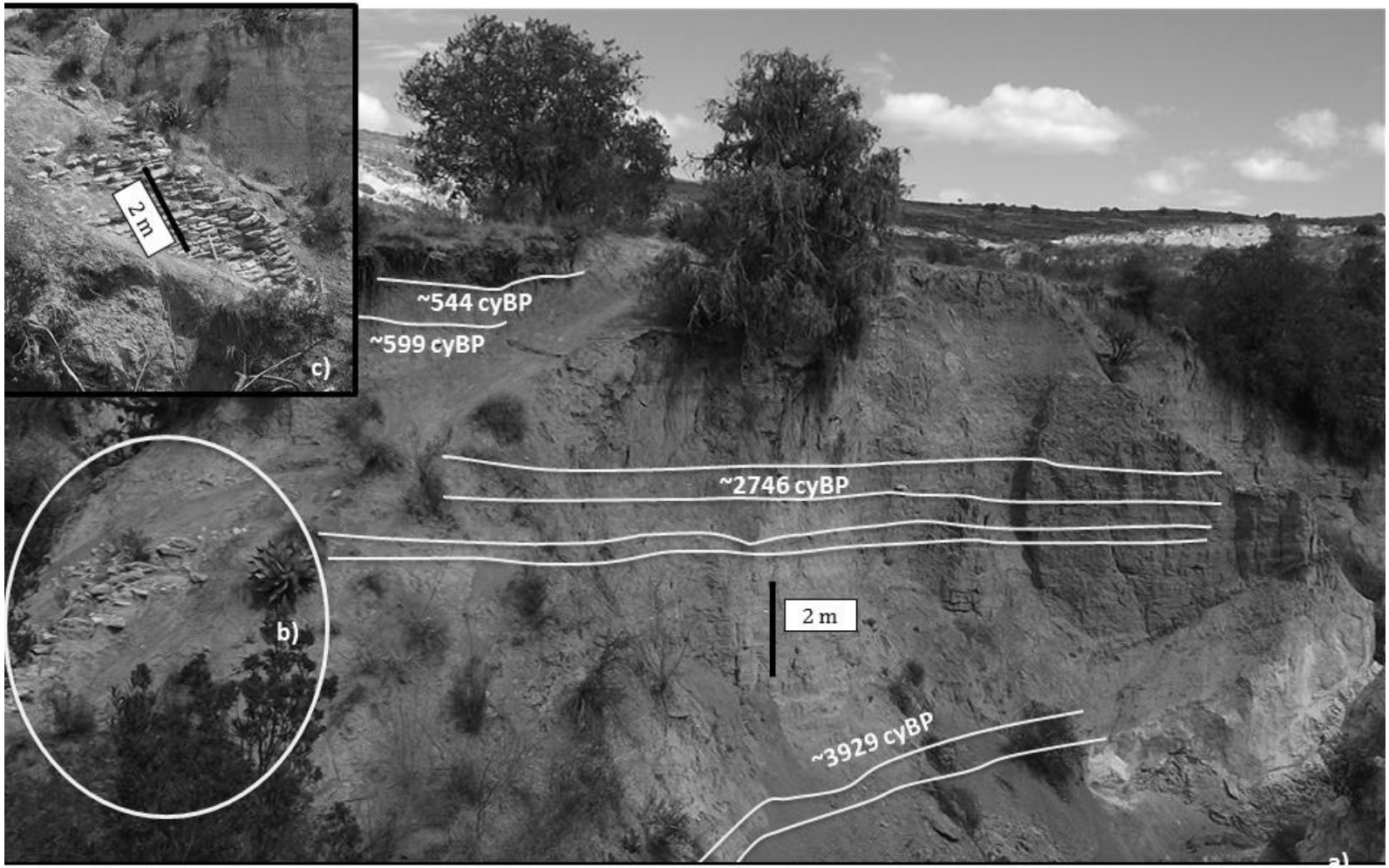

Figures 3.5. Stratigraphy and lama-bordo at S5 (a). The lama-bordo is highlighted by the white circle (b). A view from the opposite side of the lama-bordo can be viewed in the inset photo (c). The lama-bordo is located in the downstream direction. The sediments and paleosols depicted in the image were studied as Profile S5. Paleosols observed at the profile location are highlighted by white lines. The calibrated median ages for paleosols and sediments are labeled at their approximate depth.

Figures 3.6. Results from LOI, weathering indices and horizon thickness analyses. Figure 3.6a shows the thickness for each horizon type according to the median of the calibrated radiocarbon age. The data represents the combined information from all the profiles, and as no median date overlapped, each point represents the actual thickness of the particular horizon at that time. Please note that some of the thickness are only represented by one or two samples. Figures 3b and 3c show measured characteristics for profiles S4 and C2, respectively. The characteristics examined include loss on ignition (LOI) or organic content; calcium carbonate content (Carbonates); percentage of less than 2 mm particle size (<2 mm (%)); percentage of greater than 2 mm particle size (>2 mm (%)); and weathering indices based on the partial geochemical analyses of the profiles (Na/Ti).

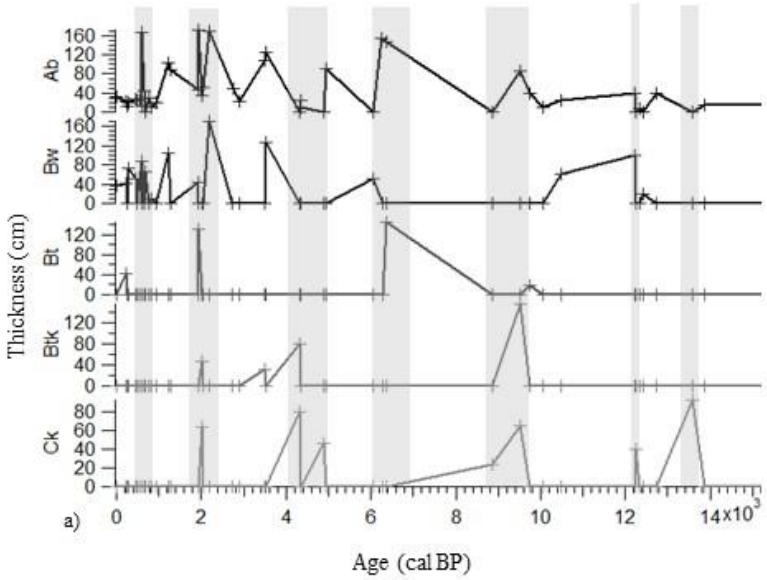

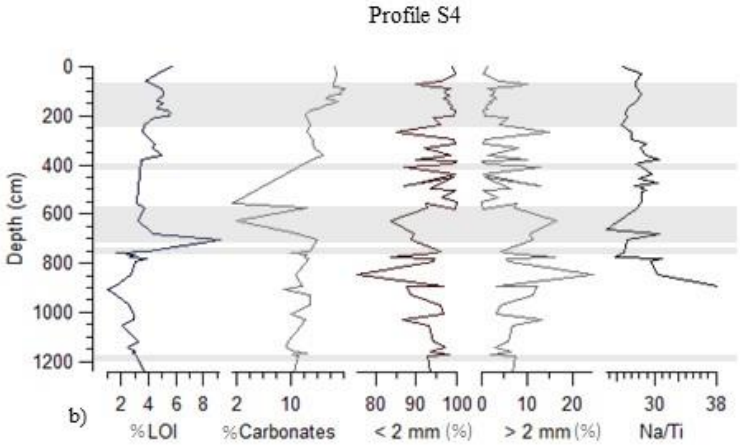

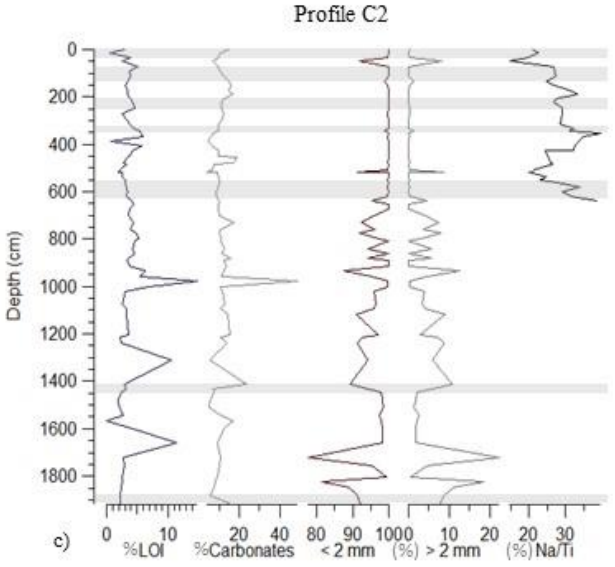

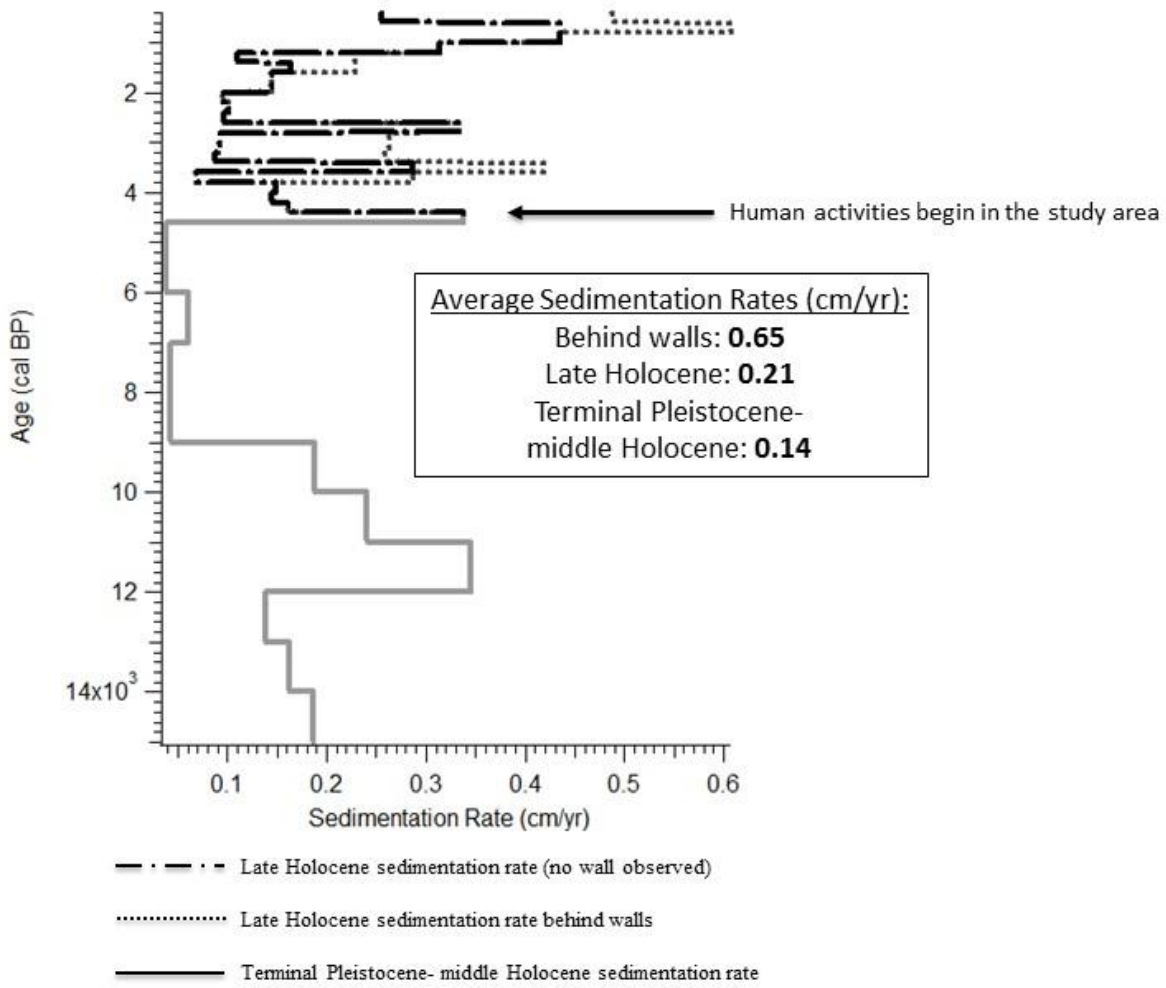

Figure 3.7. Modeled sedimentation rate (cm/yr) for the Río Culebra watershed. Rates are modeled for the Terminal Pleistocene through the late Holocene using the CLAM application (Blaauw 2012) in R software (R Development Core Team, 2008).

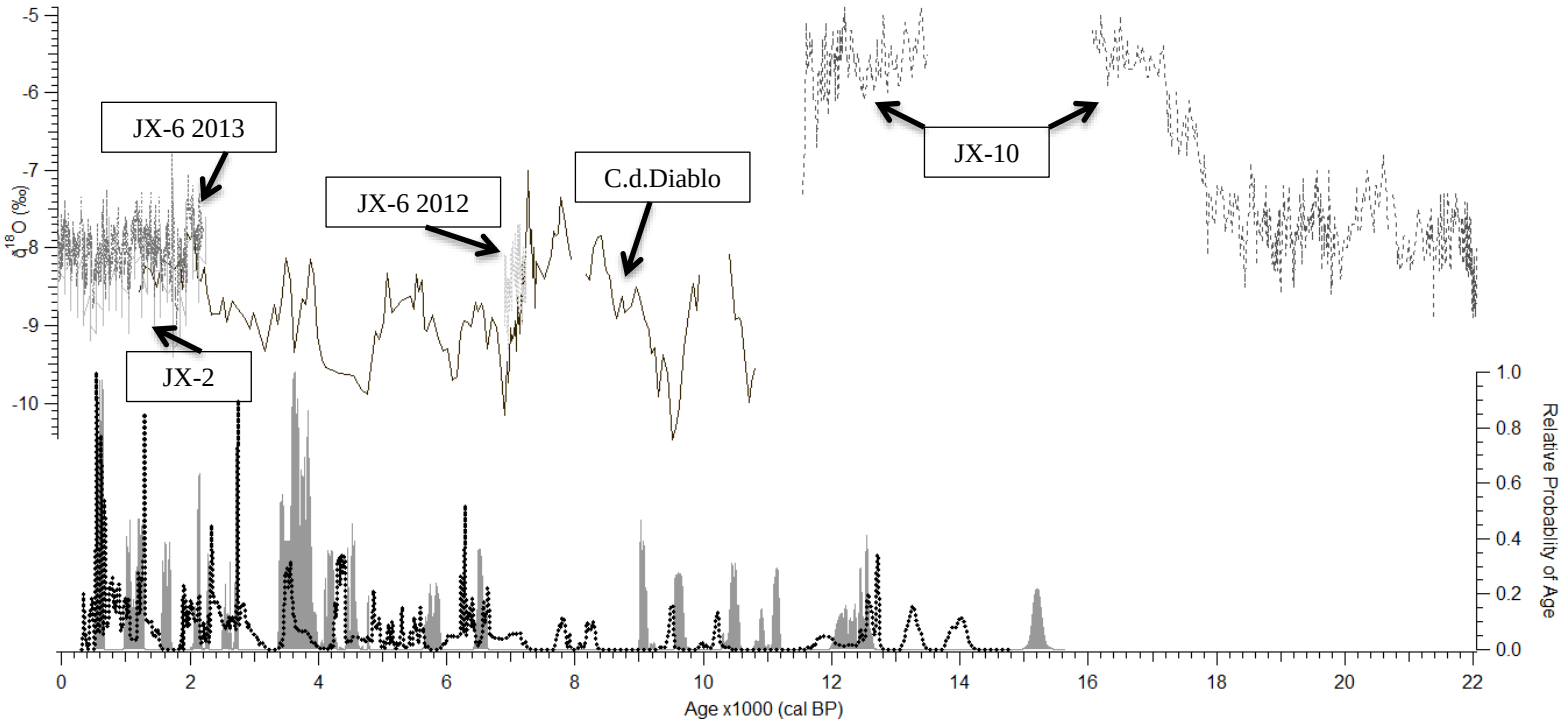

Figure 3.8. Results from qualitative assessment. The figure shows the combined stable oxygen isotope record from the Guerreran stalagmites (from Bernal et al., 2011; Lachniet et al., 2013), and the summed probability curves created from combining the relative probability of age for each calibrated radiocarbon date range of samples from paleosols and alluvium obtained in the Ríos Culebra, Inguiro and Verde watersheds (latter watershed data from Mueller et al 2012).

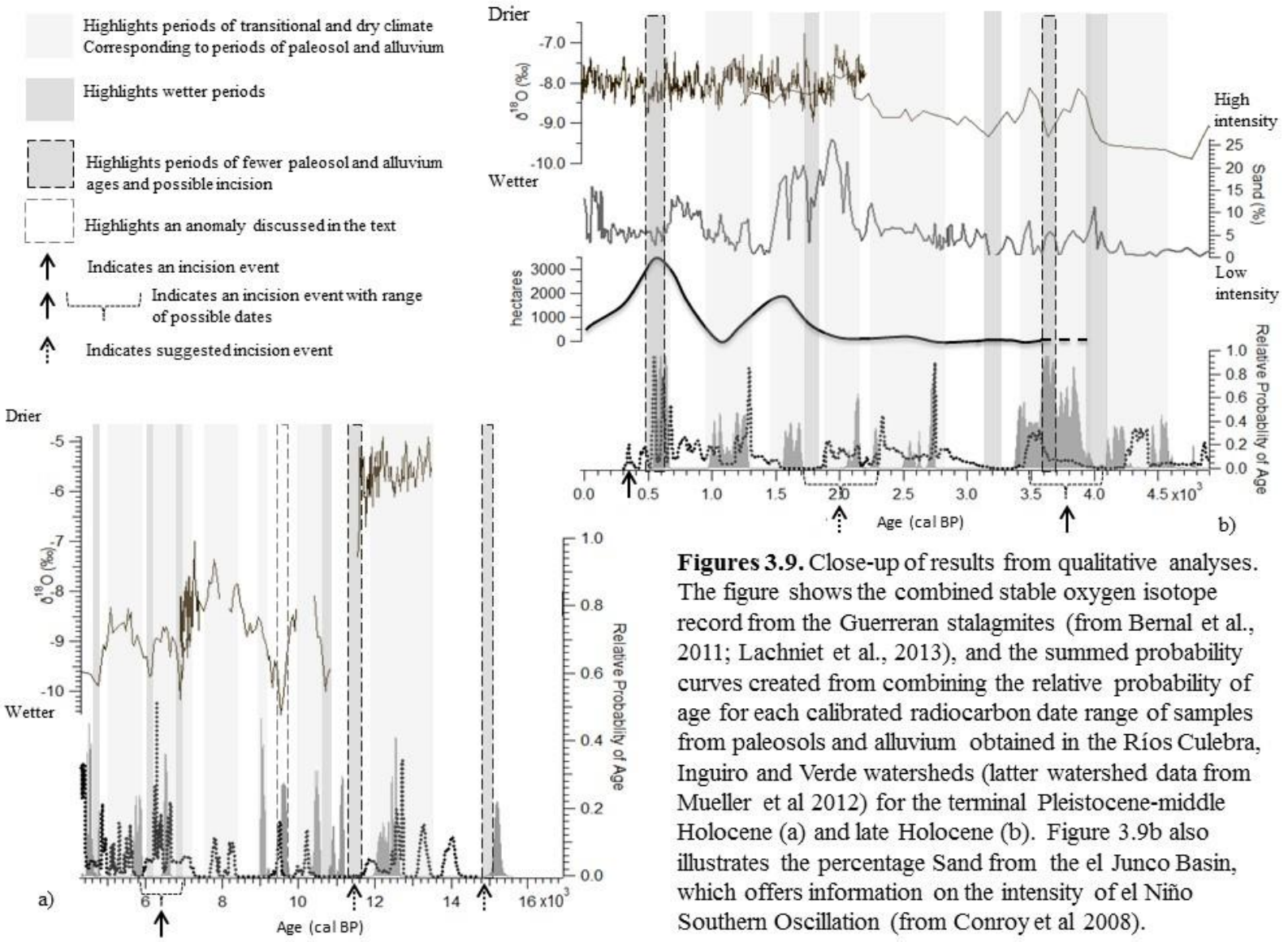

Figures 3.9. Close-up of results from qualitative analyses. The figure shows the combined stable oxygen isotope record from the Guerreran stalagmites (from Bernal et al., 2011; Lachniet et al., 2013), and the summed probability curves created from combining the relative probability of age for each calibrated radiocarbon date range of samples from paleosols and alluvium obtained in the Ríos Culebra, Inguiro and Verde watersheds (latter watershed data from Mueller et al 2012) for the terminal Pleistocene-middle Holocene (a) and late Holocene (b). Figure 3.9b also illustrates the percentage Sand from the el Junco Basin, which offers information on the intensity of el Niño Southern Oscillation (from Conroy et al 2008).

Figure 3.10. Model of arroyo cycles in the Mixteca Alta. Note that the entire river valley aggrades when the arroyo is full. The resulting valley consists of alluvium (and subsequently soils) draped over former deposits with successively younger accretion. The conditions represent the climatic conditions *suggested* for the early and middle Holocene arroyo cycles. Below the 'Stage' labels is the relationship between the *inferred* ENSO intensity and arroyo cycles during late Holocene.

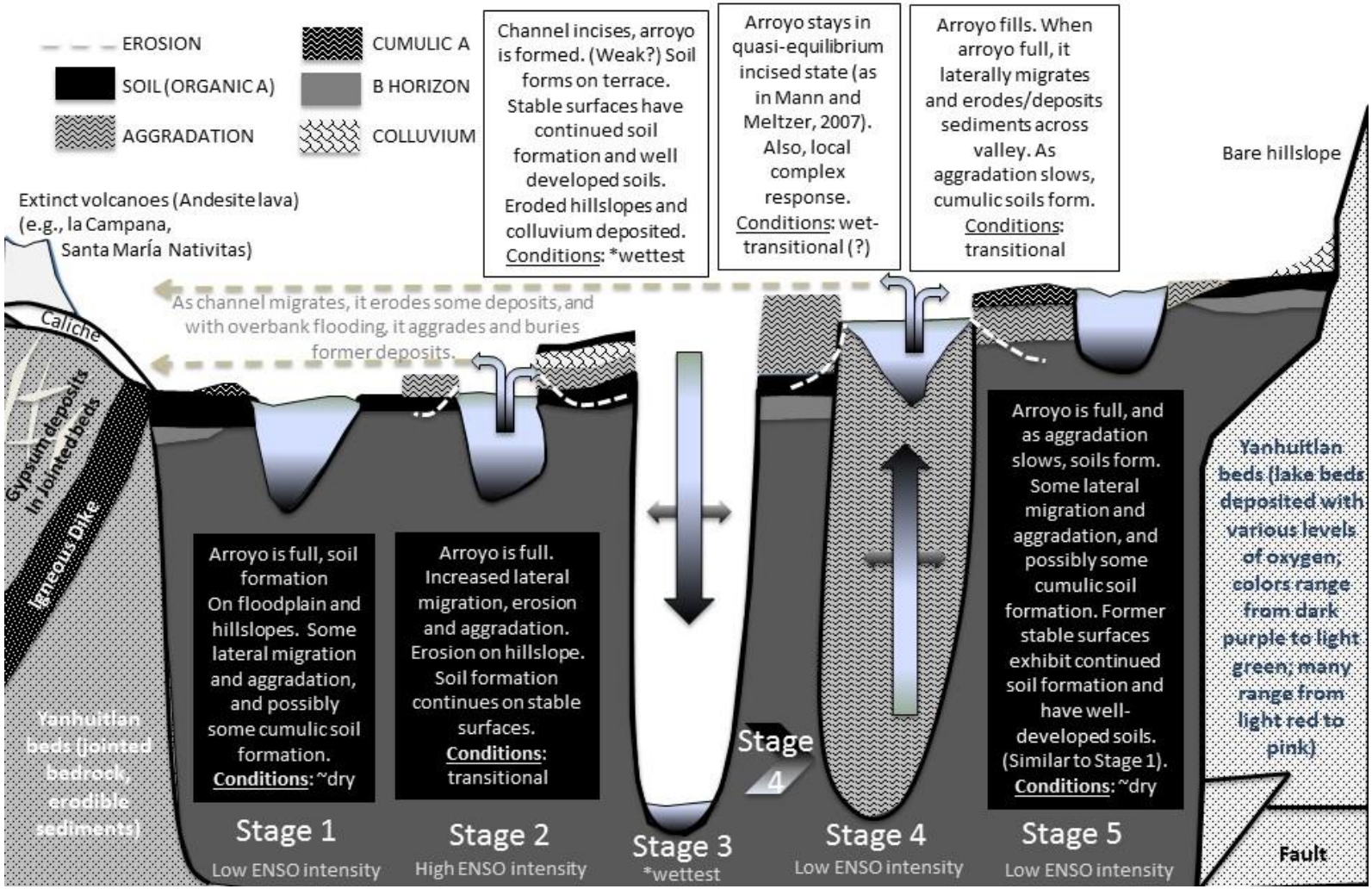

Table 3.1. Cultural phases of the Mixteca Alta. The corresponding Mesoamerican cultural period in both BP and BC/AD ages are also shown (modified from Kowalewski et al., 2009).

Mixteca Alta Cultural Phases	Ages	Mesoamerican Cultural Periods
Natividad	*700 A.D. – 1520 A.D. (1250 - 430 BP)	Post-Classic
Transición/Las Flores	200 A.D. – 700 A.D. (1750 – 1250 BP)	Transition/Classic
Ramos	300 B.C. – 350 A.D. (2250 – 1750 BP)	late and terminal Formative
Cruz	1500 B.C. – 300 B.C. (3450 – 2250 BP)	early and middle Formative

*Note: Population decreases significantly between Las Flores and Natividad phases at ~1,000 cal BP.

Table 2.2 Radiocarbon dates from the study area.

UGA[1] LAB #	Profile	Horizon	Midpoint Depth (cm)	Material	^{14}C Age	(+/-) 1 Stdev	2-sig cal range[2]	Median Age
18031	**C1**	C	600	charcoal	2150	20	2060-2300	2143
18030	**C1**	C	750	charcoal	10550	30	12421-12619	12533
9230	**C2**	Ab	222.5	soil	2060	25	1949-2114	2028
9229	**C2**	Ck	490	charcoal	8130	30	8999-9133	9063
8666	**C2**	Ab	997.5	soil	10813	33	12684-12750	12717
8651	**C3**	C	67.5	soil	1332*	24	1180-1130	1278
12644	**C3**	Ab	199	charcoal	370	20	321-499	447
8652	**C3**	C4	280	charcoal	598	24	542-651	605
12645	**C3**	Ab	366.5	charcoal	550*	25	521-633	552
12646	**C3**	C	415	charcoal	1060*	25	928-1050	961
8656	**C3**	C	471.5	soil	1471*	24	1295-1515	1356
14628	**C3**	C	545	charcoal	1720*	25	1562-1698	1626
8657	**C3**	C	670	charcoal	1154	23	983-1152	1065
8658	**C3**	C	767.5	charcoal	1281	23	1181-1278	1234
8649	**CFV**	C	bottom of cut	soil	5734	26	6451-6631	6527
8648	**CFV**	Ab	992.5	soil	23529	64	27517-27829	27677
8661	**I10**	Ab	103.5	soil	1223*	23		
14629	**I10**	Bwb	208	charcoal	1120	25	960-1166	1019
8660	**I10**	Ab	243	charcoal	1091	23	939--1057	996
8664	**I10**	C	470.5	charcoal	1964	24	1869-1987	1913
8663	**I10**	Ab	475.5	soil	1977*	25	1879-1949	1926
8662	**I10**	C	802.5	charcoal	3798	26	4039-4281	4183
12647	**LB 175**	ALLUVIUM	300	charcoal	5380*	25	6026-6279	6207
9224	**LB 175**	ALLUVIUM	below wall	charcoal	3370	25	3564-3689	3613
8643	**LB 175**	ALLUVIUM	below wall	charcoal	3384	26	3572-3692	3626
9226	**LB 175**	ALLUVIUM	below wall	charcoal	3430	25	3609-3822	3677
8650	**LB 175**	ALLUVIUM	below wall	organic sediments	6783*	26	7587-7670	7631

9225	**LB 175**	ALLUVIUM	below wall	organic sediments	6270*	30	7161-7263	7212
18033	**S11**	Ab	855	tooth enamel	25610	70	29426-30123	29716
8398	**S4**	Ab	90	soil	880*	25	690-925	784
8393	**S4**	Ab	105	charcoal	570	25	531-641	603
14633	**S4**	Ab	125	soil	1160	25	986-1175	1080
14634	**S4**	Ab	195	soil	3530*	30	3712-3891	3796
8391	**S4**	AB	246	charcoal	3540	25	3722-3896	3834
8392	**S4**	A and C	398	charcoal	3920	25	4256-4425	4360
8394	**S4**	C	517	charcoal	4060	25	4439-4784	4538
8397	**S4**	Ab	559	soil	5470	25	6212-6307	6282
8396	**S4**	Ab	587	soil	5810	25	6507-6674	6620
14630	**S4**	C	712-716	charcoal	9670	35	11808-11201	11119
8644	**S5**	Ab	67.5	soil	541	23	518-629	544
12641	**S5**	Bw	128	charcoal	620	20	553-656	599
14632	**S5**	AB	191	soil	1970	25	1873-1988	1919
8645	**S5**	C4	324	charcoal	2545	24	2504-2747	2715
12642	**S5**	Ab	434.5	charcoal	2600	25	2721-2760	2746
8646	**S5**	C	545	soil	3663*	25	3850-4150	3989
12643	**S5**	C	743	charcoal	3320*	25	3476-3630	3544
9228	**S5**	C	1080	charcoal	3360*	25	3513-3688	3604
8647	**S5**	C	1081	charcoal	3215	26	3377-3479	3427
9227	**S5**	C	1100	charcoal	3620*	25	3851-4060	3929
8653	**S6**	Ab	109	soil	1360	23	1266-1309	1291
8654	**S6**	Ab	228.5	soil	3905	26	4249-4419	4348
8395	**S7**	Ab	137	soil	1280	25	1181-1278	1233
8386	**S7**	C4	280	charcoal	1720	25	1562-1698	1626
8388	**S7**	Ab	330	charcoal	2150	25	2048-2303	2143
8387	**S7**	Ab	350	charcoal	2290	25	2184-2351	2329
8389	**S7**	Ab	522	charcoal	3280	25	3453-3565	3511

8390	**S7**	Ab	585	charcoal	3330	25	3480-3639	3567
8667	**S8**	Ab	36	soil	561	24	527-637	595
8668	**S8**	Ab	85	soil	3880	26	4238-4414	4327
9234	**X9**	Ab	252.5	soil	5610	30	6310-6446	6375
9233	**X9**	BC	450	charcoal	8690	30	9548-9703	9625
9232	**X9**	C7	785	charcoal	9280	30	10376-10573	10474
9231	**X9**	C	802.5	soil	12260*	30	14035-14309	14159
9235	**X9**	C	1700	charcoal	10350	30	12330-12250	12207
8655	**X9**	Ab	1750	soil	10587	32	12523-12670	12583
14631	**X9**	C	2300	charcoal	12760	40	15060-15348	15203
				NOCHIXTLAN				
	Yan7	paleosol	190	soil	6919*	110		7763
	Yan2	paleosol	630	soil	9246*	66		10418
	Ver6	C	200	organic sediments	5030*	40		5797
	Yuc1	C	890	organic sediments	5774*	67		6574

Notes:
[1] All radiocarbon ages were analyzed at the Center for Applied Isotopes at the University of Georgia.
[2] All dates were calibrated using the CALIB software (Stuiver et al., 2015) online and the INTCAL2013 calibration curve (Riemer et al., 2013).
* Signifying those ages not incorporated into further analyses.

Table 2.2. Radiocarbon dates from the study area. All of the dates obtained from the Culebra and Inguiro watersheds are listed here, including those dates that were discarded. The dates that were discarded from the Verde watershed (Mueller et al., 2012) are also listed. The final column of the table indicates the median date from the calibrated radiocarbon age range.

CHAPTER 4

STABLE CARBON ISOTOPE ANALYSIS OF ALLUVIAL PALEOSOL ORGANIC MATTER IN THE MIXTECA ALTA, OAXACA, MEXICO[3]

[3] Holdridge, G. and D.S. Leigh. To be submitted to *Geoarchaeology*.

Abstract

We examine $\delta^{13}C$ values from soil organic matter (SOM) from the Culebra, Inguiro and Verde watersheds (the latter was studied by Mueller et al., 2012) located in the Mixteca Alta from the terminal Pleistocene to the present. In sum, the relatively depleted terminal Pleistocene-early Holocene $\delta^{13}C$ values suggest that C_3 vegetation was more common than C_4 and Crassulacean Acid Metabolism (CAM) vegetation, while the middle Holocene $\delta^{13}C$ values are enriched and suggest the prevalence of C_4 and CAM relative to C_3 plant biomass. The late Holocene stable carbon isotope values vary, but in general they suggest slightly more C_3 versus C_4 and CAM plant biomass than the previous period. The SOM $\delta^{13}C$ values were compared against the local paleosol data, and other paleoclimatic and paleoenvironmental proxies from central and southwestern Mexico (e.g., Metcalfe et al. 2000; Caballero et al., 2010; Lachniet et al., 2013). It was found that the terminal Pleistocene through the middle Holocene paleovegetation of the watersheds in the study area reflects generally accepted changes in paleoclimate. Similar to findings in central Mexico, the paleoenvironment of these watersheds was impacted by human activities, such as agriculture during the late Holocene that affected vegetation and caused erosion. Values of $\delta^{13}C$ show a significant rise between 3,500 cal BP and 1,250 cal BP, with one notable cluster of enriched values corresponding to the Post-Classic cultural period (local Natividad phase, 1,250-500 cal BP), when the population surpassed 100,000. Since the late Formative period (local late Cruz phase, starting ~3,500 cal BP), lama-bordo (i.e., sediment check-dams) and agricultural terrace constructions were important for land use management and agriculture, which became widespread by the Post-Classic period. The

highly enriched values associated with widespread agricultural structures suggest the increased importance of maize cultivation during the late Holocene.

4.1 Introduction and Background

Paleosols are important because they provide a local source of information concerning past environmental conditions. Stable carbon isotopes from soil organic matter (SOM), in conjunction with paleosol studies and radiocarbon dates have been useful in indicating the timing of vegetation changes in the late Quaternary (Cerling et al., 1989; Driese et al., 2005; Hall and Penner, 2013; Coe et al., 2014). $\delta^{13}C$ values vary within plants, and thus in SOM for several reasons including: 1) atmospheric (CO_2) and climatic factors (precipitation and temperature) (Cerling et al., 1989); 2) physiographic factors (e.g., latitude and altitude); 3) and genetic diversity among plant varieties (Tieszen, 1991). Plant biomass and associated isotopes are especially sensitive to changes in paleoclimatic conditions in semi-arid and arid environments subject to water-stress and temperature fluctuations (Amundson et al., 1994; Ortega-Rosas et al., 2008). In some cases, analyses on bulk soil organic matter have the potential to offer evidence of landscape disturbance associated with agricultural activity (de Rouw et al., 2015), or more direct evidence, such as the past planting of maize (Johnson et al., 2007; McClung de Tapia and Adriano-Moran, 2012).

Measuring the $\delta^{13}C$ isotopic values of SOM offers information about past vegetation composition (Cerling et al., 1989). Variations in the $\delta^{13}C$ values in SOM reflect the values of the original plant community, which are different for C_3, C_4, and Crassulacean Acid Metabolism (CAM). The $\delta^{13}C$ value of C_3, C_4, and CAM results from diverse fractionation associated with

different photosynthetic pathways (Farquhar et al., 1989; Tieszen, 1991; Boutton et al., 1998). C_3 plants follow the Calvin-Benson photosynthetic pathway, C_4 plants use the Hatch-Slack Cycle (Leavitt et al., 2007), while CAM follows a variation of the C_4 pathway (Keeley and Rundel, 2003). Values are determined by comparing the $^{13}C/^{12}C$ ratio to a standard, which is typically the Pee Dee Belemnite fossil formation (PDB) (Farquhar et al., 1989).

The resulting differences between the $^{13}C/^{12}C$ and standard reflect these fractionation and metabolic variations, though these processes and resulting values may overlap. In general, typical isotopic values for C_3 plants range from -22 to -32 per mil, those for C_4 plants range from -9 to -17 per mil, and those for CAM range from -10 to -30 per mil (Boutton et al., 1998; Osmond et al., 1973). Depending on the environment, CAM may overlap significantly with either C_4 or C_3 species in terms of their $\delta^{13}C$ value, (Keeley and Rundel, 2003). The intermediate values of CAM reflect their flexibility; for example, if the $\delta^{13}C$ values are closer to the C_4 range, it implies primarily nocturnal carbon intake, whereas if values are more depleted and similar to C_3 biomass, it suggests that environmental conditions favored more direct cycling of CO_2 (Farquhar et al., 1989; Bhagwat, 2005). Unfortunately, it is thus far impossible to distinguish CAM from C_4 and C_3 ratios based on $\delta^{13}C$ values alone. A study in Baja California on modern SOM $\delta^{13}C$ showed that enriched $\delta^{13}C$ values reflected greater percentage of CAM biomass in locations with increasing summer precipitation, rather than alternating photosynthetic adaptations of this plant type (Amundson et al. 1994). Both C_4 and CAM plants have been interpreted together due to their common adaptive strategies, which are advantageous over C_3 plants in low CO_2, and drier and warmer climatic conditions.

Analyses of SOM should reflect the original average value of the vegetation, but organic matter is heterogeneous in soil and sediment (Coe et al., 2014). Some difference between the actual vegetation and the SOM values exists because it takes time for decomposing organic matter to become integrated into the soil, which may alter the $\delta^{13}C$ SOM values. The rate at which the change in isotopic values occurs is related to the rate at which the soil organic matter decomposes, and is referred to as the soil organic matter residence time or turnover rate (Boutton et al., 1998). Some studies have actually preferred SOM in modern surface soils as an indicator of present C_3 versus C_4 biomass because it represents the average of carbon inputs over a number of years (von Fischer et al., 2008).

Changes in temperature, precipitation and atmospheric CO_2 affect the amounts of C_3 versus C_4 and CAM plants in the landscape (Cerling et al., 1997; Huang et al., 2001). Both C_4 and CAM plants have an advantage over C_3 plants in dry, hot and/or saline environments (Sage, 2005). One of the main reasons for this advantage is linked to a mechanism of C_4 and CAM plants that fixes atmospheric CO_2 more efficiently (Ehleringer, 2005). Photorespiration involves the enzyme rubisco, which fixes CO_2 in all plants. In C_3 plants, air enters the stomata by diffusion and either CO_2 or O_2 can be fixed; however, if the plant metabolizes oxygen it results in photorespiration or the loss of CO_2 and energy. The amount of oxygen metabolized is a function of the O_2/CO_2 atmospheric ratio and temperature. High temperature increases the fixation of oxygen and decreases the light-use efficiency in C_3 plants. Conversely, C_4 plants avoid photorespiration by converting CO_2 into a four-carbon molecule and moving it into an internal compartment commonly known as the bundle sheath tissue, where it is concentrated around rubisco (Ehleringer, 2005; Sage, 2005). At cooler temperatures, C_3 plants assimilate

more CO_2 relative to C_4 plants, and thus the former has the competitive advantage. Conversely, higher temperatures (i.e., 35°C or above) favor C_4 plants because they reduce CO_2 assimilation and increase photorespiration losses in C_3 plants. Therefore, temperature is often a dominant factor (after CO_2) in determining or reflecting C_3 vs C_4 productivity (Ehleringer, 2005; von Fischer et al., 2008; Sage, 2008).

CAM plants are similar to C_4 in that they can also concentrate CO_2 where photosynthesis occurs, though via a different mechanism. Typically CAM plants absorb and store CO_2 biochemically during the night, and process it during the day with closed stomata, which also ensures water conservation (Ehleringer, 2005). CAM plants are limited because they need sufficient light and space to grow, and thus they cannot outcompete the faster turnover/growth of C_4 in similar environmental conditions (Keeley and Rundel, 2003).

Precipitation and moisture also affect photosynthetic pathways in plants in conjunction with CO_2 and temperature. In water-stressed environments all plants must close their stomata to reduce water loss, reducing assimilation of CO_2, but this especially occurs in C_3 plants (Sage, 2005). In general, low water, low humidity and/or high salinity increase photorespiration in C_3 vegetation, making dry and/or saline climates disadvantageous to C_3 versus C_4 and CAM plants (Ehleringer, 2005; Sage, 2005). However, in high CO_2 conditions and relatively moderate temperatures the stress on C_3 plants and photorespiration is not enough to counteract their survival, even in very dry or saline conditions (Sage, 2005). Notably, C_4 plants do not have any morphological modifications to avoid water loss *per se* (Boom et al., 2001), whereas CAM plants maximize water retention efficiency by closing their stomata during the day (Keeley and Keeley, 1989). Variability in rainfall amount and inter-annual rainfall occurrence appears very

important in conjunction with growing season temperature and CO_2 to influence the resulting dominant plant type in present day environments (Shaw et al., 2005). Average temperature during the wet or growing season is linked to differentiation in pathways, whereby C_4 and CAM plants are prevalent in summer rain regimes, and C_3 plants dominate in winter rain regimes (Ehleringer, 2005).

4.1.1 Objectives

In this paper we explore the late Quaternary paleoenvironmental changes in the Mixteca Alta in south-central Mexico as reflected in the $\delta^{13}C$ values from SOM. Stable carbon isotope data from paleosols will be presented from the Río Culebra watershed in Coixtlahuaca and Nativitas municipalities, and will include data from one profile along the Río Inguiro basin in Jicotlan. The study will also include data from the Río Verde watershed in Nochixtlan studied by Mueller et al. (2012). The $\delta^{13}C$ values from SOM represent changes in paleovegetation over the last 16,000 years. Many of the $\delta^{13}C$ values were obtained from numerically dated (primarily radiocarbon dating) organic matter within buried A horizons (these samples will be referred to as dated buried A SOM samples) from profiles examined in the Culebra, Inguiro and Verde watersheds. Other samples were obtained from undated organic matter in buried A horizons (these samples will be referred to as interpolated buried A SOM samples), and their ages were estimated using linear interpolation from other dates in the same profile (see Methods). Analyses of isotope values and descriptive properties of paleosols will be used as proxies for the local paleoenvironmental signal. This local signal will be compared to pre-existing studies of paleoclimate data from stalagmites in the nearby state of Guerrero (Bernal et al., 2011; Lachniet et al., 2013), regional changes in pollen, diatom and lake levels in central

Mexico (e.g., Metcalfe et al., 2000; Caballero et al., 2010), and overall changes in global atmospheric CO_2 as recorded in the Antarctic ice cores (Monnin et al., 2001; 2004). The main objectives of this study are twofold: 1) to determine if the $\delta^{13}C$ values from SOM are non-randomly distributed throughout the late Quaternary and possibly related to atmospheric and climate changes; and 2) to determine if non-random changes correspond to the prevailing knowledge of regional paleoenvironmental fluctuations and/or human manipulations of vegetation in the late Holocene (i.e. maize agriculture).

4.2 Study Sites

Data were collected from stratigraphic sections within deep gullies, locally known as barrancas, in the Río Culebra watershed, located in the municipalities of Coixtlahuaca and Nativitas (roughly 17° 43'N and 97° 19'W and 17° 27'N and 97° 13'W, respectively) and the Inguiro watershed in the municipality of Jicotlan (approximately 17° 27'N and 97° 13'W) (Figure 4.1). The study area is located in the Mixteca Alta, Oaxaca, Mexico, which is a sub-region of the Mixteca physio-cultural region in northern Oaxaca (see Balkansky et al., 2000). The Mixteca Alta lies approximately 2300 m amsl (above mean sea level) in the Sierra Mixteca, which is one of the sub-ranges of the Sierra Madre del Sur (Krasilnikov et al., 2013).

The high terrain of the Sierra Madre del Sur bordering the basin causes a rain shadow in the region. The North American Monsoon is the source of most precipitation in the region, the timing and duration of which is predominantly controlled by the movement of the Intertropical Convergence Zone (ITCZ), and the intensity of the El Niño Southern Oscillation (ENSO) (Trejo, 2004). The region is characterized as a semi-arid climatic regime (BSh Köppen

classification), averaging around 528 mm of rain per year, with an average annual temperature range between 13.2-18.6 ºC (Servicio Meteorologico Nacional, 2010). The warmest time of the year overlaps with the rainy season, which spans May through October, with peaks in June and September.

The geology of the study area predominantly consists of lower to middle Tertiary siltstones and claystones (shales), referred to as the Yanhuitlan Formation, which precede minor outcrops of middle Tertiary volcaniclastics and andesites (Santamaria-Diaz 2008). Quaternary alluvium fills much of the main valleys of the Ríos Culebra and Inguiro as well as their tributaries. These dryland streams have incised about 7 m to 35 m down into the Quaternary alluvium. A study of soils in the Coixtlahuaca District (Sánchez, 2004) indicated that 46% of the soils consist of Aridisols, 49% of the soils are Mollisols (or more specifically Rendolls), and the remaining 5% fall under Alfisols, Entisols, and Vertisols. The majority of the soils are associated with calcareous parent materials (Sánchez, 2004). Many of the hillslopes in the Mixteca have exposed calcrete surfaces, and both hillslopes and valley alluvium exhibit widespread barranca development (Rincon, 1999; Leigh et al., 2013). Another study by the National Institute of Statistics and Geography (INEGI, 2005) in Mexico indicates that Entisols, Vertisols and Mollisols are the primary soil types in the municipalities of Coixtlahuaca, Nativitas and Jicotlan.

The land cover (Figure 4.2) within the Culebra, Inguiro, and Verde watersheds primarily consists of human-induced pastureland, agricultural land and secondary vegetation, along with a small amount of urban land. Both Culebra and Verde watersheds also contain some bare ground and chaparral. The chaparral includes spiny and schlerophyllis scrubland (e.g.,

rosetofilous desert scrub). Primary forests are composed of mainly live oak, pine, and juniper, while secondary vegetation consists of juniper, oak and pine scrublands (Colín, 2004; INEGI landcover data, 2013). Recently, pine trees have been planted to reforest some bare hillslopes in an effort to reduce erosion (Rafael Arzate Aguirre, pers. Com.).

4.3 Methods

Stable carbon isotope analyses were conducted on the SOM from buried A horizons using profiles described and sampled in alluvium located in the Río Culebra and Río Inguiro valleys, as reported in Chapter 3. For the profiles C2, C3, S1 through S8, I10, and X9, one or more radiocarbon dates on charcoal or SOM from buried organic horizons offered ages for the strata in the profile. Some of the $\delta^{13}C$ values incorporated into this study were from the radiocarbon dates made on preserved buried A horizons, sampled within 5-10 cm of the boundary to overlying horizons. A total of 13 $\delta^{13}C$ values were obtained from the upper portion of these buried A horizons. All radiocarbon dates from charcoal and SOM from buried A horizons were calibrated using the online CALIB software (Stuiver et al., 2015) and the INTCAL13 calibration curve (Reimer et al., 2013).

Another 20 samples of buried A SOM samples were directly analyzed for percent total organic carbon (%TOC) and $\delta^{13}C$ but were not directly dated. Samples were obtained on the upper part of the buried A horizons, 10-25 cm from the boundary with the horizon above, from the following profiles: C1, C2, S4, S11, X9, and I10. Analyses were made on these profiles to observe changes in $\delta^{13}C$ according to depth and to determine the reproducibility of the isotopic signature in the SOM from this region. The ages for these $\delta^{13}C$ values from buried A SOM were

interpolated using the Classical Age Model (CLAM) of Blaauw (2010, version 2.2) with R software (R Core Team, 2013).

The $\delta^{13}C$ data from 20 buried A SOM samples from Río Verde (Mueller et al., 2012) were combined with the data from Culebra and Inguiro for further study. The $\delta^{13}C$ data from charcoal samples (18 samples in total) from buried A horizons were also included for initial comparison to the SOM from buried A horizons. Finally, SOM from modern soils were gathered from within 20 cm from the surface, in 10 cm increments. The modern samples were obtained from four representative field sites, representing various vegetation cover including grass, scrub, mixed, and forested (Table 4.1).

Radiocarbon dating and stable carbon isotope analyses were performed in the Center for Applied Isotopes (CAIS) at the University of Georgia. For radiocarbon dating, charcoal and soil samples from Culebra and Inguiro watersheds were soaked in 1N HCl at 80°C for 1 hour, then washed with deionized water on a fiberglass filter, and rinsed with diluted NaOH to remove possible contamination by humic acids. Next, the sample was soaked in 1N HCl again, washed with deionized water and dried at 60°C. For the accelerator mass spectrometry analysis, the cleaned sample was combusted at 900°C in evacuated and sealed ampoules in the presence of CuO. The resulting carbon dioxide was cryogenically purified from the other reaction products and catalytically converted to graphite using the method of Vogel (Vogel et al., 1984). Graphite $^{14}C/^{13}C$ ratios were measured using the CAIS 0.5 MeV accelerator mass spectrometer, and these ratios were compared to the ratio measured from the Oxalic Acid I (NBS SRM 4990). The sample $^{13}C/^{12}C$ ratios were measured separately using a stable isotope ratio mass spectrometer and expressed as $\delta^{13}C$ with respect to PDB, with an error of less than 0.1‰.

For stable carbon analyses of SOM in paleosols and surface soils, the samples were heated overnight at 105°C to remove any excess water, weighed, and then soaked in 1N HCl while heated overnight in a fume hood at 60°C. A drop of 1N HCl was then added to ensure the complete removal of carbonates, and the samples were dried again overnight at 60°C in a separate oven. Due to the small amount of organic carbon in the samples, they were not rinsed, but subsamples were weighed and placed in silver cups in final preparation for analysis. Next, the samples were analyzed in an elemental analyzer-stable isotope ratio mass spectrometer and expressed as $\delta^{13}C$ with respect to PDB, with an error of less than 0.1‰ (as above). Since the samples were not rinsed, and the sample size of the interpolated SOM analyzed was initially small, the percentage of total organic content was very small or registered below the detection limit of the elemental analyzer in other cases. Therefore, 12 of the 24 samples were run a second time using a larger amount of the prepared SOM sample to better determine or verify their $\delta^{13}C$ value (Table 4.1).

Other studies have incorporated the $\delta^{13}C$ values from radiocarbon dates along with samples analyzed specifically for SOM in buried As (e.g., Hall and Penner, 2013). It was determined that the two sets of $\delta^{13}C$ values are comparable because the $\delta^{13}C$ values were obtained from the total organic carbon rather than from a portion of the SOM carbon (i.e., humic acid). Furthermore, the standard preparation for radiocarbon dating is more rigorous than the standard procedure typical of $\delta^{13}C$ analysis. Replications involved re-analyzing the same paleosol SOM samples using the same pretreatment to observe how the resulting $\delta^{13}C$ values compared. We also compared the $\delta^{13}C$ values of three paleosols using both pretreatment approaches. Results are presented in Table 4.1 and discussed below.

4.3.1 Soil Residence Time and Interpolated Dates

The organic matter from many paleosols in the Coixtlahuaca region have been shown to be older than dates from charcoal, which may be due to the incorporation of older detritus, including charcoal or older SOM, and/or may be related to the long residence time of the soil (dry conditions, slow decomposition) (Rincon, 1999; Leigh et al., 2013). Although it is known that charcoal is inherently older than the soil or sediment in which it is found (Leigh et al., 2013), after examining the dated profiles, charcoal is more consistent with regard to depth as compared to buried A SOM dates (Chapter 3). Five pairs of dates, each consisting of a charcoal date paired with a buried A SOM date from the same strata (taken from Rincon, 1999 and Leigh et al., 2013) were compared to estimate the average inconsistency of the buried A SOM dates. All of the dates were calibrated using CALIB (see above for references). The difference between the calibrated range for each individual sample was examined against the differences between the calibrated ages of the charcoal and organic samples from the same strata (see Appendix III). The calibrated range for each individual sample was comparable to the differences between the calibrated ages of the charcoal and organic samples from the same strata. The seemingly erratic nature in which the organic material may incorporate older detritus means that, based on the available data, no single correction factor can account for the all of the variation in soil ages. In sum, it was concluded that the median of a calibrated date was a reasonable estimate of the age of a stratum after considering the relationship between the ages along the depth of a profile.

4.3.2 Surface Samples

Four modern surface samples were collected from the Culebra watershed and one from

the headwaters of the Río Grande (see Figure 4.1 for location). The samples were selected to represent forest (Apo): grassland (with a few scattered trees) (Ast): mixed grassland and succulent plants (Vic1): and mixed grassland, succulent and forest (Vic2). The sites with forest (e.g., Apo and Vic2) were taken from hilltops and not on the bottomland alluvium because presently trees are mainly preserved at the top of hillslopes. The sites were selected to be representative of vegetation types, and no site represented a perfectly homogenous or mixed site. The samples were collected by obtaining the top 20 cm (in 10 cm intervals) every 25 meters across a transect of 50 meters, for a total of six samples per transect. The final analyses were conducted on a mixed composite of all 0-10 cm samples within each transect for a total of four surface samples. Two modern samples originally taken to double check the radiocarbon dates from buried A SOM were also incorporated into the results. These samples come from surface soils under mixed grassland and succulent vegetation.

Any modern value will be influenced by the rise of fossil fuels in the last 200 years and the influx of 'old' CO_2 (e.g., $\delta^{13}C$ depleted) into the atmosphere known as the Suess effect (Suess, 1955; Brook et al., 2015). Values are typically depleted between 1.5‰ (Boutton et al., 1998; Wynn and Bird, 2008) and 2.0‰ (Brook et al., 2015), though the former amount has been observed in soils (Boutton et a., 1998; Wynn and Bird, 2008). An additional 1.5‰ was added to the resulting $\delta^{13}C$ values from the modern analyzed soil organic matter (Table 4.2).

4.3.3 Percentage C_4 plants

Boutton et al. (1998) developed a mass balance equation (formula (a)) for a subtropical savanah ecosystem, which was applied to this study to estimate the amount of C_4 biomass in the paleoenvironment based on the $\delta^{13}C$ values (as in Biedenbender et al., 2004; Lounejeva

Baturina et al., 2006). Formula (b) (Kelly et al., 1998) shows how the $\delta^{13}C$ values were used to calculate the percentage C_4 biomass in the study area. Since CAM in the region is important but cannot be distinguished from C_4 based on $\delta^{13}C$ values alone, the resulting calculated percentage will be assumed to represent both C_4 and CAM.

These formulas are given as follows:

$$\delta^{13}C_{meas} = x(\delta^{13}C_4) + (1-x)(\delta^{13}C_3) \quad \text{(a), and}$$

$$\%C_4 = (\delta^{13}C_{meas} - \delta^{13}C_4)/(\delta^{13}C_4 - \delta^{13}C_3) \quad \text{(b),}$$

where $\delta^{13}C_{meas}$ indicates the measured value from the SOM, $\delta^{13}C_3$ represents the average value of modern day C_3 plants in the region, and $\delta^{13}C_4$ is the average value of present CAM and C_4 plants in the region. The present values of C_4 and C_3 plants were estimated from a study done on floral isotopic diversity of highland Oaxaca by Warinner et al. (2013), which focused on wild and cultivated plants typically used by inhabitants. The average $\delta^{13}C_3$ and $\delta^{13}C_4$ values obtained for highland Oaxaca vegetation were estimated from analyses on 150 wild plants collected in transects, and found to be -28 and -13.3 per mil respectively. Estimated $\delta^{13}C$ for wild CAM plants were similar to the $\delta^{13}C_4$ values (e.g., ~14.3 per mil) (Warinner et al., 2013). Though CAM values are slightly lower, overall the study found that 80% of CAM $\delta^{13}C$ values were similar to C_4 plants (Warinner et al., 2013). As discussed in 4.3.2, due to the Suess effect (Suess, 1955; Wynn and Bird, 2008; Brook et al., 2015), an additional 1.5‰ was added to the modern $\delta^{13}C$ values used in the formula above (see Table 4.3).

4.4 Results

A total of 38 stable carbon isotope values came from the Culebra and Inguiro watersheds, listed as follows (summarized in Table 4.1): 13 values were obtained on dated buried A SOM, 20 values came from interpolated buried A SOM, six values came from analyses on modern SOM, and 18 values were obtained from dated charcoal samples. Altogether 20 stable carbon isotope values from dated buried A SOM were incorporated into this study from the Río Verde watershed (see Mueller et al., 2012).

Table 4.1 summarizes $\delta^{13}C$ values from the Ríos Culebra and Inguiro. Three dated buried A SOM samples, which already had $\delta^{13}C$ values associated with the radiocarbon date, were re-analyzed to determine the replicability of the dated buried A SOM stable carbon isotope results. In two of the cases the values were slightly enriched (comparable within 0.56 per mil), while the other sample was enriched by 2.2 per mil and clearly differed. It is possible the latter contained a fleck of charcoal that caused the value to increase. Some of the interpolated SOM samples were also re-analyzed due to small sample size, and resulting small %TOC, in order to double check the initial $\delta^{13}C$ value results. In all of these cases the second analysis, having a bigger sample size, produced $\delta^{13}C$ values that were within less than 1.65 per mil of the initial results. The averaged $\delta^{13}C$ value of the two analyses was accepted as the final value. In a few cases the small sample size produced a %TOC value that was below the detection limit of the elemental-analyzer and the initial $\delta^{13}C$ values were removed. Only the value from the second analysis was accepted. If a strata contained both an interpolated and a dated buried A SOM $\delta^{13}C$ value, the two values were averaged, and this averaged $\delta^{13}C$ value was accepted as the final value.

The percentage of total organic carbon (%TOC) obtained for the interpolated buried A SOM is presented in Table 4.2. In cases when the samples were analyzed twice, the %TOC represents the average value if the $\delta^{13}C$ values were averaged, and the re-analyzed value in the cases where only the $\delta^{13}C$ value from the second analysis was accepted. Similar to other studies, it was found that %TOC decreased with regard to depth (Figure 4.3a). Stable carbon isotope values were examined with respect to depth (Figure 4.3b) and it was found that there was no apparent pattern, but other studies have shown that a slight enrichment of $\delta^{13}C$ values may occur with depth, resulting in approximately a 2 per mil increase in values (Wynn, 2007).

The $\delta^{13}C$ values for all three watersheds range from -26.73 per mil to -15.7 per mil. The general trend in values, as ascertained from the mean and standard deviation of each period (Figure 4.4), shows more depleted values in the terminal Pleistocene through the early Holocene, more enriched values in the middle Holocene, and more depleted values in the late Holocene as compared to the middle Holocene. The range in $\delta^{13}C$ values of the terminal Pleistocene-early Holocene is -26.54 to -16.7, while the middle Holocene $\delta^{13}C$ values have a range of -24.49 to -16.1. The range of the late Holocene is -22.2 to -15.7. A closer look at the $\delta^{13}C$ values from all three watersheds indicates that some values appear to be outliers (Table 4.1 and Figure 4.4). All of the outliers came from the interpolated buried A SOM samples from site C2 in Culebra watershed, and the dated buried A SOM samples from sites Yuz9 and Ver6 in Río Verde.

The $\delta^{13}C$ values from the Culebra, Inguiro, and Verde watersheds are plotted against age (Figure 4.5), and it is apparent that the charcoal samples from the Culebra and Inguiro watersheds are consistently more depleted than the rest of the samples. The more depleted

values are expected since charcoal is derived primarily from trees (C_3 vegetation). Thus, the charcoal samples were not considered good representatives of landscape-scale vegetation patterns.

If examined apart from the late Holocene, the modern $\delta^{13}C$ values are the most depleted, even after considering the Suess effect. Altogether these come from six surface soil samples, four of which were directly analyzed for their stable carbon isotope value. The $\delta^{13}C$ values from the other two samples came from radiocarbon dating, which were used as a double check on the radiocarbon dates from SOM in buried A horizons (Chapter 3). Of the four modern categories analyzed, the $\delta^{13}C$ value for the modern forest (Apo) is the most depleted (-25.23). The modern value for grassland (Ast) is the most enriched at -20.89, but is still relatively depleted suggesting the dominance of C_3 grasses. The mixed forest (Vic2) $\delta^{13}C$ value is slightly more depleted (-24.18) than the mixed grassland (Vic1) (-21.84). The two dated samples of mixed grassland and succulent plants obtained values of -19.92 and -22.25, both of which are closer to mixed grassland and grassland values than mixed forest values. The average $\delta^{13}C$ value for all of the modern samples is -22.39, and the difference between highest and lowest value is 5.31 per mil, which equates to a difference in 36% of C_4 and CAM vegetation.

4.4.1 Calculated %C_4 and CAM

Enrichment of stable carbon isotope values was interpreted to indicate an increase of C_4 and CAM biomass in relation to C_3 plants (and is the opposite for depleted values) (e.g., Lounejeva Baturina et al., 2006; McClung de Tapia and Adriano-Moran, 2012). Typically, an increase in C_3 vegetation (e.g. indicated by depleted values) implies a wetter and/or cooler

climate, whereas an increase in C_4 and CAM biomass (e.g., indicated by more enriched values) is associated with an increase of dry and/or warm conditions.

The calculated percent of C_4 and CAM biomass is presented in Table 4.4. Incorporating all profiles, variability was high at times and is reflected in the calculated $\%C_4$ and CAM for individual values with overlapping ages (refer to both Tables 4.1 and 4.4). For example, median ages of 9,554, 9,751, and 9,833 cal BP (i.e., these ages contain overlapping calibrated radiocarbon ages) resulted in an estimated $\%C_4$ and CAM of 24, 43, and 67%, respectively. Variability in $\delta^{13}C$ values averaged to represent the same time range was within 2-18%, if the outlier values from profiles C2, Yuz9 and Ver6 (e.g., profiles with consistently lower $\delta^{13}C$ values) were removed. In general, the data is more useful when examined as a whole and to discern general trends over time.

The averaged $\%C_4$ and CAM for the Terminal Pleistocene-early Holocene (~16,000-8,200 cal BP) fluctuated within a range of 24-67%, having a median of 40% and a mean of 41%. The range in $\%C_4$ and CAM suggested it was overall wetter and/or cooler. The averaged $\%C_4$ and CAM calculated for the middle Holocene (8,200 cal BP to 4,300 cal BP) ranges from 52-76%, with a median of 55% and a mean of 51%, indicating drier and/or warmer conditions. The late Holocene (4,300 cal BP through 500 cal BP) averaged $\%C_4$ and CAM values range from 56-63%, with a median of 46% and a mean of 49%, suggesting overall dry and/or warmer conditions, but slightly moister and/or cooler than the middle Holocene. Widespread land use activities may have also affected the $\delta^{13}C$ values during the late Holocene, which will be discussed below (see section 4.5 Discussion). The $\%C_4$ and CAM for more recent $\delta^{13}C$ values (e.g., 500 cal BP to present) is the lowest estimated, having an average of 28%. Despite the

present dry and warm climate, the modern $\delta^{13}C$ values are very depleted, which may be linked to present human impact.

4.4.2 Paleovegetation and CO_2

Some authors have observed a relationship between $\delta^{13}C$ values and both climate and CO_2 earlier in the Holocene (e.g., Huang et al., 2001; Urban et al., 2015). Prior to direct measurements of CO_2 in the atmosphere, estimations of past global atmospheric CO_2 came from trapped air bubbles in the Antarctic ice sheets. The CO_2 value from the ice cores are considered proxies for global CO_2 in the past because the main source of CO_2 is in the tropics, meaning the value in the Antarctic is a result of the incorporation and mixing of the CO_2 in the atmosphere (Monnin et al., 2001; Monnin et al., 2004; Trudinger et al., 2005). In general, CO_2 values below 180 ppm are considered low enough to starve C_3 plants of CO_2, especially in conjunction with stressful climatic conditions (Bhagwat, 2005). For example, values below 180 ppm resulted in a reduction of C_3 vegetation (forests shrink) and expansion of grasses (C_4) during the last glacial maximum (LGM) (Ehlringer, 2005). After the LGM, values do fluctuate, but no values are recorded below 180 ppm (e.g., Holocene CO_2 values range between 260-280 ppm); therefore, only in conjunction with certain climatic conditions would CO_2 values affect paleovegetation ratios (as in Huang et al., 2001). In this study, there is no correlation between $\delta^{13}C$ values and CO_2, implying the $\delta^{13}C$ values reflect climatic variations, and possibly human influences in the late Holocene. It is unclear if CO_2 has impacted plant biomass in the last 100 years.

4.4.3 Local Polynomial Regression Analysis

To explore the general trends in C_4 and CAM verses C_3 vegetation from the terminal Pleistocene to the present, we analyzed all of the $\delta^{13}C$ values with a local polynomial regression to determine the most significant trends in the data (Figure 4.6). Analyses were done using the LOESS (locally weighted scatterplot smoothing) function (Cleveland et al., 1992) in R software (R Core Team, 2013). According to the analysis, the peak in the $\delta^{13}C$ values during the middle Holocene occurs around 7,000 cal BP, which is followed by a significant fall in values towards 4,900 cal BP. From 4,900 cal BP to 1,200 cal BP, the regression suggests that a significant increase in C_4 and CAM vegetation occurs during the late Holocene, which peaks between 1,000-500 cal BP. After this peak, there is a steady and significant decrease in values towards the present, and is probably impacted by the more depleted modern values, which were averaged to avoid bias. The peak around 1,000-500 cal BP and the subsequent fall in values is significant, and coincides with the Natividad phase (1,250 – 500 cal BP) and Colonial period (post 500 cal BP).

4.5 Discussion

The $\delta^{13}C$ values and the calculated $\%C_4$ and CAM are examined with regard to present and paleoenvironmental data. The results from the analyses assume that the samples are equally representative of the surrounding environment, though it is realized that vegetation does vary spatially. Increasing $\delta^{13}C$ values in soil organic matter suggest more C_4 and CAM biomass, while more depleted values reflect more C_3 vegetation (Amundson et al., 1994; Boutton et al., 1998). However, variations can occur due to sub-sampling differences; for instance, one sub-

sample may contain more charcoal resulting in more depleted values. In addition, alluvial soils, especially in arroyo stratigraphy, may contain organic content eroded from an older soil, which upon mixing with a more recent soil may affect the resulting $\delta^{13}C$ values. Finally, soil samples associated with primarily riparian vegetation will produce $\delta^{13}C$ values that represent this biomass and not the vegetation of the watershed as a whole. Despite this potential bias, this study contains a number of samples with overlapping ages and/or contexts, which reflect general changes in trends of biomass overtime, whether influenced by climatic and/or land use changes.

Since charcoal samples do not represent an integrated value of vegetation in soil organic matter, they are not incorporated into more in-depth paleovegetation trends. However, charcoal has been observed in a number of strata corresponding to different ages in the last 15,000 years, suggesting the importance of trees, or C_3 vegetation in the landscape during much of this time. A notable exception is a period of more enriched $\delta^{13}C$ values between around 9,000-4,300 cal BP, when no charcoal samples were dated. This observation suggests that the paleoclimatic conditions were not favorable to C_3 vegetation, resulting in reduced C_3 vegetation, such as trees in the landscape.

4.5.1 Modern Soils

The present day vegetation of the municipalities of Coixtlahuaca, Jicotlan and Nochixtlan is mainly induced and secondary vegetation and agricultural land. No studies have been made on the distribution of plants with different pathways in the region, but based on some of the known $\delta^{13}C$ values of certain species in the region, it is certain that the present vegetation comprises an uneven mixture of C_3, C_4 and CAM species.

Globally, drylands are experiencing an encroachment of woody vegetation (C_3) into grasslands (C_4). A study on the Chihuahua Desert suggests that this change is influenced by localized biogeophysical factors such as soil erosion, nutrient loss and reduced water infiltration. Woody perennial species have higher soil moisture extraction capacity than C_4 grasses. The expansion of these woody species results in the reduction of soil organic carbon content and surface water infiltration (Albert, 2015). Some vegetation like chaparral, which is normally found in Mediterranean climates (e.g., hot dry summer and cool, wet winters) is observed in rain shadow regions of the Sierra Madre del Sur, and is a relic of the drying climate in the Tertiary and adaptation to a long drought season (Valiente-Banuet et al., 1998). Increasing secondary woody vegetation (C_3) in the Culebra may result from the poor management of the landscape such as deforestation and uncontrolled grazing (Rafael Arzate Aguirre, pers. Com.).

Presently, CAM biomass is a significant part of the Mixteca Alta's vegetation (Valiente-Banuet, 1998; Colin, 2004; Blancas et al., 2010) and it probably had an important role in the past 16,000 years. However, a study on the local management of the Biosphere Reserve Tehuacán-Cuicatlán, which encompasses parts of Culebra and Inguiro watersheds, suggests that some native and non-native plants, including native CAM plants, are considered useful and better managed so are more abundant in the landscape than they would normally be (Blancas et al., 2010). Present day CAM $\delta^{13}C$ values in Oaxaca (Warinner et al., 2012), and in Baja California are typically enriched (Amundson et al., 1994), which would not explain the more depleted $\delta^{13}C$ values found in modern soils in this study. More recently managed forests (via government subsidies and management, Rafael Arzate Aguirre, pers. Com.) entail planting of

non-native pine trees (C_3), which possibly influenced some of the modern $\delta^{13}C$ values, especially in Sandage.

Finally, studies have shown that CO_2 affects the growth, survival and reproduction of plants in arid/semi-arid environments. With no other limitations, elevated CO_2 leads to greater *productivity* (and usually favors C_3 over the other two pathways), while local factors such as water amount and temperature mediates the influence of CO_2 (Shaw et al., 2005). In the last 200 years, the exponential rise in CO_2 to over 400 ppm is the highest it has been in the last 10 million years, which favors C_3 plants (Sage, 2005). In sum, higher erosion and other human induced disturbances, natural occurrence of C_3 woody species, and the rise in CO_2 in the last 100 years would all favor an increase in C_3 plants, and would help explain the depleted modern $\delta^{13}C$ values observed in this study.

4.5.2 Paleoenvironmental Reconstruction

The SOM $\delta^{13}C$ values from Coixtlahuaca and Nochixtlan for the terminal Pleistocene to the late Holocene were examined against local paleosol data (Mueller et al., 2012; Chapter 3), paleoclimatic and paleoenvironmental data from southwestern and central Mexico (e.g., Metcalfe et al., 2000; Caballero et al., 2010; Lachniet et al., 2013), and other tropical sources (e.g., Cariaco basin, Haug et al., 2001; El Junco Crater Lake, Conroy et al., 2008). The earliest $\delta^{13}C$ value had an age of approximately 15,800 cal BP, and thus we compare our values with external data starting at 16,000 cal BP.

Paleoclimate data are represented by a qualitative summary (Figure 4.7) of the lake data, glacial data, stalagmite data and $\delta^{13}C$ data from this study (the latter includes $\delta^{13}C$ values from Mueller et al., 2012). However, the data are variable and contradictory, in particular the lake

data, making interpretation ambigious. Therefore, when raw data were available, z-scores were calculatedin order to better discern overall trends in the paleoenvironment (Figure 4.8). The figure description of Figures 4.7 and 4.8 contain all of the references included in this summary by region and according to paleoclimate proxy.

Paleoclimate and paleoenvironmental proxies include pollen, diatom and $\delta^{18}O$ data from lake records from central Mexico, glacial studies from central Mexico, $\delta^{13}C$ data from the Cueva del Diablo stalagmite from Guerrero, and $\delta^{18}O$ data from all studied Guerreran stalagmites in southwestern Mexico. The stalagmite $\delta^{18}O$ signature represents a high-resolution reconstruction of paleoprecipitation data, while the paleolimnological and glacial data mainly exhibit general trends over time. The $\delta^{13}C$ values from the study area with overlapping calibrated radiocarbon ages were averaged together and presented in Figure 4.7.

4.5.2.1 Terminal Pleistocene-early Holocene (~16,000-8,200 cal yr BP)

In general, the terminal Pleistocene-early Holocene transition encompasses some major fluctuations corresponding to the Heinrich Stadial 1 (HS1), the Bølling-Allerod (B/A), the Younger Dryas (YD), and the 10.3 ka event (Anderson et al., 2007).

The Guerreran stalagmites reflect these fluctuations with dry conditions during HS1 and the latter part of the B/A, which are interrupted by a hiatus during the early part of the B/A representing wetter conditions (Lachniet et al 2013). The z-score calculations for the Cariaco Basin also indicate drier conditions in the YD. Pollen records indicate that cold and wet conditions during HS1 shift to cold and dry conditions during the B/A in the Patzcuaro basin, while colder and drier climate persists in the Upper Lerma basin during the HS1 and part of the B/A. Pollen records indicate that the climate during HS1 and B/A was colder and wetter in

Puebla-Tlaxcala while in the Basin of Mexico colder and drier conditions prevailed. Diatoms support the colder and drier climate in the latter basin. Additionally, glaciers start to expand during the HS1 event, and are still in expanded positions throughout most of the B/A, implying wetter and colder climate in higher altitudes.

Most pollen, diatom and stable oxygen isotope (lake) records indicate that the Younger Dryas (YD, ~12,900-11,700 cal BP) was wetter and colder, which persists through the transition to the early Holocene and until 9,500 cal BP. For example, the pollen data from the Guanajato and Michoacán area suggest that the YD through the early Holocene transition was wetter and colder, and stable oxygen isotope studies from this area also support a wetter environment. Pollen records indicate wet and cold conditions up to around 9,500 cal BP in the Puebla-Tlaxcala area and the Basin of Mexico. One exception includes the pollen record in the Patzcuaro basin, where it is transitioning from dry and cold to wet and warm in the early Holocene. Another exception is the diatom record from the Basin of Mexico, which indicates dry and warm conditions since the end of the YD through 9,500 cal BP. In addition, the diatom record in the Upper Lerma basin suggests wet and warm conditions during the YD to 9,500 cal BP, while the pollen information for the early Holocene suggests dry and cold conditions until 9,500 cal BP. Glaciers seem to slow in growth during the YD, suggesting a cold but dry climate. This slowed growth is followed by another expansion of glaciers in the early Holocene between 11,000-9,500 cal BP, which is evidence for a return to wetter and cooler conditions. The Guerreran stalagmites indicate dry conditions during the YD and 10.3 ka event, but a hiatus during the early Holocene is suggested to represent wetter conditions.

All pollen and diatom records indicate warmer conditions by 9,500 cal BP. A return to very wet conditions is observed in the $\delta^{18}O$ record around 9,500 cal yr BP (Bernal et al., 2011). Both wet and warm conditions can be connected to peak northern hemisphere insolation (Haug et al., 2001). Conditions are also wetter in the Basin of Mexico and the Puebla-Tlaxcala area starting around 9,500 cal BP according to pollen records. Diatom and pollen records from Upper Lerma basin indicate warm and wet conditions, though after 9,500 cal BP, the pollen suggests warm and dry conditions. Diatom records for the Puebla-Tlaxcala area indicate conditions are dry and warm for the entire early Holocene. Dry and warm conditions are also observed for pollen records from the Guanajuato and Michoacán area between 9,500-8,200 cal BP, which transitions to wet and warm at the end of this timespan.

The $\delta^{13}C$ data from SOM from western (Ferrand et al., 2014) and central Mexico (Lounejeva Baturina et al., 2006; Sedov et al., 2010) suggest a cold and wet terminal Pleistocene, which transitions into a drier and warmer early Holocene. Many of these conclusions in the $\delta^{13}C$ data are supported by other proxy data (e.g., phytoliths, paleosol studies and micromorphology). The $\delta^{13}C$ data from Culebra, Inguiro and Verde watersheds indicate slightly enriched values in the B/A and more depleted values in the YD. The $\%C_4$ and CAM is calculated as <41, suggesting slight dominance of C_3 vegetation. According to the z-scores, the $\delta^{13}C$ values from the study area are also depleted during the early Holocene except for a small peak (and correspondingly, a slight increase in $\%C_4$ and CAM vegetation) around 10,000-10,200 cal BP. A similar pattern is observed in the $\delta^{13}C$ values from the Cueva del Diablo stalagmite, but the small peak in enriched values occurs around 10,200 cal BP.

Paleosol studies on the Culebra, Inguiro and Verde watersheds indicate fluctuating conditions. In general, the terminal Pleistocene and early Holocene paleosols consisted of cumulic A horizons, contained clear calcium carbonate deposits ranging from nodules to deposits in root pores and ped faces, and many horizons exhibited prismatic structure. Between 14,000-13,000 and 10,000-9,000 in the Culebra watershed, paleosols have Ck and Btk horizons. Cumulic soils are evident in the Verde watershed throughout this timespan, whereas they are only apparent in the Culebra watershed starting around 9,000 cal BP. From 12,000 to 10,000 buried A horizons are typically 40 cm thick and are associated with a Bw subsoil horizon.

In general, calcium carbonate deposits indicate dry conditions. However, calcium carbonate deposits in root pores and ped faces, and in some cases masses or nodules, were discovered in buried A horizons, suggesting polygenetic soil development and antecedent dry conditions after initial soil formation. Prismatic structure and polygenetic features in these paleosols suggest fluctuating or seasonal climate. Slickensides, magnesium deposits, and more indurated calcium carbonate deposits characteristic of the terminal Pleistocene paleosols suggest slightly more intense wet and dry fluctuations during this time than subsequent periods (Mueller et al., 2012; Chapter 3).

Summary: Although climate fluctuates between wet and dry from the terminal Pleistocene through the early Holocene, the majority of the records indicate cold or cooler climate up to 9,500 cal BP. Also, during this timespan, is evidence for increasingly wetter conditions during the early Holocene. The $\delta^{13}C$ values from the Culebra, Inguiro and Verde watersheds are depleted overall, which is reflected in lower $\%C_4$ and CAM percentages. However, paleosols indicate that dry conditions, with some fluctuation around the transition to

the early Holocene, are also important up to around 9,000 cal BP. After 9,500-9,000 cal BP, the steady rise in $\delta^{13}C$ values and corresponding $\%C_4$ and CAM values in context with the regional data suggest that the terminal Pleistocene to around 9,500 cal BP reflects cooler conditions favoring C_3, followed by increasingly warmer conditions during the latter part of the early Holocene. The local paleosol data suggest an important dry component as well throughout this period.

4.5.2.2 Middle Holocene (8,200 cal BP - 4,200 cal BP)

The $\delta^{18}O$ values in the stalagmite record indicate a return to drier conditions starting around 9,300 cal BP, reaching the driest conditions around 8,200 cal BP that lasted until 7,000 cal BP. The z-score calculations support a relatively drier period in the stalagmite record during this timespan. A very brief, wet period occurred between 7,100-6,800 cal BP according to the stalagmite record, after which a return to slightly drier conditions (though still relatively wet) until 6,000 cal BP. In general, ~6,000 cal BP marks a turning point from more precipitation and insolation in N. Hemisphere to increasing aridity as the ITCZ moved south (Haug et al., 2001; Lozano-Garcia et al., 2013). The stalagmites indicate another brief wet period around 6,000 cal BP, and longer wet period between ~5,000 and 4,200 cal BP, after which the trend towards drier conditions is resumed.

All pollen records indicate warm temperatures between 8,200-4,200 cal BP, but vary between wet and dry climate. Pollen data from the Upper Lerma basin suggests overarching dry conditions up until 5,400 cal BP, with some wet periods around 7,800 cal BP and 6,000 cal BP. However, diatom data from the same basin infer persistent wet conditions since 14,000 cal BP. Between 4,800-4,200 cal BP, diatom data from the Upper Lerma basin suggest that dry

conditions exist. Wetter conditions are implied from pollen records from the Puebla-Tlaxcala area up until 7,000 cal BP, while they last in the Guanajuato and Michoacán area and the Basin of Mexico until around 6,000 cal BP. After 6,000 cal BP, the conditions in the two latter areas transition to drier, which persists through 4,200 cal BP in the Guanajuato and Michoacán area. The pollen data in the Basin of Mexico indicates that around 5,000 cal BP conditions change back to wetter until 4,200 cal BP. The diatom record for the Basin of Mexico indicates drier conditions for this timespan. The pollen record suggests drier conditions in the Patzcuaro area, though different lakes in the area show variations of wet or dry after 7,000 cal BP, and seem to alternate as dry-wet-dry up until 4,200 cal BP. Diatom records from this area support drier conditions after 7,000 cal BP. Glacier expansion around 8,200 cal BP suggests that cooler conditions were prevalent for higher altitudes and lasted until around 7,200 cal BP. No data exists for the Puebla-Tlaxcala area after 7,000 cal BP. The z-score calculations from the Cariaco basin suggest a wetter middle Holocene.

The $\delta^{13}C$ data from SOM from western (Ferrand et al., 2014) and central Mexico (Lounejeva Baturina et al., 2006; Sedov et al., 2010) support a drier middle Holocene. According to the z-scores, the $\delta^{13}C$ values from the Cueva del Diablo and Culebra, Inguiro and Verde watersheds are enriched around 8,200 cal BP, though, in the case of the study site, there is a slight downward trough around 8,000 cal BP. Conversely, the $\%C_4$ and CAM calculations indicate a high amount of C_4 and CAM biomass relative to C_3 plants, suggesting drier and warmer conditions though to 5,000 cal BP. The z-score indicates that the enriched $\delta^{13}C$ values from the Cueva del Diablo persist only until around 7,000 cal BP. After a wet spell, drier conditions return between 5,500-4,800 cal BP.

Few paleosols have been described for the middle Holocene in the Culebra, Inguiro and Verde watersheds. In the Río Verde watershed, a few buried A horizons, dating between 8,200 and 7,810 cal BP, are described as thick (up to 100 cm), with prismatic structure, and organic and clay rich. In the Culebra watershed, middle Holocene paleosols dating between 7,000 and 6,000 cal BP are cumulic, and measure over 150 cm thick. Some have prismatic structure and clay films, while others have calcium carbonate deposits. Paleosols dating between 6,000-5,000 cal BP are thinner and weaker, while others that date from 5,000-4,000 cal BP have increased calcium carbonate deposits. All horizons in both paleosols have carbonate deposits on ped faces and/or root pores. The prismatic structure and clay films support the notion of seasonality, while the carbonate deposits imply an important dry season. Thick, organic rich soil and a seasonal climate with a dry component infer grassland (Mueller et al., 2012; Chapter 3).

Summary: The warmer conditions observed in the majority of proxy data from central and southwestern Mexico corroborates the conclusion that the high percentage of C_4 and CAM calculated for the study area reflects the overarching warmer and in part drier paleoclimate during the middle Holocene.

4.5.2.3 Late Holocene (~4,200 cal yr BP to present cal BP)

Guerrero stalagmites suggest that after 4,300 cal yr BP, ENSO dominates the climatic signal in the region of southwestern (Bernal et al., 2011) and central Mexico (Lozano-Garcia et al., 2013). Many paleoenvironmental records indicate an arid or dry period around 4,200 cal BP, which is referred to as the 4.2 ka event (Walker et al., 2013). Most records indicate dry and warm conditions during this event except pollen data for the Basin of Mexico, which

suggest wetter conditions. The $\delta^{18}O$ values of the stalagmites indicate that climatic conditions around 4,800 cal BP were wetter, which started to transition to a drier climate around 4,100 cal BP, with peaks at 3,900 and 3,600 cal BP. Overall, the smoothed oxygen isotope data from the stalagmites indicate that the late Holocene climatic trend towards drier conditions started at 4,100 cal BP.

Noteably, at around 4,300 cal BP the $\delta^{13}C$ data from the Cueva del Diablo stalagmite diverges from the $\delta^{18}O$ data from this and the other Guerreran stalagmites. According to Figure 4.7, the $\delta^{13}C$ data appears to become more depleted while the $\delta^{18}O$ data becomes more enriched up until around 2,000 cal BP. Based on the z-score calculations, the $\delta^{13}C$ data becomes more enriched between 4,000-3,000 cal BP, and from 2,000-1,500 cal BP, after which there is no more $\delta^{13}C$ values available. Both the %Ti from the Cariaco Basin and the $\delta^{18}O$ data from the Guerreran stalagmites indicate drying conditions at about 4,000 cal BP. Conversely, the $\delta^{13}C$ data from western (Ferrand et al., 2014) and central Mexico records (Lounejeva Baturina et al., 2006; Sedov et al., 2010) indicate a slightly wetter late Holocene. Between 2,000-1,500 cal BP and 1,000 - 500 cal BP the z-score calculations from the following locations suggest drier conditions (see Figure 4.8): $\delta^{13}C$ data from this study, the $\%Al_2O_3$ from the Cuenca Oriental, and a higher %Sand in the El Junco basin. From 1,500-500 cal BP the $\delta^{13}C$ and $\delta^{18}O$ data from the Cuenca Oriental suggests drier conditions, while the stalagmite record and %Sand suggest wetter and lower intensity ENSO, respectively. In general, the z-scores suggest that slightly wetter conditions occur between approximately 3,500/3,000-2,000 cal BP and after 500 cal BP.

All other records continue to indicate warm conditions during the late Holocene, with either wet or dry climatic fluctuations. However, the climatic signal in most lake basins

becomes increasingly unclear due to increased widespread land use activities. The most significant aspect of all lake records during the late Holocene is that human activities, such as agriculture and deforestation, impacted the surrounding vegetation and caused erosion. Some of the trends in the z-scores, including this study, probably reflect human impact as well.

Similarly, the trend in $\delta^{13}C$ values and the results from the local polynomial regression suggests that the $\delta^{13}C$ values may not offer a clear climatic signal, but may be influenced by human activities. However, local paleosol characteristics offer insight to the paleoenvironment of the Culebra, Inguiro and Verde watersheds. The paleosols corresponding to the late Holocene vary, but most consist of silty loam with subangular blocky structure, and have calcium carbonate in root pores and ped faces. Thick (>100 cm) cumulic A horizons are prevalent in the Culebra and Inguiro watersheds. A few paleosols standout; for example, one dated to around 4,200 cal BP was well-developed with carbonate nodules indicating dry conditions around the time of the 4.2 ka event. Others dated to around 2,000 cal BP also include carbonate concretions and nodules. However, one soil along the mainstem of Rio Culebra has carbonate deposits in conjunction with redox features, meaning that a once dry, well-drained soil became engulfed by a rising water table. From ~1,300- 600 cal BP soils are cumulic but are typically less well-developed with Ab-Bw sequences. In sum, the short, but frequent and strong fluctuations in paleosol characteristics during the Holocene may reflect the extreme but short-lived variations in climate; however, it is important to note that these more recently formed soils are better preserved and more widespread (Chapter 3).

4.5.2.4 Land Use and Paleoenvironmental Reconstruction

Archaeological and geoarchaeological surveys in the Culebra and Inguiro watersheds clearly demonstrate that humans were managing the landscape by constructing lama-bordos (e.g., sediment check-dams on stream networks) and agricultural terraces on hillslopes (Kowalewski et al., 2009; Leigh et al., 2013). Starting in the Formative period (e.g., local late Cruz phase, ~3,500 cal BP), the inhabitants along two tributaries of the Río Culebra (e.g., Barrancas Sandage and Sandaxne) built lama-bordo and terrace walls, which were associated with a tipping point towards more permanent settlements and agriculture as a main food supply (Leigh et al., 2013). Slightly later during the Cruz phase (~2,850 cal BP), the lama-bordo system was evident in Ríos Inguiro (this study) and Verde as well (Mueller et al., 2012). Starting in the Ramos phase (~2,250 cal BP), the population declines through the "Transición" phase until ~1,250 cal BP (i.e. Formative through the Classic period) (Kowalewski et al., 2009). Despite general population decline, archaeological surveys (Balkansky et al., 2000; Kowalewski et al., 2009) indicate that there is a long history of land use along the lower tributary of Barrancas Sandage and along the entire Barranca Sandaxne, both tributaries of the Río Culebra. By 600 cal BP, corresponding to the end of the Post-Classic period (local Natividad phase), the indigenous population is estimated to have reached over 100,000 people. The ancient city of Inguiteria, which is situated along Río Culebra, has been identified as a major Post-Classic trading center (Kowalewski et al., 2009). Terrace walls were widespread in the region, which served as stable foundations for building habitations and as agricultural land (Balkansky et al., 2000; Kowalewski et al., 2009).

The success of any management strategy involves changes in technology and organization accompanied by environmental, cultural and socio-political changes (Brush, 2012), all occurring in a cycle of resilience, adaptation and innovation (Perez-Rodriguez and Anderson, 2013). The semi-arid environment of the Mixteca Alta does not contain many perennial streams, has intense and variable rainfall, and is prone to erosion (Rincon, 1999, Chapter 3). Water scarcity in the Mixteca Alta, as in the southwestern U.S., is a limiting factor to sedentary lifestyles; and migration would have been an adaptive strategy when water was unavailable. Conversely, agricultural structures imply a sedentary lifestyle, because they serve to conserve water and soil and they reduce vulnerability to variations in precipitation (Spielman et al., 2011). Agricultural terraces on hillslopes also help increase yields while impeding erosion, but they do have building and maintenance costs (Perez Rodriguez and Anderson, 2013). Increasingly widespread landscape management, sedentary lifestyles and communal living require some attained level of socio-cultural organization involving ceremony, politics, and religion to allow for socioecological adaptation. Land and agriculture, in particular maize agriculture, had a sacred role in the later Post-Classic Mixtec culture, which hints at its possible significance in earlier times (Joyce and Goman, 2012).

Molecular studies have shown that maize (C_4 plant) was domesticated from its wild ancestor teosinte around 9,000 cal BP, the homeland of which is the dry tropical forest in the Central Balsas River Valley in southwestern Mexico (Piperno and Flannery, 2001; Ranere et al., 2009). The earliest domesticated maize found in the Oaxacan semi-arid highlands dates to ~6,200 cal BP (Piperno and Flannery, 2001), which is long before the early structures, such as the lama-bordos and terraces observed in the Río Culebra, were first constructed in

Mesoamerica around 3,500 cal BP (Leigh et al., 2013). Adaptive terracing techniques were present in the Verde watershed by 2,990 cal BP (Mueller et al., 2012) and Inguiro, at least by 2,000 cal BP. Findings of early cultivated maize in the semi-arid/arid environments of southwestern Mexico by ~6,200 cal BP (Piperno and Flannery, 2001) and in the southwestern U.S. by ~4,000 cal BP suggest the plant was already adapted to drier environments. However, it has been suggested that it was not until cob size was large enough to serve as a primary resource that emphasis was placed on maize cultivation in places like Oaxaca. The achievement of larger cobs has been estimated to have occurred by ~3,500 cal BP (Piperno and Pearsall, 1998).

Evidence for foraging of wild plant resources, such as maguey (i.e., *Agave* spp.) and nopal (i.e., *Opuntia* spp.), dates to 12,000-9,500 cal BP in the Valley of Oaxaca (Schoenwetter and Smith, 1986). Maguey was an important plant since the Archaic period (Schoenwetter and Smith, 1986), and was probably primarily used as a source of fiber (Smith, 1986), although agave hearts are edible (Robson and Elias, 1986). Both nopal and its fruits were an important source of food (Smith, 1986). Studies of present societies show that cacti and succulent plants like maguey and nopal are still managed and at times cultivated in the Valley of Oaxaca (Warriner et al., 2013) and in the Mixteca Alta (pers. obs). Although it is hard to distinguish CAM from C_4 and C_3 plants based on isotope alones, according to the $\delta^{13}C$ values obtained for wild and cultivated CAM plants in Oaxaca, they significantly overlapped with the $\delta^{13}C$ values of wild and cultivated C_4 plants (Warinner et al., 2013). Therefore, the increased management and procurement of CAM plants during the late Holocene would also cause $\delta^{13}C$ values of SOM to increase. The maguey plant is also the primary source for pulque, an important alcoholic

beverage in the region (Warinner et al, 2013), which was possibly an important beverage in the past. Consumption of pulque would also provide impetus for intensive management or cultivation of this plant.

The increasingly more enriched $\delta^{13}C$ values between 3,500 cal BP and ~1,200 cal BP from the Ríos Culebra, Inguiro and Verde watersheds, along with the increasingly widespread land use activities such as the construction of lama-bordos and hillslope terraces, suggest that maize, and possibly some succulent plants, were becoming increasingly important. The strong peak in $\delta^{13}C$ values (circa and 500 - 1,200 cal BP) and the associated intense land management in tributary Sandage, together strongly suggest that maize agriculture constituted an important resource that helped provide sustenance to the inhabitants of the highly populated post-Classic city of Inguiteria and surrounding watersheds. The findings suggest that maize had not been adapted to the highly eroded and gully prone environment; instead, the gully prone landscape of the Mixteca Alta was adapted for maize cultivation.

Paleosol characteristics indicate that locally dry conditions existed during the late Holocene, especially around 4,000 and 2,000 cal BP. Overall, the late Holocene was not as dry as the previous period. Unlike other periods the $\delta^{13}C$ values in the late Holocene fluctuate dramatically, making the observed trend of pronounced enrichment starting ~3,500 cal BP coincident with the cultural changes that favored agricultural production of C_4 (maize) and CAM (nopal and maguey) plants. After 500 cal BP, disruption in land management due to Spanish conquest of the region (Kowalewski et al., 2009), and increased erosion caused by population decline coincided with a trend toward more depleted $\delta^{13}C$ values. This further

supports the idea that food procurement and land management were co-dependent in the late Holocene.

4.6 Conclusion

The $\delta^{13}C$ values from buried A SOM from the Río Culebra, Inguiro and Verde watersheds located in the Mixteca Alta were examined from the terminal Pleistocene to the present. In sum, the trend in $\delta^{13}C$ values from buried A SOM suggests that the terminal Pleistocene-early Holocene have mainly C_3 vegetation relative to C_4 and CAM, while the middle Holocene $\delta^{13}C$ values are enriched and suggest the prevalence of C_4 and CAM relative to C_3 plant biomass. The late Holocene stable carbon isotope values are varied, but on average, they suggest slightly more C_3 versus C_4 and CAM plant biomass than the previous time interval of the middle Holocene.

The buried A SOM $\delta^{13}C$ values and calculated $\%C_4$ and CAM were compared against the local paleosol data and other paleoclimatic and paleoenvironmental data from central and southwestern Mexico. Most paleoenvironmental proxies indicated cold or cooler climate for the terminal Pleistocene and early Holocene, while paleosols indicated that dry conditions were also important. In comparison to local and regional paleoenvironmental information, the moderate to low percentages of $\%C_4$ and CAM appear to reflect cooler temperatures during the terminal Pleistocne and early Holocene. In contrast, during the middle Holocene the majority of proxy data from central and southwestern Mexico indicate warmer conditions.. Based on these data, and the local paleosol characteristics that support the existence of dry conditions, the high

percentage of C_4 and CAM calculated for the study area probably reflects warmer and possibly drier conditions during the middle Holocene.

Paleoenvironmental data for the late Holocene indicate continued warm and dry conditions, though with more fluctuation, and less dry climate than the previous period. However, the climatic signal in most lake records becomes increasingly unclear due to human activities, such as agriculture and deforestation, which impacted the surrounding vegetation and caused erosion. Agricultural activities involving lama-bordo and hillslope terrace construction began around 3,500 cal BP (e.g., the Formative period) in the Culebra watershed, and by ~2900 cal BP in the Verde watershed. The $\delta^{13}C$ values from buried A SOM show a significant rise from this date until between 1,000-500 cal BP. Maize, an important C_4 plant in Mesoamerica, had already been domesticated and associated with the semi-arid highland of Oaxaca before 3,500 cal BP, while CAM plants of succulents and cacti formed an important part of the foraged diet since the Archaic, and possibly were managed for food and pulque production in later phases.

Landscape manipulation and transformation involves making the environment more efficient for humans (Harris, 2012), as observed in the Culebra and later in the Verde and Inguiro watersheds. The increasingly more enriched $\delta^{13}C$ values between 3,500 cal BP and 1,000 cal BP from the Ríos Culebra, Inguiro and Verde watersheds, along with the increasingly widespread land use activities, such as the construction of lama-bordos and hillslope terrace walls, suggest that intensified maize agriculture and possibly the increased management of succulent plants were becoming very important to the ecological and cultural adaptation of the

Mixteca Alta. Agriculture in the past and present not only involves managing crops but also altering the landscape to enable efficiency.

During the late Holocene, the observed land management strategies and cultural organization enabled more food production in a smaller space. The increasingly enriched $\delta^{13}C$ values in the late Holocene are constent with the idea that maize and native succulent plants were farmed and/or managed, thereby making the eroded and gullied Mixteca Alta more productive. The fall in population as well as $\delta^{13}C$ values during the Colonial period of Spanish Conquest suggests that the managed landscape was to some degree dependent on the human-environmental interactions that produced it.

4.7 References

Albert, B.M. (2015) Holocene aridification, vegetation change, sedimentation regime and limits of carbon isotope data as indicated by the alluvial pollen sites of Arroyo Grande and El Molino in North-Central Mexico. Quaternary International 377, 2-17.

Amundson, R., Francovizcaino, E., Graham, R.C. and Deniro, M. (1994) The Relationship of Precipitation Seasonality to the Flora and Stable-Isotope Chemistry of Soils in the Vizcaino Desert, Baja-California, Mexico. Journal of Arid Environments 28, 265-279.

Arzate Aguirre, Rafael, (per. Com). Coordinator of Conservation for the Biosphere Reserve Tehuacán-Cuicatlán, National Park Commission, Mexico.

Balkansky, A.K., Kowalewski, S.A., Perez Rodriguez, V., Pluckhahn, T.J., Smith, C.A., Stuiver, L.R., Beliaev, D., Chamblee, J.F., Heredia Espinoza, V.Y. and Santos Perez, R. (2000) Archaeological survey in the Mixteca Alta of Oaxaca, Mexico. Journal of Field Archaeology 27, 365-389.

Bernal, J., Lachniet, M., McCulloh, M., Mortimer, G., Morales, P., Cienfuegos, E. (2011) A Speleothem Record of Holocene Climate Variability from Southwestern Mexico. Quaternary Research 75, 104-113.

Bhagwat, A.S. (2005) Photosynthetic Carbon Assimilation of C3, C4 and CAM Pathways. In: Pessarakli, M. (Ed.), Handbook of Photosynthesis. Taylor & Francis Group, Boca Raton, pp. 367-390.

Biedenbender, S.H., McClaran, M.P., Quade, J. and Weltz, M.A. (2004) Landscape patterns of vegetation change indicated by soil carbon isotope composition. Geoderma 119, 69-83.

Blaauw, M. (2010) Methods and code for 'classical' age-modeling of radiocarbon sequences. Quaternary Geochronology 5, .

Blancas, J., Casas, A., Rangel-Landa, S., Moreno-Calles, A., Torres, I., Perez-Negron, E., Solis, L., Delgado-Lemus, A., Parra, F., Arellanes, Y., Caballero, J., Cortes, L., Lira, R. and Davila, P. (2010) Plant Management in the Tehuacán-Cuicatlán Valley, Mexico. Economic Botany 64, 287-302.

Boom, A., Mora, G., Cleef, A.M. and Hooghiemstra, H. (2001) High altitude C-4 grasslands in the northern Andes: relicts from glacial conditions? Review of Palaeobotany and Palynology 115, 147-160.

Boutton, T.W., Archer, S.R., Midwood, A.J., Zitzer, S.F. and Bol, R. (1998) delta C-13 values of soil organic carbon and their use in documenting vegetation change in a subtropical savanna ecosystem. Geoderma 82, 5-41.

Bradbury, J.P. (1989) Late Quaternary Lacustrine Paleoenvironments in the Cuenca-de-Mexico. Quaternary Science Reviews 8, 75-100.

Bradbury, J.P. (2000) Limnologic history of Lago de Patzcuaro, Michoacan, Mexico for the past 48,000 years: impacts of climate and man. Palaeogeography Palaeoclimatology Palaeoecology 163, 69-95.

Brook, G.A., Railsback, L.B., Scott, L., Voarintsoa, N-R.G. and Liang, F. (2015). Late Holocene stalagmite and tufa climate records for Wonderwerk Cave: Relationships between archaeology and climate in southern Africa. African Archaeological Review 32, 669-700.

Brush S, (2012) Traditional Management of Biodiversity. In: Gepts, P, Famula, T. R., Bettinger, R. L., Brush, S. B., Damania, A. B., McGuire, P.E., and Qualset, C. O. (Eds.), Biodiversity in Agriculture: Domestication, Evolution and Sustainability. Cambridge, Cambridge University Press, pp. 376-377.

Caballero, M., Lozano-García, S., Vázquez-Selem, L. and Ortega, B. (2010) Evidencias

de cambio climático y ambiental en registros glaciales y en cuencas lacustres del centro de México durante el último máximo glacial. Boletín de la Sociedad Geológica Mexicana 62, 359-377.

Cerling, T.E., Harris, J.M., MacFadden, B.J., Leakey, M.G., Quade, J., Eisenmann, V. and Ehleringer, J.R. (1997) Global vegetation change through the Miocene/Pliocene boundary. Nature 389, 153-158.

Cerling, T.E., Quade, J., Wang, Y. and Bowman, J.R. (1989) Carbon Isotopes in Soils and Paleosols as Ecology and Paleoecology Indicators. Nature 341, 138-139.

Cleveland, W. S., Grosse, E. and Shyu, W. M. (1992) Local regression models. In:. Chambers, J.M and Hastie, T.J. (Ed.), Statistical Models in S, Wadsworth & Brooks/Cole.

Coe, H.H.G., Macario, K., Gomes, J.G., Chueng, K.F., Oliveira, F., Gomes, P.R.S., Carvalho, C., Linares, R., Alves, E. and Santos, G.M. (2014) Understanding Holocene variations in the vegetation of Sao Joao River basin, southeastern coast of Brazil, using phytolith and carbon isotopic analyses. Palaeogeography Palaeoclimatology Palaeoecology 415, 59-68.

Colin, R.T. (2004) Tipos de Vegetacion. In: García-Mendoza, A.J., Ordóñez Díaz, M., and Briones-Salas, M. (Eds.), Biodiversidad de Oaxaca. Cuidad Universitaria, UNAM, pp. 105-115.

de Rouw, A., Soulileuth, B. and Huon, S. (2015) Stable carbon isotope ratios in soil and vegetation shift with cultivation practices (Northern Laos). Agriculture Ecosystems & Environment 200, 161-168.

Driese, S.G., Li, Z.H. and Horn, S.P. (2005) Late Pleistocene and Holocene climate and geomorphic histories as interpreted from a 23,000 C-14 yr BP paleosol and floodplain soils, southeastern West Virginia, USA. Quaternary Research 63, 136-149.

Ehleringer, J.R. (2005) The Influence of Atmospheric CO2, Temperature, and Water on the Abundance of C3/C4 Taxa. In: Ehleringer, J.R., Cerling, T.E., and Dearing, M.D. (Ed.), A History of Atmospheric CO2 and its Effects on Plants, Animals, and Ecosystems. Springer, New York, pp. 214-231.

Farquhar, G.D., Ehleringer, J.R. and Hubick, K.T. (1989) Carbon Isotope Discrimination and Photosynthesis. Annual Review of Plant Physiology and Plant Molecular Biology 40, 503-537.

Ferrand, P.A., Solleiro-Rebolledo, E., Acosta, G., Sedov, S. and Morales, P. (2014)

Archaic settlement in El Tebernal, Veracruz: First insights into paleoenvironmental conditions and resource exploitation. Quaternary International 342, 45-56.

Hall, S.A. and Penner, W.L. (2013) Stable carbon isotopes, C-3-C-4 vegetation, and 12,800 years of climate change in central New Mexico, USA. Palaeogeography Palaeoclimatology Palaeoecology 369, 272-281.

Harris, D. R.., (2012) Evolution of Agrosystems: Biodiversity, Origins, and Differential Development. In: Gepts, P, Famula, T. R., Bettinger, R. L., Brush, S. B., Damania, A. B., McGuire, P.E., and Qualset, C. O. (Eds.), Biodiversity in Agriculture: Domestication, Evolution and Sustainability. Cambridge, Cambridge University Press, pp. 21-56.

Haug, G.H., Hughen, K.A., Sigman, D.M., Peterson, L.C. and Rohl, U. (2001) Southward migration of the intertropical convergence zone through the Holocene. Science 293, 1304-1308.

Huang, Y., Street-Perrott, F.A., Metcalfe, S.E., Brenner, M., Moreland, M. and Freeman, K.H. (2001) Climate change as the dominant control on glacial-interglacial variations in C-3 and C-4 plant abundance. Science 293, 1647-1651.

INEGI (2015) Land cover data. National Institute of Statistics and Geography, Mexico website: http://www.inegi.org.mx/geo/contenidos/recnat/usosuelo/, last accessed January, 2016.

INEGI (2013) Hydrological data, National Institute of Statistics and Geography, Mexico, website, http://www.inegi.org.mx/geo/contenidos/recnat/hidrologia/descarga.aspx, last accessed January, 2016.

Johnson, K.D., Terry, R.E., Jackson, M.W. and Golden, C. (2007) Ancient soil resources of the Usumacinta River Region, Guatemala. Journal of Archaeological Science 34, 1117-1129.

Joyce A.A., and Goman, M. (2012) Bridging the theoretical divide in Holocene landscape studies: social and ecological approaches to ancient Oaxacan landscapes. Quaternary Science Reviews 55, 1-22.

Keeley, J.E. and Keeley, S.C. (1989) Crassulacean Acid Metabolism (CAM) in High Elevation Tropical Cactus. Plant Cell and Environment 12, 331-336.

Keeley, J.E. and Rundel, P.W. (2003) Evolution of CAM and C-4 carbon-concentrating mechanisms. International Journal of Plant Sciences 164, S55-S77.

Kelly, E.F., Blecker, S.W., Yonker, C.M., Olsen, C.G., Wohl, E.E., and Todd, L.C. (1998) Stable isotope composition of soil organic matter and phytoliths as paleoenvironmental indicators. Geoderma 82(1-3): 59-81.

Koch, P.L. (1998) Isotopic reconstruction of past continental environments. Annual Review of Earth and Planetary Sciences 26, 573-613.

Kowalewski, S.A., Balkansky, A. K., Walsh, L. R. S., Pluckhahn, T. J., Chamblee, J. F., Rodriguez, V. P., Espinosa, V. Y. H., Smith, C. A. (2009) Origins of the Ñuu: Archaeology in the Mixteca Alta, Mexico. University Press Colorado, Boulder.

Krasilnikov, P., Gutiérrez-Castorena, M.d.C., Ahrens, R.J., Cruz-Gaistardo, C.O., Sedov, and S., Solleiro-Rebolledo, E. (2013) The Soils of Mexico 2013. World Soil ` Series.

Lachniet, M., Asmerom, Y., Bernal, J., Polyak, V., Vaquez-Selem, L. (2013) Orbital Pacing and Ocean Circulation-Induced Collapses of the Mesoamerican Monsoon over the past 22,000 yr. Proc Natl. Acad. Sci. U.S.A. 110, 9255-9260.

Leavitt, S.W., Follett, R.F., Kimble, J.M. and Pruessner, E.G. (2007) Radiocarbon and delta C-13 depth profiles of soil organic carbon in the US Great Plains: A possible spatial record of paleoenvironment and paleovegetation. Quaternary International 162, 21-34.

Leigh, D.S., Kowalewski, S.A. and Holdridge, G. (2013) 3400 years of agricultural engineering in Mesoamerica: lama-bordos of the Mixteca Alta, Oaxaca, Mexico. Journal of Archaeological Science 40, 4107-4111.

Lounejeva Baturina, E., Morales Puente, P., Cabadas Báez, H.V., Cienfuegos Alvarado, E., Sedov, S., Vallejo Gómez, E. and Solleiro Rebolledo, E. (2006) Late Pleistocene to Holocene environmental changes from δ13C determinations in soils at Teotihuacan, Mexico. Geofísica Internacional 45, 85-98.

Lozano-Garcia, S., Torres-Rodriguez, E., Ortega, B., Vazquez, G. and Caballero, M. (2013) Ecosystem responses to climate and disturbances in western central Mexico during the late Pleistocene and Holocene. Palaeogeography Palaeoclimatology Palaeoecology 370, 184-195.

Lozano-Garcia, S., Caballero, M., Ortega, B., Sosa, S., Rodriguez, A. and Schaaf, P. (2010) Late Holocene palaeoecology of Lago Verde: evidence of human impact and climate change in the northern limit of the neotropics during the late formative and classic periods. Vegetation History and Archaeobotany 19, 177-190.

Lozano-Garcia, S., Sosa-Najera, S., Sugiura, Y. and Caballero, M. (2005) 23,000 years of vegetation history of the Upper Lerma, a tropical high-altitude basin in Central Mexico. Quaternary Research 64, 70-82.

Lozano-Garcia S & Vazquez-Selem L (2005) A high-elevation Holocene pollen record from Iztaccihuatl volcano, central Mexico. Holocene 15, 329-338.

Lozano-Garcia, M.D. and Ortega-Guerrero, B. (1998) Late Quaternary environmental changes of the central part of the Basin of Mexico; Correlation between Texcoco and Chalco basins. Review of Palaeobotany and Palynology 99, 77-93.

McClung de Tapia, E. and Cristina Adriano-Moran, C. (2012) Stable Carbon Isotopes Applied to Vegetation Reconstruction in the Teotihuacan Valley, Mexico. Boletin De La Sociedad Geologica Mexicana 64, 161-169.

Metcalfe, S.E., O'Hara, S.L., Caballero, M. and Davies, S.J. (2000) Records of Late Pleistocene-Holocene climatic change in Mexico - a review. Quaternary Science Reviews 19, 699-721.

Monnin, E., Indermuhle, A., Dallenbach, A., Fluckiger, J., Stauffer, B., Stocker, T.F., Raynaud, D. and Barnola, J.M. (2001) Atmospheric CO_2 concentrations over the last glacial termination. Science 291, 112-114.

Monnin, E., Steig, E.J., Siegenthaler, U., Kawamura, K., Schwander, J., Stauffer, B., Stocker, T.F., Morse, D.L., Barnola, J.M., Bellier, B., Raynaud, D. and Fischer, H. (2004) Evidence for substantial accumulation rate variability in Antarctica during the Holocene, through synchronization of CO2 in the Taylor Dome, Dome C and DML ice cores. Earth and Planetary Science Letters 224, 45-54.

Mueller, R.G., Joyce, A.A. and Borejsza, A. (2012) Alluvial archives of the Nochixtlan valley, Oaxaca, Mexico: Age and significance for reconstructions of environmental change. Palaeogeography Palaeoclimatology Palaeoecology 321, 121-136.

Ortega-Rosas, C.I., Guiot, J., Penalba, M.C. and Ortiz-Acosta, M.E. (2008) Biomization and quantitative climate reconstruction techniques in northwestern Mexico - With an application to four Holocene pollen sequences. Global and Planetary Change 61, 242-266.

Osmond, C.B., Allaway, W.G., Sutton, B.G., Troughto., Jh, Queiroz, O., Luttge, U. and Winter, K. (1973) Carbon Isotope Discrimination in Photosynthesis of CAM

plants. Nature 246, 40-42.

Park, J., Byrne, R., Boehnel, H., Molina Garza, R. and Conserva, M. (2010) Holocene climate change and human impact, central Mexico: a record based on maar lake pollen and sediment chemistry. Quaternary Science Reviews 29, 618-632.

Piperno DR & Flannery KV (2001) The earliest archaeological maize (Zea mays L.) from highland Mexico: New accelerator mass spectrometry dates and their implications. Proceedings of the National Academy of Sciences of the United States of America 98, 2101-2103.

Piperno, DR & Pearsall, D (1998) The Origins of Agriculture in the Lowland Neotropics, Academic Press, San Diego, pp. 400.

R Development Core Team (2008) R: A language and environment for statistical computing. R Foundation for Statistical Computing, Vienna, Austria. ISBN 3-900051-07-0, URL http://www.R-project.org.

Ranere AJ, Piperno DR, Holst I, Dickau R, & Iriarte J (2009) The cultural and chronological context of early Holocene maize and squash domestication in the Central Balsas River Valley, Mexico. Proceedings of the National Academy of Sciences of the United States of America 106, 5014-5018.

Reimer, P.J., Bard, E., Bayliss, A., Beck, J.W., Blackwell, P.G., Ramsey, C.B., Buck, C.E., Cheng, H., Edwards, R.L., Friedrich, M., Grootes, P.M., Guilderson, T.P., Haflidason, H., Hajdas, I., Hatte, C., Heaton, T.J., Hoffmann, D.L., Hogg, A.G., Hughen, K.A., Kaiser, K.F., Kromer, B., Manning, S.W., Niu, M., Reimer, R.W., Richards, D.A., Scott, E.M., Southon, J.R., Staff, R.A., Turney, C.S.M. and van der Plicht, J. (2013) INTCAL13 and MARINE13 Radiocarbon Age Calibration Curves 0-50,000 years cal BP. Radiocarbon 55, 1869-1887.

Rincon Mautner, C. (1999) Man and the Environment in the Coixtlahuaca Basin of Northwestern Oaxaca, Mexico: Two Thousand Years of Historical Ecology, Anthropology. University of Texas, Ann Arbor.

Robson, J., R., K. & Elias, J., N. (1986) Nutritional Significance of Guilá Naquitz Food Remains. In: Flannery, K. V., (Ed.), Guilá Naquitz: Archaic Foraging and Early Agriculture in Oaxaca, Mexico. Academic Press, Inc., Orlando, pp. 297-301.

Rodriguez VP & Anderson KC (2013) Terracing in the Mixteca Alta, Mexico: Cycles of Resilience of an Ancient Land-Use Strategy. Human Ecology 41, 335-349.

Sage, R.F. (2005) Atmospheric CO2, Environmental Stress, and the Evolution of C4 Photosynthesis, in: Ehleringer, J.R., Cerling, T.E., and Dearing, M. D. (Ed.), A History of Atmospheric CO2 and its Effects on Plants, Animals, and Ecosystems. Springer, New York, pp. 185-213.

Sanchez, G.A. (2004) Suelos. In: García-Mendoza, A.J., Ordóñez Díaz, M., and Briones-Salas, M. (Ed.), Biodiversidad de Oaxaca. UNAM, Ciudad Universitaria, pp. 55-66.

Schoenwetter, J., & Smith, L.S. (1986) Pollen Analysis of the Oaxaca Archaic in: Flannery, K. V., (Ed.), Guilá Naquitz: Archaic Foraging and Early Agriculture in Oaxaca, Mexico, Academic Press, Inc., Orlando, pp. 179-226.

Sedov, S., Lozano-Garcia, S., Solleiro-Rebolledo, E., McClung de Tapia, E., Ortega-Guerrero, B. and Sosa-Najera, S. (2010) Tepexpan revisited: A multiple proxy of local environmental changes in relation to human occupation from a paleolake shore section in Central Mexico. Geomorphology 122, 309-322.

Servicio Nacional Mexico (2010) Normales Climatologicas 1971-2000, Estacion 0020019: S. J. Bautista Coixtlahuaca. Comision Nacional del Agua (CONAGUA), Mexico.

Shaw, M. R., Huxman, T. E., Lund, C. P. (2005) Modern and Future Semi-Arid and Arid Ecosystems. In: Ehleringer, J.R., Cerling, T.E., and Dearing, M. D. (Ed.), A History of Atmospheric CO_2 and its Effects on Plants, Animals, and Ecosystems. Springer, New York, pp. 415-440.

Smith Jr., C. E. (1986) Preceramic Plant Remains from Guilá Naquitz. In: Flannery, K. V., (Ed.), Guilá Naquitz: Archaic Foraging and Early Agriculture in Oaxaca, Mexico. Academic Press, Inc., Orlando, pp. 265-274.

Smith, B. (2005) Photosynthesis, Respiration, and Growth. In: Pessarakli, M. (Ed.), Handbook of Photosynthesis. Taylor & Francis, Boca Raton, pp. 671-678.

Solis-Castillo, B., Golyeva, A., Sedov, S., Solleiro-Rebolledo, E. and Lopez-Rivera, S. (2015) Phytoliths, stable carbon isotopes and micromorphology of a buried alluvial soil in Southern Mexico: A polychronous record of environmental change during Middle Holocene. Quaternary International 365, 150-158.

Spielmann KA, Nelson M, Ingram S, & Peeples MA (2011) Sustainable Small-Scale Agriculture in Semi-Arid Environments. Ecology and Society 16, 26 [online].

Stuiver, M., Reimer, P. J., and Reimer, R. (2015) CALIB Radiocarbon Calibration,

Version 7.1html ed., http://calib.qub.ac.uk/calib/

Suess, H. E. (1955), Radiocarbon concentration in modern wood, Science, 122(3166), 415–417.

Tieszen, L.L. (1991) Natural Variations in the Carbon Isotope Values of Plants Implications for Archaeology, Ecology, and Paleoecology. Journal of Archaeological Science 18, 227-248.

Trejo, I. (2004) Clima. In: Garcia-Mendoza, A.J., Ordonez, M., and Briones-Salas, M. (Ed.), Biodiversidad de Oaxaca. Universidad Nacional Autonoma de Mexico, Cuidad Universitaria, pp. 67-86.

Urban, M.A., Nelson, D.M., Street-Perrott, F.A., Verschuren, D. and Hu, F.S. (2015) A late-Quaternary perspective on atmospheric pCO_2, climate, and fire as drivers of C-4-grass abundance. Ecology 96, 642-653.

USGS, Global Multi-resolution Terrain Elevation Data (2010) (GMTED2010), United States Geological Survey website (2010),http://topotools.cr.usgs.gov/-gmtedviewer/; last accessed March 2016.

Valiente-Banuet, A., Flores-Hernandez, N., Verdu, M. and Davila, P. (1998) The chaparral vegetation in Mexico under nonmediterranean climate: The convergence and Madrean-Tethyan hypotheses reconsidered. American Journal of Botany 85, 1398-1408.

Vogel, J.S., Southon, J.R., Nelson, D.E. and Brown, T.A. (1984) Performance of Catalytically Condensed Carbon for Use in Accelerator Mass-Spectometry. Nuclear Instruments & Methods in Physics Research Section B-Beam Interactions with Materials and Atoms 5, 289-293.

von Fischer, J.C., Tieszen, L.L. and Schimel, D.S. (2008) Climate controls on C-3 vs. C-4 productivity in North American grasslands from carbon isotope composition of soil organic matter. Global Change Biology 14, 1141-1155.

Warinner, C., Robles Garcia, N. and Tuross, N. (2012) Maize, beans and the floral isotopic diversity of highland Oaxaca, Mexico. Journal of Archaeological Science 40, 868-873.

Wynn, J.G. (2007) Carbon isotope fractionation during decomposition of organic matter in soils and paleosols: Implications for paleoecological interpretations of paleosols. Palaeogeography Palaeoclimatology Palaeoecology 251, 437-448.

Wynn, J.G., Bird, M.I. (2008) Environmental controls on the stable carbon isotopic composition of soil organic carbon: implications for modelling the distribution of C-3 and C-4 plants, Australia. Tellus Series B-Chemical and Physical Meterology 60(4): 604-621.

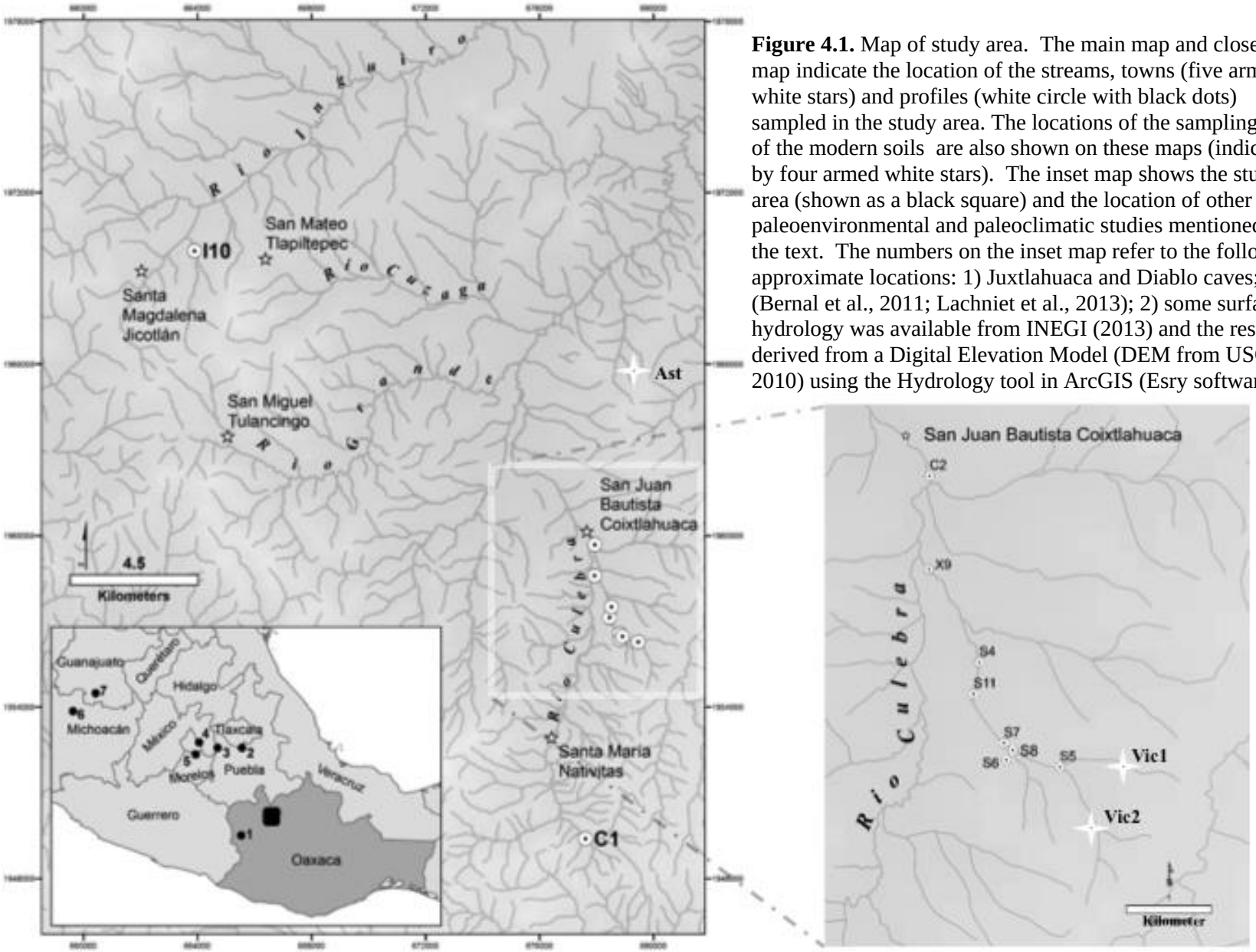

Figure 4.1. Map of study area. The main map and close-up map indicate the location of the streams, towns (five armed white stars) and profiles (white circle with black dots) sampled in the study area. The locations of the sampling sites of the modern soils are also shown on these maps (indicated by four armed white stars). The inset map shows the study area (shown as a black square) and the location of other paleoenvironmental and paleoclimatic studies mentioned in the text. The numbers on the inset map refer to the following approximate locations: 1) Juxtlahuaca and Diablo caves; (Bernal et al., 2011; Lachniet et al., 2013); 2) some surface hydrology was available from INEGI (2013) and the rest derived from a Digital Elevation Model (DEM from USGS, 2010) using the Hydrology tool in ArcGIS (Esry software).

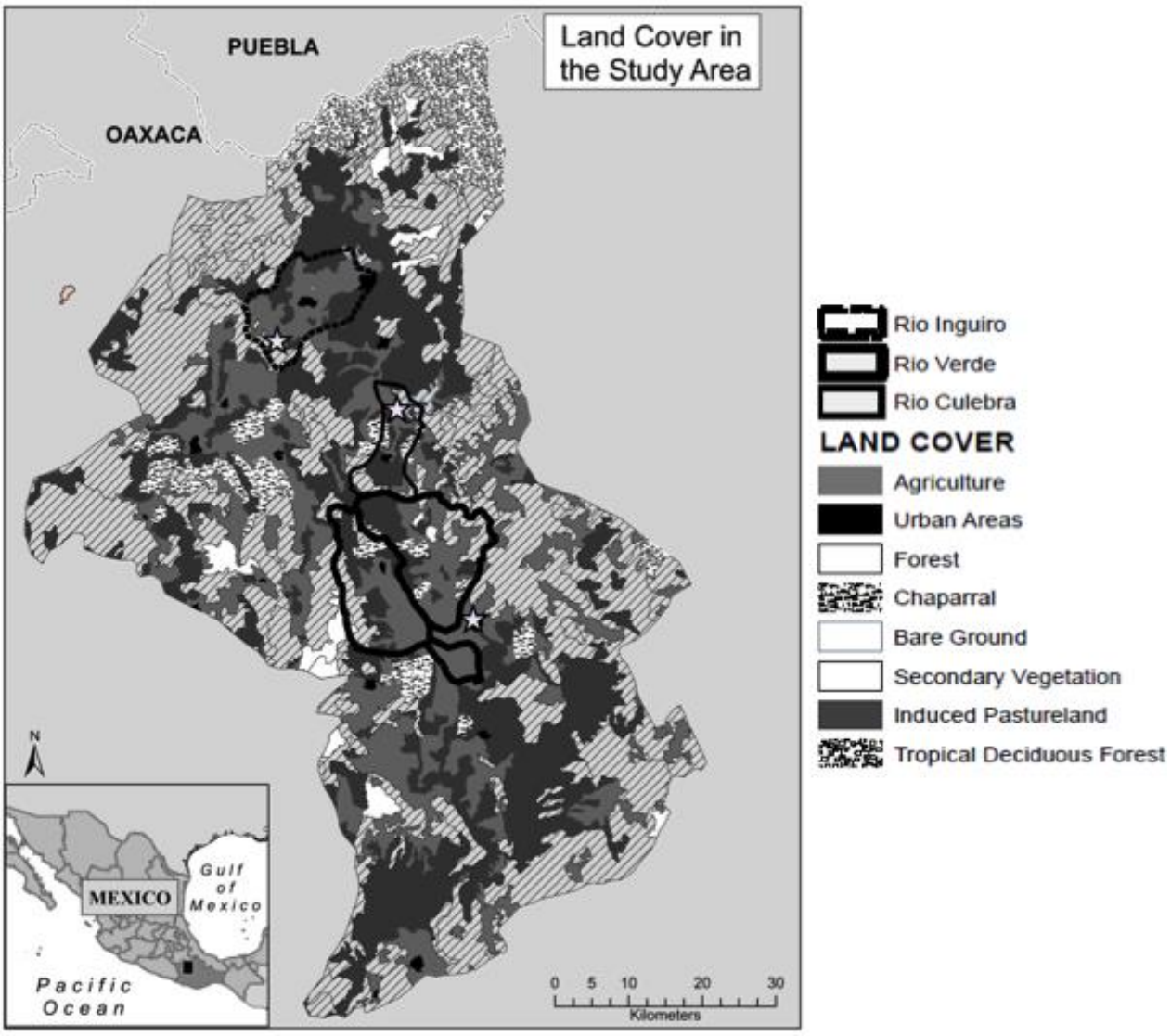

Figure 4.2. Land cover map of the region. The outline of the study area involves the watersheds of Rio Culebra, Inguiro, and parts of Verde. The stars show the location of the three municipalities associated with the watersheds. (Land cover data from INEGI, 2015).

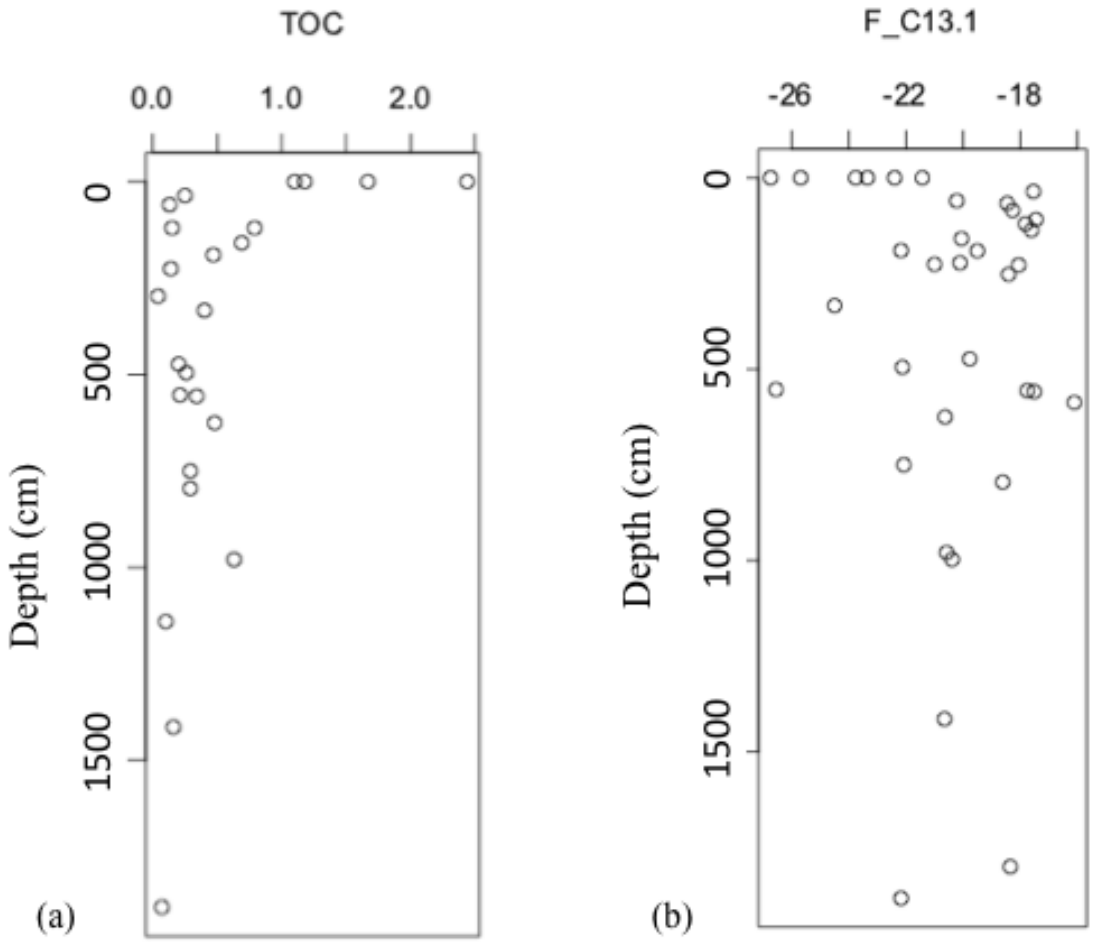

Figures 4.3. Relationship between depth and %TOC (a), and $\delta^{13}C$ (b). Only the interpolated buried Ab SOM samples were analyzed for %TOC and are incorporated into Figure 4.3a. Figure 4.3b includes $\delta^{13}C$ values from interpolated and radiocarbon dated buried Ab samples. No charcoal values were incorporated into these graphs.

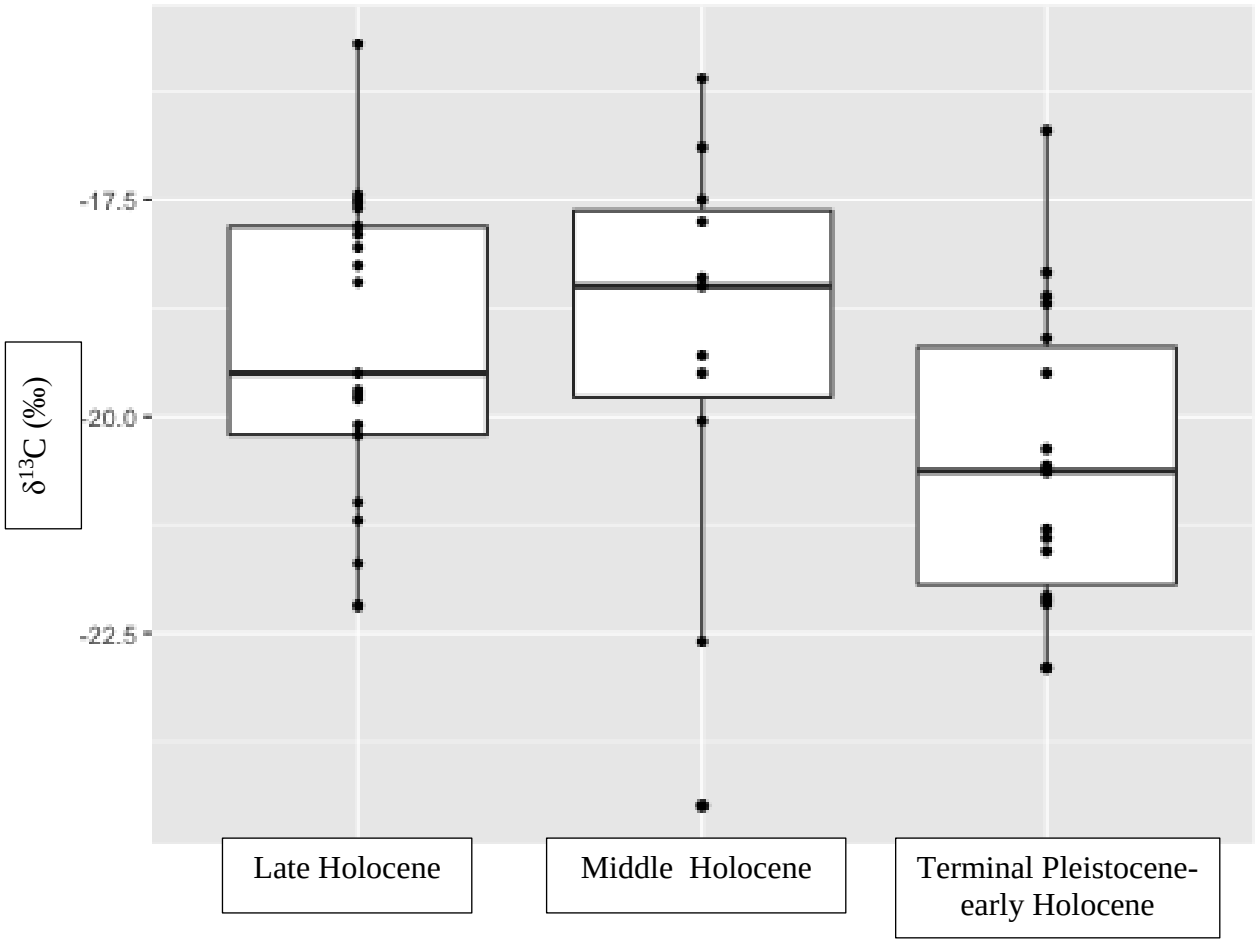

Figure 4.4. Distribution of δ13C values from the Culebra, Verde and Inguiro watersheds (not including the charcoal sample values) including the mean (black horizontal line), the standard deviation (box), and the individual δ13C values (black dots) for different time periods. The modern values reflect the +1.5‰ related to the Suess effect.

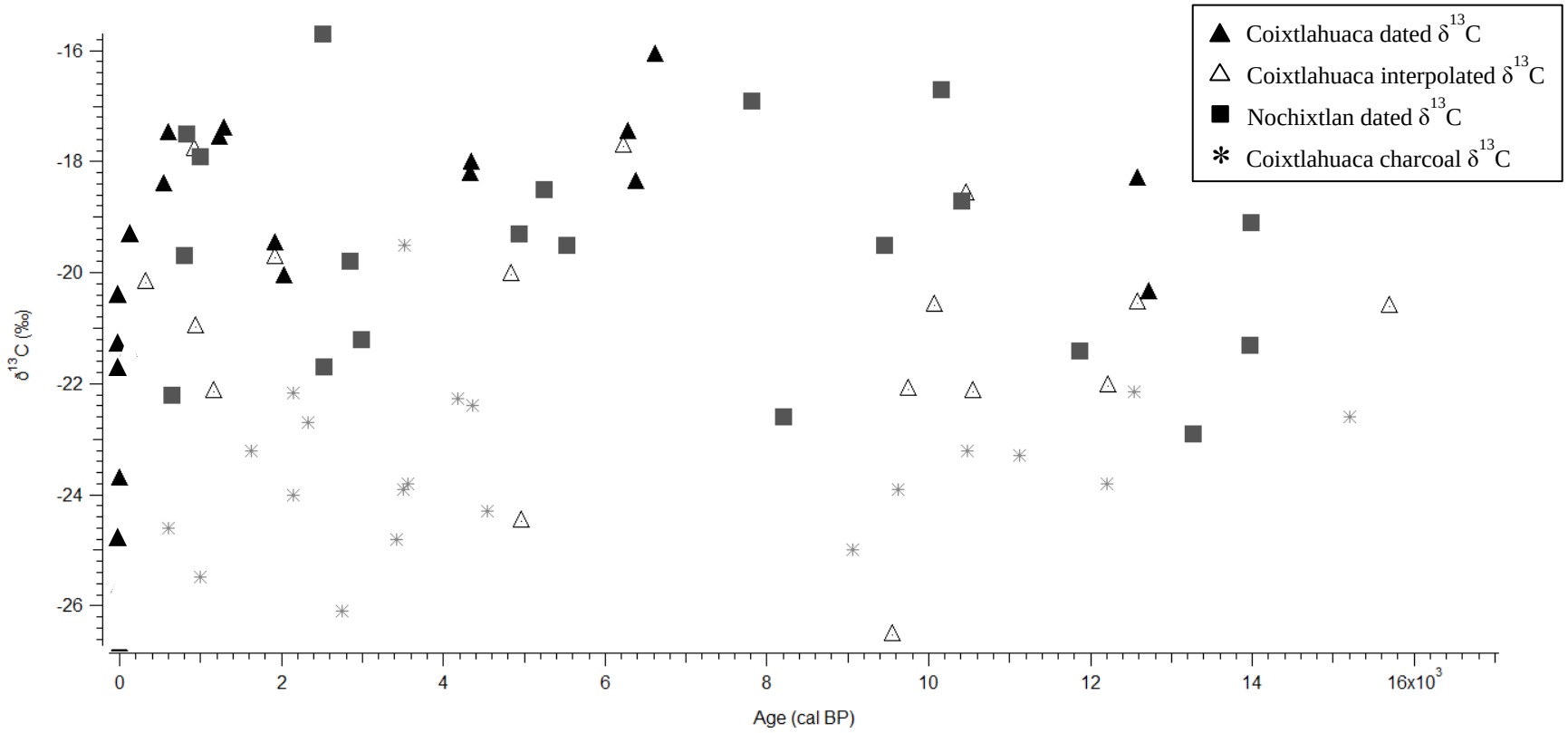

Figure 4.5. Variation of all $\delta^{13}C$ values from the Culebra, Inguiro and Verde watersheds from the terminal Pleistocene through the late Holocene. The median age was calculated for all ages from the interpolated or actual calibrated age range. The $\delta^{13}C$ values from Rio Verde are denoted by closed, black squares. The closed black triangles and open triangles represent the $\delta^{13}C$ values from the dated and interpolated buried Ab samples, respectively, from the Ríos Culebra and Inguiro watersheds. The light gray star shapes represent the $\delta^{13}C$ values from the charcoal samples from the Ríos Culebra and Inguiro watersheds. The modern values reflect the +1.5‰ related to the Suess effect.

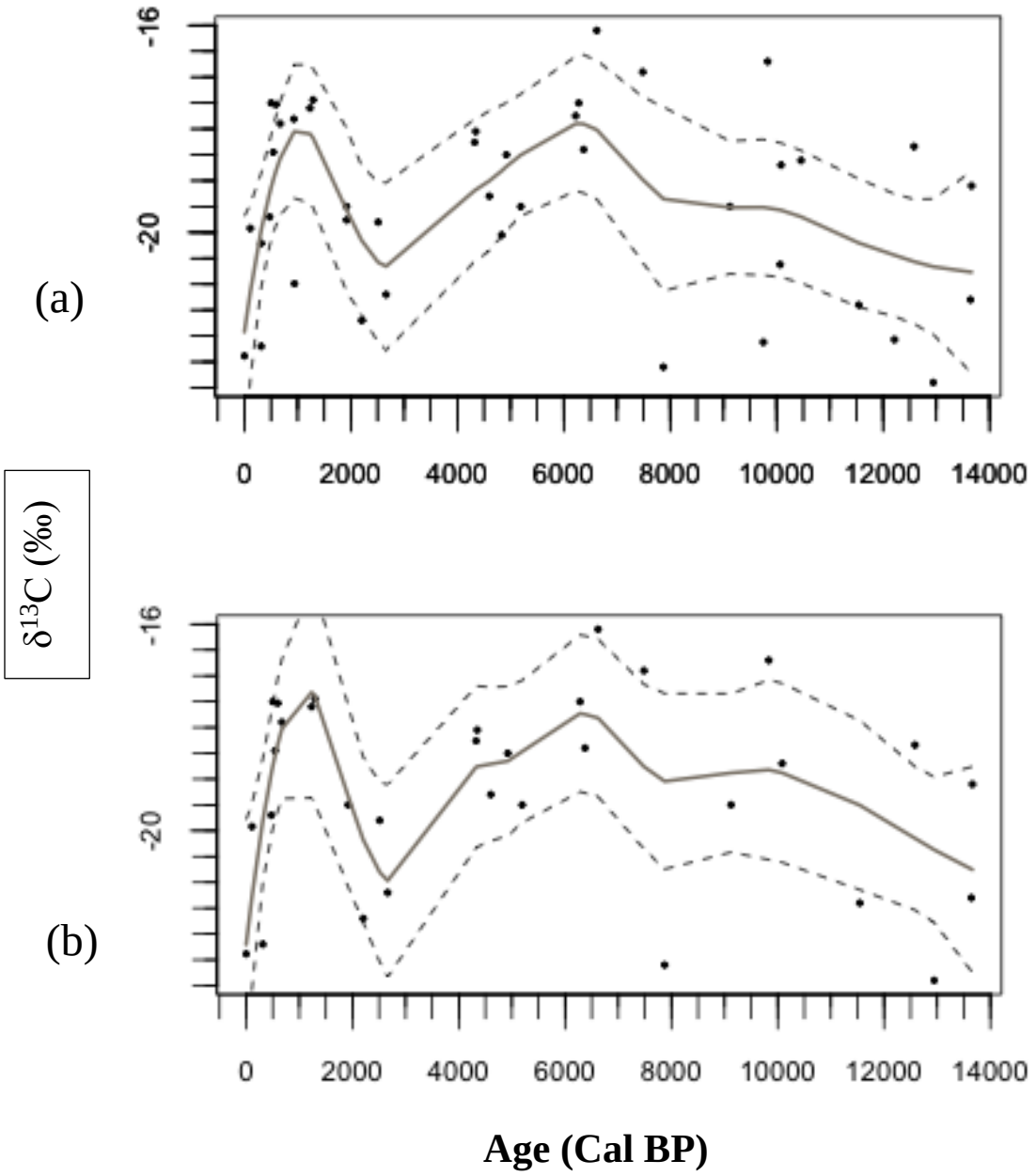

Figures 4.6. Local polynomial regression indicating the main trend of all $\delta^{13}C$ values over time. Graph 4.6a excludes the outliers, while graph 4.6b excludes both outliers and the interpolated $\delta^{13}C$ values. Neither of the graphs include the $\delta^{13}C$ values from the charcoal samples. Note two peaks in the data, the first of which is in the middle Holocene and the second is in the late Holocene, between ~1,250-500 cal BP. The analysis was made in R statistical software (R core team) using the **LOESS** function (Cleveland et al 1992). The modern values are averaged and reflect the +1.5‰ related to the Suess effect.

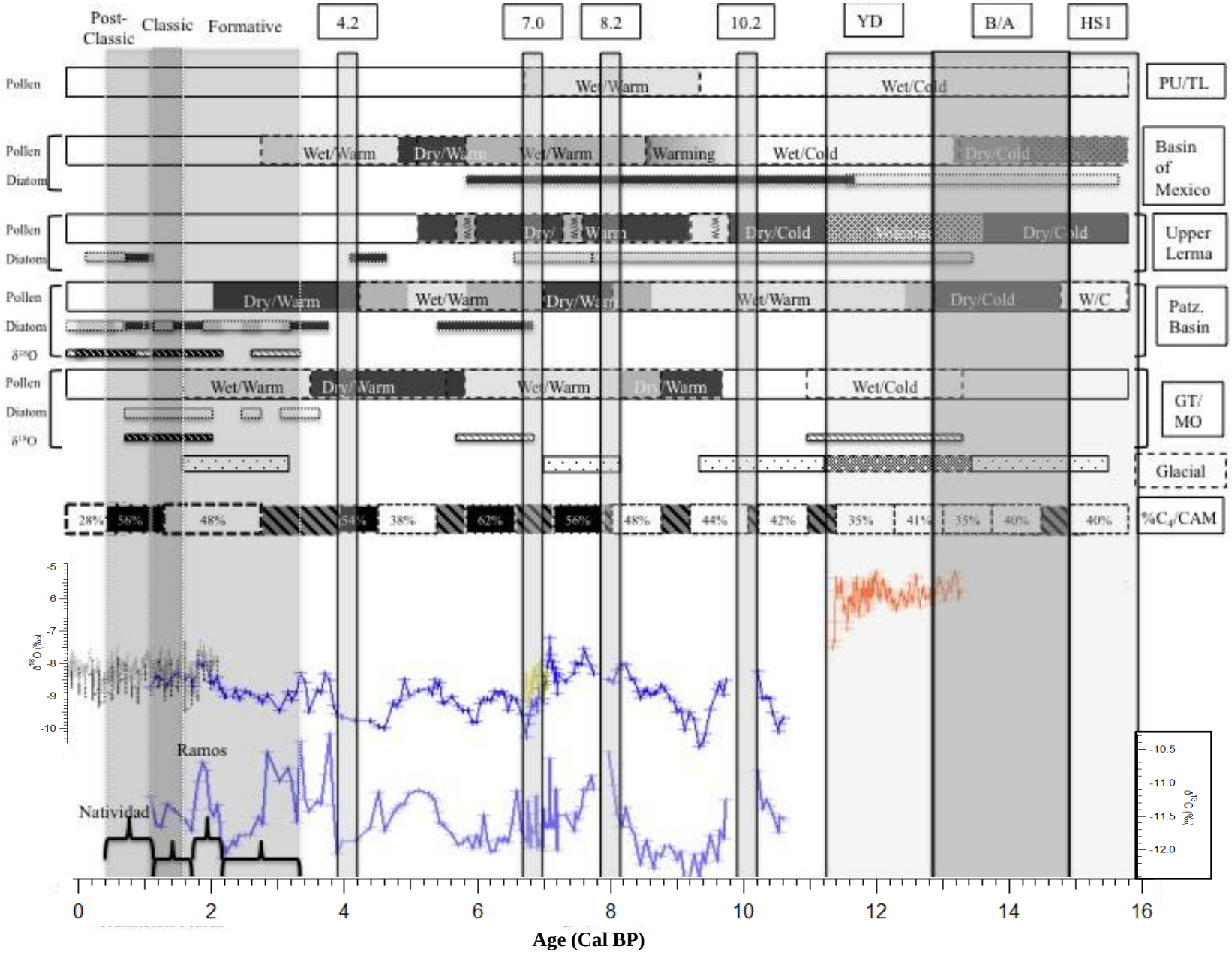
Post-Classic
Classic
Formative
4.2
7.0
8.2
10.2
YD
B/A
HS1
Pollen
Wet/Warm
Wet/Cold
PU/TL
Pollen
Diatom
Wet/Warm
Dry/Warm
Wet/Warm
Warming
Wet/Cold
Dry/Cold
Basin of Mexico
Pollen
Diatom
Dry/Cold
Upper Lerma
Pollen
Diatom
δ18O
Dry/Warm
Wet/Warm
Wet/Warm
Dry/Cold
W/C
Patz. Basin
Pollen
Diatom
δ13O
Wet/Warm
Wet/Warm
Wet/Cold
GT/ MO
Glacial
28%
56%
48%
54%
38%
62%
56%
48%
44%
42%
35%
41%
35%
40%
40%
%C4/CAM
δ18O (‰)
Ramos
Natividad
δ13C (‰)
0
2
4
6
8
10
12
14
16
Age (Cal BP)

Note: Caption refers to figure on previous page.

Figure 4.7. Summary of the climate data in central and southwestern Mexico for the last 16,000 years. This information is organized by region (listed on right) and type of proxy data (listed on left) for the upper portion (top 1/4th) of the figure. Below this regional organization is information concerning glaciers from central Mexico, %C4 and CAM and paleosol information from the study area and the Río Verde basin. The second portion of the graph shows the $\delta^{18}O$ signature from stalagmites in Guerrero, Mexico and CO_2 information.

Information for figure and in text is summarized from the following articles: 1) Puebla-Tlaxcala (Metcalfe et al., 2000); 2) Basin of Mexico (from Metcalfe et al., 2000; Lozano-Garcia and Ortega-Guerrero, 1998; Lozano-Garcia and Vazquez-Selem) 3) Upper Lerma (Metcalfe et al., 2000; Lozano-Garcia et al., 2005;) ; 4) Lake Patzcuaro, Lake Zirahuen, Lake Zacapu (Metcalfe et al., 2000; Bradbury, 1989; Bradbury, 2000; Lozano-Garcia et al., 2013); 5) Guanajato and Michoacán (Metcalfe et al., 2000; Park et al., 2010); 6) Glaciers: (Metcalfe et al., 2000; Lozano-Garcia and Vazquez-Selem, 2005; Vazquez-Selem and Heine, 2011); 7) $\%C_4$/CAM (this study, Rio Verde information from Mueller et al., 2012); 8) paleosol information (Mueller et al., 2012; Chapter 3); 9) $\delta^{18}O$ from Guerreran stalagmites (Bernal et a., 2011; Lachniet et al., 2013); 10) past atmospheric CO2 from the Antarctic ice cores (Monnin et al 2001; 2004); lake carbonate isotope data (Lozano-Garcia et al., 2010); 11) $\delta^{13}C$ data (this study, includes data from Verde watershed, Mueller et al., 2012); 12) archaeological time periods (Kowalewski et al., 2009, Kowalewski, pers. com).

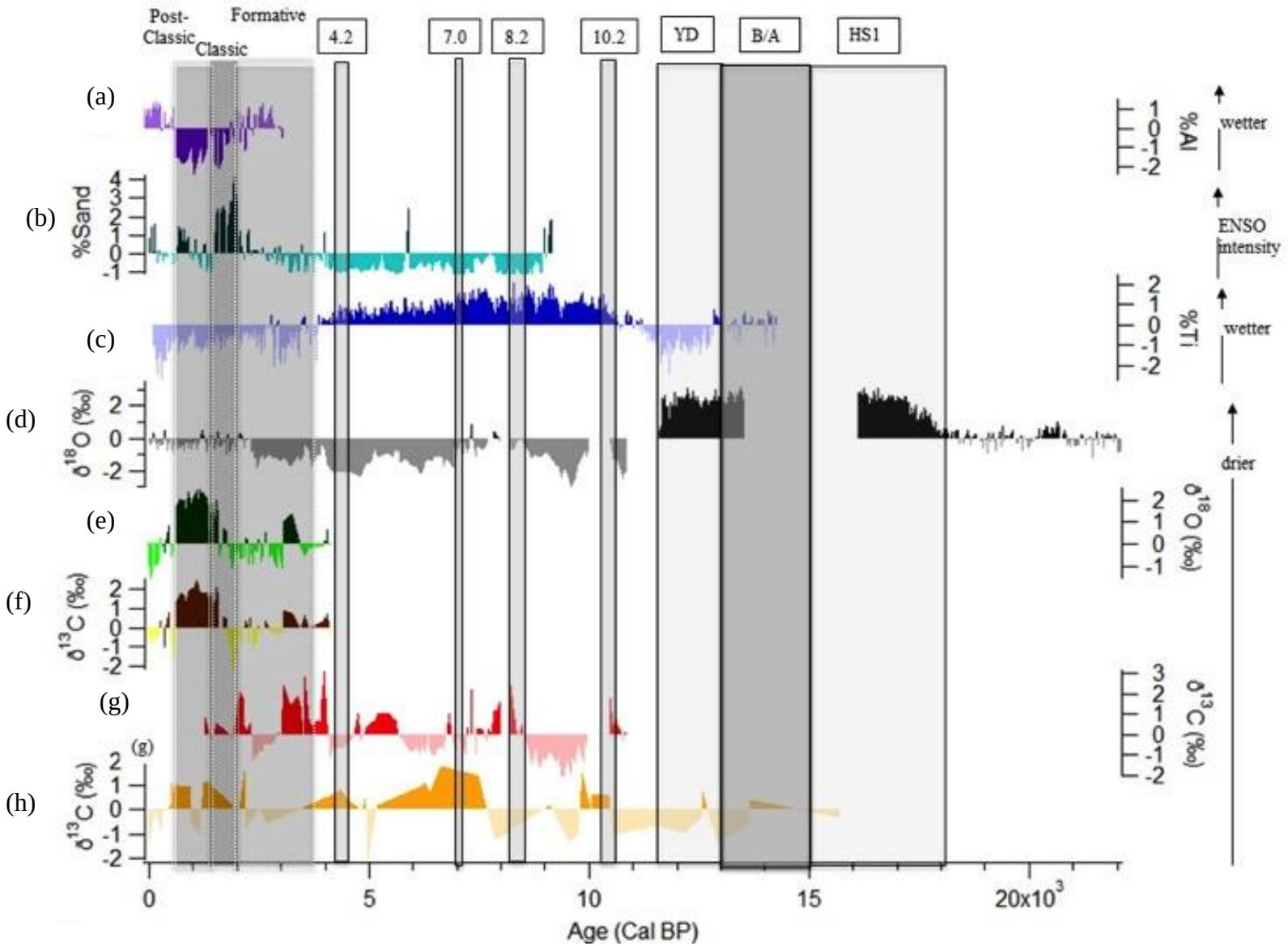

Figure 4.8. Z-score calculations for selected paleoclimatic datasets.

Note: Caption refers to figure on previous page.

Figure 4.8. Z-score calculations for selected paleoclimatic datasets. Information for figure and in text is summarized from the following studies: (a) $\%Al_2O_3$ from Cuenca Oriental (Bhattacharya et al. 2015); (b) % Sand from El Junco Basin (Conroy et al., 2008); (c) %Ti from Cariaco Basin (Haug et al., 2001); (d) $\delta^{18}O$ (‰)from Guerreran stalagmites (Bernal et a., 2011; Lachniet et al., 2013); (e) $\delta^{18}O$ (‰) from Cuenca Oriental (Bhattacharya et al. 2015); (f) $\delta^{13}C$ (‰) from Cuenca Oriental (Bhattacharya et al. 2015); (g) (d) $\delta^{13}C$ (‰) from the Cueva del Diablo (Guerrero) (Bernal et a., 2011); and (h) $\delta^{13}C$ data (this study, includes data from Verde watershed, Mueller et al., 2012).

Table 4.1. Results of the $\delta^{13}C$ values analyses. The results include analyses made on dated and interpolated buried A SOM samples, as well as from charcoal samples from the Culebra and Inguiro watersheds. The ages from the dated buried A SOM and charcoal samples were calibrated using the online CALIB software (Stuiver et al., 2015) and the INTCAL2013 calibration curve (Riemer et al., 2013). The ages of the interpolated buried A SOM samples were estimated using the Classical Age Model (CLAM) of Blaauw (2010, version 2.2) with R software (R Core Team, 2013).

Site	Depth (cm)	Calibrated Age (2-sig)	Median	$\delta^{13}C$ values Analysis 1[1]	$\delta^{13}C$ values Analysis 2	Paleosol $\delta^{13}C$ values from C14 dating	Charcoal $\delta^{13}C$ values	Final $\delta^{13}C$[2]	Total Organic Carbon[3]
Apo	Forest	NA	MODERN	-26.73	NA	NA	NA	-25.23	1.1
Ast	Grassland	NA	MODERN	-22.39	NA	NA	NA	-20.89	1.67
Vic	Mixed grass/ succulent	NA	MODERN	-23.34	NA	NA	NA	-21.84	2.44
Vic	Mixed grass/forest/ succulent	NA	MODERN	-25.68	NA	NA	NA	-24.18	1.18
C1	395	2060-2300c	NA	NA	NA	NA	-23.6	-23.6	NA
C1	800	12421-12619c	NA	NA	NA	NA	-23.7	-23.7	NA

C1	300	NA	NA	-22.27	NA	NA	NA	-22.27	0.13
C1	950	NA	NA	-22.14	NA	NA	NA	-22.14	0.4
C2	190	1073-1251*	1162	-22.17	NA	NA	NA	-22.17	0.47
C2	222	1949-2114	2028	NA	NA	-20.1	NA	-20.1	NA
C2	334	4898-5019*	4959	-24.49	NA	NA	NA	-24.49	0.4
C2	490	89999-9133c		NA	NA	NA	-25	-25	
C2	553	9468-9640*	9554	(-30.17[i])	-22.91	NA	NA	-22.91	0.35
C2	979	12550-12611*	12581	NA	-20.57	NA	NA	-20.57	0.63
C2	997	12684-12750	12717	NA	NA	-20.38	NA	-20.38	
C2	1414	15589-15798*	15694	-20.28	-21	NA	NA	-20.64	0.16
C2	1882	18828-19218*	10553	(-20.18[i])	-22.17	NA	NA	-22.17	0.07
I10	Mixed grassland/ succulent	***	MODERN	NA	NA	-21.42	NA	-19.92	NA
I10	36	NA	NA	-20.92	-19.29	NA	NA	-20.11	0.25
I10	226	881-998*	940	-20.58	-21.4	NA	NA	-20.99	0.14
I10	243	939-1057c	NA	NA	NA	NA	-25.49	-25.49	NA
I10	473	1855-1987*	1921	**-20.21**	**-19.98**	**-19.42**	NA	-19.76	0.2
I10	802	4039-4281c	NA	NA	NA	NA	-22.26	-22.26	NA
S11	120	NA	NA	(-19.41[i])	-20.95	NA	NA	-20.95	0.15
S4	Mixed grassland/ succulent	***	MODERN	NA	NA	-23.75	NA	-22.25	NA
S4	60	286-349*	318	-20.1	NA	NA	NA	-20.21	0.13

S4	105	531-641c	NA	NA	NA	NA	-24.6	-24.6	NA
S4	120	881-978*	930	-17.81	NA	NA	NA	-17.81	0.79
S4	398	4256-4425c	NA	NA	NA	NA	-22.4	-22.4	NA
S4	517	4439-4784c	NA	NA	NA	NA	-24.3	-24.3	NA
S4	556	6173-6274*	6224	(-28.74[4])	**-17.99**	**-17.5**	NA	-17.75	0.34
S4	559	6212-6307	6282	NA	NA	-17.5	NA	-17.5	NA
S4	587	6507-6674	6620	NA	NA	-16.1	NA	-16.1	NA
S4	712	11808-11201c	NA	NA	NA	NA	-23.3	-23.3	NA
S4	750	11986-12444*	12215	-21.24	-22.89	NA	NA	-22.07	0.29
S4	1140	24852-26488*	25670	-21.06	-22.04	NA	NA	-21.55	0.1
S5	280	1562-1698c	NA	NA	NA	NA	-23.2	-23.2	NA
S5	67	518-629	544	NA	NA	-18.45	NA	-18.45	NA
S5	191	1873-1988	1919	NA	NA	-19.5	NA	-19.5	NA
S5	434	2721-2760c	NA	NA	NA	NA	-26.1	-26.1	NA
S5	1081	3377-3479c	NA	NA	NA	NA	-24.8	-24.8	NA
S6	109	1266-1309	1291	NA	NA	-17.44	NA	-17.44	NA
S6	228	4249-4419	4348	NA	NA	-18.05	NA	-18.05	NA
S7	137	1181-1278	1233	NA	NA	-17.6	NA	-17.6	NA
S7	330	2048-2303c	NA	NA	NA	NA	-24	-24	NA
S7	350	2184-2351c	NA	NA	NA	NA	-22.7	-22.7	NA
S7	522	3453-3565c	NA	NA	NA	NA	-23.9	-23.9	NA
S7	585	3480-3639c	NA	NA	NA	NA	-23.8	-23.8	NA

S8	36	527-637	595	NA	NA	-17.53	NA	-17.53	NA
S8	85	4238-4414	4327	NA	NA	-18.26	NA	-18.26	NA
Sand	500	3457-3571	NA	NA	NA	-19.5	NA	-19.5	NA
X9	159	4720-4946*	4833	-20.05	NA	NA	NA	-20.05	0.69
X9	252	6310-6446	6375	NA	NA	-18.4	NA	-18.4	NA
X9	450	9548-9703c[l]	NA	NA	NA	NA	-23.9	-23.9	NA
X9	495	9675-9827*	9751	-21.52	-22.72	NA	NA	-22.12	0.34
X9	625	9994-10139*	10067	-20.81	-20.44	NA	NA	-20.62	0.48
X9	785	10376-10573c	NA	NA	NA	NA	-23.2	-23.2	NA
X9	795	10335-10582*	10459	**-19.72**	**NA**	**-17.5**	NA	-18.61	0.29
X9	1750	12330-12250c	NA	NA	NA	NA	-23.8	-23.8	NA
X9	1800	12524-12670	12583	NA	NA	-18.34	NA	-18.34	NA
X9	2300	15060-15348c	NA	NA	NA	NA	-22.6	-22.6	NA

Notes:

1The $\delta^{13}C$ values from the interpolated buried A SOM samples are presented in Analysis 1 and 2.

2If more than one $\delta^{13}C$ value was obtained for a corresponding profile and depth, they are averaged and presented in the Final $\delta^{13}C$ column.

3The percentage of the total organic carbon (%TOC) for the interpolated buried A SOM analyses are presented in this column. These values represent an averaged value if the $\delta^{13}C$ values were averaged.

*$\delta^{13}C$ values with interpolated ages.

"c" = $\delta^{13}C$ values for charcoal ages.

"**22.1**" = $\delta^{13}C$ values from dated buried A SOM that were re-analyzed to determine their duplicability.

4 $\delta^{13}C$ values removed from further analysis.

*** $\delta^{13}C$ values from surface A SOM that were dated to estimate soil residence time.

Table 4.2. The resulting modern $\delta^{13}C$ values after applying correction for the Suess effect. The italized values represent the final accepted values.

Site Name	Vegetation type	Raw δ13C	*Final δ13C (+1.5‰)*	δ13C (+2.0‰)
Apo	Forest	-26.73	*-25.23*	-24.73
Ast	Grassland	-22.39	*-20.89*	-20.39
S4	Mixed grassland/succulent	-23.75	*-22.25*	-21.75
Vic1	Mixed grass/succulent	-23.34	*-21.84*	-21.34
Vic2	Mixed grass/forest/ succulent	-25.68	*-24.18*	-23.68
I10	mixedMixed grassland/succulent	-21.42	*-19.92*	-19.42

Table 4.3. The modern $\delta^{13}C$ values used in calculating $\%C_4$ and CAM. The italized values represent the final accepted values.

Vegetation Type	δ13C Value	*(+1.5‰)*	(+2.0‰)
C3 wild	-28	*-26.5*	-26
C3 cultivated	-27.3		
C4 wild	-13.3	*-11.8*	-11.3
C4 cultivated	-12		
CAM wild	14.3		
CAM cultivated	13.1		

Table 4.4. Calculated percentages of C_4 and CAM. The percentages were calculated from the $\delta^{13}C$ values, excluding charcoal, from the Verde, Culebra and Inguiro watersheds.

Site	Median	Final $\delta^{13}C^2$	%C4 and CAM (no correction)	Final %C4 and CAM (+1.5)	%C4 and CAM (+2.0)
Apo (forest)	0	-25.23	19	**9**	5
Ast (grass)	0	-20.89	48	**38**	35
S4 (Mixed grassland/succulent)	0	-22.25	39	**29**	26
Vic1 (mixed grass/succulent)	0	-21.84	42	**32**	28
Vic2 (mixed grass/forest/succulent)	0	-24.18	26	**16**	12
I10 (Mixed grassland/succulent)	112	-19.92	55	**45**	41
Yan5	313	-22.2	39	**29**	26
S4	318	-20.21	53	**43**	39
Yutz7	473	-19.7	56	**46**	43
Yux3	503	-17.5	71	**61**	58
S5	544	-18.45	65	**55**	51
S8	595	-17.53	71	**61**	58
Yan2	673	-17.9	69	**59**	55
S4	930	-17.81	69	**59**	56
I10	940	-20.99	48	**37**	34
C2	1162	-22.17	40	**29**	26
S7	1233	-17.6	71	**61**	57
S6	1291	-17.44	72	**62**	58
S5	1919	-19.5	58	**48**	44
I10	1921	-19.76	56	**46**	42
C2	2028	-20.1	54	**44**	40
Ver6	2183	-15.7	84	**73**	70
Yuz8	2203	-21.7	43	**33**	29
Yutz4	2513	-19.8	56	**46**	42
Yutz4	2663	-21.2	46	**36**	33
S8	4327	-18.26	66	**56**	53
S6	4348	-18.05	68	**57**	54
Yuz5	4603	-19.3	59	**49**	46
X9	4833	-20.05	54	**44**	40
Yan1	4923	-18.5	65	**54**	51
C2	4959	-24.49	24	**14**	10

Yutz4	5193	-19.5	58	**48**	44
S4	6224	-17.75	70	**60**	56
S4	6282	-17.5	71	**61**	58
X9	6375	-18.4	65	**55**	52
S4	6620	-16.1	81	**71**	67
Yuz5	7483	-16.9	76	**65**	62
Yuz9	7873	-22.6	37	**27**	23
Yutz7	9123	-19.5	58	**48**	44
C2	9554	-22.91	35	**24**	21
X9	9751	-22.12	40	**30**	26
Yan4	9833	-16.7	77	**67**	63
X9	10067	-20.62	50	**40**	37
Yan2	10083	-18.7	63	**53**	50
X9	10458	-18.61	64	**54**	50
C2	10553	-22.17	40	**29**	26
Yan8	11543	-21.4	45	**35**	31
S4	12215	-22.07	40	**30**	27
C2	12581	-20.57	51	**40**	37
X9	12583	-18.34	66	**56**	52
C2	12717	-20.38	52	**42**	38
Yuz9	12943	-22.9	35	**24**	21
Yuz12	13643	-21.3	46	**35**	32
Yutz4	13663	-19.1	61	**50**	47
C2	15694	-20.64	50	**40**	36
S4	25670	-21.55	44	**34**	30

CHAPTER 5

CONCLUSION

5.1 Introduction

The incomplete understanding of present and past climatic change and the variability of hydrological response to climate and land use change in dryland tropical regions is cause for great concern. The problems of dryland regions in Mexico are no exceptions, with only a few investigations into the nature and causes of erosion in dryland stream systems (Julio Falfan of ConAgua, pers. Com., Rafael Arzate Aguirre of the Reserva de la Biosfera, pers. Com., and as stated in Butzer et al., 2008; Mueller et al., 2012). The state of Oaxaca is home to many indigenous populations, whose livelihoods depend on their local environment. The highly degraded landscape of the Mixteca Alta embodies the dilemma of dryland desertification. Oaxaca is in one of the two poorest states in Mexico, and many people partially rely on government aid and intervention. The Mixteca Alta is one of the poorest areas in Oaxaca, not only in terms of financial needs, but also in relation to its impoverished environment. Foraging and managing of local plants, cultivating, and animal herding provide sustenance and supplementary income to the rural population of this region. Several national organizations, including the National Park Service, have worked with local communities to implement governmentally subsidized conservation measures. However, without more information on the

various causes of degradation and the variability of local dryland stream systems, it is difficult to assess the short and long-term effectiveness of these solutions on a basin-wide scale.

Examination of the late Quaternary environment and geomorphology of the incised, ephemeral tributaries forming the Río Culebra watershed offered insight about causes of erosion and hydrological variability of the region. This integrated study confirmed the variable and intricate nature of semi-arid dryland fluvial systems. Climate change, land use factors, and innate watershed characteristics (e.g., influential natural factors) have an integrated role in producing erosion and modifying stream response during the late Holocene. Despite present conservation efforts, climate change, present land use, and legacy effects from prehistoric and Colonial land use all impede a straightforward solution to restoring the landscape on a basin wide scale.

The arroyos of the Río Culebra watershed, and much of the Mixteca Alta, are particularly complex as they involve both perennial and ephemeral streams, all of which incise and aggrade on a cyclical timescale (Bull, 1997; Graf, 2002). As such, no stepped terraces are observed in the valley, meaning more than 15,000 years of alluvial deposits reflecting hydrologic responses to external drivers are entangled in the valley alluvium. Although the Culebra watershed only covers 82 km^2, the findings shed light onto better understanding the desertification problem in the entire Mixteca Alta, and other drylands worldwide.

5.2 Climate and Hydrology: Long-Term Variability

The earliest date of cut-and-fill stratigraphy at ~15,000 cal BP demonstrates that at least since the terminal Pleistocene, arroyo cycles have been a significant feature of the

geomorphology of the Mixteca Alta. The easily erodible geology of the Yanhuitlan beds in the Mixteca Alta makes these areas extremely vulnerable to any climatic and land use changes (as in McAuliffe and McFadden, 1997).

The semi-arid climate of the Mixteca Alta results from the rain shadow effect of the high Mexican orography, in particular the Sierra Madre del Sur. Precipitation in the region is variable and intensity is high. The current rainy season is attributed to the timing and strength of the North American Monsoon, which are affected by both la Niña and El Niño phases of El Niño Southern Oscillation (Vera et al., 2006).

The ephemeral tributary arroyos of the Río Culebra have many traits in common with other sand-gravel dominated headwater dryland streams including rectangular channel form, lack of armouring, subtle bedforms, and variable but intense scour-and-fill (Hassan et al., 2009; Billi, 2011; Lucia et al., 2016). The channel morphology comprises a single-threaded main channel that has some braiding with bars and minor channels. Minimum bedload yield of 17 and 45 t day^{-1} measured during individual runoff events from Barrancas Sandage and Sauce, respectively, indicate that the watershed has high bedload yield typical of other semi-arid environments. Floods in the Culebra watershed are extremely flashy and highly concentrated, though they are often relatively shallow. High bedload yield and shallow floods in conjunction with the various traits expressed above support high bedload flux under relatively low shear stress and equal mobility of particles as observed in other ephemeral streams (e.g., Reid et al., 1996; Lucia et al., 2016). Examining the alluvium-paleosol chronology of the Culebra, Inguiro, and Verde (Mueller et al., 2012) watersheds against the high-resolution $\delta^{18}O$ signature from Guerreran stalagmites (Bernal et al., 2011; Lachniet et al., 2013) suggested that incision occured

during wetter periods, which corresponds to findings in other studies (Harden et al., 2010). This comparison also suggested that alluvial deposition and paleosol formation occurred during transitional wet and dry periods, which correspond to relatively drier periods than those associated with incision and offers support for the "wet-dry-wet" model of arroyo cycles (Waters and Haynes, 2001; Hereford, 2002; Huckleberry and Duff, 2008, Harden et al., 2010). Overarching paleosol characteristics since the latest Pleistocene support the idea that wet and dry fluctuations are an important component of the climate, and in general, support the idea that alluvium/paleosol deposition/formation was prevalent during relatively drier, transitional wet and dry periods. The importance of dry conditions in the area is demonstrated by the widespread Stage I $CaCO_3$ deposited on ped faces and in root pores in most horizons (Birkeland, 1984).

The $\delta^{13}C$ values obtained from buried soil organic matter exhibit a non-random distribution through time and reflect overarching climate change from the terminal Pleistocene to the early Holocene. When compared to various climatic proxies for central Mexico (e.g., Lozano-Garica and Ortega-Guerrero, 1998; Metcalfe et al., 2000), as well as to the $\delta^{18}O$ from stalagmites in southwestern Mexico (Bernal et al., 2011; Lachniet et al; 2013), the calculated percentages of $\%C_4$ and CAM reflected both temperature and moisture fluctuations. The transition of low to moderate percentages of C_4 and CAM biomass in the terminal Pleistocene and early Holocene toward high percentages in the middle Holocene signals the transition from cool and dry towards warm and dry conditions. The late Holocene stable carbon isotope values were varied and confounded by land use changes.

The variability and polygenetic nature of many paleosols limited their use to reconstruct past climatic and environmental conditions, though they did provide some insight about past conditions. Paleosols offered useful information on the paleohydrology associated with arroyo cycles (as in Aslan and Autin, 1998). Unweathered alluvium and paleosol formation in alluvium are two end members of alluvial stratigraphy. Paleosols represent relatively stable surfaces that may be local or widespread, where and/or when aggradation slows or ceases. The value of alluvial paleosols is how they fit into the range of alluvial deposits, how the variations in the stratigraphy reflect paleohydrology, and how this provides information about prevailing environmental conditions. For example, cumulic A horizons form on floodplains when aggradation is slow enough to allow for pedogenesis. Cumulic A horizons were observed in both the Culebra and Verde watersheds from the late Pleistocene to the late Holocene, but not noted in the present-day arroyos, suggesting the prehistoric cumulic A horizons form in less flashy conditions than that presently.

Observations from present bedload yield, flow characteristics, channel bed morphology, and stratigraphy offered further insight on interpreting and understanding the Quaternary alluvial stratigraphy (as in Reid, 2002; Billi, 2008). The nature of sediment characteristics of flows and bedload yield in present-day systems suggested that similar traits observed in stratigraphy reflect similar flood regimes in the past. For example, massive, coarse sandy to fine gravel matrix-supported deposits in some alluvial strata resemble the deposits of present flash floods. Overall finer deposits, with clear laminations and thin beds are observed in present patchy floodplain deposits, contrasting with the prevalence of even finer deposits in the alluvial

stratigraphy. The overall finer deposits support more extensive floodplain construction during aggradation phases.

5.3 Anthropogenic Drivers

Past and present land use has impacted sedimentation rates, sediment supply, vegetation cover and type, and channel form. The Cruz phase (3,500 cal BP to 2,000 cal BP) agricultural constructions were observed from the headwaters to the basin outlet in Barranca Sandage (~4 km^2) (Leigh et al., 2013), and according to an archaeological survey they were continuously used through the Natividad phase, despite population fluctuations (Kowlewski et al., 2009). In contrast to the Cruz phase, lama-bordos and terrace walls were observed throughout much of the Culebra watershed in the Natividad phase, which has an area of 82 km^2. Sedimentation rates behind lama-bordo walls during the late Holocene were more than two times higher than that in the earlier Holocene and terminal Pleistocene, demonstrating the effectiveness of lama-bordos as sediment traps. However, it appears that sedimentation rates were not affected on a widespread scale until the Natividad phase.

Vegetation type, and the present scarcity of vegetation cover, has resulted from natural and cultural factors. The region's present biodiversity, including endemic succulent plants, forestland, grasses, and woody vegetation, is a product of climate change, as well as prehistoric and recent land use. Prehistoric impact on local vegetation is reflected in the $\delta^{13}C$ values from buried A soil organic matter, showing a significant rise from ~3,500 cal BP until between 1,000-500 cal BP. The increasingly enriched $\delta^{13}C$ values in the late Holocene suggest that intensified maize agriculture and possibly the increased management of succulent plants were

becoming very important to the ecological and cultural adaptation of the Mixteca Alta, and that by the Natividad phase these species dominated parts of the landscape. It is unclear to what extent deforestation took place in the past. Present agricultural land is not well managed and vulnerable to erosion, and deforestation has resulted in much soil loss and reduction in biomass. Various activities such as pumping water downstream and modern constructions on the Culebra and its tributaries including fords, bridges, and check dams have all resulted in internal channel adjustments including the formation of knickpoints.

5.4 Epilogue

Comparing the alluvium-paleosol stratigraphy to regional climatic change aided in connecting paleohydrology to climatic drivers before intensive land use, but there were still issues of equifinality. The comparison was complicated by the fact that the beginning of agriculture in the region overlapped with the transition from the influence of the North Atlantic on the spatio-temporal variability of the North American Monsoon to ENSO as the dominant influence (Bernal et al., 2011). During the late Holocene, climate appears to have been the dominant driver until the Natividad phase. Prior to the Natividad phase, land use activities interacted with climate to produce hydrologic changes at a local scale, whereas during and after the Natividad phase, widespread land use interacted with climate to affect changes on the watershed scale. The subsequent abandonment of the lama-bordo system may have affected the timing and nature (i.e., threshold-crossing event) of the most recent incision event around 1650 AD (Leigh et al., 2013), but did not cause the incision per se. Instead, prehistoric land use altered sedimentation rates and storage in the landscape, as well as vegetation type and cover,

and the arrival of the Spanish resulted in further land use change, all of which interacted with climate (e.g., precipitation amount and/or intensity) resulting in incision (Perroy et al., 2012).

For the past 15,000 years arroyo cycles have occurred as a result of external climatic drivers compounded by local internal conditions. It is only during the late Holocene that arroyos are influenced by human activities, and despite the new variable they persisted. The present system of Río Culebra appears to be in complex response (as in Schumm, 1979), adjusting to the long-term and short-term influences of late Holocene climate variation, legacies of prehistoric land-use change, and modern land use. A forum on erosion and conservation in the Mixteca Alta brought together local communities and local and national governmental agencies including the National Park Service and Forest Service. From the presentations and discussions in this forum, it was clear that local community leaders realize the need to preserve and manage their environment and that unsustainable land use activities and climate change cause land degradation. The Mexican government provides subsidies to reduce degradation and implement conservation measures, however much of it depends on local labor, and available funding is limited.

Evaluations of conservation measures have produced varying results (e.g., Fox et al., 2016). Despite the well-conserved headwaters in Barranca Sandage, sediment yield was still relatively high, suggesting that basin-wide conservation is needed. Interestingly, prehistoric farmers installed check dams and terraces on a basin-wide scale; on Barranca Sandage earlier on, and along the Culebra during the Natividad phase. Even so, the high sedimentation rates and build up of material appeared to have had long-term effects, which emphasizes the need to consider conservation at various temporal and spatial scales in the future.

5.5 References

Arzate Aguirre, Rafael, (per. Com). Coordinator of Conservation for the Biosphere Reserve Tehuacán-Cuicatlán, National Park Commission, Mexico.

Aslan, A., Autin, W.J., 1998. Holocene flood-plain soil formation in the southern lower Mississippi Valley: Implications for interpreting alluvial paleosols. Geological Society of America Bulletin 110, 433-449.

Bernal, J., Lachniet, M., McCulloh, M., Mortimer, G., Morales, P., Cienfuegos, E., 2011. A Speleothem Record of Holocene Climate Variability from Southwestern Mexico. Quaternary Research 75, 104-113.

Billi, P., 2008. Bedforms and sediment transport processes in the ephemeral streams of Kobo basin, Northern Ethiopia. Catena 75, 5-17.

Billi, P., 2011. Flash flood sediment transport in a steep sand-bed ephemeral stream. International Journal of Sediment Research 26, 193-209.

Birkeland, P.W., 1984. Soils and Geomorphology. Oxford University Press, New York.

Butzer, K.W., Abbott, J.T., Frederick, C.D., Lehman, P.H., Cordova, C.E., Oswald, J.F., 2008. Soil-geomorphology and "wet" cycles in the Holocene record of North-Central Mexico. Geomorphology 101, 237-277.

Bull, W.B., 1997. Discontinuous ephemeral streams. Geomorphology 19, 227-276.

Falfan, Julio of ConAgua (pers. Com.). Meterologist at the Nation Comission of Water in Oaxaca.

Graf, W.L., 2002. Fluvial Processes in Dryland Rivers. The Blackburn Press, Caldwell.

Harden, T., Macklin, M.G., Baker, V.R., 2010. Holocene flood histories in south-western USA. Earth Surface Processes and Landforms 35, 707-716.

Hassan, M.A., Marren, P.M., Schwartz, U., 2009. Bar structure in an arid ephemeral stream. Sedimentary Geology 221, 57-70.

Hereford, R., 2002. Valley-fill alluviation during the Little Ice Age (ca. AD 1400-1880), Paria River basin and southern Colorado Plateau, United States. Geological Society of America Bulletin 114, 1550-1563.

Huckleberry, G., Duff, A.I., 2008. Alluvial cycles, climate, and puebloan settlement shifts near Zuni Salt Lake, New Mexico, USA. Geoarchaeology-an International Journal 23, 107-130.

Kowalewski, S.A., Balkansky, A. K., Walsh, L. R. S., Pluckhahn, T. J., Chamblee, J. F., Rodriguez, V. P., Espinosa, V. Y. H., Smith, C. A., 2009. Origins of the Nuu: Archaeology in the Mixteca Alta, Mexico. University Press Colorado, Boulder.

Lachniet, M., Asmerom, Y., Bernal, J., Polyak, V., Vaquez-Selem, L., 2013. Orbital Pacing and Ocean Circulation-Induced Collapses of the Mesoamerican Monsoon over the past 22,000 yr. Proc Natl. Acad. Sci. U.S.A. 110, 9255-9260.

Leigh, D.S., Kowalewski, S.A., Holdridge, G., 2013. 3400 years of agricultural engineering in Mesoamerica: lama-bordos of the Mixteca Alta, Oaxaca, Mexico. Journal of Archaeological Science 40, 4107-4111.

Lozano-Garcia, M.D., Ortega-Guerrero, B., 1998. Late Quaternary environmental changes of the central part of the Basin of Mexico; Correlation between Texcoco and Chalco basins. Review of Palaeobotany and Palynology 99, 77-93.

Lucia, A., Recking, A., Martin-Duque, J.F., Storz-Peretz, Y., Laronne, J.B., 2013. Continuous monitoring of bedload discharge in a small, steep sandy channel. Journal of Hydrology 497, 37-50.

McFadden, L.D., McAuliffe, J.R., 1997. Lithologically influenced geomorphic responses to Holocene climatic changes in the Southern Colorado Plateau, Arizona: A soil-geomorphic and ecologic perspective. Geomorphology 19, 303-332.

Metcalfe, S.E., O'Hara, S.L., Caballero, M., Davies, S.J., 2000. Records of Late Pleistocene-Holocene climatic change in Mexico - a review. Quaternary Science Reviews 19, 699-721.

Mueller, R.G., Joyce, A.A., Borejsza, A., 2012. Alluvial archives of the Nochixtlan valley, Oaxaca, Mexico: Age and significance for reconstructions of environmental change. Palaeogeography Palaeoclimatology Palaeoecology 321, 121-136.

Perroy, R.L., Bookhagen, B., Chadwick, O.A., Howarth, J.T., 2012. Holocene and Anthropocene Landscape Change: Arroyo Formation on Santa Cruz Island, California. Annals of the Association of American Geographers 102, 1229-1250.

Poesen, J., Nachtergaele, J., Verstraeten, G., Valentin, C., 2003. Gully erosion and environmental change: importance and research needs. Catena 50, 91-133.

Reid, I., Powell, D.M. and Laronne, J.B., 1996. Prediction of bed-load transport by desert flash floods. Journal of Hydraulic Engineering-Asce, 122(3): 170-173.

Reid, I., 2002. Sediment Dynamics of Ephemeral Channels, in: Bull, L.J., Kirkby, M.J. (Eds.), Dryland Rivers: Hydrology and Geomorphology of Semi-Arid Channels. John Wiley & Sons Ltd., Wests Sussex.

Schumm, S.A., 1974. Geomorphic thresholds and complex response of drainage systems, in Morisawa, M, ed., Fluvial Geomorphology. State University of New York at Binghamton, Publications in Geomorphology, pp. 299-310.

Schumm, S.A., 2005. River Variability and Complexity. Cambridge University Press, Cambridge.

Valentin, C., Poesen, J., Li, Y., 2005. Gully erosion: Impacts, factors and control. Catena 63, 132-153.

Vera, C., Higgins, W., Amador, J., Ambrizzi, T., Garreaud, R., Gochis, D., Gutzler, D., Lettenmaier, D., Marengo, J., Mechoso, C.R., Nogues-Paegle, J., Silva Dias, P.L., Zhang, C., 2006. Toward a unified view of the American Monsoon Systems. Journal of Climate 19, 4977-5000.

Waters, M.R., Haynes, C.V., 2001. Late Quaternary arroyo formation and climate change in the American Southwest. Geology 29, 399-402.

APPENDIX I

FLOOD AND BEDLOAD DATA

Table 1.a. The sediment weight and flow data for each flood is offered in the table. Each flood number corresponds to the total sediments removed from the pit traps during each flood. The sediments were weighed in the field (WET kg) upon removal from the pit trap. Some subsamples were oven dried to remove water and estimate a correction factor. removed for further study were first air dried and then oven dried while others were to produce a correction factor resulting in the dry weight. flood in the 2013-2014 rains seasons

SANDAGE

Flood Date	Flood No.	Box ID	Sediment Weight WET (kg)	Sediment Weight DRY (kg)	Max Stage (cm)	Q ($m^3 s^{-1}$)	Trap opening (m)	% of channel	Total Sed. (kg)	Tonnes /day	Notes
6/11/2013	1	N	370	281.2	0.15	0.6897	0.09	2.4	5905.2	5.91	N trap not full
6/11/2013		S	508	386.08			0.09	2.4	8107.68	8.11	
6/27/2013	2	N	150	75	0.07	0.19	0.11	2.9	1312.5	1.31	N trap mud at bottom; S pit trap sediment begins at 10-15 cm below top
6/27/2013		S	441	335.16					5865.3	5.87	
7/7/2013	3	N	23	12.5	0.08	0.24	0.09	2.4	262.5	0.26	S trap full; N trap sediment at bottom 10 cm
7/7/2013		S	526	399.76					8394.96	8.39	
7/12/2013	4	N	450	342	0.12	0.47	0.09	2.4	7182	7.18	N and S traps full; missed sediments
7/12/2013		S	502	381.52					8011.92	8.01	

7/21/2013	5	N	532	404.32	0.39	4.01	0.09	2.4	9501.52	9.50	N and S traps full; missed sediments
7/21/2013		S	561	426.36					10019.46	10.02	
9/2/2013	6	N	540	410.4	0.65	9.66	0.09	2.4	9849.6	9.85	N and S traps full; missed sediments
9/2/2013		S	507	385.32					9247.68	9.25	
9/26/2013	7	N	156	75.24	0.08	0.22	0.025	0.7	5718.24	5.72	S trap full; N trap sediments at bottom 30 cm
9/26/2013		S	483	367.08					27898.08	27.90	
10/1/2013	8	N	51	38.76	0.075	0.16	0.05	1.3	1472.88	1.47	S trap full; N trap sediments at bottom 30 cm
10/1/2013		S	409	310.84			0.07	1.8	8392.68	8.39	
6/18/2014	9	N	484	367.84	1.2	25.02	0.08	2.1	11035.2	11.04	N and S traps full; missed sediments
6/18/2014		S	486	369.36			0.09	2.4	9603.36	9.60	
6/24/2014	10	S	455	345.8	0.09	0.29	0.09	2.4	4841.2	4.84	N and S traps not full; M trap full
6/24/2014		N	372	282.72					3958.08	3.96	
6/24/2014		M	449	341.24					4777.36	4.78	
7/4/2014	11	N	312	237.12	0.39	4.31	0.09	2.4	3793.92	3.79	N, S, and M traps full; missed sediments
7/4/2014		S	473	359.48					5751.68	5.75	
7/4/2014		M	442	335.92					5374.72	5.37	
7/24/2014	12	N	454	345.04	0.36	3.76	0.09	2.4	5520.64	5.52	N, S, and M traps full; missed sediments
7/24/2014		S	470	357.2					5715.2	5.72	
7/24/2014		M	428	325.28					5204.48	5.20	
8/10/2014	13	N	417	316.92	0.67	10.76	0.09	2.4	5387.64	5.39	N, S, and M traps full; missed sediments
8/10/2014		S	434	329.84			0.09	2.4	5607.28	5.61	
8/10/2014		M	442	335.92			0.05	1.1	10077.6	10.08	
9/15/2014	14	N	363	275.88	0.15	0.68	0.09	2.4	3862.32	3.86	N, S, and M traps full; missed sediments
9/15/2014		S	509	386.84			0.09	2.4	5415.76	5.42	
9/15/2014		M	532	404.32			0.05	1.1	10108	10.12	

Table 1.b. The sediment weight and flow data for each flood is offered in the table. Each flood number corresponds to the total sediments removed from the pit traps during each flood. The sediments were weighed in the field (WET kg) upon removal from the pit trap. Some subsamples were oven dried to remove water and estimate a correction factor. removed for further study were first air dried and then oven dried while others were to produce a correction factor resulting in the dry weight. flood in the 2013-2014 rains seasons

SAUCE

Flood Date	Flood No.	Box ID	Sediment Weight WET (kg)	Sediment Weight DRY (kg)	Max Stage (cm)	Q ($m^3 s^{-1}$)	Trap opening (m)	% of channel	Total Sed. (kg)	Tonnes /day	Notes
6/11/2013	1	1	526	399.76	0.51	20.46	0.05	0.5	16789.92	16.79	All traps full, missed sediments
6/11/2013		2	521	395.96	0.51	20.46	0.05	0.5	16630.32	16.64	
6/11/2013		3	526	399.76	0.51	20.46	0.05	0.5	16789.92	16.79	
6/11/2013		4	540	410.4	0.51	20.46	0.05	0.5	17236.8	17.24	
6/11/2013		5	533	405.08	0.51	20.46	0.05	0.5	17013.36	17.02	
6/24/2013	2	1	526	399.76	0.035	0.19	0.11	1.1	7195.68	7.2	Traps 3, 4, and 5 almost full
6/24/2013		2	468	355.68	0.035	0.19	0.11	1.1	6402.24	6.41	
6/24/2013		3	517	392.92	0.035	0.19	0.11	1.1	7072.56	7.08	
6/24/2013		4	540	410.4	0.035	0.19	0.11	1.1	7387.2	7.39	
6/24/2013		5	493	374.68	0.035	0.19	0.11	1.1	6744.24	6.75	
7/12/2013	3	1	7	5.32	0.025	0.11	0.132	1.3	79.8	0.08	All traps contain only mud and water
7/12/2013		2	4.5	3.42	0.025	0.11	0.11	1.1	61.56	0.07	
7/12/2013		3	4.5	3.42	0.025	0.11	0.12	1.2	58.14	0.06	
7/12/2013		4	7	5.32	0.025	0.11	0.12	1.2	90.44	0.1	
7/12/2013		5	33	25.08	0.025	0.11	0.127	1.3	401.28	0.41	

7/24/2013	4	1	1.5	1.14	0.02	0.08	0.11	1.1	20.52	0.03	Trap 1 contains mud and water
7/24/2013		2	1.5	1.14	0.02	0.08	0.11	1.1	20.52	0.03	
7/24/2013		3	1.5	1.14	0.02	0.08	0.11	1.1	20.52	0.03	
7/24/2013		4	1.5	1.14	0.02	0.08	0.11	1.1	20.52	0.03	
7/24/2013		5	4.5	3.42	0.02	0.08	0.11	1.1	61.56	0.07	
9/2/2013	5	1	432	328.32	0.35	8.5	0.11	1.1	5909.76	5.91	Trap 1 not full
9/2/2013		2	528	401.28	0.35	8.5	0.132	1.3	6019.2	6.02	
9/2/2013		3	476	361.76	0.35	8.5	0.5	5	1447.04	1.45	
9/2/2013		4	572	434.72	0.35	8.5	0.5	5	1738.88	1.74	
9/2/2013		5	510	387.6	0.35	8.5	0.5	5	1550.4	1.56	
9/29/2013	6	1	518	393.68	0.07	0.59	0.025	0.25	31494.4	31.5	All traps full; missed sediments
9/29/2013		2	546	414.96	0.07	0.59	0.025	0.25	33196.8	33.2	
9/29/2013		3	468	355.68	0.07	0.59	0.5	5	1422.72	1.43	
9/29/2013		4	467	354.92	0.07	0.59	0.5	5	1419.68	1.42	
9/29/2013		5	533	405.08	0.07	0.59	0.5	5	1620.32	1.63	
10/13/2013	7	1	101	76.76	0.1	1.06	0.025	0.25	6140.8	6.15	Traps 1, 2 not full; 3, 4, 5 no top
10/13/2013		2	204	155.04	0.1	1.06	0.025	0.25	12403.2	12.41	
10/13/2013		3	474	360.24	0.1	1.06	0.5	0.5	1440.96	1.45	
10/13/2013		4	513	389.88	0.1	1.06	0.5	0.5	1559.52	1.56	
10/13/2013		5	556	422.56	0.1	1.06	0.5	0.5	1690.24	1.7	
6/18/2014	8	1	541	411.16	0.9	58.68	0.08	0.7	11512.48	11.52	All traps full; missed sediments
6/18/2014		2	522	396.72	0.9	58.68	0.08	0.7	11108.16	11.11	
6/18/2014		3	508	386.08	0.9	58.68	0.5	4.4	1737.36	1.74	
6/18/2014		4	579	440.04	0.9	58.68	0.5	4.4	1980.18	1.99	

6/18/2014		5	552	419.52	0.9	58.68	0.5	4.4	1887.84	1.89	
6/26/2014	9	1	424	322.24	0.05	0.33	0.08	0.8	8056	8.06	Trap 1, 2 almost full; 3, 4, 5 no top
6/26/2014		2	472	358.72	0.05	0.33	0.08	0.8	8968	8.97	
6/27/2014		3	440	334.4	0.05	0.33	0.5	5	1337.6	1.34	
6/26/2014		4	511	388.36	0.05	0.33	0.5	5	1553.44	1.56	
6/27/2014		5	532	404.32	0.05	0.33	0.5	5	1617.28	1.62	
7/9/2014	10	1	485	368.6	0.33	7.7	0.08	0.8	9215	9.22	All traps full; missed sediments
7/9/2014		2	487	370.12	0.33	7.7	0.08	0.8	9253	9.26	
7/9/2014		3	455	345.8	0.33	7.7	0.5	5	1383.2	1.39	
7/9/2014		4	507	385.32	0.33	7.7	0.5	5	1541.28	1.55	
7/9/2014		5	569	432.44	0.33	7.7	0.5	5	1729.76	1.73	
7/24/2014	11	1	109	82.84	0.44	13.13	0.08	0.8	2071	2.08	Traps 1 almost full; 3, 4, 5 no top
7/24/2014		2	501	380.76	0.44	13.13	0.08	0.8	9519	9.52	
7/24/2014		3	440	334.4	0.44	13.13	0.5	5	1337.6	1.34	
7/24/2014		4	511	388.36	0.44	13.13	0.5	5	1553.44	1.56	
7/24/2014		5	470	357.2	0.44	13.13	0.5	5	1428.8	1.43	
8/10/2014	12	1	0	0	0.11	1.24	0.08	0.8	0	0	Trap 1 mud at bottom
8/10/2014		2	239	181.64	0.11	1.24	0.08	0.8	4541	4.55	

8/10/2014		3	413	313.88	0.11	1.24	0.5	5	1255.52	1.26	
8/10/2014		4	380	288.8	0.11	1.24	0.5	5	1155.2	1.16	
8/10/2014		5	356	270.56	0.11	1.24	0.5	5	1082.24	1.09	
9/21/2014	13	11	491	373.16	0.55	23.2	0.115	1.1	3358.44	3.36	All traps full; missed sediments
9/21/2014		12	227	172.52	0.55	23.2	0.05	0.5	3622.92	3.63	
9/21/2014		13	380	288.8	0.55	23.2	0.09	0.9	3465.6	3.47	
9/21/2014		14	571	433.96	0.55	23.2	0.05	0.5	9113.16	9.12	
9/21/2014		15	362	275.12	0.55	23.2	0.09	0.9	3301.44	3.31	
9/21/2014		16	387	294.12	0.55	23.2	0.05	0.5	6176.52	6.18	
9/21/2014		17	562	427.12	0.55	23.2	0.04	0.4	11105.12	11.11	
9/21/2014		18	623	473.48	0.55	23.2	0.11	1	4734.8	4.74	
9/21/2014		19	403	306.28	0.55	23.2	0.05	0.5	6431.88	6.44	
9/21/2014		20	339	257.64	0.55	23.2	0.05	0.5	5410.44	5.42	

APPENDIX II

PROFILE DESCRIPTIONS

Table II.a. The table shows the location information of the profiles.

Profile Name	Site ID	Site #	Zone	Easting	Northing	Barranca	Field Notes
Sauce	C1	SAU004	14Q	677603	1949394	Sauce	Several cut and fills in headwater tributaries of Río Culebra.
Confluence Site	C2	435	47Q	322171	1958692	Culebra/Sandage/ Sandaxne	Well represented alluvium-paleosol sequence at confluence of tributary and midpart of the main stem.
Río Culebra Confluence	C3	118	14Q	677933	1959690	Culebra	Well represent alluvium-paleosol sequence on midpart of main strem, Río Culebra.
Meander Bend	I10	362	14Q	663885	1969963	Tributary to Inguiro (JIcotlan)	Well represented alluvium-paleosol sequence associated with several lama-bordos.
Tusk-Horse	S11	564	14Q	678419	1957101	Sandage	Cut-and-fill stratigraphy with part of fossil mammoth tusk and other Pleistocene horse jaw with several teeth. Note highly oxidized C and Bw horizon.
Magdalena Culvert	S4	122	14Q	678514	1957512	Sandage	Well represented alluvium-paleosol sequence along downstream part of tributary arroyo Sandage.

Victor's Lama-bordo	S5	192	14Q	679457	1956286	Sandage	Well represented alluvium-paleosol sequence associated with very well-preserved ancient lama-bordo in upper section of tributary Sanage. Alluvial incision associated with allostratigraphy cuts into endeque and older (?) paleosol.
Flores Amarillas	S6	426	14Q	678905	1956480	Sandage	Well represented alluvium-paleosol sequence on midstream tributary of Sandage. Located upstream from lama-bordo wall. Thick, older paleosol also observed in lower strata as in S5.
Island Site	S7	68	14Q	678802	1956564	Sandage	Well represented paleosol-alluvial sequence associated with (2?) ancient lama-bordo(s) on tributary of Sandage.
Juniper Site	S8	424	14Q	678832	1956368	Sandage	Profile in first order tributary to Sandage. Connects hillslope sediments to valley.
Cliff Site	X9	436	14Q	677926	1958596	Culebra/Sandage/Sandaxne	Well represented paleosol-alluvial sequence at lower part of tributary just before joins main stem; includes lower cut and fill
Cuganda Sur	/	514	14Q	677587	1959131	Inguiteria	Profile on shoulder near summit of hillslope. Note paleosol beneath endeque.
Sandaxne Site	/	112	14Q	678421	1957945	Sandaxne	Allostraigraphy containing mammoth bones and teeth in massive deposits (colluvium?), stratifraphically below a well-

							defined paleosol, and above clear fluvial deposits.
Inguirjo Site	/	475	14Q	663822	1970732	Inguiro	Well represent paleosol-alluvial sequence along mainstem of the Río Inguiro, Jicotlan.
Two Coyote	/	Cul029	14Q	675527	1962009	Culebra	Cut-and-fill stratigraphy in the downstream part of mainstem, Rio Culebra. Some well-defined paleosols noted.

Table II.b. Juniper Site Profile Description

Depth (cm)	Horizon	Color (Dry)	Texture	Structure	Boundary	Remarks	C-14 Samples
0-12	C1	10YR 6/2	sil/mgr	3cogr	clear	much angular Yanhuitlan (moderate gravel)	
12-30	C2	10YR 5.5/2	sil	2fgr	clear	less gravel than C1	
30-42	Ab	10YR 5/2	sil	1mgr	clear	few gravel clasts of mostly endeque (pottery sherd)	#201 bulk
42-55	C3	10YR 5/2	sil	1mgr	clear	less gravel than C1 (similar to C2)	
55-67	Ab1'	10YR 5/1	sil	2fsbk	clear	few gravel Yanhuitlan (potsherd)	
67-80	Ab2'	10YR 5/2	sil	2msbk	clear	moderate amount of Yanhuiltan and endeque gravel (potsherd)	
80-90	2Ab3'	10YR 5/2	sicl	3msbk	clear	tells him went from hillslope to Yanhuitlan beds	#140; #202 bulk
90-106	2AB	10YR 5/3	sicl	3cosbk	gradual	abundant secondary CaCO3 nodules and root filaments, uncertain whether nodules are redeposited endeque or in situ	,
106-136	2Bt1bk	10YR 4/2	sicl	3cosbk	clear	faint, thin, discontinuous, clay films on ped faces. Abundant secondary CaCO3 nodules and root filaments	
136-170	2Bt2bk	10YR 6/4	sil	1fsbk	gradual	few, thin, discontinuous clay films. CaCO3 as above but with larger nodules	
170-190	2Ck	10YR 7/4	sil	1cosbk		CaCO3 root filaments (no nodules)	

Table II.c. Flores Amarillas Profile Description

Depth (cm)	Horizon	Color (Dry)	Texture	Structure	Boundary	Remarks	C-14 Samples
(A section)							
0-21	C		cos	sg	A		
21-64	Ab	10YR 4/3	sl	1fsbk	C	cumulic	C14#244
64-71	C2	10YR 5/2	fgr-cos	laminated	G	Endeque and Yanhuitlan clasts. Fining upward sequences.	
71-82	C3	10YR 4/2.5	sil	2msbk	A	Some root disturbance (krotovina).	C14#243
82-104	2Ab	10YR 4/2	sil	1fsbk	G	Common Yanhuitlan and endeque clasts.	
104-129	2Ab2	10YR 4/1	sil	2msbk	C		C14#160
129-170	2Ab3	10YR 4/1	sicl	3msbk	G		
170-221	C4	10YR 5/2	sil	2mpr	C	Common endeque nodules. Few Yanhuitlan nodules. CaCO3 in root pores.	C14#242
221-245	Ab'	10YR 3/2	sicl	3mpr	A	CaCO3 in root pores and ped faces. Few Yanhuitlan clasts.	C14#161
245-250	C5	10YR 6/2	sil	m	C	fine-medium endeque gravel.	
250-296	Ck6	10YR 6/2	sil	1fsbk	D	Common endeque nodules. Common, distinct CaCO3 in root pores. Few faint CaCO3 on ped faces.	
296-348	BC(k) - AC?	10YR 5/1	sil	3msbk	G	Common endeque nodules. Common, distinct CaCO3 in root pores and on ped faces. Yanhuitlan clasts.	
348-368+	C7	10YR 6/2	sil	1vfsbk		Few, distinct CaCO3 in root pores and on ped faces. Yanhuitlan and endeque clasts. (Much less CaCO3 than above).	

(B section)							
348-434	C7				G		
434-547	C8	10YR 6/3	sil to si	1fsbk	G	Silty loam grades up to silt. Abundant endeque clasts grades down to common. Abundant, distinct, CaCO3 in roots.	C14#162
547-567+	Bw?	10YR 6/3	sil - sicl?	2mpr		Fine to medium Yanhuitlan gravel. Common endeque clasts. Common, distinct CaCO3 in root pores.	

Table II.d. Island Site Profile Description

Depth (cm)	Horizon	Color (Dry)	Texture	Structure	Boundary	Remarks	C-14 Samples
(A Section) SE EDGE OF ISLAND							
0-35 cm	A	7.5YR 5/2	csl	moderate granular	clear	Normally graded coarse sandy loam at base. Sandy loam at top.	
35-76 cm	C1	10YR 6/2	(p)sl	single grain	abrupt	Thinly bedded, both gravel and sand lenses, few cobbles. Many endeque clasts. Many Yanhuitlan clasts.	C14#18
MAIN PROFILE						***All profile has filaments except A and C1.**	
0-37 cm	A	7.5YR 5/2	fsl	moderate granular	clear	Normally graded coarse sandy loam at base. Sandy loam at top.	
37-78 cm	C1	10YR 6/2	sl	massive (sg?)	abrupt	Thinly bedded with few gravel lenses. There are endeque and Yanhuitlan clasts.	
78-111 cm	Ab1	10YR 5/1	sil	2msbk	gradual	Horizon somewhat transitional to underlying Ab2. Upper 10 cm slightly darker. Few medium gravel clasts. Thin humic clay films coating medium gravel clasts.	
111-182 cm	Ab2	10YR 3/1	sil	3cgr + 3vcsbk	gradual	Common granuals, some of which are endeque. Few very fine filaments of CaCO3 and root pores.	C14#15
182-225 cm	C2	10YR 7/2	sil	3cpr	abrupt	Few endeque granuals. Charcoal sample (14C # 13) at 223-225 cm.	C14#13
225-263 cm	C3	10YR 7/2	sl/sicl/sil	3cpr	abrupt	Many endeque clasts. Stratified beds ranging from endeque rich sandy loam with gravel to silty clay loam beds. Includes reworked	

						pottery sherds. Includes 1-2 cm thick charcaol lens 245-249 cm deep. Charcoal lens is ashy.	
263-300 cm	C4	10YR 7/2	sil	3mpr	clear	Very few Yanhuitlan and endeque clasts.	
300-335 cm	Ab1'	10YR 5/2	sicl	3mpr	gradual	Very few Yanhuitlan and endeque clasts. Charcoal sample (14C # 14) at 324-330 cm. Few thin granular beds near base, probably endeque?	C14#14
335-430 cm	Ab2'	10YR 4/2	sicl	3cpr	diffuse	(ABC) Very few endeque clasts. Pot sherd recovered. Includes rock cluster 5 m NW of profile.	
430-470 cm	Ab3'	10YR 5/3	sil	2msbk	clear	Very few endeque clasts.	
470-484 cm	C5	10YR 7/3	sil	massive	abrupt	Common CaCO3 concretions, possibly transported Yanhuitlan beds.	
(B Section) 2.30 m NW of Main Profile							
484-610 cm	Ab"	10YR 4/2	l	1msbk	very abrupt	536-550 cm particularly gravelly zone, sampled separately. (Pulse of sediment in swale?) (Horizon paleochannel fills that grade up to ABC?) Charcoal sample (14C# 17) at 580-590 cm. Weakly stratified with thick and thin beds. Some beds include abundant endeque. Gravel, few thin silt lenses. Gravel beds very poorly sorted within matrix.	C14#16, #17, #19
610-640 cm	C6	10YR 7/3	sil	massive	massive	Suggestive of reworked Yanhuitlan bedrock.	

Table II.e. Meander Bend Profile Description

Depth (cm)	Horizon	Color (Dry)	Texture	Structure	Boundary	Remarks	C-14 Samples
(A section)							
0-25	Ap	10YR 4/2	fsl	3msbk	A		#174
25-36	C	10YR 5/3	sil	1msbk	C	Contains few angular gravels	
36-59	Ab	10YR 4/2	sil	1msbk	C	Very few gravels	#175, #177
59-84	Bw1b	10YR 4.5/3	sil	2msbk	G		
84-101	Bw2b	10YR 4/3	sil	2msbk	G		
101-125	Ab'	10YR 4/2.5	sil	2msbk	C	Carbonate root filaments	#178
125-143	C2	10YR 8/1	cobbles	sg	A	Clast supported cobbles in P-gravel matirx	
143-160	C3	2.5Y 4.5/4	sl	sg	A	Much medium gravel, basal contact. Clearly erodes underlying horizon.	
160-226	Bwb	2.5Y 4/4	ssil	1msbk	A	P-gravel bed at 192-196 cm. Sandy loam bed at 210-214 cm. Slightly darker possible AB at 198-210 cm that contains much charcoal; large charcoal fleck at 243 cm.	#78, #176
226-246	Ab"	2.5Y 4/2	sil	2msbk	C		177?
246-257	C4	2.5Y 4/3	gl	sg	VA	Many medium and large gravels.	
257-279	C5	2.5Y 5/3	fsl	1msbk	A		
279-336	C6	2.5Y 5/3	m-chr	sg			
(B section)							
336-357	C7	2.5Y 5/3	sil	m	C	Very few gravel clasts. Faint laminations towards base.	

357-374	C8	2.5Y 4.5/3	sil	m	A	Contains many vesicles, as if incipient A horizon.	
374-427	C9	2.5Y 5/3	sil	1msbk	C	Contains a flood gravel bed at 405-410 cm depth.	
427-473	C10	2.5Y 5/3	s	sg	VA	Plane bedded rhythmites, gravelly sand graded up to fine sand (about 5-6 cm), contains coarse gravel and cobbles elsewhere on outcrop. Groundwater preculating in zone under underlying silty loam unit. Erosionally truncated underlying unit.	#183
473-592	2Ab1	2.5Y 4/2	sicl	2msbk	C	Ocassional angular gravels, lens of cobble to left of main profile. Interpreted as reworked culural material (little charcoal). Many fine CaCO3 nodules in upper 30 cm.	#94, #181, #182
592-645	2Ab2	2.5Y 5/2	sicl	3copr	A	Abundant, fine-medium gravel, somewhat bedded. Medium carbonate nodules at 600-615 cm. Prominent cobble layer at base at 629-645 cm laterally extensive gravelly zone in zone that interfingers L-B.	#93
645-775	Btb	2.5Y 5/2	sic	3vcpr		Contains Mk films on ped faces. Clay films which gradually diminish towards base. Lots of time represented by this horizon. A prominent L-B structure is upstream (left in photos) from this profile at 700-750 cm.	#84, #85, #92, #180
775-850+	C11	2.5Y 5/4	l (sl at base)	m		Abundant charcoal, classic fining upward sequence.	#179

Table II.f. Victor's Lama-Bordo Profile Description

Depth (cm)	Horizon	Color (Dry)	Texture	Structure	Boundary	Remarks	C-14 Samples
(A Section)							
0-65 cm	C1	10YR 5/2	grl	3mgr	abrupt	plowed. Weakly stratified with fine to medium gravel in lower half.	
65-90 cm	Ab	10YR 4/2	sil	3cogr	gradual	(14C#109) bulk	C14#109
90-142 cm	Bw	10YR 4.5/1	sil	1cosbk	diffuse	common, fine gravel throughout. No bedding, massive. (14C# 110)	C14#111
142-188 cm	Ab'	10YR 4/1	hsil	3msbk	diffuse	fine CaCO3 filaments throughout rootlet holes. (14C# 110) (potsherd, chert flake at 160 cm)	C14#110
(B Section)							
188-232 cm	Bw'	10YR 5/2	sil	3mgr	clear	CaCO3 in rootlets and faint CaCO3 on ped faces	C14#113
232-251 cm	C2	10YR 5/1	grl	m	clear	lots of endeque granules. Freguent large gravel and cobble	
251-306 cm	C3	10YR 5/2	sil	3copr	clear	lots of endeque granules. Freguent large gravel and cobble. CaCO3 infilling rootlets and ped faces (as above)	
306-336+ cm	C4	see C4 in C section				lots of endeque granules (14C# 110)	C14#112
(C Section)							
306-431 cm	C4	10YR 5/2	sil	1copr to m	clear	CaCO3 infillings of rootlets, NOT ped faces	C14#116
431-480 cm	Ab'	10YR 4/1	hsil	1fgr to m	gradual	very few CaCO3 infillings, many endeque granules	C14#114, #115, #117, #119
(D Section)							
480-517 cm	C5	10YR 4/2	l	m	clear	abundant endeque granules. Fine, medium gravel	
517-540 cm	C6	10YR 5/3	l gravel	sg	very abrupt		

540 - see C7 in E section	C7	10Yr 6/2	ssi	laminated and thinly saturated		few thing beds of reworked endeque	C14#118
(E Section)							
540-569 cm	C7				abrupt		
569-590 cm	Ab"	10YR 4/1	sil	2msbk	clear	few endeque granules. Few rootlet fillaments of CaCO3. corresponds to very top of intact of preserved lama-bordo rocks.	
590-700 cm	C8	10YR 4/1, 10YR 5/2, 10YR 4/2	si to grsil	thinly stratified	see section F	typical 5-15 cm beds of laminated silts to poorly sorted gravelly silty loam	C14#120
(F Section)							
700-900 cm	C8				diffuse	(cont. from above) and with depth below 8m (especially below 8m) increasing frequency of sandy loam beds and sandy gravel beds. * All planar beds; do not exhibit cross-beds.	C14#121, #122, #129
(G Section)							
900-1123 cm	C9				very abrupt	as above in C8, but with prominent 5- 15cm thick beds of rounded endeque and Yanhuitlan gravels. All planar beds. Many, distinct, normally graded beds. D90 size typically 4-5 cm. Endeque gravel well rounded vs. Yanhuitlan gravel subangular and angular. Basal bed is laminated silty sand, 1100-1123 cm. (seperate bags of gravel, Gravel sample 1: 960-970 cm, and Gravel sample 2: 1010-1020 cm.) Some beds are distinctly graded from gravel up to silty clay and as indeed are rhythmites. ***Absolutely no evidence of human disturbance in rhythmite beds.	C14#128

1123-1164 cm	Ab1"	10YR 4/2 and 10YR 6/4	sil	1msbk	clear	many inclusions of endeque granules. 10YR 6/4 beds may be krotovina and possibly old plow zone.	C14#124, #127
1164-1200 cm	Ab2"	10YR 3/2	sil	1msbk	clear	definite 10YR 6/4 krotovina, very few endeque granules	C14#123, #125
1200-1230 cm	Ab3"k					same as above, but with prominent CaCO3 filaments	C14#126

Table II.g. Confluence Profile Description

Depth (cm)	Horizon	Color (Dry)	Texture	Structure	Boundary	Remarks	C-14 Samples
(A Section)							
0-19	A	10YR 4/2	sil	2msbk	G		
19-32	C1	10YR 5/3	sil	1msbk	G	graded towards sand at base	
32-41	C2	10YR 5/4	ls	sg	A		
41-53	Ab	10YR 5/2	sil	2msbk	G	top 5 cm bulk	#148
53-64	C3	10YR 4/5.2	sil	m	C	very faint laminae	
64-83	Ab'	10YR 4/2	sil	2msbk	C	top 5 cm bulk	#147
83-93	Bw1	10YR 4/2.5	sil	2msbk	C	thin discontinuous CaCO3 on ped faces and root filaments	
93-155	Bw2	10YR 3.5/3	sil	2msbk	G	thin discontinuous CaCO3 on ped faces and root filaments	
155-194	BC	10YR 5/3	sil	1cosbk to m	C	BC due to color??	
194-204	Ab"						
(B Section)							
194-222	Ab"	10YR 4/2	sil	2vcosbk	G		#149, #150, #152
222-250	Bwb"	10YR 4/3	sil	2cosbk	G		
250-273	BCb"	10YR 4/3	sil	1cosbk to m	A		
273-287	C4	10YR 6/3	fine sand	laminated	A	faint planar bed laminations	#151

287-295	C5	10YR 7/4 and 10YR 5/2	si to vfs	laminated	VA	distinct plane bed laminations	
295-304	C6	10YR 5/4	s and fgr	sg	VA	contains 2 potsherds	
304-325	C7	10YR 7/4 and 10YR 5/2	si to vfs	laminated	VA	distinct plane bed laminations, but contains some soft sedimentary deformation structures	
325-344	C8	10YR 6/2	si	m	VA		
344-364	Ab1"'	10YR 4/1	sic	3vcopr	G	contains many sub mm vesicles	
364-390	Ab2"'	10YR 4/2	sic	3copr	G		#153
(C Section) Eastern Profile							
340-360	Ab1"'	10YR 4/1	sic	3vcopr	G	bounded above by very abrupt contact with laminated sands that contain some pebbles to gravel. (same zone/bed werein Natividad pot sherds were found. The top of the Ab appears truncated by erosion (many rivulets).	#154
360-395	Ab2"'	10YR 4/2	sicl	2copr	D		#155, #172
395-420	C9	10YR 4/3	sil	1copr to m	C		#170
420-449	Ab	10YR 4/2	sicl	2msbk	C		
449-469	C10	10YR 5/3	si	laminated bedding	C	appears to have disrupted laminated bedding	#171
469-478	Ab""	10YR 3/1	sil	2msbk	C		#166
478-490	C11	10YR 7/1 and 10YR 3/1	sil	laminated	A		
490-535	C12	2.5Y 4/2	sil	2csbk	A	on 3/14/11 we may have put this boundary at 530 cm.	

535-570	C13	2.5Y 6/3	ssil	laminated	VA		#156, #157
570-591	C14	2.5Y 5/3	sil	2msbk	G	darker topset at 570-573 cm sampled on 3/14/11 for C14	
591-612	C15	2.5Y 5/3	ssil	m and thinly bedded	C		
612-723	C16	2.5Y 7/4 (si) and 2.5Y 5/3 (sil)	si and sil	laminated and thinly bedded	G	contains a few beds of distinctly laminated silts and fine sands, otherwise there is lamination throughout, but most of it is deformed/disturbed abundant large pieces of charcoal (collected some). Few dark beds (10YR 4/2) are present, but not buried A horizons.	#168, #169, #173
723-765	C17	2.5Y 5/3	sil	1msbk to m	C	exhibits faint thin bedding and few organic lenses	#167
765-800	C18	2.5Y 5/3	sl	m		exhibits faint thin bedding	

Table II.h. Cuganda Sur Profile Description

Depth (cm)	Horizon	Color (Dry)	Texture	Structure	Boundary	Remarks	C-14 Samples
0-22	A	10YR 4/2	sil	1fgr	VA	Endeque. F, d, S-I CaCO3 nodules (2 mm gr sized). From break up of endeque	#234
22-39	Ck	10YR 7/2	sil	1fsbk	A	small endeque/nodules? Layers/massive-petrocalcic?	
39-58	Ck2	10YR 6/2	sil	2fsbk	C	very similar to above only more structure	
58-77	C	10YR 6/3	sil	1fsbk	G	f, f-med gr Endeque clasts (YAN beds derived C)	
77-131	C2	10YR 5/4	sil	2msbk	C	very similar to above only stronger structure and more abundant Endeque clasts towards bottom. C-a, med to co gr Endeque clasts. Vf, f-med Yanhuitlan clasts.	
131-152	C3	10YR 5//2	sil	2msbk	VA	c, f-m Endeque clasts. Vf, f gr, Yanhuitlan clasts	
152-195	Ab	10YR 4/1	sicl	2mwedge	G	c, p, CF on PF. F, d, masses, I, CaCO3 on PF.	#235
195-273	Ab2	10YR 4/2	sicl	2mpr	C	c-a, p, strong CF on PF. C, p, med-co CaCO3 masses I-S on PF. F, d, Mg dep on PF. F, d, slickenslides. Few, very small charcoal flecks.	#236
273-300	AC	10YR 4/2	sil	2fpr		c, d, CF on PF. F, f, CaCO3 on PF. F, d, CaCO3 in RP. Organic fill on PF, root disturbance. F, med Endeque clasts	

Table II.i. Inguiro Site Profile Description

Depth (cm)	Horizon	Color (Dry)	Texture	Structure	Boundary	Remarks	C-14 Samples
(A Section)							
0-22	A	10YR 5/2	sl	2fgr	C	gravel-cobble colluvial inclusions	
22-39	C	10YR 5/2	vfsl	2cogr	A	c, f-co Endeque clasts. F-c gravel- cobble colluvial inclusions	
39-65	2Ab	10YR 4/2	sil	3cogr	C	c,d CaCO3 on ped faces	C14#239
65-81	2Ab2	10YR 5/2	sil	3cogr	A	f, d, Ca CO3 on ped faces. F, gravel - cobble colluvial inclusions	
81-111	C2	10YR 5/3	m	1msbk	VA	f, d, CaCO3 on root pores. F, f, CaCO3 on some ped faces. F, coare gravel colluvial inclusions.	
111-133	C3	10YR 5/3	si/cogr	sg	VA	p, yanhuitlan clasts. F, endeque clasts. Biggest clast is 5 x 5 cm. Silty layer bounded by 2 gravel layers. The lower gravel layer fines up to the silty layer.	
133-165	C4	2.5Y 5/3	sl	m	D	lenses of cos-coarse gravel in matrix of silt.	C14#200
165-190	2Ab'	2.5Y 4/2	sil	1msbk	A	patches of diffuse boundary 2.2Y 5/3. c,p, CaCO3 in root pores. F,f Yanhuitlan clasts.	C14#238
190-260	2Ab2'	1.5Y 4/2	sil	3mweg	C	f, p, CaCO3 in root pores. F,f, CaCO3 on some ped faces. F,f, endeque clasts.	C14#237
260-302	2Ab3'	2.5Y 4/2; 2.5Y 6/3	sil	3fp2	A	f, f, CaCO3 on root pores	
302-359	2Ab4'	2.5Y 4/2; 2.5Y 6/3	sil	2fp2	G	f, p, CaCO3 in root pores. F,vf-f Endeque and Yanhuitlan clasts.	

359-403	AC	SEE BELOW					C14#201, #202
(B Section)							
372-412	AC	10YR 4/1	sil	2fp2	C	f,d, CaCO3 in root pores	
412-424	Ck	10YR 5/2	sil	2vfpr	G	f, coarse endeque clasts. F, d, I CaCO3 masses. F, p, CaCO3 in root pores.	
424-437	C5	10YR 6/2	sil-fs	m	VA	f, f-med Endeque clasts. F, f, Yanhuitlan clasts	
437-442	C6	2.5YR 6/2	fs, f-m gr	sg	VA	lenses of sand-gravel sized Yanhuitlan clasts. F, f endeque clasts.	
442-473	C7	2.5YR 6/3	ls	m	VA	f, d, I, CaCO3 noduels. C, f, endeque and Yanhuitlan clasts	
473-530	C8	10YR 6/3; 2.5YR 6/2	cos; fs-sil	laminated, fining upward seq	VA	fluvial beds, bands of beds with few f-co sized endeque clasts, and common Yanhuitlan clasts	
530-548	C9	10YR 6/2	fs- stones	sg	VA	coarsening upward bed. Mixed detrital	
548-550+	SEE BELOW						
(C Section)							
548-589	Bw	7.5YR 6/3	sil	2fsbk	A	F,D, CaCO3 in root pores. F,d CaCO3 on ped faces	
589-610	Bk	7.5YR 7/2; 7.5YR 8/1	sil	2fsbk	A	c,p, CaCO3 on ped faces	
610-643	Ck	7.5YR 7/2	sil	1fsbk	A	f,d, S, CaCO3 nodules	
643-716	C10	7.5YR 7.3	s-cos	m/1fsbk	C	fluvial deposits, with coarse sand- gravel sized endeque and Yanhuitlan clasts	
716-759	2Bt	7.5YR 5/3	si-cogr	sg, laminated	VA	c,p,f-med, I CaCO3 masses	
759-792	C11	7.5YR 7/3	sicl	3mpr	C	(color is moist) c, f, endeque clasts. F, m Yanhuitlan clasts. C,d, cf on ped faces	

792-823	C12	7.5YR 7/3	fsl	1msbk	A	f,f, CaCO3 in root pores. Cf endeque and Yanhuitlan clasts
823-925	C13	10YR 4/3; 10YR 5/4; 10YR 5/3	cl	m/1msbk	A	pathy. F, d, f, I CaCO3 masses at 852-853 cm and 110 lenses of endeque and carbonate nodules. (coarse rocks are between 2-4 cm)
925-950+	C14	2.5Y 5/3	sic	m		non-homogenous

Table II.j. Sandaxne Site Profile Description

Depth (cm)	Horizon	Color (Dry)	Texture	Structure	Boundary	Remarks	C-14 Samples
(A Section)							
0-10	C		sil	sg-m	VA	influxes of cos-med gr poorly sorted colluvium common as Yanhuitlan clasts and few co Endeque clasts. Silty matrix.	#228
10-50	Ab	10YR 5/4	sil	2fsbk	A	CaCO3 in root pores. Few, fine, Yanhuitlan and Endeque clasts. F, f, CF on PF. C, d CaCO3 on PF (one side). Bdy disturbed by modern root pores and krotavina	
50-82	Ab2	10YR 6/2	sil	1fsbk	A	similar to Ab above, but less organic	#229
82-124	C2	10YR 7/2	sil	1vfsbk	G	c, f, CaCO3 on PF. C, d, CaCO3 in root pores. F, vf-cos, Yanhuitlan and Endeque clasts	
124-135	C3	10YR 7/2	sil	sg-1vfsbk	VA	same as C2 only layer cos-med gr sized Yanhuitlan and Endeque clasts (2-4 mm) sg inclusions (this is colluvial layer)	
125-148	C4	10YR 6/3	sil	1vfsbk	A	cos-gr sized inclusions of colluvial common Yanhuitlan and few Endeque clasts. CaCO3 in RP only	
148-190	C5	10YR 6/3	sil	2vfsbk		similar to C4 colluvial inclusions. This layer is different because it contains only one layer of gr-cob sized colluvial inclusions	
(B Section)							
150-161	C5	10YR 7/2	sil	2vfsbk	A	f,f-mg Endeque clasts. F, f-m Yanhuitlan clasts. Layer bottom marked by 4-5 cm cobbles and gr layer 1-2 cobbles thick	

161-299	C6	a) 10YR 7/2, lighterwith CaCO3 on PF; b) 10YR 6/3, darker without CaCO3	sil	2vfsbk	A	CaCO3 in RP. c, d, CaCO3 on PF. C-a Yanhuitlan Clasts cos-cogr cobble. f-med gr Endeque clasts. Layer bottom marked by 8-10 cm cobles and f-co gr (1-2 cobbles thick) and co sand (on profile). Mastedon Hueso vertical in profile 175-194 cm. Other mastedon bone fragments in 207-217 cm near profile B, 45 cm across. *huesos near A- in situ at 313 cm and are of bones at 198-235 cm aaf	
299-335	C7	10YR 6/3	sil	2fsbk	VA	f, d, CaCO3 on PF. F, d, CaCO3 on RP. C, m-cos, f-m gr, Yanhuitlan clasts. F, m-cos, f-m gr Endeque clasts	
335-389	Ab'	10YR 5/3	sil	3msbk	VA	c, cos- co gr Yanhuitlan clasts. Some darker minerals. F, d, CaCO3 on PF. C, d, CaCO3 in RP.	#226
389-405	Ab2'	10YR 4/3	sicl	3fpr	A	c-a, cos-cogr Yanhuitlan clasts in bottom of layer. F, f-m gr, Endeque clasts. F, d CaCO3 on PF. F, d, CaCO3 in RP.	#225
405-432	Ab3'	10YR 4/4	sicl	3fpr	C	c,d, CaCO3 in RP. F, d, CaCO3 on PF (some). F, cos-cogr, Yanhuitlan clasts. F, cos-co gr Endeque clasts. Similar to Ab2' but fewer Yanhuitlan clasts.	
432-442	C8	10YR 5/4	si-cogr	sg-1fsbk	C	some paleosol matrix but much colluvial c-a, f-cos to cogr cobble (2 mm)Yanhuitlan clasts and f-c Endeque clasts (as sg).	
442-458	C9	10YR 4/4	sil-cogr	sg-2fsbk	A	c-a, cos-fgr Yanhuitlan clasts inclusions. F, f, CaCO3 on PF. F, d, CaCO3 in RP. Smaller clasts in general and almost no Endeque clasts, and darker color distinguished this from above	
458-464	C10	10YR 4/3	sicl	1fsbk	C	c, m-cos/co gr Yanhuitlan clasts. F, d, CaCO3 on PF and in RP. Mud organic layer within- fluvial deposit?	#223, #224, #222

464-469	C11	10YR 5/4	cos-cogr (2-3 cm)	m/sg		colluvial

Table II.k. Sauce Site Profile Description

Depth (cm)	Horizon	Color (Dry)	Texture	Structure	Boundary	Remarks	C-14 Samples
PROFILE 1							
550-552	C1	10YR 5/3	fgr-fsi	sg	A	fining up sequence- here only sampled gravel-sand but above nail it continues as m-fs and si.	
552-580	C2	10YR 5/4	gr (~5 cm)-sil	sg-massive	C	finign upward sequence at bottom mainly gravel fines up to sil which has more structure though weak. Sil also has CaCO3 on PF and RP. ~5 cm band of reddish clay (subsample of sil). At 2-11 cm some cross trough bedding noticeable to right.	
580-603	C3	10YR 5/2	gr (~10 cm)-fsl	sg-massive	VA	large cut at bottom fining up to fs-sl, followed by two more fining upward sequences to top with noteable cross trough bedding. Sl with structure contains charcoal. More structure in part of sl; sl also contains CaCO3 on RP and PF. In the gravel (~2 cm max) to fsl layers the bedding is very apparent, but only in the bottom gravel part is the cross trough bedding clear. These beds contain some clay chunks	
603-613	C4	10YR 6/2	fg-sl	sg-massive	VA	fining up sequence. No sedimentary structures, thus plain beds. Towards top in the sl it is more massive. The sl also contains some charcoal but it is not noticeable across whole layer. More structure or more consolidated than in layers to bottom and top.	
613-650	C5	10YR 5/4	gr (~2 cm) - sl (or sil)	sg/bedding	A	Around 5 main fining upward sequences and some up to sl and others sil. The top cm consists of sil which is above the sl with CaCO3 in RP and on PF and more massive structure (possible 1fsbk). This sub-layer has	#296

						much charcoal and seems like below this sub-layer with charcoal in some parts, there is trough cross bedding noticeable and rythmites noticeable in upper m-fs part of fining upward sequence	
650-655	C6	10YR 5/2	gr (~3 cm)-c	massive	A	This layer is very mixed with grains in more random order in a clay matrix. It has more clay than other layers and it is unclear whether it is planor beds fining up to sl or fs or sil - the latter is usually with rythmites and sl with cross-trough bedding	
655-720	C7	10YR 5/4	cos-sl or sil	sg-massive	? (break in stratigraphy)	Seems like beds mainly trough in co-fs and rythmites in fs-sil. Some beds cogr to sl beds have CaCO3 on PD and RP and are 1msbk-1fsbk- but only from 150 cm downwards. Below 170 cm change in profile it juts out and it is unclear the transition to the next layer.	#295
720-796	C8	10YR 5/3	gr (~12 cm) - ms	sg	VA	Profile from here juts out at angle - due to preservation. Where the trough cross bedding is noticeable in entire outcrop that is where cut 1 is located. These sedimens are from bottom of this cut and fill and no bedding structure is clear. Looking at where justs out in 'cross-section" see planar beds.. i.e., looking west or towards cut 6.	
796-875	Bt	10YR 4/3	sicl	2msbk (ang?)	D	F, f CaCO3 in RP; c, c, Mg in RP and PF. Or humus in PF/RP? - vf, inclusions, f, charcoal. F, vf CF on PF. F,f-m nodules of Endeque	
875-903+	Bt2	10YR 4/3	sicl	1msbk (ang?)		c, c, CF on PF. C, C, CaCO3 in RP and f, c, CaCO3 on PF. C, c, Mg in RP- what is coating on some PF? Very similar to BT1 but has weaker structure and more CaCO3, clay	

						coatings may be clearer because fresher sample?	
PROFILE 2							
675-701	C1	10YR 6/3	sil	2msbk	D	C, CL, CaCO3 on PF; c, f-m, charcoal throughout; c, c, vf-m organic flecks; some clay on RP (red); f, f-c, f Endeque clasts.	#305
701-726	C2	10YR 6/3	sil	3msbk	C	increase in organic material and burnt charcoal mixed. Redder color and increase in size of patches. Also slightly larger peds. F, vf-f endeque clasts. C, c, CaCO3 on RP. Decrease in CaCO3 on PF from above and further down in horizon. F, c, CaCO3 on PF. increase in sand towards bottom; decrease in charcoal, vf, f-m, pieces of charcoal. Look larger and more mdern than those in layer above.	
726-737	C3	10YR 6/3	f-ms-sil	sg-massive	A	pretty homogenous layer of sand before seemlingly stable time (C1 and C2).	
737-779	C4	10YR 6/2; 10YR 6/3	sl	2msbk	A	C, c, CaCO3 in RP which decreases towards top. Vf, CaCO3 on PF. F, vf-f Endeque clasts. C, vf, charcoal flecks. Largest sandy layer at bottom mm and silty material throughout. Has more structure than layers above and below but similar in material to these other layer. Overall 2-3 organic layers and 4 fining upward sequences	
779-815	C5	10YR 6/2	cos-fs	sg	C	finer towards top mainly medium sand grains and maybe finer part of sequence from below	
815-840	C6	10YR 6/3	gr-fs	sg	C	intermixed layers of mainly m-cos with gravel up to 5 cm intersperesed more gravel observed towards bottom.	
840-887	C7	10YR 6/3	gr-fs (max 10 cm)	sg	VA	bottom of cut mainly 2 cm gravel to medium sand. Much coarser material at bottom and at	

						bottom intermixed with older gravel layer. Maybe copart of fining up sequence from C8 to C7
887-892	C8	10YR 6/2	fgr-fs	sg	VA	mainly coarse sand- part of older gr-s layer which later cut cuts into
892-894	C9	10YR 6/3	ms-si	sg	VA	fining upward sequence and dated ms-silt
894-910	C10	10YR 6/3	sil-fs	sg	C	rythmite beds still noticeable but cemented mainly silt - very weak strcutre started
910-930	Ab1	10YR 5/1	sl	2mgr	D	"organic layer" cumulic A in paleoswale allowed time to develop weak structure. C, vf-f Endeque clasts. C, vf flecks of charcoal; f-c, vf-m Yanhuitlan and volcanic clasts; f clay in RP- red.
930-989	AC	10YR 5/1	gr-s	sg (1fgr)	VA	"part of cumulic A" but this layer consists of mainly gravel to sand with 2-3 intermittent darker layers- of organic material or well developed A- (i.e., periods of stability)? Organic A layers here are weaker than above and finer with many inclusions. Mainly C12 layers of fs-fgr up to 3 cm max. Around 5 fill layers of mainly fs and cos.
989-1002	Ab'	10YR 6/2	sl	2mgr	VA	part of same cumulic horizon as Ab1 bottom towards righ combines into 1 (i.e., towards cut edge or hillslope and tribfurcates towards center of paleoarroyo
1002-1045	C11	10YR 6/3	si-gr	sg	C	fining upward sequence from gravel (majority between 2-5 cm) upper gravel and sand layers (mainly ms-gr up to 2 cm). Ab at top and bottom is a silty layer containing C-14 material. Probably antoher set of fining upward sequences starting from C12.
1045-1089	C12	10YR 6/3	fs-gr	sg	VA	several layers of gr-s at bottom of fill (between 12-20 cm is size range for larger gravel) and

1089-1097+	2Ab	10YR 4/1	sil	2msbk	…	mainly m-cos and between 2-5 cm gravel. To right and left of profile are intermittent with silty layer and evidence for cross-trough bedding c,c, CF on PF; humic (or Mg??) - coatings on PF. F, f-m Endeque, Yanhuitlan and volcanic clasts. Cery late color for A - post pedogenically altered?

Table II.l. Cliff Site Profile

Depth (cm)	Horizon	Color (Dry)	Texture	Structure	Boundary	Remarks	C-14 Samples
UPPER PROFILE							
0-159	C	10YR 6/4	gr- fsl	planar bed, massive	VA	Colonial. Many 10-15 cm beds of m,vco Gravel, thinly stratified.	
159-205	Ab	10YR 3/2	sicl	3copr	G	many 10-15 cm beds of m-vco gr, Colonial	#263
205-305	Ab2	10YR 3/1	sicl	3copr	D	very many fine CaCO3 filaments on PF	#264
305-390	Btb	10YR 3/3	sicl	2mpr - weaker? But clay films	D	moderately thick CF on PF, CaCO3 filaments on PF	
390-450	Bt2b	10YR 4/3	sicl	3msbk	G	mk films on PF, CaCO3 filaments on PF	
450-495	BCb	10YR 4/4	sicl	2msbk	C	possible faint bedding	#262
495-535	Ab'	10YR 4/3	sicl	3msbk	D	many CaCO3 on PF, complete PF coatings	#261
535-553	Btb'	10YR 4/4	sicl	2msbk	C	thin CF on PF	
553-585	C2	10YR 4/6	sl	m	C	f, med gr beds and faint bedding	
585-625	C3	10YR 6/4	f/s	m	VA		
625-636	Ab"	10YR 4/2	sil	3cosbk	G		#260
636-685	C4	10YR 6/3	si	m/bedded	C	bedded with several fine, gravel beds about 3-4 cm thick	
685-740	C5	10YR 6/3	si	m	C	faintly bedded	
740-754	C6	10YR 6/4	mgr to s	indv. Beds	A		
754-795	C7	10YR 6/4; 10YR 4/2	si and sil	planar beds	G	abundant charcoal	#259
795-820	Ab"'	10YR 4/2	sicl	2cosbk	D		#258
820-880	Bwb	10YR 4/3	sil	2msbk	C		

880-910	C8	10YR 6/4	s	thinly bedded	A	f, fine gr layers	#257
910-930+	C9	10YR 6/3	si	laminated	f, p gr lenses	flame structures, disrupted laminae	
LOWER PROFILE							
1550-1700	C1	10YR 6/4	si, s, fgr	rhythmically bedded	C	numerous beds of gravel graded up unto silt. Silt and fine snd beds show planar and cross beds laminations . Gr beds contain distinct clasts of Yanhuitlan clasts (many well rounded Yanhuitlan clasts).	#263
1700-1750	C2	10YR 6/4; 10YR 5/2	si-sicl	laminated thinly stratified	A	abundant charcoal. Transitional to prominent A horizon	#265
200-240	Ab	10YR 3/2	sic	3copr	G		#266
240-340	Bw	10YR 6/6	sicl	2msbk	D		
340-490	C3	10YR 6/5	si, s, fgr	rhythmically bedded		numerous beds of gravel graded up unto silt. Silt and fine snd beds show planar and cross beds laminations . Gr beds contain distinct clasts of Yanhuitlan clasts (many well rounded Yanhuitlan clasts).f, f, med Endeque clasts. F, f-m Yanhuitlan clasts. Cos-gr lenses at 325-332 cm	
490-505	Ab"		fsl	1fsbk	C	many med-cos Endeque clasts many beds (esp silt and fine sand) show cross stratification/cross beds.	#276, #278
505-587	C9		fg-sic	laminated beds	VA	Majority of gr/s clasts are of Yanhuitlan beds and some subangular endeque. Gr/s to si/cl fining upward sequences. Basal unit (bottom 4 cm) fining upward sequences of mud has dark brown to	

					black. (non silt but sandy clay rich has reddish color.)	
587-602	C10		med-cogr sic	laminated beds	A	cross trough bedding, gravel (up to 5 cm) to fs-sic fining upward sequence. Majority are subangular Yanhuitlan beds clasts and angular Endeque clasts. upper boundary is a muddy (4 cm thick) layer is overlain by a cos-fs layer (about 1 cm thick). From 602- 615 cm are fgr- fs cross trough bedding. Below this, from 615-652 cm are mixed cross and planar beds of fgr-fs. Bottom 15-20 cm (from 652-672 cm) contains definite cross cross trough bedding of gravel and cobbles (diameter 10 cm). Beds contain Yanhuitlan and Endeque angular to rounded clasts.
602-672	C11		fgr-fs	laminated beds	VA	
672-742+	C12		mainly sicl, also fining upward(?-no) fgr-sic			#274, #275

Table II.m. Río Culebra Confluence Profile

Depth (cm)	Horizon	Color (Dry)	Texture	Structure	Boundary	Remarks	C-14 Samples
(A Section)							
0-15	A	10YR 5/2	sil	1msbk	G	f, d, CaCO3 in RP and PF. C, f-med, Yanhuitlan and endeque clasts. (part of cumulic horizon or disturbed due to modern LB.)	
15-49	A2	10YR 5/2	sil	1msbk	VA	vf, f-med Endeque clasts. F, d CaCO3 in RP and PF. Common Yanhuitlan clasts.	#189
49-72	C	10YR 5/2	fs-cogr	laminated s, m	VA	3 fining upward sequences of fs-cogr of mainly Yanhuitlan clasts, but includes some Endeque clasts.	
72-109	Ab'	10YR 6/2	sil	3cogr	G	f, f, CaCO3 on PF and RP. F, f, Yanhuitlan clasts, f, f, endeque clasts. Much fewer than in Ab and Ab2.	#188
109-136	C2	10YR 6/3	sil	1cogr	C	common, fine- medium Yanhuitlan clasts. F, f-m endeque clasts.	
136-149	C3	10YR 6/3	sil-sg	1mgr	A	a, f Yanhuitlan clasts, few, fine-medium Endeque clasts. Separated from V above due to the abundance of Yanhuitlan clasts. Fluvial deposits.	
149-173	C4	10YR 6/3	sil	2cogr	D	few, fine endeque clasts, and no Yanhuitlan clasts.	
173-190	C5	10YR 6/2; 10YR 6/3	sil/sicl	3cogr/1msbk	A	patchy due to diffuce boundary. Redox features BPF, I, I dif, (10YR 6/4). F, d, CaCO3 in RP.	
190-224	Ab"	10YR 5/1	sil	2msbk	G	f, f, Endeque clasts and f, f, Yanhuitlan clasts. Some oxidation	#187, #255

						on PF. F, d, CaCO3 in RP. Sherd at 205 cm.	
224-270	Ab2"	10YR 4/1	sicl	2mpr	C	f, f, clay films, on 1 side of PF. f, d, f-med, S-I CaCO3 nodules. f, d, CaCO3 in RP. vf, f, endeque and Yanhuitlan clasts.	
270-300+	Ck1	10YR 6/2	sil	m		f, f, CaCO3 on PF and RP. f, d, f-med, S, CaCO3 nodules.	
(B Section)							
300-312	Ck1				C		
312-334	Ck2	10YR 4/3; 10YR 4/2	sil	2mgr	A	f, d, CaCO3 in RP. f, d, f-med, I CaCO3 masses. f, f, Yanhuiltan and Endeque clasts.	#256
334-343	2Ab	10YR 3/1; 10YR 4/3	sil	2msbk	C	f, d, CF on PF. f, d, CaCO3 in RP.	#193
343-352	2Ab2	10YR 3/2; 10YR 4/3	sicl	2msbk	A	f, p, CaCO3 in RP. F, d, CF on PF. f, d, f-med, I, CaCO3 masses.	
352-385	2Ab3	10YR 3/1	sicl	3cosbk	A	f, d, CF on PF. f, d, CaCO3 in PF. f, p, CaCO3 in RP. f, d, f-med, S CaCO3 nodules	#186, #194
385-426	2Ab4	10YR 3/1	sil	2cogr	D	f, d, CaCO3 in RP.	
426-451+	C7						
(C Section)							
426-479	C8	10YR 6/2; 10YR 5/2	sil	1msbk	A	c, d, CaCO3 in RP and PF. f, d, Endeque clasts. f, med Yanhuitlan clasts.	
479-483	C9	10YR 6/3	fine gravel (2mm), and fine-coarse sand	2mgr	A	c, f, Yanhuitlan clasts. f, f, endeque clasts. f, d, CaCO3 in RP.	

483-507	Ck	10YR 6/3; 10YR 6/2	fine to medium gravel to silt	2mgr	A	no bedding or laminations. Fining upward sequences. CaCO3 in root pores. c, d, f-med, I, CaCO3 masses. c, m, Yanhuitlan clasts. f, vf, Endeque clasts.	#252
507-516	C10	10YR 6/2	fs-mgr	2mgr	A	c, f, CaCO3 on PF. f, d CaCO3 in RP. f, f, Endeque clasts.	#253
516-519	C11	10YR 6/3	sil-fs	sg	C	f, p, Yanhuitlan clasts. f, f, endeque clasts.	
519-553	C12	10YR 6/3	fs-fgr	1fgr	G	si on bottom coarsesns up and is overlain by fsl cs- fgr. Above this is sil and csfs. C, d, CaCO3 in RP.	
553-562	2Ab"	10YR 6/3; 10YR 5/3	sil	2fsbk	C	f, f, CaCO3 on PF. F, d, CaCO3 in RP. Silty lenses from 555-557 cm and from 561-562 cm, which has 1fgr structure. Cumulic A. Color of CaCO3 in pores is 10YR 7/2.	
562-582	2Ab2"	10YR 5/3; 10YR 5/2	sil	1msbk	G	c, d, CaCO3 in RP and PF.	#195
582-598	2Ab3"	10YR 5/3; 10YR 5/2	sil	2msbk	G	c, d, CaCO3 in RP and on PF. Contains silty patches (10YR 6/3).	#196, #254
598-620	2AB	10YR 4/2	sil	2mpr	C	d, f, CF on PF. F, d, CaCO3 in RP and on PF. At 618-620 cm there are abundant, med-gravel sized Endeque clasts.	
620-638	Btk	10YR 4/3	sicl	2mpr	G	f, d, CF on PF (10YR 3/2). f, d, fine-medium, S, CaCO3 nodules. f, d, CaCO3 in RP and on PF.	#197
638-672	Btkss	10YR 4/2	sicl	2mpr	C	f, p, med-co, S-I, CaCO3 concentrations. f, d, slickenslides on PF. c, d, CaCO3 in RP and on PF.	

672-775	Btkss	10YR 4/2	sicl	3copr	G	c, p, slickensides. f, p CaCO3 in RP. f, f-med, Endeque clasts. f, p, med-co, I, CaCO3 nodules.	#190
775-820+	Ck	10YR 4/3	sicl- sil	1mpr		f, p, co, I, CaCO3 very cemented nodules. F, d, CF on PF in upper gradual boundary to few beneath where grades down to sil.	
(D Section)							
810-841	Ck	10YR 5/2	sil	2msbk	VA		#191
841-881	C13	10YR 6/2	sil	1msbk	VA	From 841-842 is layer of abundant med-co endeque clasts. Throughout horizon, c, f-med endeque clasts.	
881-890	C14	10YR 6/3	fs-mgr		VA	no obvious bedding. Cut and fill pinches out to west of horizon	
890-934	C15	10YR 6/2	sil	1cogr	A	f, f, Endeque clasts.	#257
934-979	Ck	10YR 6/3	sil	1msbk	C	c, med-co, I-S, CaCO3 nodules.	
979-1019	3Ab	10YR 4/2	sil	2msbk	G	c, f, Endeque clasts. F, f-med, I, CaCO3 nodules.	#192
1019-1055+	C16	10YR 6/3	vfsil	2fgr		c, f, Endeque clasts. F, f, Yanhuiltlan clasts.	
(E Section)							
1019-1074	C16				C		
1074-1095	Ck'	10YR 7/2	sil	1msbk	A	a, p, CaCO3 on ped faces. F, f-med, Yanhuitlan clasts.	
1095-1119	C17	7.5YR 7/2	sil	1msbk; 2cogr	A	c, f-med, Yanhuitlan clasts. A, f, endeque clasts. F, CaCO3 in RP.	
1119-1204	Ck '	10YR 5/4	sil	2msbk	C	c, d, f-med, S, CaCO3 nodules. C, vf, Yanhuitlan clasts.	
1204-1212	Ck2'	10YR 6/4	ls	1msbk	VA	a, Yanhuitlan clasts. Main difference between these horizon are fewer CaCO3 nodules than above and more abundant Yanhuitlan	

						clasts. There are also few, fine, Endeque clasts.
1212-1239	C18	10YR 8/2	su	m-gr	A	(from here down, the tape makes a 20 degree angle with the profile). Consists of gravel to cobbles in silty matrix, not well sorted, thus is remnants of a colluvium?- need to see. Some stones lie flat in at upper boundary. Cobbles measure 10-15 cm in diam. Few endeque clasts.
1239-1309	C19	2.5Y 7/3	tuff, ms	m	A	tuff is deposited the mud/debris flow underneath. More massive like between 1269-1309 cm, contains some roots. From 1269-1309 cm bedding is obvious, from f-med sand to silt sized particles. Fining upwards.
1309-1443	C20	10YR 5/4; 10YR 6/4	f-cos	sg		consists of fine pebbles to boulder sized debris, mixed with sand sized particles. Very poorly sorted, definit debris flow. Larger boulders measure about 25 x 25 x 15cm.
(F Section)						
1414-1431	4Ab	10YR 6/2.5	sl	2cogr	C	(very weak A), a, vf Endeque clasts. F, co Endeque clasts. F, f, Yanhuitlan clasts. A, d, Mg deposits in RP. F, d, Mg I nodules.
1431-1448	AC	10YR 7/2	fsl	1cogr	G	f, d, f Mg nodules and in RP. C, f, Endeque clasts

1448-1480	C21	10YR 6/2	fsl	2vcgr	C	c, d, f-m Mg nodules and in RP. A, vf, Endeque clasts. C, co Endeque clasts
1480-1511	C22	10YR 7/2	sil	1fsbk	G	a, f-m Endeque clasts. F, f gr inclusions
1511-1545	C23	10YR 8/2	sil	1msbk	G	f, m-co Yanhuitlan clasts. A, vf-f Endeque clasts
1545-1569	C24	10YR 8/1	sil	1msbk	G	f, f, Endeque clasts. Seems like consolidated Endeque, more massive precipitates
1569-1595	C25	10YR 8/1	sil	m/1msbk	D	c, f-m endeque clasts. Less 'consolidated' than in C4
1595-1661	C26	10YR 7/3	sil	1msbk	G	f, m-co Yanhuitlan clasts. C, (but fewer than in C5) f-m endeque clasts
1661-1724	C27	10YR 6/2	sil	2msbk	C	same as C6
1724-1757	Bwb	10YR 5/3	sicl	2mpr	C	c,f, CF. c, d, CaCO3 in RP. C, d, CaCO3 on PF
1757-1804	BC	10YR 6/3	sicl	1mpr	C	f,f, CF. F, d, CaCO3 in RP and f, f, CaCO3 on PF
1804-1815+	C28	10YR 6/2	sil	2cogr		
(G Section)						
1815-1822	C28				C	see Section F
1822-1848	C29	10YR 7/2	sil	2mpr	D	c, d, CaCO3 on PF. F, m-co Endeque clasts
1848-1882	C30	10YR 7/2; 10YR 8/1; 10YR 5/3	sil; si-sil; sicl	2mpr; 1msbk; 3cogr	C	mixed layer due to slope or slopewash? (10YR 8/1 endeque massive layer. f, f, CF. (flake/chip included in layer- cultural?). F, d, CaCO3 on PF. C, d, CaCO3 in RP.
1882-1920	5Ab	10YR 5/3	sicl	1msbk-3cogr	C?- D	f, d, CF on PF. C, d, CaCO3 in RP. F, d, CaCO3 on PF

1920-1955	Btk	10YR 5/3	sicl	1msbk	D	horizon contains parts of both A and B. Patches of 10YR 6/3 A horizon. f, vco, 10YR 8/1 CaCO3, I, S, nodules between peds.
1955-2023	Btk	10YR 5/3	sicl	2msbk		f, p, CaCO3, I, S, 10YR 8/1, vc-ext-co, nodules. C, p, CF on PF.
2023-2143+	C31		sicl	massive		porous structure with pebbles and boulders interdispersed.. Debris flow/mudflow?

Table II.n. Magdalena Culvert Profile

Depth (cm)	Horizon	Color (Dry)	Texture	Structure	Boundary	Remarks	C-14 Samples
MAIN PROFILE							
0-81	C1	10YR 5/4	sil	1cosbk	clear	Few beds of gravelly loam especially at base. Gravel includes Yanhuitlan and endeque clasts.	
81-110	Ab1	10YR 4/2	sil	2msbk	diffuse	Many granules of Yanhuitlan and endeque class. Faint CaCO3 in very fine root pores . Contains potsherds.	#30, #31
110-140	Ab2	10YR 3/2	sil	3msbk	gradual	Many granules of Yanhuitlan and endeque class. Faint CaCO3 in very fine root pores . Contains potsherds.	#29
140-164	Ab3	10YR 4/2	sil	3cosbk	gradual	Common, distinct CaCO3 in fine root pores. Yanhuitlan and Endeque clasts included. Includes pottery.	
164-205	Ab4	10YR 3/2	sil	3mpr	gradual	Abundant CaCO3 in fine root pores. Yanhuitlan and Endeque clasts included. NO pottery.	#28
205-247	ABb	10YR 4/2.5	sil	2msbk	diffuse	Common, distinct CaCO3 in fine root pores. Yanhuitlan and Endeque clasts included. NO pottery.	#22
247-291	Bwb	10YR 4/3	sil	2msbk	diffuse	Common distinct CaCO3 in fine root pores. Yanhuitlan and Endeque clasts included. NO pottery. Very fine and medium gravelly zone.	

291-334	BCb	10YR 4.5/3	sil	2msbk	abrupt	Common distinct CaCO3 in fine root pores. Yanhuitlan and Endeque clasts included. NO pottery. Very fine and medium gravelly zone; BUT less gravel than above.	
334-364	C2	10YR 4/2 (sil) 10YR 5/4 (gr)	sil grl	lmsbk	abrupt	Poorly stratified silty loam and gravel loam. Silt loam in mist of gravel loam.	
364-380	C3	10YR 6/3, 10YR 4/2	si	m	very abrupt	Bedded, CaCO3 filamentation remained same since 291 cm. Faint lamination in light silts. Darker beds in middle, but disturbed.	#23
380-385	C4	10YR 4/4	l	m	very abrupt	Very poorly sorted with many granules.	
385-396	C5	10YR 6/4	si	m	very abrupt	Laminated (somewhat distorted). Same CaCO3 filaments as in C4.	
396-407	A and C	10YR 4/2 (A) 10YR 4/3 (C)	l (A) l (C)	m (A) m (C)	clear	Graded bed with organic enrichment in top 3 cm.	#26, #27
407-437	C6	10YR 4/3	grsil	m	matching horizon with outcrop to W	*407-554 represents a thick stratum of flood events with some graded beds and many thick strata.	
MAIN PROFILE							
407-437	C6	10YR 4/3	grsil	m			
437-454	C7	10YR 5/3	si	m	very abrupt	Few granules. CaCO3 as above from 385-399 cm.	
454-475	C8	10YR 4/4	grl	m	very abrupt	Poorly bedded granules mixed with a little 10YR 6/3 silt.	
475-487	C9	10YR 5/3	grsil	m	very abrupt		
487-491	C10	10YR 4/4	gsl	m	very abrupt		

491-500	C11	10YR 5/3	si	m	very abrupt		
500-506	C12	10YR 4/4	grsl	m	very abrupt		
506-511	C13	10YR 6/3	si	m	very abrupt		
511-535	C14	10YR 5/3	grl	m	abrupt		#32
535-548	C15	10YR 6/3	grsi	bedded	very abrupt	Contains few thin beds of granules (flood beds).	
548-554	C16	10YR 6/2	sil	m	abrupt		
554-580	Ab1'	10YR 3/2	heavy silt loam	3mpr breaks to 3msbk	gradual	NO CaCO3 filaments as above. Few very small concretions.	#25
580-?	Ab2'	10YR 5/1	sicl	3copr breaks to 3msbk	N/A		#24
(A Section)							
560-580	Ab'	10YR 4/3	sil	(3copr -)(3?)1msbk		from diffuse boundary above (previous profile)	#268
580-685	Ab2'	10YR 4/2	sil	2msbk	G	f, f-m, endeque clasts; c, d, CaCO3 in RP; vf, m, Yanhuitlan clasts both increase towards bottom to common	
685-709	Ab3'	10YR 5/2	sil	2msbk	A	f, f-m, Yanhuitlan and Endeque clasts; little less common than above. F, f, CaCO3 in RP.	#269
709-754	C	10YR 6/2	sil	2msbk	C	mix of s, si and gr and not well organized possible colluvial input ? Color? structure with lenses of Yanhuitlan and Endeque clasts. Throughout A matrix are c, f, Endeque and Yanhuitlan clasts. Lens located at	#272
754-761	Ab"	10YR 5/3	sil	2fsbk	A	c, d, carbonate on PF; c, d, carbonate in RP; c, f-m, Yanhuitlan and endeque clasts	
761-767	C17	10YR 5/4	sil	sg	C	colluvial deposits bordering a colluvial	

767-783	C18	10YR 6/3	sil	massive	G	colluvial layer bordered by fluvial lens on bottom with f, med Endeque clasts. F, f, Yanhuiltan clasts, different from above and below by increaseing Endeque and decreasing Yanuitlan clasts	
783-788	C19	10YR 5/4	sil; f-cos, fgr	sg-massive	C	c, f-m, Yanhuitlan clasts; f, f-m, Endeque clasts; increase in Endeque clasts; fluvial fining upwards sequences gr-si.	
788-797	C20					darker layer with charcoal (ashy…?)	
797-850	C21	10YR 4/4	lsi/ls-fgr	laminated	C	mainly a, vf-m Yanhuitlan clasts and f, f, Endeque clasts in laminated planar and possibly cross trough beds	
850-897	C22	10YR 4/4	ls-cogr	laminated planar	VA	different from abaove based on particle size. F, f-m gr endeque clasts; a, f-vco Yanhuitlan clasts	
897-913	C23	10YR 5/4	sil-s	massive		some laminated beds observable. Vf, f, Endeque clasts; f, f-m, Yanhuitlan clasts	
	C24						
(B Section)							
897-937	C25	10YR 5/4	sil-fgr	massive-sg	VA	a, f-m, Yanhuitlan clasts (as gr and s); f, f-m, Endeque clasts; same laminations in si-fs and s-gr beds	#273
937-977	C26	10YR 4/3	sil-fgr	massive	C	f, f, laminated beds; a few gravel lenses; with mainly Yanhuitlan and some Endeque clasts. Fining up sequences	#271
977-1009	C27	10YR 6/3	sil-fgr	2mgr	G	f-c, f-m, Yanhuitlan and f, f, Endeque inclusions	
1009-1032	C28	10YR 5/3	si/sil	massive-1fsbk	C	c, d, CaCO3 in RP; original fining upward sequence from s-gr below?	
1032-1056	C29	10YR 6/2	sil-fgr	sg-1fgr	A	majority endeque f-m gr clasts; f, f, Yanhuitlan clasts	
1056-1122	C30	10YR 6/3	si-cos	massive/laminated	VA	similar to above, but no structure and smaller clasts; c, f-m, endeque clasts	

1122-1145	C31	10YR 6/3	sil-fgr	1fsbk	A	f, d, CaCO3 in RP; f, f-m, Yanhuitlan clasts, f, f, Endeque clasts
1145-1167	2Ab	10YR 4/3	sl	1fsbk	D	in sandy deposit; soil development, c, f, Yanhuitlan clasts; f, f, Endeque clasts
1167-1172	A/ C	10YR 4/3	si-fs/scl	massive	G	fluvial depsoits of some A horizontal clasts mixed with rip-up clasts of A horizon(from other part) with color of 10YR 3/3. Some charcoal
1172-1176	C32	10YR 5/4	scl	massive	C	f, f-m, Yanhuiltan clasts
1176-1182	C33	10YR 4/4	sicl	?	A	organic layer
1182-1248	C34	10YR 5/4	sicl	massive	D	f-c, f-m, Yanhuitlan and f, f-m, Endeque inclusions

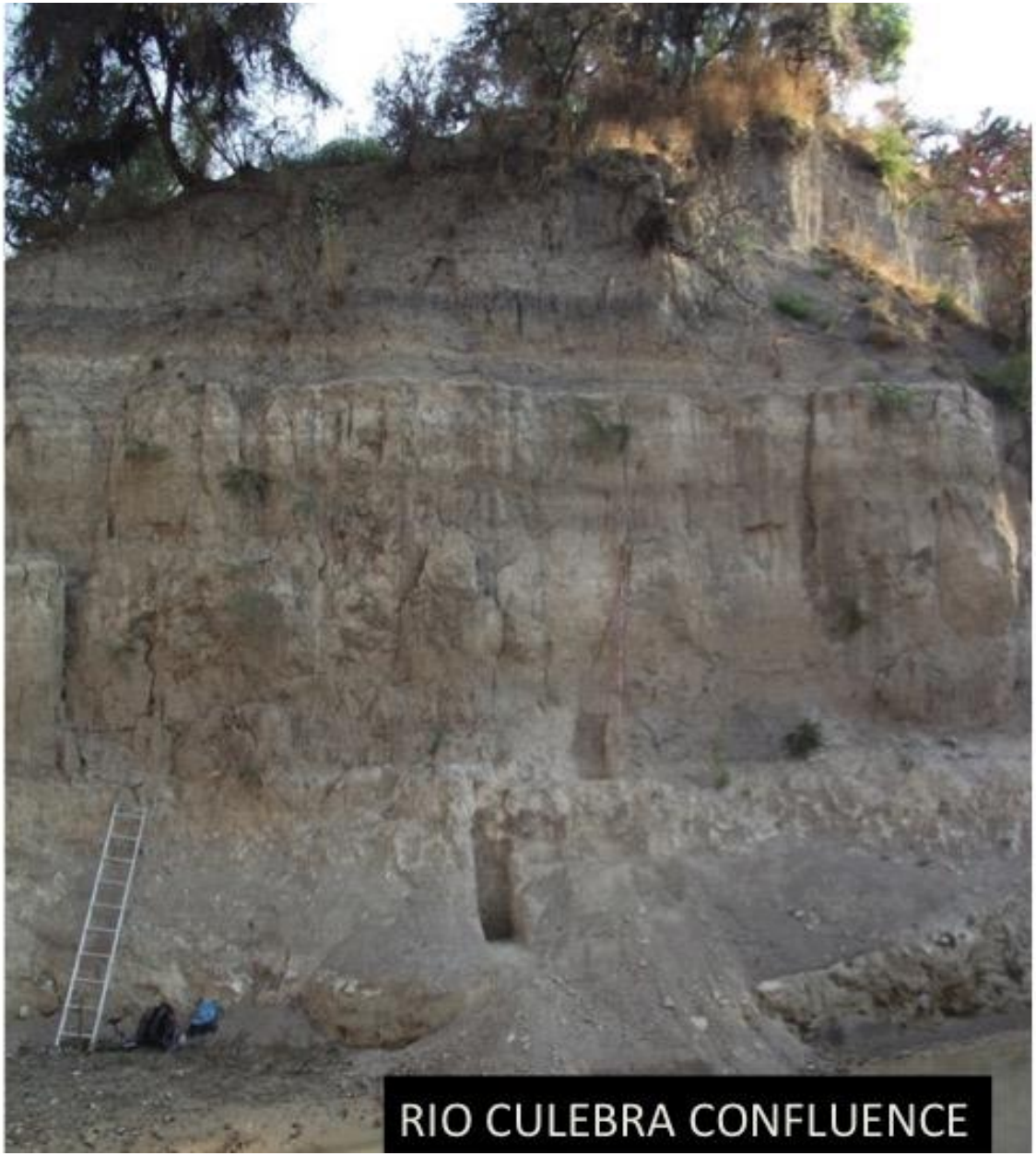
RIO CULEBRA CONFLUENCE


SAUCE


SAUCE


CONFLUENCE SITE


CLIFF SITE


CLIFF SITE

MAGDALENA CULVERT


ISLAND SITE


VICTOR'S LAMA-BORDO SITE


FLORES AMARRILAS


FLORES AMARILLAS


JUNIPER SITE

Table II.o. The table shows the formulas used in the CLAM application (Blaauw, 2012) in R software (R Development Core Team, 2008) to model sedimentation rate (cm/yr) for each profile. The results from estimated sedimentation rates are shown in Table II.p. Each formula included terms dmin = 0 and dmax = (the maximum depth of each profile when average rates with overlapping dates to create Figure 3.8.

Profile	Formula in CLAM
X9 (Cliff Site)	Clam("CLF", type = 1, its = 10000, accrate = 1)
C1 (Confluence)	Clam("CON", type = 2, its = 1000, accrate = 1)
S6 (Flores Amarillas)	Clam("FAM", type = 1, its = 1000, accrate = 1)
S8 (Juniper Site)	Clam("JUN", type = 1, its = 10000, accrate = 1)
S7 (Island Site)	Clam("IS", type = 1, its = 1000, accrate = 1)
S5 (Victor's Lama-bordo)	Clam("LBV", type = 1, its = 1000, accrate = 1, hiatus = 599)
S4 (Magdalena Culvert)	Clam("Mag", type = 1, its = 1000, hiatus = 542, accrate = 1)
I10 (Meander Bend)	Clam"("MB", type = 3, its = 1000, accrate = 1)
C2 (Río Culebra Confluence)	Clam("RCC", type = 1, its = 10000, accrate = 1)

Table II.p. The table shows the results from estimated sedimentation rates using the formula and procedures as described in Table II.o.. Only strata that did not contain any major hiatus or well-developed paleosol formation (excluding cumulic paleosols), and which fell within two radiocarbon ages (versus modeled ages).

Site ID	Depth (cm)	Age (Median Cal BP)	Rate (cm/yr)
S5	119	599	0.98
S5	127	607	0.98
I10	243	996	0.25
C3	767	1065	0.75
S7	137	1223	0.35
S7	280	1626	0.09
I10	470	1913	0.25
S7	330	2143	0.13
S7	351	2329	0.14
S5	191	2746	3.03
S7	522	3511	0.92
S5	1075	3604	4.55
S4	246	3834	0.28
S4	398	4360	0.63
X9	253	6375	0.06
C2	490	9063	0.14
X9	450	9629	0.4
X9	785	10474	0.55
X9	1749	12207*	0.55
X9	1750	12213**	0.14
X9	1799	12583	0.14
X9	1800	12581	0.19
C2	997	12710*	0.14
X9	2289	15201*	0.19

APPENDIX III

SUMMED PROBABILITY PLOTS AND AGE CALIBRATION

The CALIB downloadable software program was used to calibrate all of the dates from Coixtlahuaca. The paleosol and alluvium dates from Coixtlahuaca and Nochixtlan were combined and collected into two different cumulative probability curves.

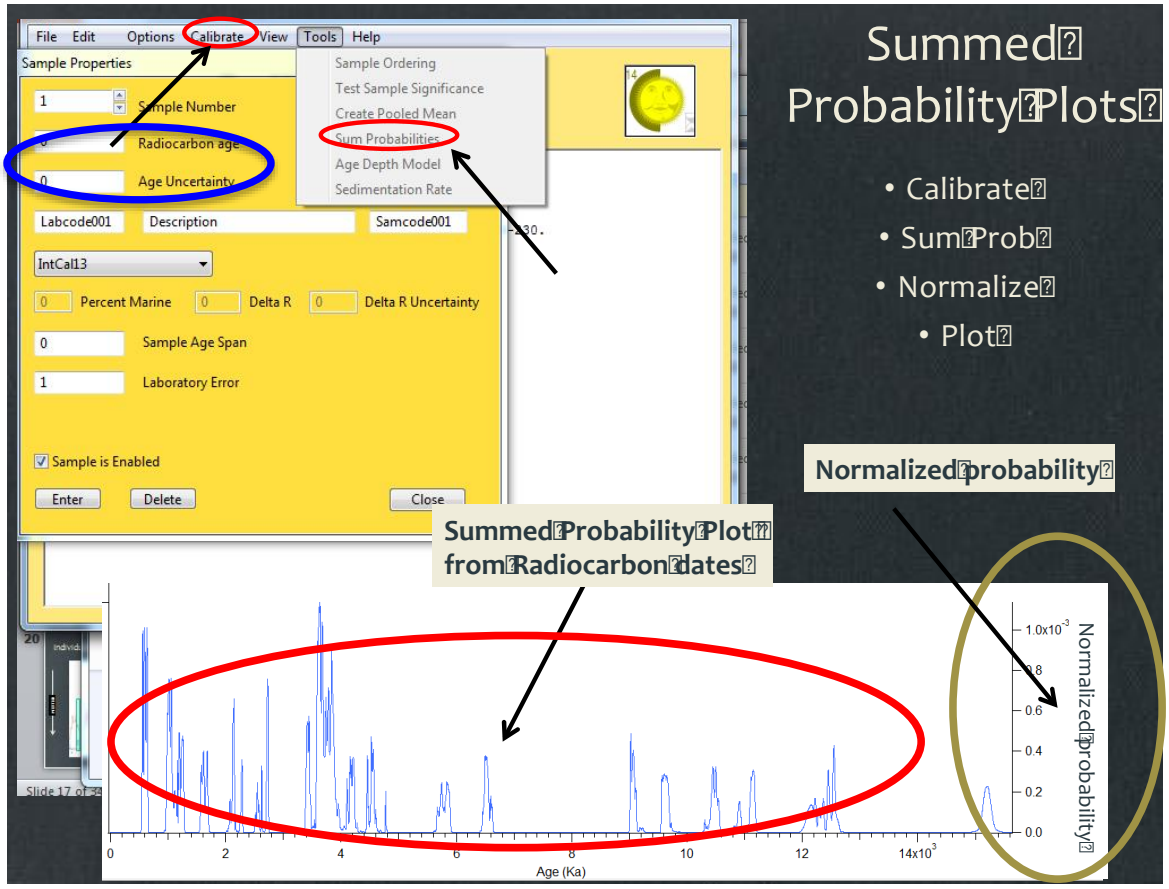

After downloading software, I set my options and tools as follows to make the two Sum Probability Curves, one for paleosols and one for alluvium (See Figure Xa). Under the heading

CALIBRATION I defined how I wanted the calibration to be displayed. I checked the 1- and 2-sigma precisions and calibration in years BP. I also checked "write distribution file". Then, under **OPTIONS**, I chose **plot options,** and selected ***Single Sample Cumulative Probability***. I also checked: "Make postscript Plot File". Next, I clicked on **File>Open> New**. I entered in the C-14 Radiocarbon age and the Age Uncertainty for the paleosols, changing the Labcode number for each successive entry. After I entered all of the dates for the paleosols, I clicked on **CALIBRATE**.

To obtain the Summed Probability values, I clicked on **TOOLS**>Summed Probabilities. I opened each of the individual calibrated files and the summed probability files located in the **CALIB** folder into wordpad, saved as text, and then imported these into EXCEL. I used the same procedure to make a Sum Probability Curve for the alluvium. The Sum Probability Curves were plotted in IGOR with the stable oxygen isotope data from the stalagmites from Guerrero and qualitatively compared (see text for graphs).

In order to conduct the quantitative analysis, I edited the probability curve values in Excel, so that they matched the dates and corresponding stable oxygen isotope values from the stalagmites. For example, I only kept the dates and corresponding probability information from the probability curves that were the same as the dates corresponding to the stalagmite isotope values. The probability information from the cumulative curves was used to divide the paleosol or alluvium dates into two further categories: either corresponding to a dated alluvium or paleosol, or having a value of zero (i.e., no probability of being a date associated with either one). The result were 2 pairs of data, each having a date and an isotope value, which corresponded to one of the following 4 categories: isotope values corresponding to dated paleosols (Category: Paleosol1), isotope information corresponding to dated alluvium Category:

Alluvium1), isotope values not corresponding to dated paleosols (Category: Paleosol0), and isotope data not relating to dated alluvium (Category: Alluvium0). These categories were further subdivided into those based on age (e.g., early vs. late Holocene) and on overarching climatic phenomena (e.g., ENSO, North Atlantic). Any significant difference between categories was detected by conducting t-tests and non-parametric tests (e.g., Mann-Whitney and Wilcoxon tests). Since there were so few paleosol and no alluvium dates from the late Pleistocene, the quantitative analysis only incorporated dates since the Terminal Pleistocene (in this study after ~16.0 cal ka BP). A similar procedure was used in filtering the sand data from el Junco, and the Sum Probability Curves for alluvium and paleosols.

Table III.a. The table shows the relationship between radiocarbon ages obtained from charcoal and soil organic matter (i.e., bulk in table) from the same strata. Radiocarbon samples are from Rincon, 1999 and this study. Calibrated ages were made using CALIB online software (see above for references).

14C Charcoal Dates	14C Bulk Dates	Range of Calibrated Ages for Charcoal	Difference in Range of Calibrated Ages for Charcoal	Range of Calibrated Ages for Bulk	Difference in Range of Calibrated Ages for Bulk	Range of Differences between Bulk and Charcoal Calibrated Ages
1	107	1-25	24	22-266	244	21-241
1500	1530	1176- 1710	534	1343-1526	183	167-184
1920	2370	1628-2058	430	2210-2705	495	582-647
2240	2580	1947-2691	744	2350-2923	573	403-232
4430	4570	4866-5286	420	5040-5464	424	174-178
		Average:	**430.4**		**383.8**	**269.4-296.4**

Average Variability in Calibrated Ages for both Charcoal and Bulk	407.1
Average Variability in the Difference between Bulk and Charcoal Calibrated Ages	282.9
T-test Results:	0.088354041